Similar but different: Oncogenic MAPK pathway mutations in colorectal cancer

Jasmin Barry Post

Similar but different: oncogenic MAPK pathway mutations in colorectal cancer

ISBN: 9789463756709

Printed by: Ridderprint | www.ridderprint.nl
Layout by: Jasmin B. Post
Cover design by: Jasmin B. Post

Publication of this thesis was financially supported by ChipSoft B.V..

Similar but different: Oncogenic MAPK pathway mutations in colorectal cancer

Gelijk doch verschillend:
Oncogene mutaties in de MAPK-signaaltransductiecascade in darmkamer
(met een samenvatting in het Nederlands)

Proefschrift

ter verkrijging van de graad van doctor aan de
Universiteit Utrecht
op gezag van de
rector magnificus, prof.dr. H.R.B.M. Kummeling,
ingevolge het besluit van het college voor promoties
in het openbaar te verdedigen op

dinsdag 3 december 2019 des middags te 2.30 uur

door

Jasmin Barry Post

geboren op 1 april 1989
te Mississauga, Ontario, Canada

PROMOTOR:

Prof. dr. J.E. van Rheenen

COPROMOTOR:

Dr. H.J.G. Snippert

CONTENTS

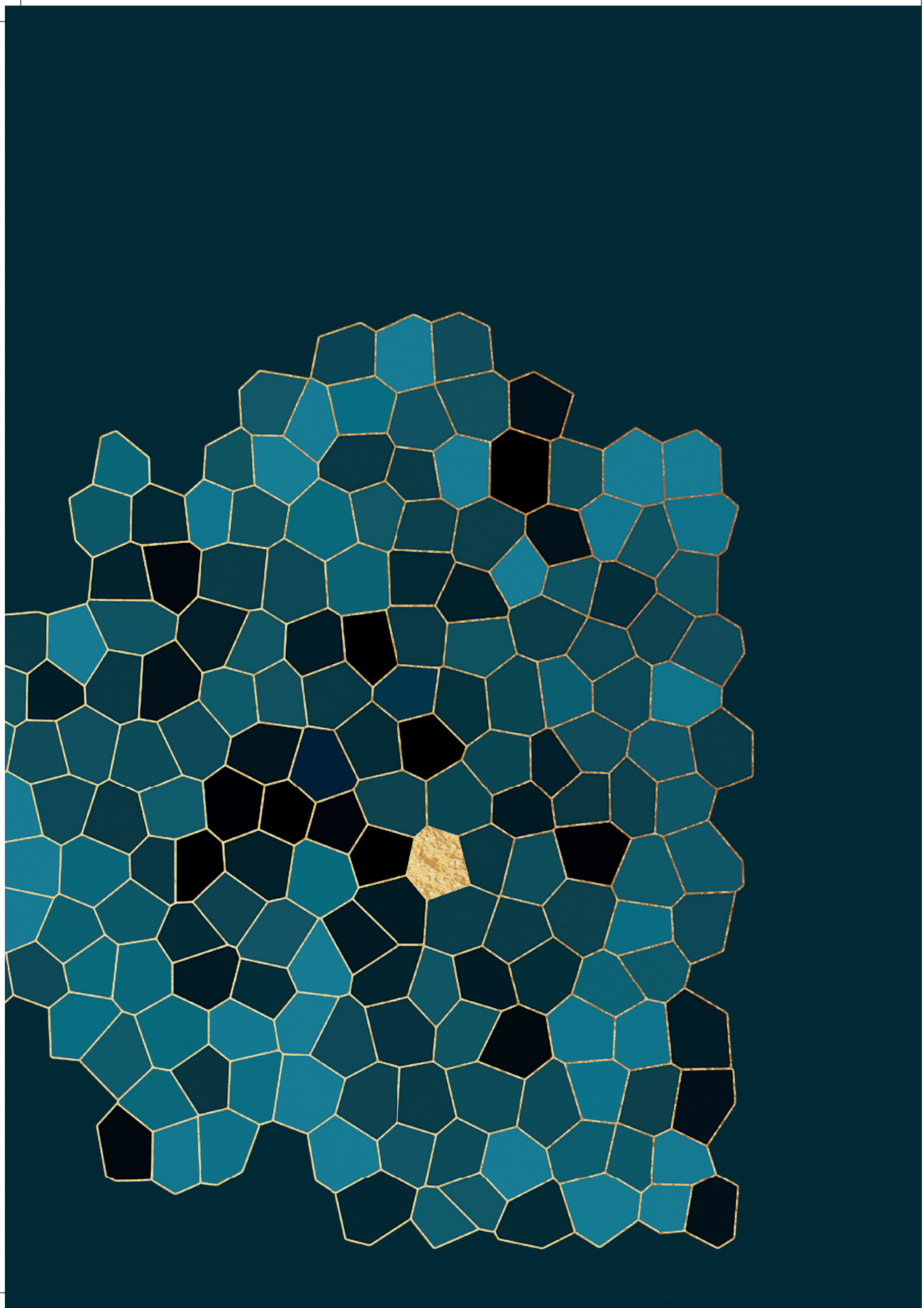

CHAPTER 1

DISEASE MODELING IN TUMOR ORGANOIDS: DISCRIMINATING BETWEEN ONCOGENIC *RAS* AND *BRAF* VARIANTS

Jasmin B. Post, Jeanine M.L. Roodhart and Hugo J.G. Snippert

Under review at Trends in Cancer

ABSTRACT

RAS and BRAF proteins are frequently mutated in colorectal cancer (CRC) and have been associated with therapy resistance in metastatic CRC patients. The RAS protein family consists of four isoforms, which are highly similar in their amino acid sequence and molecular structure, leading to the initial hypothesis that RAS proteins can act as redundant entities in physiological and pathological settings. However, there is compelling evidence that RAS proteins have isoform specific and context dependent functions. In particular, oncogenic *RAS* and *BRAF* variants seem to have different oncogenic potential and therapeutic outcomes. In the most extreme scenarios, intertumoral or even intratumoral heterogeneity in drug response is observed between identical *KRAS* mutant clones. In this review, we describe the evidence supporting similarities and differences between oncogenic *RAS* and *BRAF* variants in CRC development, histology, and therapy resistance. In addition, we describe the potential of patient-derived tumor organoids for personalized therapy, as well as CRC organoid biobanks and CRC disease modeling using genome editing as preclinical model systems to study the similarities and discrepancies between oncogenic EGFR pathway mutations on tumor growth and drug response.

KEYWORDS

RAS, BRAF, CRC, Organoids, Targeted therapy

1

RAS AND *BRAF* ONCOGENES: NOTHING SEEMS THE SAME

The RAS protein family consists of four different isoforms, i.e. HRAS, NRAS, and KRAS splice variants 4A and 4B, that are expressed in a wide range of tissues[1–5]. All four isoforms are highly similar in amino acid sequence (80%) and molecular structure. Most of their sequence variation is concentrated at their C-terminal hypervariable region (HVR)[2,6–8], which mediates isoform-specific membrane localization[9–12] (**See Box 1** for information on the signaling networks that involve RAS proteins).

Although RAS isoforms are ubiquitously expressed and despite their high sequence similarity, the prevalence of oncogenic mutations and mutation types across RAS isoforms are not equally distributed between different cancers. First, between RAS isoforms, *KRAS* is most frequently mutated in cancer, which occurs in 22% across all cancers, whereas mutations in *NRAS* and *HRAS* are found in 8% and 3% of cancer cases, respectively[1,13]. Second, the relative mutation frequency at hotspot locations differs between RAS isoforms, with G12 mutations most often detected in *KRAS* (83%), Q61 mutations frequently found in *NRAS* (63%), and an even distribution between all three hotspot locations (codon 12, 13 and 61) observed in *HRAS*[1,2,13,14]. Third, most cancer types prefer specific oncogenic RAS isoforms for their transformation. For instance, *KRAS* mutations predominate in pancreatic (90%)[2,15–17], colorectal (50%)[2,18,19] and lung (20%) cancers[2,18,20–24]. *NRAS* mutations are most frequent in myeloid malignancies and cutaneous melanomas [23,24], while *HRAS* mutations are common for head and neck and bladder cancers[2,23]. Together, these epidemiological observations suggest that RAS isoforms are not equal *in vivo,* but have rather unique functions and oncogenic potentials in a tissue- and mutation-specific manner.

Colorectal cancer (CRC) patients with mutant *KRAS* display resistance to epidermal growth factor receptor (EGFR) inhibition with monoclonal antibodies (cetuximab and panitumumab)[25–31]. As mutations in *NRAS* turn out to associate with resistance to anti-EGFR targeted therapy as well[28–33], all metastatic CRC (mCRC) patients harboring mutations in *RAS* are now excluded from anti-EGFR targeted therapy[34–37]. Unfortunately, these studies could not be performed for mutation-specific isoforms due to insufficient sample size of patient numbers. However, based on the epidemiological data alone, it is conceivable that there are significant differences between mutant hotspots and perhaps even between variants at one specific codon (e.g. D, V or C substitutions at G12 and G13 or between Q61 variants R, L or K).

Furthermore, other MAPK pathway mutations beyond *RAS*, such as $BRAF^{V600E}$, have also been associated with anti-EGFR therapy resistance in CRC patients[28–30,32,38,39]. Although initially *BRAF* mutations were not considered as negative predictive biomarkers to anti-EGFR therapy[28,29,38,39], currently the beneficial effect of anti-EGFR treatment is considered to be only very modest and anti-EGFR treatment is not recommended for this group[36,37]. Further complicating the stratification of mCRC patients for targeted therapy of the MAPK pathway is the distinct histopathological nature (i.e. mucinous, primary tumor location and tumor grade) of colorectal tumors expressing mutant *BRAF* or *KRAS* variants[33,40–43].

In summary, overall epidemiological observations seem at odds with the almost uniform classification of tumors with a mutant EGFR signaling pathway. For CRC patients for example,

BOX 1. RAS SIGNALING IN CANCER.

RAS proteins are GTPases which protein conformation cycles between GDP-bound inactive and GTP-bound active states[6,187]. RAS activation is promoted by guanine nucleotide exchange factor (GEF) binding, which facilitates the release of GDP and thereby promotes the association of nucleotide-free RAS proteins with cytoplasmic GTP. Conversely, GTPase-activating proteins (GAPs) regulate RAS inactivation by inserting a positively charged arginine finger into the GTP-binding pocket, thereby accelerating RAS' intrinsic rate of GTP hydrolysis[1,187,188]. When active, RAS proteins can activate many downstream effector pathways, including the two main cancer-related signaling cascades: the RAS-RAF-MEK-ERK and PI3K-AKT-mTOR axes[2,188–192]. Hereby, RAS proteins regulate a large variety of cellular processes, such proliferation, differentiation, migration and survival (**Fig. I**). Oncogenic mutations in *RAS* are found in approximately 15-30% of human cancers and often involve the mutational hotspot codons 12, 13 and 61[13]. All hotspot codons are positioned in close proximity to the GTP-binding pocket, desensitizing RAS proteins for GAP-mediated GTP hydrolysis upon their mutation [71,75,76].

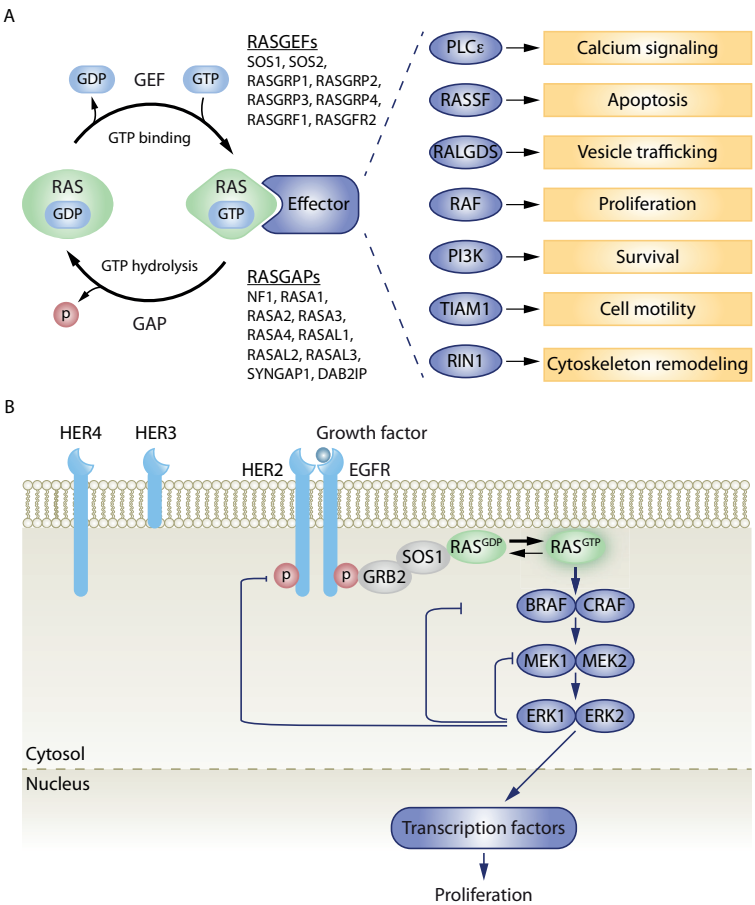

Figure I. Schematic representation of RAS signaling. (**A**) The GTP-GDP exchange of RAS molecules is depicted. RAS nucleotide exchange factors (GEFs) activate GDP-bound inactive RAS proteins by facilitating the release of GDP, thereby promoting GTP loading of RAS. The binding of GTP induces a conformational change in RAS, allowing it to bind to various downstream effectors that regulate a wide range of cellular effects. The inactivation of GTP-bound RAS proteins is regulated by RAS GTPase activating proteins (GAPs) that accelerate RAS' intrinsic GTP hydrolysis rate, causing RAS to return to its GDP-bound inactive state. (**B**) The mitogen-activated protein kinase (MAPK)

pathway is shown. Growth factor binding to members of the human epidermal growth factor family (EGFR, HER2, HER3, and HER4) induces receptor dimerization, followed by autophosphorylation. Adaptor protein GRB2 in turn binds to phosphorylated HER family receptors and recruits the GEF SOS1 to the plasma membrane, where it stimulates RAS activation. Active RAS proteins subsequently recruit and activate RAF proteins (BRAF and CRAF), resulting in the initiation of a phosphorylation cascade where RAF activates MEK1/2, and MEK in turn ERK1/2. ERK proteins have over 200 downstream substrates, among others transcription factors, and as such regulates many biological processes, including cell proliferation, migration, and differentiation. Activated ERK proteins are also involved in negative feedback regulation of the MAPK pathway. Either by directly phosphorylating EGFR-MAPK pathway components or by inducing the expression of negative feedback regulators. SOS, son of sevenless; RASGRP, RAS guanine-releasing protein; RASGRF, RAS-specific guanyl-nucleotide-releasing factor; NF1, neurofibromin 1; RASA, RAS GTPase-activating protein; RASAL, RAS GAP-activating-like protein; SYNGAP1, synaptic RAS GTPase activating protein 1; DAP2IP, DAB2 interacting protein; PLCε, phospholipase Cε; RASSF, RAS association domain-containing family; RALGDS, RAL guanine nucleotide dissociation stimulator; RAF, RAF proto-oncogene, serine/threonine protein kinase ; PI3K, phosphoinositide 3-kinase; TIAM1, T-lymphoma invasion and metastasis-inducing 1; RIN1, RAS and Rab interactor 1; EGFR, epidermal growth factor receptor; MEK, MAPK kinase; ERK, extracellular signal-regulated kinase[196].

the main stratification is solely based on mutant RAS versus BRAF, but not on RAS isoforms or specific mutational substitutions. In this review, we provide an overview on the similarities and differences between different oncogenic *RAS* and *BRAF* mutations observed in various experimental studies of CRC. We examine their implication for targeted therapy of the MAPK pathway and the potential of new pre-clinical model systems to study and cross-compare oncogenic RAS and BRAF variants to improve personalized cancer therapy.

ISOFORM DIFFERENCES: KRAS VS NRAS VS HRAS

Lessons learned from mouse development and tissue homeostasis

The ubiquitous expression pattern of RAS proteins in a wide range of adult tissues[4,44], in combination with their structural similarity, led to the hypothesis that the four isoforms perform redundant functions *in vivo.* However, during development, clear differences in expression patterns are observed, with *HRAS* expression deviating from *KRAS* and *NRAS*[4,44,45]. Mouse genetics in particular, indicate an essential role for KRAS, but not N- or HRAS, during embryonic development[46–49]. However, the phenotype of *KRAS* null embryos becomes more severe in a heterozygous *NRAS* background. Vice versa, *NRAS* null embryos die during development or just after birth when heterozygous for *KRAS*, indicating redundant roles for KRAS and NRAS during development[47]. Intriguingly, when the *KRAS* gene was elegantly modified to encode for *HRAS* expression, no defects were observed during embryonic development[50,51]. Thus, the essential role of KRAS for normal embryonic mouse development is determined by its distinctive expression profile and not by an isoform-unique function.

General RAS isoform differences in cancer

In contrast to development, observations from cancer studies suggest different functions for the RAS isoforms, in particular considering their varying mutation frequencies across tissues (**Figure 1**). Affected tissues that originate from the same germ layer seem to associate with specific mutant isoforms. For instance, mutations in *KRAS* predominate in cancers from endodermal origin (e.g. lung, pancreas, colon)[16,17,19–24], while *NRAS* mutations predominate

	colorectal cancer			lung cancer			pancreas cancer			melanoma			endometr. cancer			haem. neoplasias			urinary bl. cancer			lymph. neoplasias			thyroid cancer			up. aero. tr. cancer			small int. cancer			ovary cancer			biliary tr. cancer			stomach cancer			esoph. cancer		
new cases 2019 (*1000)	146			228			57			96			4.3			94			80			82			52			53			11			23			12			28			18		
% of all cancers	8.3			12.9			3.2			5.5			75			5.3			4.6			4.7			3.0			3.0			0.6			1.3			0.7			1.6			1.0		
	KRAS	NRAS	HRAS	K	N	H	K	N	H	K	N	H	K	N	H	K	N	H	K	N	H	K	N	H	K	N	H	K	N	H	K	N	H	K	N	H	K	N	H	K	N	H	K	N	H
mutation prevalence (%)	33.1	3.7	0.6	17.3	1.2	0.5	64.2	0.5	0	1.8	16.9	1.3	16.7	3.2	0.2	4.2	9.6	0.8	5.7	1.7	8.0	6.1	7.2	0.2	2.4	8.2	4.1	1.9	1.5	5.0	36.1	1.5	0	13.2	1.4	0.1	19.9	2.8	0.5	5.8	0.6	0.7	1.6	0.1	0.3
relative mutation spectrum per gene (%) G12D	34.6	17.4	0	19.6	NA	NA	47.8	NA	NA	11.3	3.3	0	32.6	NA	NA	24.2	31.3	0	26.1	0	7.4	20.1	21.7	NA	18.3	0.4	0.6	38.1	6.1	10.6	40.9	NA	NA	39.0	NA	NA	46.2	14.5	NA	36.1	NA	NA	36.7	NA	NA
G12V	22.2	3.1	0	21.4	NA	NA	31.3	NA	NA	16.1	0.4	5.6	23.7	NA	NA	8.3	5.0	0	20.4	0	23.8	7.6	3.2	NA	10.3	0	7.4	5.2	0	14.0	15.5	NA	NA	38.3	NA	NA	19.4	0	NA	11.5	NA	NA	14.3	NA	NA
G12C	8.0	8.5	0	39.6	NA	NA	2.5	NA	NA	0	0.8	0	9.1	NA	NA	2.5	3.6	0	12.1	7.3	3.5	2.5	4.9	NA	8.9	0.9	1.4	10.3	0	3.9	5.5	NA	NA	5.4	NA	NA	7.1	1.8	NA	5.3	NA	NA	4.1	NA	NA
G12A	5.8	0.6	0	6.7	NA	NA	1.3	NA	NA	3.2	0.8	0	11.2	NA	NA	5.3	4.1	0	6.4	0	0.4	5.2	3.0	NA	2.7	0	1.4	3.1	0	1.1	6.4	NA	NA	5.5	NA	NA	5.3	0	NA	8.0	NA	NA	4.1	NA	NA
G12S	5.5	2.7	2.9	3.3	NA	NA	1.5	NA	NA	8.1	0.8	0	2.3	NA	NA	5.5	9.5	0	4.5	0	6.0	4.5	6.5	NA	8.9	0.3	1.1	7.2	44.9	22.3	5.0	NA	NA	1.5	NA	NA	8.7	0	NA	3.8	NA	NA	6.1	NA	NA
G13D	18.6	3.3	0	3.0	NA	NA	1.5	NA	NA	16.1	1.6	5.6	14.8	NA	NA	19.9	15.0	1.8	7.6	0	1.1	22.8	14.8	NA	11.2	0.1	0.9	10.3	4.1	5.0	16.8	NA	NA	4.5	NA	NA	4.6	0	NA	20.1	NA	NA	14.3	NA	NA
G13C	0.5	0.6	0	3.7	NA	NA	0.1	NA	NA	1.6	0.3	0	1.0	NA	NA	0.7	1.5	0	0	0	0.4	0.9	1.6	NA	0.4	0.1	0.6	2.1	0	0.6	0	NA	NA	0.8	NA	NA	0.6	1.8	NA	1.5	NA	NA	4.1	NA	NA
G13V	0.1	1.2	0	0.1	NA	NA	0	NA	NA	0	0.9	0	0.5	NA	NA	0	3.9	0	0	0	1.8	0	2.1	NA	0	0.1	0.3	1.0	0	5.0	0.5	NA	NA	0.3	NA	NA	0.3	0	NA	0.3	NA	NA	2.0	NA	NA
Q61H	0.8	2.9	0	1.1	NA	NA	1.7	NA	NA	1.6	4.4	8.3	1.0	NA	NA	4.6	4.0	1.8	2.5	2.4	0	9.2	7.2	NA	0.9	0.8	0.9	0	0	1.7	0.9	NA	NA	1.1	NA	NA	2.4	0	NA	2.4	NA	NA	0	NA	NA
Q61R	0.2	14.5	0	0.2	NA	NA	0.5	NA	NA	6.5	27.6	8.3	0	NA	NA	0.5	8.0	0	0	29.3	18.1	1.6	10.8	NA	17.0	76.4	48.4	1.0	12.2	5.6	0	NA	NA	0	NA	NA	0.2	34.5	NA	0.9	NA	NA	0	NA	NA
Q61K	0.1	24.5	0	0.2	NA	NA	0.1	NA	NA	0	34.8	38.9	0	NA	NA	0.2	7.6	0	1.3	12.2	4.3	0.2	12.9	NA	3.6	16.8	20.3	3.1	10.2	5.0	0	NA	NA	0	NA	NA	0.1	20.0	NA	0.9	NA	NA	0	NA	NA
Q61L	0.3	7.5	0	0.2	NA	NA	0.1	NA	NA	4.8	10.0	13.9	0.5	NA	NA	0.9	1.7	1.8	1.9	19.5	12.1	1.4	5.1	NA	1.3	2.0	1.4	0	8.2	7.3	0.5	NA	NA	0	NA	NA	0.5	3.6	NA	0.6	NA	NA	0	NA	NA
A146T	0.7	0	0	0	NA	NA	0.1	NA	NA	1.6	0.3	2.8	0	NA	NA	3.0	0.1	0	1.9	0	0	4.5	1.0	NA	0	0	0	1.0	0	0	0.9	NA	NA	0	NA	NA	0.5	0	NA	1.5	NA	NA	0	NA	NA
A146V	0.2	0	0	0	NA	NA	0	NA	NA	1.6	0.1	0	0	NA	NA	1.1	0.1	0	1.3	0	0	2.0	0	NA	1.3	0	0	0	0	0	0	NA	NA	0	NA	NA	0	0	NA	0	NA	NA	2.0	NA	NA

Figure 1. Mutation spectrum and frequency of *RAS* mutations in human cancers.
Estimated number of new cancer cases in 2019 in the USA from the annual report of the American Cancer Society 2019, USA. Relative frequency of mutation spectrum per cancer type is from COSMIC database, Wellcome Trust Sanger Institute, UK. Color hues: for relative numbers 50% is red and 0% is white. For new cancer cases in 2019, 50% of all new cases is red (881 thousand) and 0% is white. NA: not applicable due to small sample size (<30 cases). The order of cancer types (from left to right) is based on the absolute number of *KRAS* mutant tumors in 2019.

in cancers originating from the neural crest (e.g. skin)[23,24], and *HRAS* mutations are most frequent in cancers originating from the transitional zone (e.g. bladder)[23]. Mouse genetics supports that the transforming capacity of mutant RAS is dependent on the right combination of tissue and isoform expression level. For instance, the introduction of $HRAS^{G12V}$ at the *KRAS* locus ($K^{HRASV12}$), equalizing their expression patterns and levels, induced other tumorigenic lesions than $KRAS^{G12V}$ [51]. Interestingly, $K^{HRASV12}$ mice developed tumor types that are normally associated with *NRAS* mutations, such as papillomas and hematopoietic malignancies[51], possibly due to the similar membrane localizations of NRAS and HRAS proteins and the NRAS-like expression pattern imposed by the *KRAS* gene body[7,8,10,12,44].

RAS isoform differences in mCRC

The prevalence of *KRAS* mutations is high in CRC (35-50%), whereas mutations in *NRAS* are rare and are only identified in 4-11% of the cases[28,32,33,37,41,52–54]. Most mutations in *KRAS* affect codon 12 and 13, comprising 90% of all *KRAS* mutations, which is followed by mutations in codon 61 (4%)[29,30,32,33,41]. In contrast to *KRAS*, mutations in *NRAS* more often involve codon 61 (57%) than codon 12 (30%) or 13 (13%)[29,32,33,41] (**Figure 2A**). Apart from mutation frequencies, *KRAS* mutations are detected at similar frequencies across all stages of CRC, whereas *NRAS* mutations tend to occur in later stages of CRC development[41] (**Figure 2B**). Furthermore, *NRAS* mutations associate with left-sided tumors and *KRAS* mutations with right-sided tumors[40,41,52,54] (**Figure 2C**). Remarkably, the observed differences in incidence, primary tumor location and histology remain largely unexplained. Most insights however are obtained from mouse models in which mutant *KRAS* or *NRAS* expression can be activated from their endogenous locus.

Mutant $KRAS^{G12D}$ expression at endogenous levels, but not $NRAS^{G12D}$, creates only hyperplasia of colonic epithelium with crypt lengthening. Adenocarcinoma development is observed upon combined loss with APC. The difference in the oncogenic potential between the two isoforms is likely due to lack of sufficient MEK and ERK activation by $NRAS^{G12D}$ [55]. Indeed, overexpression of mutant KRAS is sufficient to produce tumor formation in the intestine[56], suggesting that increasing amounts of MAPK pathway activation facilitates tumorigenesis. In a similar fashion, endogenous $KRAS^{G12D}$ is expressed at a higher level than $NRAS^{G12D}$ in murine hematopoietic cells and induces a more aggressive myeloproliferative disorder. Here, abundant KRAS expression resulted in higher levels of total RAS-GTP than by $NRAS^{G12D}$, suggesting that the overall level of MAPK pathway activation is critical for the difference in severity of the disease[57]. Indeed, initiation of hematopoietic malignancies by mutant $NRAS^{G12D}$ has been observed to occur in a dose-dependent manner[58]. The same phenomenon has been described for the development of melanoma, which was efficiently induced by the endogenous expression of $KRAS^{G12D}$, but not by $NRAS^{G12D}$. Intriguingly, once melanomas were formed, the histology and growth rates of the tumors expressing different oncogenic RAS isoforms were indistinguishable, indicating that the transforming potential of isoforms presumably result from their endogenous expression levels, is most pronounced during tumor initiation[59].

The different tumorigenic potentials of RAS isoforms result from complex integration of upstream signals to downstream signaling cascades. Signaling strength likely differs per mutant isoform, although variations within their signaling relay cannot be excluded. For instance, deviating signaling output might originate from distinct membrane localization of

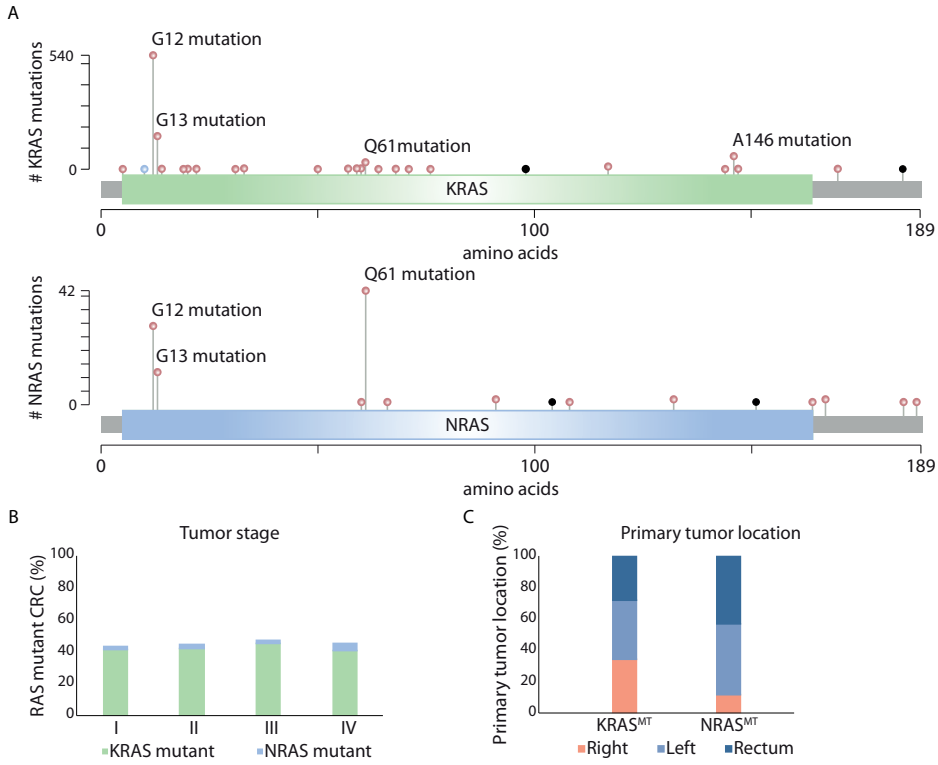

Figure 2. Differences between *KRAS* and *NRAS* oncogenes in mCRC.
(**A**) Absolute number and distribution of mutations in *KRAS* and *NRAS* in CRC from 2137 patients (cBioportal, combined data from 5 studies[116,117,193–195]). Red, blue and black dots indicate missense, inframe and truncating mutations, respectively. Green and blue boxes indicate regions in *KRAS* and *NRAS* with extensive homology to the RAS protein family. (**B**) Percentage of CRC patients with *KRAS* and *NRAS* mutations across different tumor stages (I-IV)[41]. (**C**) Distribution (%) of primary tumor locations (right or left colon, or rectum) across *KRAS* and *NRAS* mutant CRCs[41].

RAS isoforms[7,10–12,60]. Indeed, on the cellular level, studies in mouse models and CRC cell lines have demonstrated that $KRAS^{G12D}$ mutant cells promote cell proliferation in the intestine while enhancing their sensitivity to apoptosis[55,61]. Conversely, $NRAS^{G12D}$ mutations do not promote proliferation of intestinal cells, but do suppress the induction of apoptosis[55].

HOTSPOT MUTATION DIFFERENCES: CODON-SPECIFIC *RAS* ONCOGENES IN MCRC

Differences between hotspot mutations in RAS oncogenes

All RAS isoforms share similar hotspot mutations, i.e. codon substitutions at position 12, 13, 61 and to lesser extent 146. Peculiarly, the relative mutation frequencies per hotspot differ per RAS isoforms in mCRC. Importantly, the prognostic value for disease progression differs per isoform and mutant hotspot combination[33,40,52]. For *KRAS*, mutations in codon 12 and 13, but not codon 61, are relative frequent and associated with poor prognosis. In contrast, codon 61

mutations are predominantly observed in *NRAS* mutant tumors[40,52]. Furthermore, colorectal tumors with codon 61 mutations in *NRAS* are associated with poor prognosis, while *NRAS* codon 12 mutant CRCs have a similar prognosis as wild-type *RAS/BRAF* tumors[40,52]. In concordance, mutual exclusivity with *KRAS* mutations has mainly been observed for *NRAS* codon 61, but not *NRAS* codon 12, mutant mCRCs[40]. These observations are in line with observations in mouse models, where endogenous expression of $NRAS^{Q61R}$, but not $NRAS^{G12D}$, promotes melanoma development. Similar to observations made for KRAS versus NRAS driven malignancies, $NRAS^{Q61R}$ mutants showed highest abundance of total RAS-GTP levels as compared to $NRAS^{G12D}$ [59]. Moreover, *NRAS* codon 61 mutations induce pronounced activation of the MAPK pathway, while *NRAS* codon 12 mutants promote signaling via PI3K and AKT, and as such potentially influences their contribution to colorectal tumor development [62].

Recently, genetic mouse models were reported that revealed an intermediate hyperplasia phenotype for $KRAS^{G13D}$ expression in colonic epithelium when compared to wild-type and $KRAS^{G12D}$ colons, in line with intermediate levels of RAS-ERK activation[63]. Similar findings were made when comparing the transformative capacities of endogenously expressed $KRAS^{A146T}$ and $KRAS^{G12D}$ mutations in the colonic epithelium. Mechanistically, the different levels of downstream activation of the MAPK signaling pathway per mutant form of KRAS seems responsible for the different tumorigenic phenotypes, with enhanced MAPK signaling causing increased tumorigenic potential[64]. For human mCRC, there is debate about the differences between codon 12 and 13 mutations in *KRAS* for overall survival[65–69], among others reflecting the challenging characterization of downstream pathway activation per mutation while excluding influences of tumor subtypes, stages and mutational backgrounds.

Molecular insights from structural differences

Structural analysis of oncogenic KRAS proteins provide mechanistic insights underlying the various cellular phenotypes observed in CRCs with different *KRAS* mutations. Most prominent are mutated codons 12 and 13 that reside in the p loop of RAS, which is a positively charged region involved in the binding of the negatively charged phosphate of GTP[70,71]. Amino acid substitutions with bulkier side chains at codon 12 and 13 affect the phosphate binding pocket in RAS proteins and thereby cause steric hindrance in GTP hydrolysis[70]. In contrast, the glutamine residue at codon 61 is important for stabilizing RAS in its transition state when the phosphate group of GTP undergoes hydrolysis[72,73]. Mutations at codon 61 impairs coordinated GTP hydrolysis[71,74–76].

In general, biochemical studies confirmed that the intrinsic GTP hydrolysis rate was reduced for most KRAS mutants, indicating prolonged periods of GTP loading *in vivo*[64,71,76]. The most pronounced reduction on intrinsic GTP hydrolysis rate was observed for G12A, G12R, Q61H and Q61L mutant proteins, whereas an intermediate effect was observed in G12D, G12V, an G13D KRAS oncogenes (**Figure 3**). Striking, G12C shows no reduction in intrinsic GTP hydrolysis rates. Indeed, in vivo hydrolysis rates become significantly faster for $KRAS^{WT}$ due to additional GAP activity, but their effect become negligible or even obsolete for KRAS mutant proteins, including G12C[64,71,76].

Counteracting GTP hydrolysis are GDP-GTP exchange rates that in normal cells is facilitated by GEF proteins. $KRAS^{G13D}$, $KRAS^{Q61L}$ and $KRAS^{A146T}$ mutants show intrinsic higher exchange rates compared to other mutant and $KRAS^{WT}$ proteins[63,64,71,76] (**Figure 3**). Easier GDP to GTP

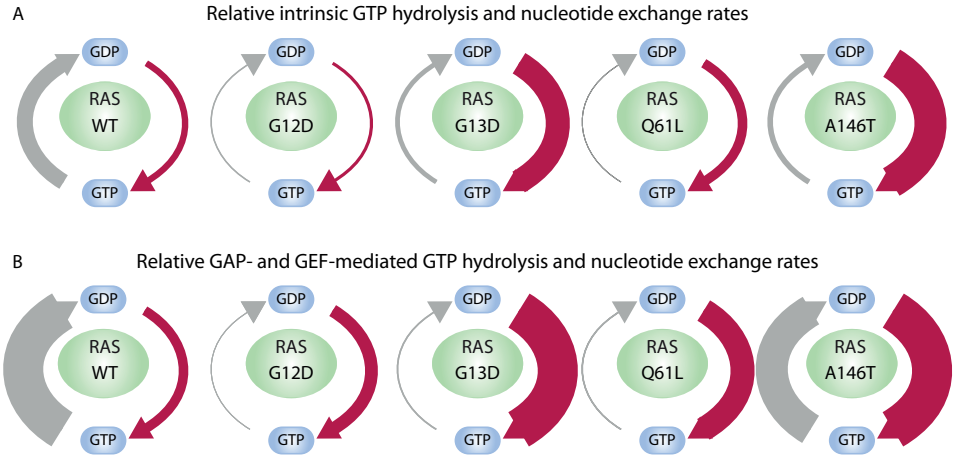

Figure 3. GTP hydrolysis and nucleotide exchange rates of oncogenic RAS proteins.
Schematic representation of intrinsic (**A**) and GAP- and GEF-mediated (**B**) GTP hydrolysis and nucleotide exchange rates of wild-type RAS (WT) as well as mutant RAS proteins (G12D, G13D, Q61L and A146T). Thickness of arrows represents rates of GTP hydrolysis (grey) and nucleotide exchange (red) relative to WT RAS proteins. Pictures are adapted from Smith et al. (2013)[76].

exchange in G13D, Q61L and A146T mutants might lead to increased probability of these KRAS mutants to auto-activate. As a consequence, $KRAS^{G13D}$, $KRAS^{Q61L}$ and $KRAS^{A146T}$ oncoproteins might be less dependent on GEF-mediated regulation for their activation[64,71,76]. Elevated basal RAS signaling might explain the poor prognosis of mCRC patients that harbor tumors with *KRAS* mutations at codon 13 when they do not receive targeted therapy against the MAPK pathway[65–67]. Independently, phosphoproteomic analysis of different *KRAS* mutations in isogenic CRC cell lines demonstrated that the largest difference in downstream signaling was observed between *KRAS* codon 12 and codon 13 mutant cells[77].
Elevated basal RAS signaling might explain the poor prognosis of mCRC patients that harbor tumors with *KRAS* mutations at codon 13 when they do not receive targeted therapy against the MAPK pathway[65–67]. Independently, phosphoproteomic analysis of different *KRAS* mutations in isogenic CRC cell lines demonstrated that the largest difference in downstream signaling was observed between *KRAS* codon 12 and codon 13 mutant cells[77].
In addition, the type of amino acid substitutions affecting the same codon (e.g. codon 12) can also influence downstream signaling cascades and biological effects[78–80]. For example, G12C and G12V substitutions in *KRAS* increase anchorage-independent growth, whereas G12D mutations enhance EGF-independent proliferation[78,79]. Yet, why the mutation frequencies are unevenly distributed remains unresolved, and are presumably the result of tissue-specific mutational processes (mutation signatures) in combination with natural selection[81].

ONCOGENIC BRAF ISOFORMS IN CRC

Oncogenic BRAF mutations in CRC

Active RAS promotes BRAF recruitment to the plasma membrane and binds BRAF at its

RAS binding domain in the N-terminal region. RAS binding induces a conformational change that promotes BRAF and CRAF hetero- and homodimerization and kinase activation, resulting in the activation of downstream effectors MEK and ERK[82–84]. *BRAF* activating mutations are present in approximately 10% of CRCs of which the majority affects codon 600[28,29,85–87,30,33,39–43,53]. Mutations in the activation segment of BRAF, e.g. V600E, causes a release from its auto-inhibitory conformation and enhances BRAF kinase activity, resulting in RAS-independent ERK activation[83–85,87,88]. Kinase-impaired mutations in *BRAF*, such as D594G, have also been detected in CRCs[40], which rely on CRAF binding for downstream ERK activation[85,89]. In addition, *BRAF* fusion genes have been detected in mCRC patients that are the results of structural chromosome rearrangements[90,91]. BRAF fusions are chimeric proteins that predominantly consist of the BRAF kinase domain fused to a wide range of 5' fusion partners that replace the N-terminal domain with auto-inhibitory activity[43,84,92–94] (Submitted manuscript by Stangl et al., 2019). Whereas strong kinase activating alterations in *BRAF*, e.g. V600E and *BRAF* fusions, occur in a mutually exclusive manner with mutations in *KRAS* and *NRAS*[29,40,42,91,95], $BRAF^{D594G}$ mutations are more likely to co-occur with *RAS*, albeit at lower frequencies than observed in $BRAF^{WT}$ tumors[40,85].
Similar to $KRAS^{G12D}$ transgenic mice, it has been demonstrated that endogenous $BRAF^{V600E}$ expression in colonic epithelial cells induces hyperplasia and serrated epithelial formations, resembling human *BRAF* mutant mCRC phenotypes[96].

ONCOGENIC *RAS* AND *BRAF* VARIANTS IN ANTI-EGFR THERAPY RESPONSE

Multiple studies have shown that frequent mutations in *KRAS* at codon 12 and 13 are negative predictive biomarkers for response to anti-EGFR targeted therapy[28,29,32,97]. Rare mutations like mutant NRAS or codons 61, 117 and 146 mutations in *KRAS,* are also associated with resistance to EGFR inhibition[28,30,32,33,98–101]. Yet their low incidence makes it difficult to interpret their independent predictive value for response to EGFR inhibition. Therefore, CRC patients with less common *RAS* mutations are often grouped to create sufficient statistical power to evaluate their response to anti-EGFR targeted therapy[29,31,38]. Consequently, all *RAS* mutant tumors together show significant reduced response to EGFR inhibition, and led to the exclusion of all *NRAS* and *KRAS* mutant mCRC patients from EGFR targeted therapy[29,31,36,102]. However, various tumor characteristics are indicative of critical differences between codon-specific *RAS* mutant tumors and raise the possibility that these tumors might also differ in response to treatment. There are several lines of evidence indicating that patients with colorectal tumors harboring *NRAS* codon 12 or *KRAS* codon 13 mutations might actually benefit from anti-EGFR targeted therapy[65–67,103]. Similarly, *NRAS* mutant mCRC patients that relapsed to anti-EGFR therapy often revealed codon 61 mutations, but not codon 12 or 13[98], indicating different tumorigenic potential *in vivo*. Similar to mCRC patients with $KRAS^{G12D}$ tumors, patients with colorectal tumors with $BRAF^{V600E}$ mutations do not respond to anti-EGFR therapy with monoclonal antibodies[28,30,32,36,38,102]. Besides oncogenic $BRAF^{V600E}$ mutations, it has been reported that other genetic alterations in *BRAF*, such as *BRAF* fusion genes, can also promote resistance to EGFR inhibition via sustained MAPK signaling[104] (Submitted manuscript by Stangl et al., 2019).

DIFFERENT COLORECTAL TUMOR TYPES

KRAS versus BRAF mutant tumors

Both oncogenic *KRAS* and *BRAF* mutations create hyperplasia in colonic epithelia of mice and are implicated in tumor progression of the classical adenoma-carcinoma sequence of CRC with both roles being mostly mutual exclusive. Despite their overlapping roles, data is accumulating that indicates that both oncogenes might drive distinct routes towards tumorigenesis.

The majority of 'classical' CRCs develop from APC-deficient adenomatous polyps, which can progress into adenocarcinomas often after acquisition of activating mutations in *KRAS* and loss-of-function mutations in TP53[42,105–110]. A small number of CRCs develop from the serrated neoplasia pathway[111], which are initiated by MAPK pathway activating mutations without the prior loss of APC[42,107,112,113]. Whereas $KRAS^{G12D}$ mutations are often found in classical APC-deficient adenomas, $BRAF^{V600E}$ mutations are more likely to occur in sessile serrated adenomas[42,107,111–115]. It is not understood why different oncogenes are employed to activate the MAPK pathway. Even more so, WNT pathway activation that is achieved independent of *APC* loss, e.g. RNF43 mutations, is more often associated with $BRAF^{V600E}$ mutations than with oncogenic *KRAS* variants[42,109,112,116,117] (**Figure 4**).

It is difficult to dissect the cause and consequence of *KRAS* and *BRAF* oncogenic mutations on tumor phenotypes and mutational co-occurrence with specific WNT pathway mutations. For instance, hypermutator phenotypes, including micro-satellite instability (MSI), is more frequently observed in CRCs with $BRAF^{V600E}$ mutations compared to wild-type and *KRAS* mutant tumors[33,40–43,107,113,115,116,118] (**Figure 4**).

Moreover, sessile serrated and MSI CRCs are often detected in the right colon, show a mucinous phenotype and are poorly differentiated compared to non-serrated and micro-satellite stable (MSS) colorectal tumors, respectively[40,111–113,116,118] (**Figure 4**).

Furthermore, $BRAF^{V600E}$ and $KRAS^{G12D}$ mutant CRCs show different metastatic behavior. *BRAF* mutant CRCs display a higher incidence of peritoneal metastases versus *KRAS* mutant CRCs that show more pronounced liver and lung metastases[33,40] (**Figure 4**). Like *KRAS* codon-specific mutations and phenotypes, patients with $BRAF^{D594}$ colorectal tumors display a different clinicopathology than $BRAF^{V600E}$, resembling CRCs that are wild-type for the MAPK pathway[40].

MAPK pathway mutations in right- versus left-sided mCRCs

Following the biased distribution sessile and MSI tumors along the colonic tract, the incidence of specific MAPK pathway mutations also varies between right- and left-sided mCRCs. A high number of *BRAF* and *KRAS* mutations have been detected in right-sided tumors, in contrast to better prognostic *NRAS* and RAS^{WT} tumors in the left colon[40,41,125–127,52,54,119–124].

Besides differences in mutational patterns, right- and left-sided CRCs also show differences in tumor-specific gene expression patterns. In particular, MSS mCRCs that are located in the right colon and that are wild-type for both *KRAS* and *BRAF* have a gene expression signature that is reminiscent of a *BRAF* mutant, MSI/serrated adenomas[123]. In concordance, targeted therapy against EGFR improved progression free survival of patients with left-sided but not

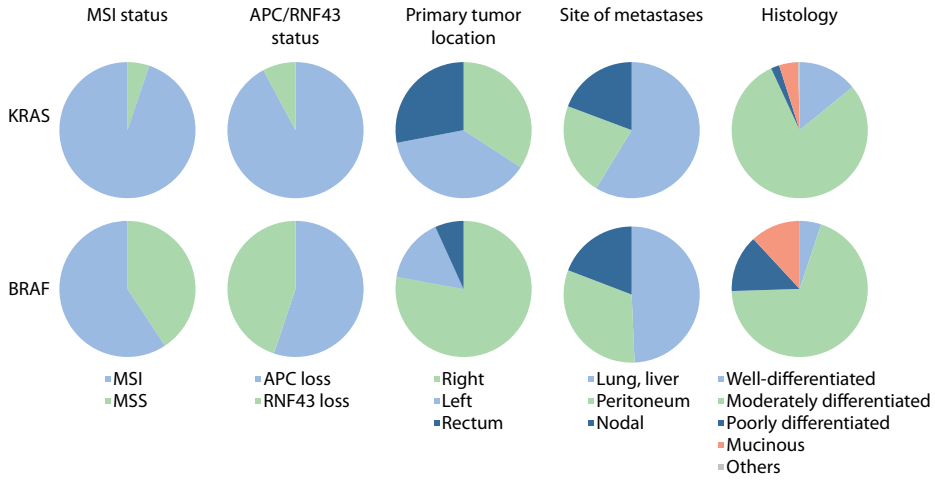

Figure 4. Differences between *BRAF* and *KRAS* mutant CRCs.
Similarities and differences between *KRAS* and *BRAF* mutant CRC features presented in pie-charts, such as the distribution (%) of microsatellite instability (MSI)[41], co-occurrence with aberrant activation of WNT signaling by loss of APC or RNF43, primary[41] and metastatic tumor locations, and histological features[41]. Data obtained from cBioportal of 5 studies combined[116,117,193–195].

right-sided colorectal tumors that were wild-type for *KRAS* and *BRAF*[119,120,123,128–130].

ORGANOIDS AS PREDICTIVE MODELS FOR CRC THERAPY RESPONSE

Patient-derived xenografts (PDXs) and CRC-derived cell lines have been instrumental model systems in cancer research to study long-lasting questions regarding RAS oncogenes. Both model systems have their own set of advantages and disadvantages. The use of PDX models allows the growth of three dimensional (3D) tumors that resemble patient tumor histology and *in vivo* drug testing of preclinical cancer treatments. Unfortunately, PDX experiments are slow, low-throughput, expensive and can exhibit mouse-specific clonal dynamics[131–134]. Conversely, the use of human CRC cell lines allows high-throughput drug screening experiments due to their infinite growth potentials in low-cost culture conditions. Furthermore, cell lines are relatively easy to manipulate, which has been extensively exploited to artificially overexpress RAS isoforms. Unfortunately, cell line generation is very inefficient and requires their adaptation to two dimensional (2D) culture conditions. This often results in a biased selection towards cells from advanced cancer stages that lack apical-basal polarity and that do not represent the entire range of tumor types as presented by cancer patients[131–133,135–139]. Furthermore, recent data accumulates that supraphysiological levels of RAS oncogenes are not reflective of true tumor biology, where the vast majority of oncogenic RAS versions are expressed at endogenous levels[140–144]. For example, the transformative potential of MAPK pathway mutants seems to follow the 'just right' hypothesis, where threshold levels of overall MAPK activity determine tumorigenesis and underscore the critical role for endogenous expression levels in model systems. Indeed, cell lines with oncogenic knock-in mutations

improve reliability of drug response[145]. Many studies have used SW48[80,146], LIM1215 or HCT116 isogenic cell lines that contain different oncogenic *KRAS* mutations (Horizon Discovery) for cross-comparisons[67,77,80,147,148]. However, all three CRC cell lines are MSI and show loss of *MLH1* expression accordingly[149–151], which is a genetic background that is typical for *BRAF* mutant and not for *KRAS* mutant CRCs. Moreover, the parental cancer cell lines are unfortunately not truly indicative of an unaffected EGFR signaling pathway as SW48 cells contain hyperactivating mutations in *EGFR*[152], LIM1215 cells contain a small fraction of $KRAS^{G13D}$ mutant clones[153], while HCT-116 contains $KRAS^{G13D}$ and $PIK3CA^{H1047R}$ driver mutations[149,150]. Hence, additional cancer models are required to fill the gap between PDX and human cell line models for the investigation of drug response in the context of mutant *RAS* and *BRAF* in human CRC.

Organoid models for predicting therapy response

The development of 3D organoids has resulted in a physiological relevant *in vitro* cancer model that can function as an intermediate platform in between cell lines and PDX models for precision medicine in cancer therapy (**Figure 5**). When embedded in a 3D matrix and provided with the right cocktail of niche factors, epithelial cancer cells can grow into self-organizing polarized organotypic structures[154,155]. Established organoid cultures retain both stem and differentiated cell types and can be established from a wide range of tissues[155,156]. In addition, the organoid technology allows the *ex vivo* expansion of limited patient-derived tumor material from biopsies as well as matched normal organoids with high efficiencies, enabling direct comparison between tumor and healthy tissues[132,133,154,157]. To date, several patient-derived tumor organoid (PDTO) biobanks have been established from various healthy and malignant tissues, including primary and metastatic colon[154,155,158–162], breast[159,163], esophageal[159,162], pancreatic[157,159] and ovary[159,164] cancer tissues. Importantly, these studies have demonstrated, even after successive passaging, that PDTOs display histopathological, genetic and epigenetic features that resemble the original tumors[154,158,159,162,163,165]. Furthermore, histopathological phenotypes were retained upon orthotopic transplantation of organoids into immune-deficient mice[154,159].

Proof-of-concept drug screening in tumor organoids has demonstrated the feasibility of the organoid system for investigating molecular mechanisms involved in drug sensitivity, which recapitulates genotype-phenotype correlations of therapy responses observed in cancer patients[158,159]. Subsequent high-throughput screening experiments in organoids from breast[163], ovary[164], endometrial[159] and colon[159] cancers have demonstrated that *in vitro* drug responses in PDTOs show high concordance with drug responses obtained with *in vivo* PDTOs upon their xenografting in mice. More importantly, experiments in gastro-intestinal[162], pancreatic[157] and breast[163] tumors demonstrated a high degree of similarity in drug response between patients and their corresponding tumor organoids, underscoring the predictive value of living PDTO biobanks for therapy response in individual patients.

Limitations of organoid models for predicting therapy response

Biobanks of patient-derived CRC organoids are representative for the clinical diverse disease, including multiple subtypes, with a wide range of genetic backgrounds and *in vitro* drug responses that resemble those observed in matched patients. Nevertheless, this cancer

model system also comes with a set of limitations. In particular, the organoid system solely consists of epithelial structures and as such lacks blood vessels, stroma and immune cells. As a result, PDTOs belonging to the consensus molecular subtype 4 (CMS4), which are tumors characterized by prominent transforming growth factor b (TGF-b) activation and stromal invasion, are generally missing in CRC biobanks[154]. In addition, prevalent cross-talk between CRC cells and the tumor microenvironment (TME), known to affect tumor progression and therapy resistance[162,166–168], is lacking. In addition to potentially altered drug responses, therapies targeting tumor stroma cannot be tested.

Furthermore, a mouse-derived extracellular matrix (ECM) is required for the growth of PDTOs. This ECM contains predominantly structural proteins, such as laminin and collagen IV. Nevertheless, remnants of various other mouse-derived known and unknown factors, including TGF-b, EGF and insulin-like growth factor 1 (IGF-1)[169,170], can be present, which quantities might differ per ECM batch. Recent advances in the development of well-defined synthetic hydrogels has shown that growth of human intestinal organoids can be established with synthetic gels that support integrin signaling. In the near future, continuous innovation of synthetic replacement of mouse-derived matrices will increase the efficiency and reproducibility of long-term PDTO growth[171,172].

Recently, additional optimizations have been implemented on the original reported culture conditions, such as the removal of p38 MAPK inhibitors and/or hypoxic conditions, in order to achieve optimal efficiency of PTDO derivation and growth [154]. In addition, these refined culture conditions also increase the cellular diversity, improving the physiological fidelity of *in vitro* intestinal organoids[173,174]. Nevertheless, the composition of the organoid-specific culture media with respect to signaling molecules might affect drug sensitivities, either direct or indirect by influencing cellular composition of the organoid. Moreover, cross-comparison of drug responses between different types of PDTOs with tailored media compositions, can be challenging.

The fact that tumors showcase significant intra-tumoral heterogeneity is currently well documented, and creates immense challenges for modeling drug measurements in a personalized manner. Accurate cancer modeling requires inclusion of all possible tumor clones that contain diverse genomes with adaptive potential. As applies to all model systems, exclusion of a minor clone in the PDTO culture that possesses drug resistance, might very well lead to discrepancies between drug responses *in vitro* and the original tumor. Although PDTOs have shown to be heterogenous[175], clonal dynamics and evolution during culture can alter the composition[154,165]. Drug screens on numerous characterized organoid biobanks are helpful to improve our understanding of genotype-phenotype correlations. Moreover, the reproducible and scalable aspects of the organoid cancer model is optimal for industrial screening platforms to identify new drug candidates in a pre-clinical setting.

Continuous improvement of controlled culture conditions that supports the establishment of all possible CRC subtypes, correct cellular composition and co-culture systems with stroma will likely enhance the value of PDTOs for personalized therapy design, development of new anti-cancer strategies and drug innovation.

CRC organoid models to investigate RAS and BRAF isoforms

CRC organoid biobanks represent a broad range of CRC subtypes, including rare hyperplastic

polyps and sessile serrated adenomas[154,158]. Furthermore, they retain the genomic and epigenetic mutation profiles observed in CRC, such as loss-of-function mutations in *TP53* and the WNT signaling pathway together with MAPK pathway activating mutations[154,158,161]. Consistent with results from the clinic, drug screen experiments demonstrated a high degree of sensitivity to EGFR inhibition in $KRAS^{WT}$ tumor organoids[159,161], whereas resistance was observed in those with *KRAS*, *NRAS* and *BRAF* mutations[158,161,176]. In addition, a significant response to BRAF inhibition was observed in CRC organoids expressing mutant $BRAF^{V600E}$, but not in $BRAF^{WT}$ organoids, which corresponded with a significant decrease in MAPK signaling[162,175]. However, treatment of mutant *BRAF* CRC organoids with BRAF inhibitors failed to induce apoptosis, resembling drug responses observed in *BRAF* mutant mCRC patients[162,177].

Subsequent extensive drug screening of mCRC organoid biobanks has demonstrated the utility of this system to identify drug combinations to target mutant *RAS* CRCs. Again, this study showed the high degree of anti-EGFR therapy resistance in CRC organoids with activating mutations in *KRAS*. Furthermore, $BRAF^{V600E}$ and $NRAS^{Q61K}$ mutant organoids were highly resistant to EGFR inhibition, in line with observations from the clinic[176]. Growth factor depletion experiments support the resistance phenotype of *BRAF* mutant organoids to EGFR inhibition, showing that CRC organoids with mutations in *BRAF* exhibit EGF independence[154]. In independent experiments, drug screens on other *BRAF* mutant organoid lines led to conflicting results, showing differential outcomes to EGFR inhibition[165,178]. Similar heterogeneous responses to EGFR inhibition have recently been observed between *KRAS* mutant organoid cultures[165,176,178]. Similar observations were made by depletion of growth factors from organoid culture media, showing that about 50% of *KRAS* mutant CRC organoid lines remained dependent on EGF signaling for successful growth[154]. Together, these findings demonstrate the potential intertumoral heterogeneity in drug response between *KRAS* mutant tumors.

In an even more extreme case, differential responses to EGFR targeted therapy were observed between CRC organoid subclones that were derived from the same parental tumor tissue and all contained the same oncogenic mutation in *KRAS*[165,178]. Heterogeneity in MAPK activity has recently been shown in organoids, where gradients of MAPK pathway activation exist along the differentiation axis of PDTOs, irrespective of the mutational status of *KRAS* [179]. On the contrary, cell type-specific MAPK signaling was absent in the presence of $BRAF^{V600E}$ expression[179]. Together, this suggests that additional factors, such as allele frequencies and cell types, can influence MAPK pathway activation and therapy outcome in CRCs with oncogenic *KRAS* mutations. Hence, additional and more controlled model systems are required to investigate the oncogenic potential of *KRAS* and *BRAF* variants in the presence and absence of EGFR inhibition.

Cancer modeling using organoids and CRISPR/Cas9

Recent advances in genetic manipulations, such as the CRISPR/Cas9 technology and plasmid delivery methods, have facilitated organoid engineering for disease modeling[180]. Several studies have shown the utility of the CRISPR technology for studying stepwise colorectal cancer tumorigenesis via classical and serrated neoplasia pathways[181–183]. Here, sequential knock-in and -out strategies in healthy human colon organoids indicated that the type of

niche growth factor independency correlated with CRISPR-induced mutations in matched signaling pathways. For instance, oncogenic KRAS promoted independency towards EGF-mediated signaling, but only became fully independent with co-occuring mutation in PI3K[183]. Engraftment efficiencies, tumor growth and invasion of transplanted CRISPR-engineered organoids correlated with increased number of signaling pathway mutations that established growth factor independence [181–183]. Similar strategies have also been applied in PDTOs as well as healthy organoids to create isogenic lines for studying the impact of oncogenic *KRAS* on targeted inhibition of the EGFR pathway. Subsequent drug screening demonstrated that a single oncogenic mutation in *KRAS* is sufficient to confer EGFR therapy resistance irrespective of its tumorigenic state[176]. However, this study used intermittent EGFR inhibition for selection of *KRAS* mutant knock-in lines, which might have resulted in the loss *KRAS* mutant clones that display a lower degree of resistance. Reminiscent of the aforementioned niche growth factor dependency study, CRISPR-mediated $KRAS^{G12V}$ knock-in mutations in healthy intestinal organoids was not sufficient to completely substitute for EGF-mediated signaling upon growth factor depletion[183]. Identical findings were made by the Clevers lab[182]. Importantly, this suggests that selection strategies on induced phenotype by growth factor depletion might be biased and most likely reflect acquired resistance during targeted therapy. Introduction of antibiotic resistance cassettes are therefore favorable to model primary resistance, which potentially reveals a more heterogenous range of sensitivities to EGFR inhibition between different engineered organoid lines. A similar EGF independency selection strategy was recently performed in a CRISPR-screen to identify whether depletion of members from the RASGAP family could confer resistance to anti-EGFR therapy in CRC. Subsequently, the only positive hit, i.e. loss of NF1 results in EGFR signaling independence[184], was confirmed using targeted introduction of loss-of-function alleles that were selected for using antibiotic resistance cassettes.

To model differences between oncogenic variants during primary resistance and their role during early tumor progression future knock-in strategies should use phenotype-independent selection strategies (**Figure 5**).

FUTURE DIRECTIONS AND CONCLUDING REMARKS

In this review, we have discussed the differences between oncogenic *RAS* and *BRAF* variants in CRC development, progression and therapy resistance. An increasing number of studies demonstrate the variable effects of different oncogenic MAPK pathway mutations on CRC histopathology and therapy outcome, indicating that a personalized approach in mCRC treatment requires consideration of mutation type. Unfortunately, the sample sizes of patient cohorts in clinical trials when subdivided per mutation in *RAS* and *BRAF* are usually too small to reach significant conclusions about their predictive role in therapy response.

The relatively high success rate of organoid establishment from various cancer subtypes, together with their high scalability and reproducibility *in vitro*, allows intensive drug screening to identify new treatment regimens. This, as well as the high resemblance between drug responses in PDTOs and cancer patients, are indicative that PDTOs can be substitutes for current resource intensive PDX models at the pre-clinical stage of drug discovery. Subsequently, PDX models will remain tremendously important for validating drug sensitivity,

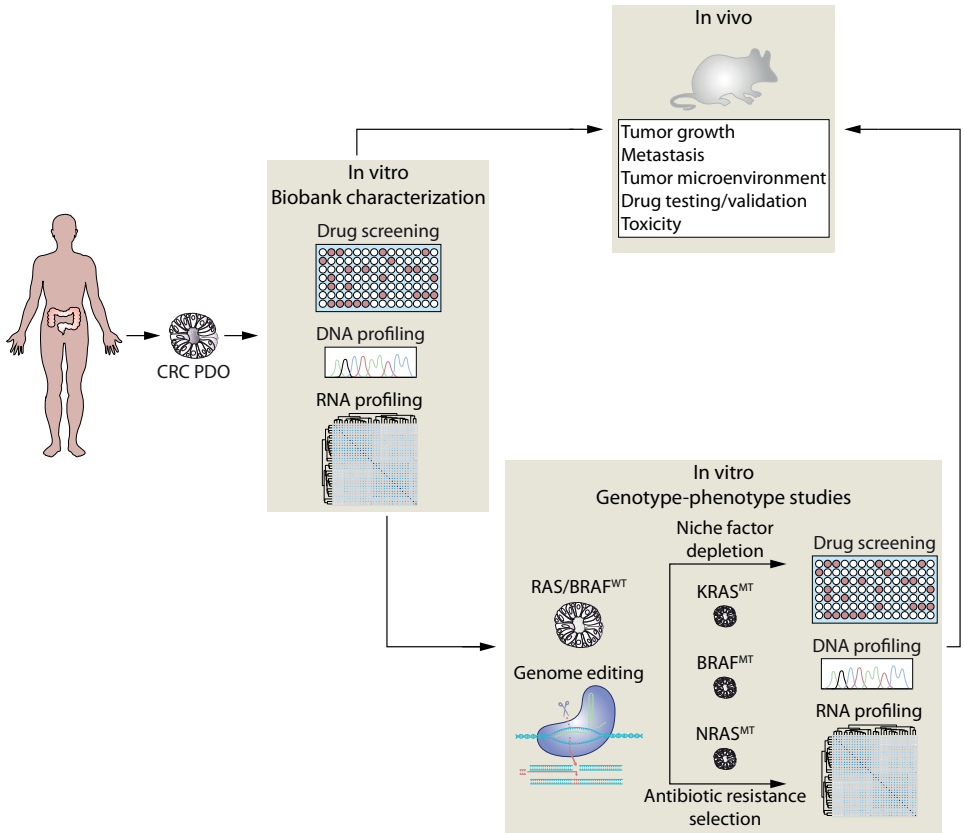

Figure 5. Patient-derived CRC organoids for personalized treatment and genotype-phenotype correlations. Patient-derived organoid (PDO) biobanks of CRCs allow full characterization of patient-specific tumor DNA and RNA profiles with in vitro drug responses. Subsequently, CRC PDOs can be genetically modified using the CRISPR/Cas9 technology to introduce or remove cancer mutations, for instance to create isogenic organoid lines with various mutations in endogenous MAPK oncogenes. The use of isogenic organoid lines reveals intrinsic effects of oncogenic mutations on RNA expression, chromosomal instability and drug response. Xenotransplantation of CRC PDOs in mice recapitulate the original native tumor histology and can be used to investigate tumor growth and metastatic properties, as well as interactions with the tumor microenvironment. The reliable and scalable nature of organoid models enable high-throughput drug screening, after which resource-intensive *in vivo* drug screen experiments can validate "hits" in combination with overall toxicity evaluation.

dosage and adverse toxicity[159,176]. Another benefit of using PDX models for validation is that organoid systems lack the TME, which will affect treatment outcome. This holds especially true for drugs that target effectors in the microenvironment, such as the anti-angiogenic drug regorafenib, that showed no effect on CRC PTDOs *in vitro*, whereas a marked reduction in tumor size and vasculature was observed upon orthotopic transplantation in mice[162]. Recent advances are made in the development of organoid co-culture systems with immune[168,185] and mesenchymal cells[168,186] that might further optimize accurate prediction of therapy response. Apart from basic studies and drug development, current drug screening methodologies on PDTOs might fail to correctly predict therapy response in a personalized setting due

to immense intra-tumoral heterogeneity in the patient's tumor. The derivation of multiple different PTDO subclones from the same tumor mass revealed the clonal differences on the genetic level, but also in terms of variability in drug response[165,178]. This indicates that multi-site tumor sampling might be required to optimize inclusion of all possible subclones in the analysis to predict drug response of an individual tumor.

We envision further optimization of organoid drug screening platforms, such as automated high-throughput image-based drug screening[161], together with improved genome editing strategies to increase our understanding on the specific role of various mutant *RAS* and *BRAF* oncogenes in therapy resistance. Ultimately, this knowledge will facilitate optimal patient stratification for successful treatment regimes.

SCOPE OF THIS THESIS

In metastatic colorectal cancer (mCRC), resistance to EGFR-targeted therapy is associated with MAPK pathway activating mutations. As a result, mCRC patients with such mutations, like oncogenic RAS, are currently excluded from anti-EGFR targeted therapy. However, an increasing amount of evidence supports the notion that not all oncogenic RAS proteins are equal, but impose isoform- and mutation-specific phenotypes in a context-dependent manner. Diverging phenotypes are likely to exist for most types of activating mutations. Unfortunately, these concepts are challenging to support with clinical evidence, as ideal stratification of patient cohorts per mutation type would severely dilute the desired patient numbers to draw significant conclusions.
In this thesis we have investigated the similarities and discrepancies between various oncogenic MAPK pathway mutations that are prevalent in CRC progression and therapy resistance with the aim to improve future patient stratification for treatment regimens. We used patient-derived organoids from CRC samples that maintain the histopathological features of the native tumor, including high concordance of somatic mutations, transcriptome and drug response between matched primary tumors and derived organoids cultures. Subsequently, patient-derived CRC organoids were genetically modified using CRISPR/Cas9 technology to introduce oncogenic mutations of interest.

Chapter 2 provides a guide to create state-of-the-arty genetic model systems using the CRISPR/Cas9 technology for homologous recombination. We describe strategies to enhance current genome editing efficiencies in various model systems, including hard-to-transfect cell lines and 3D organoids, allowing us to study oncogene-induced mutation effects at endogenous expression levels.
In **chapter 3**, we used CRISPR-mediated knock-out strategies to reveal that of all RASGAPs only the loss of NF1 promotes EGFR signaling independence. In comparison to oncogenic KRAS, we show that the degree of EGFR independence is less robust in NF1-deficient organoids. Furthermore, we observed that enhanced growth of NF1-deficient organoids mainly manifests itself in growth condition supplemented with EGF, demonstrating that the loss of NF1 acts as an amplifier of RAS-MAPK signaling.
In **chapter 4,** we characterize 5' gene fusion partners of BRAF that replace its autoinhibitory domain, thereby creating oncogenic BRAF variants. In particular, potential 5' gene fusion partners of BRAF influence BRAF localization and its efficacy to activate downstream signaling. While all BRAF fusions exhibit resistance to EGFR inhibition, they revealed differential responses to targeted therapy of downstream MAPK pathway components. Patients with mCRC expressing BRAF fusions are relatively rare and no specific therapeutic strategy is present. Our data indicate that these mutant tumors should be excluded from anti-EGFR targeted therapy.
In **chapter 5**, we investigate codon- and isoform-specific mutations in *RAS* and *BRAF* in mCRC progression and therapy resistance. Using CRISPR-mediated homologous recombination we created a panel of isogenic patient-derived organoid lines to study the similarities and discrepancies between various oncogenic mutations in the MAPK pathway. We show

that different oncogenic MAPK pathway mutations impose distinct phenotypes in a context-dependent manner, in accordance with observations in mCRC patients. Furthermore, we show that *RAS* and *BRAF* mutant organoids are still dependent on upstream EGFR signaling, as tumor growth and corresponding levels of MEK-ERK activation decreased upon pan-HER inhibition.

Finally, we summarize the main findings of this thesis in **chapter 6** and discuss the novel insights on oncogenic RAS and BRAF signaling in CRC biology.

REFERENCES

1. Cox AD, Der CJ. Ras history: The saga continues. *Small GTPases*. 2010;1(1):2-27. doi:10.4161/sgtp.1.1.12178
2. Hobbs GA, Der CJ, Rossman KL. RAS isoforms and mutations in cancer at a glance. *J Cell Sci*. 2016;129(7):1287-1292. doi:10.1242/jcs.182873
3. Simanshu DK, Nissley D V., McCormick F. RAS Proteins and Their Regulators in Human Disease. *Cell*. 2017. doi:10.1016/j.cell.2017.06.009
4. Fiorucci G, Hall A. All three human ras genes are expressed in a wide range of tissues. *BBA - Gene Struct Expr*. 1988;950(1):81-83. doi:10.1016/0167-4781(88)90076-0
5. Leon J, Guerrero I, Pellicer A. Differential expression of the ras gene family in mice. *Mol Cell Biol*. 2015;7(4):1535-1540. doi:10.1128/mcb.7.4.1535
6. Johnson CW, Reid D, Parker JA, et al. The small GTPases K-Ras, N-Ras, and H-Ras have distinct biochemical properties determined by allosteric effects. *J Biol Chem*. 2017;292(31):12981-12993. doi:10.1074/jbc.M117.778886
7. Omerovic J, Laude AJ, Prior IA. Ras proteins: Paradigms for compartmentalised and isoform-specific signalling. *Cell Mol Life Sci*. 2007;64(19-20):2575-2589. doi:10.1007/s00018-007-7133-8
8. Castellano E, Santos E. Functional specificity of Ras isoforms: So similar but so different. *Genes and Cancer*. 2011;2(3):216-231. doi:10.1177/1947601911408081
9. Nussinov R, Tsai CJ, Jang H. Oncogenic ras isoforms signaling specificity at the membrane. *Cancer Res*. 2018;78(3):593-602. doi:10.1158/0008-5472.CAN-17-2727
10. Nussinov R, Tsai CJ, Chakrabarti M, Jang H. A new view of ras isoforms in cancers. *Cancer Res*. 2016;76(1):18-23. doi:10.1158/0008-5472.CAN-15-1536
11. Nussinov R, Tsai CJ, Jang H. Is Nanoclustering essential for all oncogenic KRas pathways? Can it explain why wild-type KRas can inhibit its oncogenic variant? *Semin Cancer Biol*. 2018;(December 2017):0-1. doi:10.1016/j.semcancer.2018.01.002
12. Parker JA, Mattos C. The Ras-Membrane Interface: Isoform-Specific Differences in the Catalytic Domain. *Mol Cancer Res*. 2015;13(4):595-603. doi:10.1158/1541-7786.MCR-14-0535
13. Prior I a, Lewis PD, Mattos C. UKPMC Funders Group UKPMC Funders Group Author Manuscript A comprehensive survey of Ras mutations in cancer. *Cancer Res*. 2012;72(10):2457-2467. doi:10.1158/0008-5472.CAN-11-2612.A
14. Cox AD, Fesik SW, Kimmelman AC, Luo J, Der CJ. Drugging the undruggable RAS: Mission Possible? *Nat Rev Drug Discov*. 2014;13(11):828-851. doi:10.1038/nrd4389
15. Haigis KM. KRAS Alleles: The Devil Is in the Detail. *Trends in Cancer*. 2017;3(10):686-697. doi:10.1016/j.trecan.2017.08.006
16. Smit VT, Boot AJ, Smits AM, Fleuren GJ, Cornelisse CJ, Bos JL. KRAS codon 12 mutations occur very frequently in pancreatic adenocarcinomas. *Nucleic Acids Res*. 1988;16(16):7773-7782. https://www.ncbi.nlm.nih.gov/pubmed/3047672.
17. Almoguera C, Shibata D, Forrester K, Martin J, Arnheim N, Perucho M. Most human carcinomas of the exocrine pancreas contain mutant c-K-ras genes. *Cell*. 1988;53(4):549-554. doi:10.1016/0092-8674(88)90571-5
18. Haigis KM. KRAS Alleles: The Devil Is in the Detail. *Trends in Cancer*. 2017. doi:10.1016/j.trecan.2017.08.006
19. Bos JL, Fearon ER, Hamilton SR, et al. Prevalence of ras gene mutations in human colorectal cancers. *Nature*. 1987;327(6120):293-297. doi:10.1038/327293a0
20. Rodenhuis S, Slebos RJC. Clinical significance of ras oncogene activation in human lung cancer. *Cancer Res*. 1992;52(9 SUPPL.).
21. Li Z, Zheng J, Weiss LM, Shibata D. c-K-ras and p53 mutations occur very early in adenocarcinoma of the lung. *Lung Cancer*. 2002;12(1-2):154. doi:10.1016/0169-5002(95)96453-3
22. Graziano BSL, Gamble GP, Newman NB, et al. N o n – S m a l l - Ce l l Lu n g Ca n c e r. 2019;17(2):668-675.
23. Bos JL. The ras gene family and human carcinogenesis. *Mutat Res Genet Toxicol*. 1988;195(3):255-271. doi:10.1016/0165-1110(88)90004-8
24. J.L. B. ras Oncogenes in human cancer: A review. *Cancer Res*. 1989;49(17):4682-4689. http://ovidsp.ovid.com/ovidweb.cgi?T=JS&PAGE=reference&D=emed2&NEWS=N&AN=1989213649.
25. Van Cutsem E, Köhne C-H, Hitre E, et al. Cetuximab and Chemotherapy as Initial Treatment for Metastatic Colorectal Cancer. *N Engl J Med*. 2009;360(14):1408-1417. doi:10.1056/NEJMoa0805019
26. Douillard JY, Siena S, Cassidy J, et al. Randomized, Phase III trial of panitumumab with infusional fluorouracil, leucovorin, and oxaliplatin (FOLFOX4) Versus FOLFOX4 alone as first-line treatment in patients with previously untreated metastatic colorectal cancer: The PRIME study. *J Clin Oncol*. 2010;28(31):4697-4705. doi:10.1200/JCO.2009.27.4860

27. Karapetis CS, Khambata-Ford S, Jonker DJ, et al. *K-ras* Mutations and Benefit from Cetuximab in Advanced Colorectal Cancer. *N Engl J Med*. 2008. doi:10.1056/NEJMoa0804385
28. Peeters M, Oliner KS, Parker A, et al. Massively parallel tumor multigene sequencing to evaluate response to panitumumab in a randomized phase III study of metastatic colorectal cancer. *Clin Cancer Res*. 2013;19(7):1902-1912. doi:10.1158/1078-0432.CCR-12-1913
29. Douillard J-Y, Oliner KS, Siena S, et al. Panitumumab–FOLFOX4 Treatment and RAS Mutations in Colorectal Cancer . *N Engl J Med*. 2013;369(11):1023-1034. doi:10.1056/nejmoa1305275
30. Loupakis F, Ruzzo A, Cremolini C, et al. KRAS codon 61, 146 and BRAF mutations predict resistance to cetuximab plus irinotecan in KRAS codon 12 and 13 wild-type metastatic colorectal cancer. *Br J Cancer*. 2009;101(4):715-721. doi:10.1038/sj.bjc.6605177
31. Allegra CJ, Rumble RB, Hamilton SR, et al. Extended RAS gene mutation testing in metastatic colorectal carcinoma to predict response to anti-epidermal growth factor receptor monoclonal antibody therapy: American society of clinical oncology provisional clinical opinion update 2015. *J Clin Oncol*. 2016;34(2):179-185. doi:10.1200/JCO.2015.63.9674
32. De Roock W, Claes B, Bernasconi D, et al. Effects of KRAS, BRAF, NRAS, and PIK3CA mutations on the efficacy of cetuximab plus chemotherapy in chemotherapy-refractory metastatic colorectal cancer: A retrospective consortium analysis. *Lancet Oncol*. 2010;11(8):753-762. doi:10.1016/S1470-2045(10)70130-3
33. Schirripa M, Cremolini C, Loupakis F, et al. Role of NRAS mutations as prognostic and predictive markers in metastatic colorectal cancer. *Int J Cancer*. 2015;136(1):83-90. doi:10.1002/ijc.28955
34. European Medicines Agency. CHMP summary of opinion—erbitux. *http://www ema.europa.eu/docs/en_GB/document_library/Summary_of_opinion/human/000558/WC500155463.pdf*.2013;1(November):14-15.
35. Amgen. EPAR - Summary For The Public: Vectibix (panitumumab). 2015;44(0):1-4. http://www.ema.europa.eu/docs/en_GB/document_library/EPAR_-_Summary_for_the_public/human/000741/WC500047704.pdf%0Ahttp://www.ema.europa.eu/ema/index.jsp?curl=pages/medicines/human/medicines/000741/human_med_001128.jsp&mid=WC0b01ac058001d124.
36. Van Cutsem E, Cervantes A, Adam R, et al. ESMO consensus guidelines for the management of patients with metastatic colorectal cancer. *Ann Oncol*. 2016;27(8):1386-1422. doi:10.1093/annonc/mdw235
37. Sepulveda AR, Hamilton SR, Allegra CJ, et al. Molecular biomarkers for the evaluation of colorectal cancer: Guideline from the American society for clinical pathology, college of American pathologists, association for molecular pathology, and American society of clinical oncology. *Arch Pathol Lab Med*. 2017;141(5):625-657. doi:10.5858/arpa.2016-0554-CP
38. van Brummelen EMJ, de Boer A, Beijnen JH, Schellens JHM. BRAF Mutations as Predictive Biomarker for Response to Anti-EGFR Monoclonal Antibodies . *Oncologist*. 2017;22(7):864-872. doi:10.1634/theoncologist.2017-0031
39. Van Cutsem E, Köhne CH, Láng I, et al. Cetuximab plus irinotecan, fluorouracil, and leucovorin as first-line treatment for metastatic colorectal cancer: Updated analysis of overall survival according to tumor KRAS and BRAF mutation status. *J Clin Oncol*. 2011;29(15):2011-2019. doi:10.1200/JCO.2010.33.5091
40. Summers MG, Smith CG, Maughan TS, Kaplan R, Escott-Price V, Cheadle JP. BRAF and NRAS locus-specific variants have different outcomes on survival to colorectal cancer. *Clin Cancer Res*. 2017;23(11):2742-2749. doi:10.1158/1078-0432.CCR-16-1541
41. Ogura T, Kakuta M, Yatsuoka T, et al. Clinicopathological characteristics and prognostic impact of colorectal cancers with NRAS mutations. *Oncol Rep*. 2014;32(1):50-56. doi:10.3892/or.2014.3165
42. Morkel M, Riemer P, Bläker H, Sers C. Similar but different: distinct roles for KRAS and BRAF oncogenes in colorectal cancer development and therapy resistance. *Oncotarget*. 2015;6(25):20785-20800. doi:10.18632/oncotarget.4750
43. Rimbert J, Tachon G, Junca A, Villalva C, Karayan-Tapon L, Tougeron D. Association between clinicopathological characteristics and RAS mutation in colorectal cancer. *Mod Pathol*. 2018;31(3):517-526. doi:10.1038/modpathol.2017.119
44. Leon J, Guerrero I, Pellicer A. Differential expression of the ras gene family in mice. *Mol Cell Biol*. 2015. doi:10.1128/mcb.7.4.1535
45. Newlaczyl AU, Coulson JM, Prior IA. Quantification of spatiotemporal patterns of Ras isoform expression during development. *Sci Rep*. 2017;7:1-7. doi:10.1038/srep41297
46. Koera K, Nakao K, Miyoshi J, et al. K-ras is essential for the development of the mouse embryo. *Oncogene*. 1997;15:1151-1159.
47. Johnson L, Greenbaum D, Cichowski K, et al. K-ras is an essential gene in the mouse with partial functional overlap with N-ras [published erratum appears in Genes Dev 1997 Dec 1;11(23):3277]. 1997;11(19):2468-2481.
48. Umanoff H, Edelmann W, Pellicer A, Kucherlapati R. The murine N-ras gene is not essential for growth and development. *Proc Natl Acad Sci*. 1995;92(5):1709-1713. doi:10.1073/pnas.92.5.1709

49. Esteban LM, Vicario-Abejon C, Fernandez-Salguero P, et al. Targeted Genomic Disruption of H-ras and N-ras, Individually or in Combination, Reveals the Dispensability of Both Loci for Mouse Growth and Development. *Mol Cell Biol*. 2001;21(5):1444-1452. doi:10.1128/MCB.21.5.1444-1452.2001
50. Potenza N, Vecchione C, Notte A, et al. Replacement of K-Ras with H-Ras supports normal embryonic development despite inducing cardiovascular pathology in adult mice. *EMBO Rep*. 2005;6(5):432-437. doi:10.1038/sj.embor.7400397
51. Drosten M, Simon-Carrasco L, Hernandez-Porras I, et al. H-Ras and K-Ras oncoproteins induce different tumor spectra when driven by the same regulatory sequences. *Cancer Res*. 2017;77(3):707-718. doi:10.1158/0008-5472.CAN-16-2925
52. Cercek A, Braghiroli MI, Chou JF, et al. Clinical features and outcomes of patients with colorectal cancers harboring NRAS mutations. *Clin Cancer Res*. 2017;23(16):4753-4760. doi:10.1158/1078-0432.CCR-17-0400
53. Vaughn CP, Zobell SD, Furtado L V., Baker CL, Samowitz WS. Frequency of KRAS, BRAF, and NRAS mutations in colorectal cancer. *Genes Chromosom Cancer*. 2011;50(5):307-312. doi:10.1002/gcc.20854
54. Irahara N, Baba Y, Nosho K, et al. NRAS mutations are rare in colorectal cancer. *Diagnostic Mol Pathol*. 2010;19(3):157-163. doi:10.1097/PDM.0b013e3181c93fd1
55. Kendall KR, Wang Y, Cheung A, et al. Differential effects of oncogenic K-Ras and N-Ras on proliferation, differentiation and tumor progression in the colon. *Nat Genet*. 2008;40(5):600-608. http://ovidsp.ovid.com/ovidweb.cgi?T=JS&PAGE=reference&D=medc&NEWS=N&AN=18372904.
56. Janssen KP, Marjou F El, Pinto D, et al. Targeted expression of oncogenic K-ras in intestinal epithelium causes spontaneous tumorigenesis in mice. *Gastroenterology*. 2002;123(2):492-504. doi:10.1053/gast.2002.34786
57. Li Q, Haigis KM, McDaniel A, et al. Hematopoiesis and leukemogenesis in mice expressing oncogenic Nras G12D from the endogenous locus. *Blood*. 2011;117(6):2022-2032. doi:10.1182/blood-2010-04-280750
58. Wang J, Liu Y, Li Z, et al. Endogenous oncogenic Nras mutation initiates hematopoietic malignancies in a dose- and cell type-dependent manner. *Blood*. 2011;118(2):368-379. doi:10.1182/blood-2010-12-326058
59. Burd CE, Liu W, Huynh M V, et al. Selection in Melanoma. 2015;4(12):1418-1429. doi:10.1158/2159-8290.CD-14-0729.Mutation-Specific
60. Nussinov R, Tsai CJ, Jang H. Oncogenic ras isoforms signaling specificity at the membrane. *Cancer Res*. 2018;78(3):593-602. doi:10.1158/0008-5472.CAN-17-2727
61. Keller JW, Haigis KM, Franklin JL, Whitehead RH, Jacks T, Coffey RJ. Oncogenic K-RAS subverts the antiapoptotic role of N-RAS and alters modulation of the N-RAS: Gelsolin complex. *Oncogene*. 2007;26(21):3051-3059. doi:10.1038/sj.onc.1210103
62. Posch C, Sanlorenzo M, Vujic I, et al. Phosphoproteomic Analyses of NRAS(G12) and NRAS(Q61) Mutant Melanocytes Reveal Increased CK2α Kinase Levels in NRAS(Q61) Mutant Cells. *J Invest Dermatol*. 2016;136(10):2041-2048. doi:10.1016/j.jid.2016.05.098
63. Johnson CW, Lin Y-J, Reid D, et al. Isoform-Specific Destabilization of the Active Site Reveals a Molecular Mechanism of Intrinsic Activation of KRas G13D. *Cell Rep*. 2019;28(6):1538-1550.e7. doi:10.1016/j.celrep.2019.07.026
64. Poulin EJ, Bera AK, Lu J, et al. Tissue-specific oncogenic activity of K-RasA146T. *Cancer Discov*. April 2019:CD-18-1220. doi:10.1158/2159-8290.CD-18-1220
65. Mao C, Huang YF, Yang ZY, Zheng DY, Chen JZ, Tang JL. KRAS p.G13D mutation and codon 12 mutations are not created equal in predicting clinical outcomes of cetuximab in metastatic colorectal cancer: A systematic review and meta-analysis. *Cancer*. 2013;119(4):714-721. doi:10.1002/cncr.27804
66. Tejpar S, Celik I, Schlichting M, Sartorius U, Bokemeyer C, Van Cutsem E. Association of KRAS G13D tumor mutations with outcome in patients with metastatic colorectal cancer treated with first-line chemotherapy with or without cetuximab. *J Clin Oncol*. 2012;30(29):3570-3577. doi:10.1200/JCO.2012.42.2592
67. De Roock W, Jonker DJ, Di Nicolantonio F, et al. Association of KRAS p.G13D mutation with outcome in patients with chemotherapy-refractory metastatic colorectal cancer treated with cetuximab. *JAMA - J Am Med Assoc*. 2010. doi:10.1001/jama.2010.1535
68. Imamura Y, Morikawa T, Liao X, et al. Specific mutations in KRAS codons 12 and 13, and patient prognosis in 1075 BRAF wild-type colorectal cancers. *Clin Cancer Res*. 2012;18(17):4753-4763. doi:10.1158/1078-0432.CCR-11-3210
69. Jones RP, Sutton PA, Evans JP, et al. Specific mutations in KRAS codon 12 are associated with worse overall survival in patients with advanced and recurrent colorectal cancer. *Br J Cancer*. 2017. doi:10.1038/bjc.2017.37
70. Chen CC, Er TK, Liu YY, et al. Computational Analysis of KRAS Mutations: Implications for Different Effects on the KRAS p.G12D and p.G13D Mutations. *PLoS One*. 2013;8(2):6-13. doi:10.1371/journal.pone.0055793

71. Hunter JC, Manandhar A, Carrasco MA, Gurbani D, Gondi S, Westover KD. Biochemical and Structural Analysis of Common Cancer-Associated KRAS Mutations. *Mol Cancer Res*. 2015;13(9):1325-1335. doi:10.1007/s40520-017-0795-7
72. Buhrman G, Wink G, Mattos C. Transformation Efficiency of RasQ61 Mutants Linked to Structural Features of the Switch Regions in the Presence of Raf. *Structure*. 2007;15(12):1618-1629. doi:10.1016/j.str.2007.10.011
73. Lu S, Jang H, Nussinov R, Zhang J. The Structural Basis of Oncogenic Mutations G12, G13 and Q61 in Small GTPase K-Ras4B. *Sci Rep*. 2016;6:1-15. doi:10.1038/srep21949
74. Novelli ET, First JT, Webb LJ. Quantitative Measurement of Intrinsic GTP Hydrolysis for Carcinogenic Glutamine 61 Mutants in H-Ras. *Biochemistry*. 2018;57(44):6356-6366. doi:10.1021/acs.biochem.8b00878
75. Lu S, Jang H, Nussinov R, Zhang J. The Structural Basis of Oncogenic Mutations G12, G13 and Q61 in Small GTPase K-Ras4B. *Sci Rep*. 2016;6. doi:10.1038/srep21949
76. Smith MJ, Neel BG, Ikura M. NMR-based functional profiling of RASopathies and oncogenic RAS mutations. *Proc Natl Acad Sci*. 2013;110(12):4574-4579. doi:10.1073/pnas.1218173110
77. Hammond DE, Mageean CJ, Rusilowicz E V., Wickenden JA, Clague MJ, Prior IA. Differential reprogramming of isogenic colorectal cancer cells by distinct activating KRAS mutations. *J Proteome Res*. 2015;14(3):1535-1546. doi:10.1021/pr501191a
78. Ihle NT, Byers LA, Kim ES, et al. Effect of KRAS oncogene substitutions on protein behavior: Implications for signaling and clinical outcome. *J Natl Cancer Inst*. 2012;104(3):228-239. doi:10.1093/jnci/djr523
79. Stolze B, Reinhart S, Bulllinger L, Fröhling S, Scholl C. Comparative analysis of KRAS codon 12, 13, 18, 61, and 117 mutations using human MCF10A isogenic cell lines. *Sci Rep*. 2014;5:1-9. doi:10.1038/srep08535
80. Gamba S, Camaj P, Heinemann V, et al. Effect of KRAS exon 2 mutations on antitumor activity of afatinib and gefitinib. *Anticancer Drugs*. 2015;26(4):371-378. doi:10.1097/CAD.0000000000000196
81. Ostrow SL, Simon E, Prinz E, et al. Variation in KRAS driver substitution distributions between tumor types is determined by both mutation and natural selection. *Sci Rep*. 2016;6. doi:10.1038/srep21927
82. Weber CK, Slupsky JR, Andreas Kalmes H, Rapp UR. Active ras induces heterodimerization of cRaf and BRaf. *Cancer Res*. 2001;61(9):3595-3598.
83. Wan PT, Wan PT, Garnett MJ, et al. Mechanism of activation of the RAF-ERK signaling pathway by oncogenic mutations of B-RAF. *Cell*. 2004;116(6):855-867. papers2://publication/uuid/6A789316-AB6F-4316-B640-A6CE5046EAE0.
84. Lavoie H, Therrien M. Regulation of RAF protein kinases in ERK signalling. *Nat Rev Mol Cell Biol*. 2015;16(5):281-298. doi:10.1038/nrm3979
85. Zheng G, Tseng L-H, Chen G, et al. Clinical detection and categorization of uncommon and concomitant mutations involving BRAF. *BMC Cancer*. 2015;15(1):779. doi:10.1186/s12885-015-1811-y
86. Rowland A, Dias MM, Wiese MD, et al. Meta-analysis of BRAF mutation as a predictive biomarker of benefit from anti-EGFR monoclonal antibody therapy for RAS wild-type metastatic colorectal cancer. *Br J Cancer*. 2015;112(12):1888-1894. doi:10.1038/bjc.2015.173
87. Holderfield M, Deuker MM, McCormick F, McMahon M. Targeting RAF kinases for cancer therapy: BRAF-mutated melanoma and beyond. *Nat Rev Cancer*. 2014;14(7):455-467. doi:10.1038/nrc3760
88. Yao Z, Torres NM, Tao A, et al. BRAF Mutants Evade ERK-Dependent Feedback by Different Mechanisms that Determine Their Sensitivity to Pharmacologic Inhibition. *Cancer Cell*. 2015;28(3):370-383. doi:10.1016/j.ccell.2015.08.001
89. Wan PTC, Garnett MJ, Roe SM, et al. Mechanism of activation of the RAF-ERK signaling pathway by oncogenic mutations of B-RAF. *Cell*. 2004;116(6):855-867. doi:10.1016/S0092-8674(04)00215-6
90. Mertens F, Johansson B, Fioretos T, Mitelman F. The emerging complexity of gene fusions in cancer. *Nat Rev Cancer*. 2015;15(6):371-381. doi:10.1038/nrc3947
91. Kloosterman WP, Coebergh Van Den Braak RRJ, Pieterse M, et al. A systematic analysis of oncogenic gene fusions in primary colon cancer. *Cancer Res*. 2017;77(14):3814-3822. doi:10.1158/0008-5472.CAN-16-3563
92. Ross JS, Wang K, Chmielecki J, et al. The distribution of BRAF gene fusions in solid tumors and response to targeted therapy. *Int J Cancer*. 2016;138(4):881-890. doi:10.1002/ijc.29825
93. Chong H, Guan KL. Regulation of Raf through phosphorylation and N terminus-C terminus interaction. *J Biol Chem*. 2003;278(38):36269-36276. doi:10.1074/jbc.M212803200
94. Heidecker G, Huleihel M, Cleveland JL, et al. Mutational activation of c-raf-1 and definition of the minimal transforming sequence. *Mol Cell Biol*. 2015;10(6):2503-2512. doi:10.1128/mcb.10.6.2503
95. Cisowski J, Sayin VI, Liu M, Karlsson C, Bergo MO. Oncogene-induced senescence underlies the mutual exclusive nature of oncogenic KRAS and BRAF. *Oncogene*. 2016;35(10):1328-1333. doi:10.1038/onc.2015.186
96. Carragher LAS, Snell KR, Giblett SM, et al. V600EBraf induces gastrointestinal crypt senescence and

promotes tumour progression through enhanced CpG methylation of p16INK4a. *EMBO Mol Med*. 2010;2(11):458-471. doi:10.1002/emmm.201000099

97. Diaz LA, Williams RT, Wu J, et al. The molecular evolution of acquired resistance to targeted EGFR blockade in colorectal cancers. *Nature*. 2012;486(7404):537-540. doi:10.1038/nature11219
98. Bettegowda C, Sausen M, Leary RJ, et al. Detection of circulating tumor DNA in early- and late-stage human malignancies. *Sci Transl Med*. 2014;6(224):224ra24. doi:10.1126/scitranslmed.3007094
99. Misale S, Di Nicolantonio F, Sartore-Bianchi A, Siena S, Bardelli A. Resistance to Anti-EGFR therapy in colorectal cancer: From heterogeneity to convergent evolution. *Cancer Discov*. 2014;4(11):1269-1280. doi:10.1158/2159-8290.CD-14-0462
100. Misale S, Yaeger R, Hobor S, et al. Emergence of KRAS mutations and acquired resistance to anti-EGFR therapy in colorectal cancer. *Nature*. 2012;486(7404):532-536. doi:10.1038/nature11156
101. Van Emburgh BO, Sartore-Bianchi A, Di Nicolantonio F, Siena S, Bardelli A. Acquired resistance to EGFR-targeted therapies incolorectal cancer. *Mol Oncol*. 2014;8(6):1084-1094. doi:10.1016/j.molonc.2014.05.003
102. Sepulveda AR, Hamilton SR, Allegra CJ, et al. Molecular biomarkers for the evaluation of colorectal cancer: Guideline from the American society for clinical pathology, college of American pathologists, association for molecular pathology, and American society of clinical oncology. *Arch Pathol Lab Med*. 2017. doi:10.5858/arpa.2016-0554-CP
103. Van Emburgh BO, Arena S, Siravegna G, et al. Acquired RAS or EGFR mutations and duration of response to EGFR blockade in colorectal cancer. *Nat Commun*. 2016;7:1-9. doi:10.1038/ncomms13665
104. Schrock AB, Zhu VW, Hsieh WS, et al. Receptor Tyrosine Kinase Fusions and BRAF Kinase Fusions are Rare but Actionable Resistance Mechanisms to EGFR Tyrosine Kinase Inhibitors. *J Thorac Oncol*. 2018;13(9):1312-1323. doi:10.1016/j.jtho.2018.05.027
105. Dow LE, O'Rourke KP, Simon J, et al. Apc Restoration Promotes Cellular Differentiation and Reestablishes Crypt Homeostasis in Colorectal Cancer. *Cell*. 2015;161(7):1539-1552. doi:10.1016/j.cell.2015.05.033
106. Sansom OJ, Reed KR, Hayes AJ, et al. Loss of Apc in vivo immediately perturbs Wnt signaling, differentiation, and migration. *Genes Dev*. 2004;18(12):1385-1390. doi:10.1101/gad.287404
107. Rosenberg DW, Yang S, Pleau DC, et al. Mutations in BRAF and KRAS differentially distinguish serrated versus non-serrated hyperplastic aberrant crypt foci in humans. *Cancer Res*. 2007;67(8):3551-3554. doi:10.1158/0008-5472.CAN-07-0343
108. Fearon ER, Vogelstein B. A genetic model for colorectal tumorigenesis. *Cell*. 1990;61(5):759-767. doi:10.1016/0092-8674(90)90186-I
109. Borowsky J, Dumenil T, Bettington M, et al. The role of APC in WNT pathway activation in serrated neoplasia. *Mod Pathol*. 2018;31(3):495-504. doi:10.1038/modpathol.2017.150
110. Boutin AT, Liao WT, Wang M, et al. Oncogenic Kras drives invasion and maintains metastases in colorectal cancer. *Genes Dev*. 2017;31(4):370-382. doi:10.1101/gad.293449.116
111. Yamane L, Scapulatempo-Neto C, Reis RM, Guimarães DP. Serrated pathway in colorectal carcinogenesis. *World J Gastroenterol*. 2014;20(10):2634-2640. doi:10.3748/wjg.v20.i10.2634
112. Yachida S, Mudali S, Martin SA, Montgomery EA, Iacobuzio-Donahue CA. Beta-catenin nuclear labeling is a common feature of sessile serrated adenomas and correlates with early neoplastic progression after BRAF activation. *Am J Surg Pathol*. 2009;33(12):1823-1832. doi:10.1097/PAS.0b013e3181b6da19
113. Stefanius K, Ylitalo L, Tuomisto A, et al. Frequent mutations of KRAS in addition to BRAF in colorectal serrated adenocarcinoma. *Histopathology*. 2011;58(5):679-692. doi:10.1111/j.1365-2559.2011.03821.x
114. Yong HK, Kakar S, Cun L, Deng G, Kim YS. Distinct CpG island methylation profiles and BRAF mutation status in serrated and adenomatous colorectal polyps. *Int J Cancer*. 2008;123(11):2587-2593. doi:10.1002/ijc.23840
115. Han Y, Zhou ZY. Clinical features and molecular alterations of traditional serrated adenoma in sporadic colorectal carcinogenesis. *J Dig Dis*. 2011;12(3):193-198. doi:10.1111/j.1751-2980.2011.00495.x
116. Muzny DM, Bainbridge MN, Chang K, et al. Comprehensive molecular characterization of human colon and rectal cancer. *Nature*. 2012;487(7407):330-337. doi:10.1038/nature11252
117. Yaeger R, Chatila WK, Lipsyc MD, et al. Clinical Sequencing Defines the Genomic Landscape of Metastatic Colorectal Cancer. *Cancer Cell*. 2018. doi:10.1016/j.ccell.2017.12.004
118. Gupta R, Sinha S, Paul RN. The impact of microsatellite stability status in colorectal cancer. *Curr Probl Cancer*. 2018;42(6):548-559. doi:10.1016/j.currproblcancer.2018.06.010
119. Brulé SY, Jonker DJ, Karapetis CS, et al. Location of colon cancer (right-sided versus left-sided) as a prognostic factor and a predictor of benefit from cetuximab in NCIC CO.17. *Eur J Cancer*. 2015;51(11):1405-1414. doi:10.1016/j.ejca.2015.03.015
120. Boeckx N, Koukakis R, Op de Beeck K, et al. Effect of Primary Tumor Location on Second- or Later-line Treatment Outcomes in Patients With RAS Wild-type Metastatic Colorectal Cancer and All Treatment Lines in Patients With RAS Mutations in Four Randomized Panitumumab Studies. *Clin Colorectal Cancer*.

2018;17(3):170-178.e3. doi:10.1016/j.clcc.2018.03.005
121. Nitsche U, Stögbauer F, Späth C, et al. Right sided colon cancer as a distinct histopathological subtype with reduced prognosis. *Dig Surg*. 2016;33(2):157-163. doi:10.1159/000443644
122. Loupakis F, Yang D, Yau L, et al. Primary tumor location as a prognostic factor in metastatic colorectal cancer. *J Natl Cancer Inst*. 2015;107(3). doi:10.1093/jnci/dju427
123. Missiaglia E, Jacobs B, D'Ario G, et al. Distal and proximal colon cancers differ in terms of molecular, pathological, and clinical features. *Ann Oncol*. 2014;25(10):1995-2001. doi:10.1093/annonc/mdu275
124. Samowitz WS, Curtin K, Schaffer D, Robertson M, Leppert M, Slattery ML. Relationship of Ki-ras mutations in colon cancers to tumor location, stage, and survival: A population-based study. *Cancer Epidemiol Biomarkers Prev*. 2000;9(11):1193-1197.
125. Yamauchi M, Morikawa T, Kuchiba A, et al. Assessment of colorectal cancer molecular features along bowel subsites challenges the conception of distinct dichotomy of proximal versus distal colorectum. *Gut*. 2012;61(6):847-854. doi:10.1136/gutjnl-2011-300865
126. Lee DW, Han SW, Cha Y, et al. Association between mutations of critical pathway genes and survival outcomes according to the tumor location in colorectal cancer. *Cancer*. 2017;123(18):3513-3523. doi:10.1002/cncr.30760
127. Takane K, Akagi K, Fukuyo M, Yagi K, Takayama T, Kaneda A. DNA methylation epigenotype and clinical features of NRAS-mutation(+) colorectal cancer. *Cancer Med*. 2017;6(5):1023-1035. doi:10.1002/cam4.1061
128. Holch JW, Ricard I, Stintzing S, Modest DP, Heinemann V. The relevance of primary tumour location in patients with metastatic colorectal cancer: A meta-analysis of first-line clinical trials. *Eur J Cancer*. 2017;70:87-98. doi:10.1016/j.ejca.2016.10.007
129. Tejpar S, Stintzing S, Ciardiello F, et al. Prognostic and predictive relevance of primary tumor location in patients with ras wild-type metastatic colorectal cancer retrospective analyses of the CRYSTAL and FIRE-3 trials. *JAMA Oncol*. 2017;3(2):194-201. doi:10.1001/jamaoncol.2016.3797
130. Boeckx N, Janssens K, Van Camp G, et al. The predictive value of primary tumor location in patients with metastatic colorectal cancer: A systematic review. *Crit Rev Oncol Hematol*. 2018;121(June 2017):1-10. doi:10.1016/j.critrevonc.2017.11.003
131. Sachs N, Clevers H. Organoid cultures for the analysis of cancer phenotypes. *Curr Opin Genet Dev*. 2014;24(1):68-73. doi:10.1016/j.gde.2013.11.012
132. Tuveson D, Clevers H. Cancer modeling meets human organoid technology. *Science (80-)*. 2019;364(6444):952-955. doi:10.1126/science.aaw6985
133. Drost J, Clevers H. Organoids in cancer research. *Nat Rev Cancer*. 2018. doi:10.1038/s41568-018-0007-6
134. Ben-David U, Siranosian B, Ha G, et al. Genetic and transcriptional evolution alters cancer cell line drug response. *Nature*. 2018;560(7718):325-330. doi:10.1038/s41586-018-0409-3
135. Chantret I, Barbat A, Dussaulx E, Brattain MG, Zweibaum A. Epithelial Polarity, Villin Expression, and Enterocytic Differentiation of Cultured Human Colon Carcinoma Cells: A Survey of Twenty Cell Lines. *Cancer Res*. 1988;48(7):1936-1942.
136. Masters JRW. Human cancer cell lines: Fact and fantasy. *Nat Rev Mol Cell Biol*. 2000. doi:10.1038/35043102
137. Kamb A. At a crossroads in oncology. *Curr Opin Pharmacol*. 2010. doi:10.1016/j.coph.2010.05.006
138. Gazdar AF, Gao B, Minna JD. Lung cancer cell lines: Useless artifacts or invaluable tools for medical science? *Lung Cancer*. 2010. doi:10.1016/j.lungcan.2009.12.005
139. Gillet JP, Varma S, Gottesman MM. The clinical relevance of cancer cell lines. *J Natl Cancer Inst*. 2013. doi:10.1093/jnci/djt007
140. Sarkisian CJ, Keister BA, Stairs DB, Boxer RB, Moody SE, Chodosh LA. Dose-dependent oncogene-induced senescence in vivo and its evasion during mammary tumorigenesis. *Nat Cell Biol*. 2007;9(5):493-505. doi:10.1038/ncb1567
141. Pérez-Mancera PA, Tuveson DA. Physiological Analysis of Oncogenic K-Ras. *Methods Enzymol*. 2005;407:676-690. doi:10.1016/S0076-6879(05)07053-9
142. Snippert HJ, Schepers AG, Van Es JH, Simons BD, Clevers H. Biased competition between Lgr5 intestinal stem cells driven by oncogenic mutation induces clonal expansion. *EMBO Rep*. 2014;15(1):62-69. doi:10.1002/embr.201337799
143. Haigis KM, Kendall KR, Wang Y, et al. Differential effects of oncogenic K-Ras and N-Ras on proliferation, differentiation and tumor progression in the colon. *Nat Genet*. 2008;40(5):600-608. doi:10.1038/ng.115
144. Deng Q, Liao R, Wu BL, Sun P. High Intensity ras Signaling Induces Premature Senescence by Activating p38 Pathway in Primary Human Fibroblasts. *J Biol Chem*. 2004;279(2):1050-1059. doi:10.1074/jbc.M308644200
145. Di Nicolantonio F, Arena S, Gallicchio M, et al. Replacement of normal with mutant alleles in the genome of normal human cells unveils mutation-specific drug responses. *Proc Natl Acad Sci*. 2008;105(52):20864-

20869. doi:10.1073/pnas.0808757105
146. De Roock W, Piessevaux H, De Schutter J, et al. KRAS wild-type state predicts survival and is associated to early radiological response in metastatic colorectal cancer treated with cetuximab. *Ann Oncol*. 2008;19(3):508-515. doi:10.1093/annonc/mdm496
147. Costa-Cabral S, Brough R, Konde A, et al. CDK1 Is a synthetic lethal target for KRAS mutant tumours. *PLoS One*. 2016;11(2). doi:10.1371/journal.pone.0149099
148. Perera D, Venkitaraman AR. Oncogenic KRAS triggers MAPK-dependent errors in mitosis and MYC-dependent sensitivity to anti-mitotic agents. *Sci Rep*. 2016;6. doi:10.1038/srep29741
149. Suter CM, Norrie M, Ku SL, Cheong KF, Tomlinson I, Ward RL. CpG island methylation is a common finding in colorectal cancer cell lines. *Br J Cancer*. 2003;88(3):413-419. doi:10.1038/sj.bjc.6600699
150. Ahmed D, Eide PW, Eilertsen IA, et al. Epigenetic and genetic features of 24 colon cancer cell lines. *Oncogenesis*. 2013;2(0424). doi:10.1038/oncsis.2013.35
151. Mouradov D, Sloggett C, Jorissen RN, et al. Colorectal cancer cell lines are representative models of the main molecular subtypes of primary cancer. *Cancer Res*. 2014;74(12):3238-3247. doi:10.1158/0008-5472.CAN-14-0013
152. Forbes SA, Bindal N, Bamford S, et al. COSMIC: Mining complete cancer genomes in the catalogue of somatic mutations in cancer. *Nucleic Acids Res*. 2011;39(SUPPL. 1). doi:10.1093/nar/gkq929
153. Misale S, Yaeger R, Hobor S, et al. Emergence of KRAS mutations and acquired resistance to anti-EGFR therapy in colorectal cancer. *Nature*. 2012;486(7404):532-536. doi:10.1038/nature11156
154. Fujii M, Shimokawa M, Date S, et al. A Colorectal Tumor Organoid Library Demonstrates Progressive Loss of Niche Factor Requirements during Tumorigenesis. *Cell Stem Cell*. 2016;18(6):827-838. doi:10.1016/j.stem.2016.04.003
155. Sato T, Stange DE, Ferrante M, et al. Long-term expansion of epithelial organoids from human colon, adenoma, adenocarcinoma, and Barrett's epithelium. *Gastroenterology*. 2011;141(5):1762-1772. doi:10.1053/j.gastro.2011.07.050
156. Clevers H. Modeling Development and Disease with Organoids. *Cell*. 2016. doi:10.1016/j.cell.2016.05.082
157. Tiriac H, Belleau P, Engle DD, et al. Organoid profiling identifies common responders to chemotherapy in pancreatic cancer. *Cancer Discov*. 2018;8(9):1112-1129. doi:10.1158/2159-8290.CD-18-0349
158. Van De Wetering M, Francies HE, Francis JM, et al. Prospective derivation of a living organoid biobank of colorectal cancer patients. *Cell*. 2015;161(4):933-945. doi:10.1016/j.cell.2015.03.053
159. Pauli C, Hopkins BD, Prandi D, et al. Personalized in vitro and in vivo cancer models to guide precision medicine. *Cancer Discov*. 2017;7(5):462-477. doi:10.1158/2159-8290.CD-16-1154
160. Weeber F, van de Wetering M, Hoogstraat M, et al. Preserved genetic diversity in organoids cultured from biopsies of human colorectal cancer metastases. *Proc Natl Acad Sci*. 2015;112(43):13308-13311. doi:10.1073/pnas.1516689112
161. Betge J, Rindtorff N, Sauer J, et al. Multiparametric phenotyping of compound effects on patient derived organoids. *bioRxiv*. January 2019:660993. doi:10.1101/660993
162. Vlachogiannis G, Hedayat S, Vatsiou A, et al. Patient-derived organoids model treatment response of metastatic gastrointestinal cancers. *Science (80-)*. 2018. doi:10.1126/science.aao2774
163. Sachs N, de Ligt J, Kopper O, et al. A Living Biobank of Breast Cancer Organoids Captures Disease Heterogeneity. *Cell*. 2018;172(1-2):373-386.e10. doi:10.1016/j.cell.2017.11.010
164. Kopper O, de Witte CJ, Lõhmussaar K, et al. An organoid platform for ovarian cancer captures intra- and interpatient heterogeneity. *Nat Med*. 2019;25(5):838-849. doi:10.1038/s41591-019-0422-6
165. Roerink SF, Young MD, Alexandrov B, et al. Intra-tumour diversification in colorectal cancer at the single-cell level. *Nature*. 2018;556:457-462. doi:10.1038/s41586-018-0024-3
166. Calon A, Lonardo E, Berenguer-Llergo A, et al. Stromal gene expression defines poor-prognosis subtypes in colorectal cancer. *Nat Genet*. 2015;47(4):320-329. doi:10.1038/ng.3225
167. Isella C, Terrasi A, Bellomo SE, et al. Stromal contribution to the colorectal cancer transcriptome. *Nat Genet*. 2015;47(4):312-319. doi:10.1038/ng.3224
168. Qin X, Sufi J, Vlckova P, et al. Single-Cell Signalling Analysis of Heterocellular Organoids. *bioRxiv*. January 2019:659896. doi:10.1101/659896
169. Vukicevic S, Kleinman HK, Luyten FP, Roberts AB, Roche NS, Reddi AH. Identification of multiple active growth factors in basement membrane matrigel suggests caution in interpretation of cellular activity related to extracellular matrix components. *Exp Cell Res*. 1992;202(1):1-8. doi:10.1016/0014-4827(92)90397-Q
170. Hughes CS, Postovit LM, Lajoie GA. Matrigel: a complex protein mixture required for optimal growth of cell culture. *Proteomics*. 2010. doi:10.1002/pmic.200900758
171. Gjorevski N, Sachs N, Manfrin A, et al. Designer matrices for intestinal stem cell and organoid culture. *Nature*. 2016. doi:10.1038/nature20168
172. Broguiere N, Isenmann L, Hirt C, et al. Growth of Epithelial Organoids in a Defined Hydrogel. *Adv Mater*.

2018. doi:10.1002/adma.201801621
173. Fujii M, Matano M, Toshimitsu K, et al. Human Intestinal Organoids Maintain Self-Renewal Capacity and Cellular Diversity in Niche-Inspired Culture Condition. *Cell Stem Cell*. 2018. doi:10.1016/j.stem.2018.11.016
174. Mead BE, Ordovas-Montanes J, Braun AP, et al. Harnessing single-cell genomics to improve the physiological fidelity of organoid-derived cell types. *BMC Biol*. 2018. doi:10.1186/s12915-018-0527-2
175. Van De Wetering M, Francies HE, Francis JM, et al. Prospective derivation of a living organoid biobank of colorectal cancer patients. *Cell*. 2015;161(4):933-945. doi:10.1016/j.cell.2015.03.053
176. Verissimo CS, Overmeer RM, Ponsioen B, et al. Targeting mutant RAS in patient-derived colorectal cancer organoids by combinatorial drug screening. *Elife*. 2016. doi:10.7554/elife.18489
177. Kopetz S, Desai J, Chan E, et al. Phase II pilot study of vemurafenib in patients with metastatic BRAF-mutated colorectal cancer. *J Clin Oncol*. 2015;33(34):4032-4038. doi:10.1200/JCO.2015.63.2497
178. Schumacher D, Andrieux G, Boehnke K, et al. Heterogeneous pathway activation and drug response modelled in colorectal-tumor-derived 3D cultures. *PLoS Genet*. 2019;15(3):e1008076. doi:10.1371/journal.pgen.1008076
179. Brandt R, Uhlitz F, Riemer P, Giesecke C, Schulze S, El- IA. Cell type-dependent differential activation of ERK by oncogenic KRAS or BRAF in the mouse intestinal epithelium. *bioRxiv 340844*. 2018;(June):0-2. doi:https://doi.org/10.1101/340844
180. Bollen Y, Post J, Koo B-K, Snippert HJG. How to create state-of-the-art genetic model systems: strategies for optimal CRISPR-mediated genome editing. *Nucleic Acids Res*. 2018;46(13):6435-6454. doi:10.1093/nar/gky571
181. Lannagan TRM, Lee YK, Wang T, et al. Genetic editing of colonic organoids provides a molecularly distinct and orthotopic preclinical model of serrated carcinogenesis. *Gut*. 2019;68(4):684-692. doi:10.1136/gutjnl-2017-315920
182. Drost J, Van Jaarsveld RH, Ponsioen B, et al. Sequential cancer mutations in cultured human intestinal stem cells. *Nature*. 2015. doi:10.1038/nature14415
183. Matano M, Date S, Shimokawa M, et al. Modeling colorectal cancer using CRISPR-Cas9-mediated engineering of human intestinal organoids. *Nat Med*. 2015. doi:10.1038/nm.3802
184. Post JB, Hami N, Mertens AEE, Elfrink S, Bos JL, Snippert HJG. CRISPR-induced RASGAP deficiencies in colorectal cancer organoids reveal that only loss of NF1 promotes resistance to EGFR inhibition. *Oncotarget*. 2019;10(14).
185. Neal JT, Li X, Zhu J, et al. Organoid Modeling of the Tumor Immune Microenvironment. *Cell*. 2018. doi:10.1016/j.cell.2018.11.021
186. Öhlund D, Handly-Santana A, Biffi G, et al. Distinct populations of inflammatory fibroblasts and myofibroblasts in pancreatic cancer. *J Exp Med*. 2017. doi:10.1084/jem.20162024
187. Simanshu DK, Nissley D V., McCormick F. RAS Proteins and Their Regulators in Human Disease. *Cell*. 2017;170(1):17-33. doi:10.1016/j.cell.2017.06.009
188. Vigil D, Cherfils J, Rossman KL, Der CJ. Ras superfamily GEFs and GAPs: Validated and tractable targets for cancer therapy? *Nat Rev Cancer*. 2010;10(12):842-857. doi:10.1038/nrc2960
189. Engelman JA, Luo J, Cantley LC. The evolution of phosphatidylinositol 3-kinases as regulators of growth and metabolism. *Nat Rev Genet*. 2006;7(8):606-619. doi:10.1038/nrg1879
190. Nakhaeizadeh H, Amin E, Nakhaei-Rad S, Dvorsky R, Ahmadian MR. The RAS-effector interface: Isoform-specific differences in the effector binding regions. *PLoS One*. 2016;11(12):1-20. doi:10.1371/journal.pone.0167145
191. Malumbres M, Barbacid M. RAS oncogenes: the first 30 years. *Nat Rev Cancer*. 2003;3:459. https://doi.org/10.1038/nrc1097.
192. Drosten M, Dhawahir A, Sum EYM, et al. Genetic analysis of Ras signalling pathways in cell proliferation, migration and survival. *EMBO J*. 2010;29(6):1091-1104. doi:10.1038/emboj.2010.7
193. Guda K, Veigl ML, Varadan V, et al. Novel recurrently mutated genes in African American colon cancers. *Proc Natl Acad Sci U S A*. 2015. doi:10.1073/pnas.1417064112
194. Brannon AR, Vakiani E, Sylvester BE, et al. Comparative sequencing analysis reveals high genomic concordance between matched primary and metastatic colorectal cancer lesions. *Genome Biol*. 2014. doi:10.1186/s13059-014-0454-7
195. Giannakis M, Mu XJ, Shukla SA, et al. Genomic Correlates of Immune-Cell Infiltrates in Colorectal Carcinoma. *Cell Rep*. 2016. doi:10.1016/j.celrep.2016.03.075
196. McKay MM, Morrison DK. Integrating signals from RTKs to ERK/MAPK. *Oncogene*. 2007. doi:10.1038/sj.onc.1210394

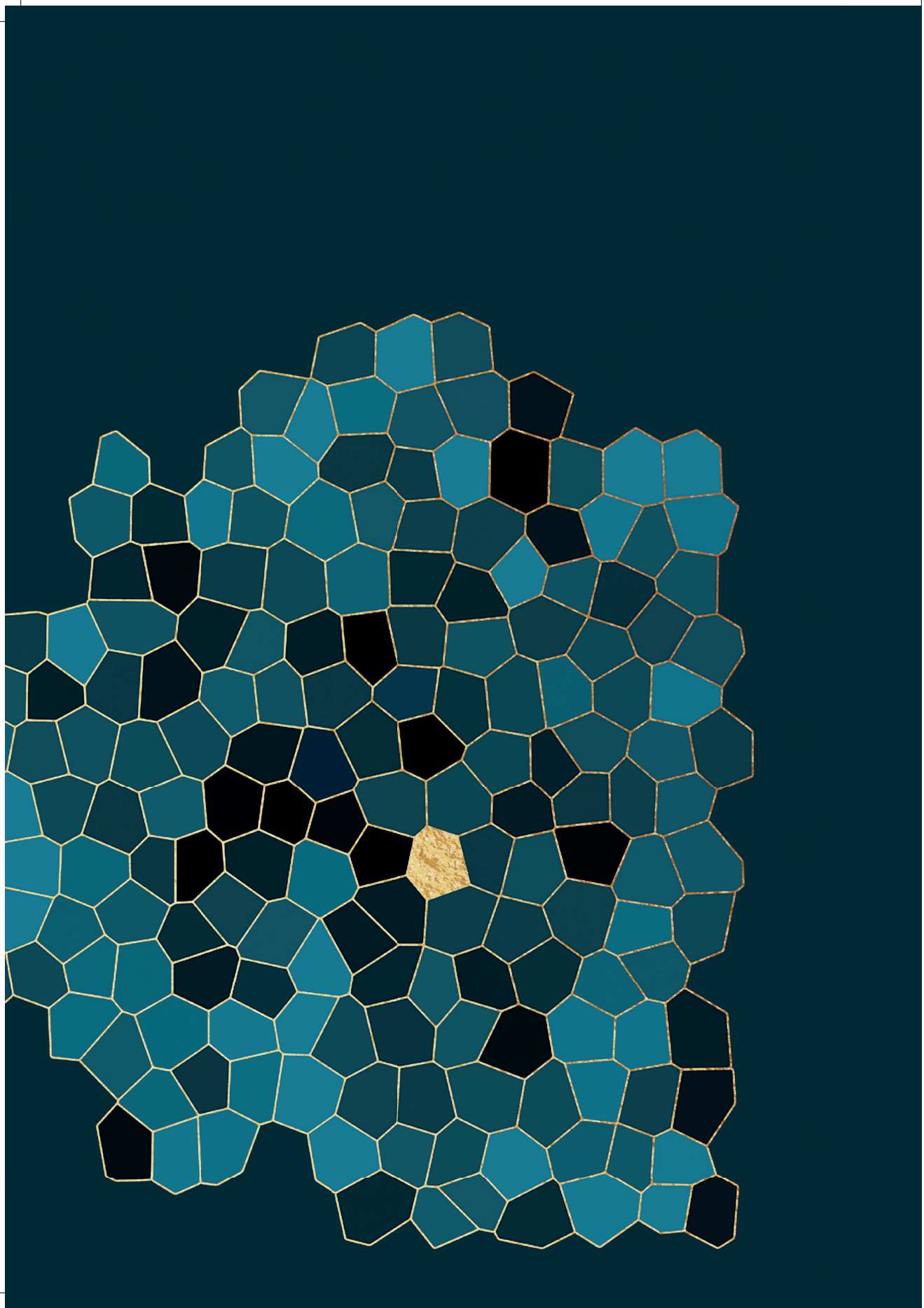

CHAPTER 2

HOW TO CREATE STATE-OF-THE-ART GENETIC MODEL SYSTEMS: STRATEGIES FOR OPTIMAL CRISPR-MEDIATED GENOME EDITING

Yannik Bollen, Jasmin B. Post,
Bon-Kyong Koo and Hugo J.G. Snippert

Nucleic Acids Research. 2018. 46(13): 6435-6454

ABSTRACT

Model systems with defined genetic modifications are powerful tools for basic research and translational disease modeling. Fortunately, generating state-of-the-art genetic model systems is becoming more accessible to non-geneticists due to advances in genome editing technologies. As a consequence, solely relying on (transient) overexpression of (mutant) effector proteins is no longer recommended since scientific standards increasingly demand genetic modification of endogenous loci. In this review, we provide up-to-date guidelines with respect to homology-directed repair (HDR)-mediated editing of mammalian model systems, aimed at assisting researchers in designing an efficient genome editing strategy.

INTRODUCTION

Mammalian model systems with defined genetic modifications are powerful tools for basic research and disease modeling. Unfortunately, precise manipulation of the mammalian genome has remained resource extensive and laborious for years, forcing many researchers to prioritize user-friendly techniques such as transgenic overexpression. The recent development of a novel generation of designer nucleases, e.g. Cas9, in combination with a better understanding of DNA repair mechanisms, is greatly improving the generation of new model systems with defined genetic modifications. Indeed, these more accurate model systems will increasingly represent a new standard that researchers have to incorporate into their studies.

Optimal design of precise genome editing strategies is subject to many considerations that depend to a large extent on the nature of the desired modification and the cellular context in which it is pursued. While double-strand breaks (DSBs) generated by designer nucleases are sufficient to introduce deletions and rearrangements at defined genomic loci[1–3], accurate replacement or insertion of genetic material generally requires the co-introduction of a donor template that carries the modification. Moreover, the composition of the donor template can be altered to favor a particular DSB repair pathway by which the modification will be introduced into the host genome.

DSBs naturally occur during DNA replication or as a consequence of environmental factors. Fortunately, homology directed repair (HDR) pathways, e.g. homologous recombination, accurately repair DSBs by using homologous DNA as a template[4,5]. Indeed, the requirement for a homologous template during HDR can be exploited to facilitate the replacement or insertion of genetic material. This mode of genome editing can be stimulated by a designer nuclease-generated DSB at the genomic locus of interest and the on-site presence of an artificial DNA template that contains (i) the new or modified genetic code and (ii) flanking regions that contain sufficient homology to the cleaved genomic strands (**Figure 1**). In a natural setting however, a homologous sister chromatid is only readily available to serve as a template during and shortly after DNA replication. Outside the late-S, G2 and M-phase of the cell cycle, most cells actively suppress HDR to favour non-homologous end joining (NHEJ)-mediated DSB repair[6–8]. As a result, classical HDR-mediated genome editing is largely restricted to proliferative cells[9]. In contrast to HDR, NHEJ directly ligates break ends without the need of homology and is active in both proliferating and post-mitotic cells[10]. NHEJ-mediated DSB repair has recently been exploited to introduce exogenous DNA into genomes of post-mitotic cells such as mature neurons and cardiac muscle cells[11,12]. Along similar lines, the microhomology-mediated end joining (MMEJ) pathway can also be stimulated to facilitate precise genome editing in both proliferative and post-mitotic cells[13–15].

Although NHEJ- and MMEJ-based genome editing protocols are important innovations that enable editing in post-mitotic cells, both strategies are subject to their own set of limitations. NHEJ in particular has a tendency to generate errors during DSB repair, which may lead to inaccurate junctions during integration of the donor template[12,15]. More importantly, since NHEJ ligates the cleaved genomic strands, introducing exogenous DNA (e.g. cDNA encoding fluorescent proteins) is only possible at the exact genomic location where the DSB

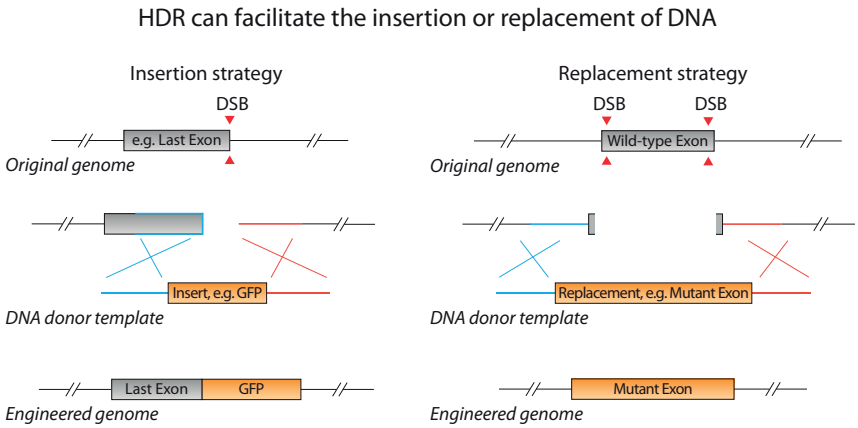

Figure 1. Exploiting HDR for insertion or replacement of DNA.
Left panel: DNA Insertion strategy. A nuclease induced DSB near the stop codon triggers HDR mediated insertion of sequence in-between the homology regions of the donor template. Right panel: DNA replacement strategy. In this example, replacing an exon for a mutant variant will be accommodated via its excision by dual targeting of the nuclease to both ends of the exon (using two gRNA), followed by HDR between the DNA break extremities and the homology regions of the donor template. HDR via the 5' and 3' homology regions is indicated in blue and red, respectively.

was generated. In similar fashion, the microhomology involved in MMEJ-mediated donor integration does not tolerate significant positional divergence between the nuclease cleavage site and the desired integration site.

While mammalian genome editing via HDR remains the least error prone and most flexible strategy, traditional protocols often suffer from low editing efficiency. Fortunately, novel generations of designer nucleases and new insights into the molecular mechanisms of HDR have led to the development of more efficient HDR-mediated genome editing protocols. In this review we discuss the latest research and condense it into 'best practice guidelines' for researchers who would like to generate mammalian model systems with precisely defined genetic modifications.

strategy, traditional protocols often suffer from low editing efficiency. Fortunately, novel generations of designer nucleases and new insights into the molecular mechanisms of HDR have led to the development of more efficient HDR-mediated genome editing protocols. In this review we discuss the latest research and condense it into 'best practice guidelines' for researchers who would like to generate mammalian model systems with precisely defined genetic modifications.

DESIGNER NUCLEASES

Mouse genomes can be edited with bp-resolution using HR-mediated repair of naturally occurring DSBs in cultured ES cells[16]. For decades, this procedure has been successfully used to generate new mouse models with specific integrations of exogenous DNA, so-called knock-in mouse models. Since the timing and location of DSBs could not be controlled, efficiency of

HR-mediated knock-ins varied significantly between different integration-sites, e.g. genes of interest. In addition to the desired genomic modification, the donor template often included a positive selection cassette to allow selection for donor integration. Furthermore, the homology arms were extended up to 5 kb in length to increase the likelihood that the DNA template would span a naturally occurring DSB[17].

The development of designer nucleases that can target virtually all DNA loci of interest significantly enhanced the efficiency of precise genome editing, since integration of the donor template is no longer dependent on the spontaneous occurrence of a DSB near the site of interest[18]. The first use-cases of designer nucleases for precise genome editing in mammalian cells involve Zinc-finger nucleases (ZFN), which were succeeded by transcription-activator like effector nucleases (TALENs)[19,20]. Specificity of both ZFN and TALENs depends on a sequence-specific DNA binding domain to guide a non-specific DNA cleavage module, frequently the FokI nuclease domain. Generation of a DSB requires dual targeting in a specific spatial bi-orientation since FokI requires dimerization for nuclease activity. While ZFN and TALENs have proven effective, their usability has been limited by the requirement to pre-engineer sequence-specific DNA binding domains for each genomic target site, followed by experimental testing of nuclease activity for each ZFN or TALEN pair.

More recently, class II nucleases of the bacterial clustered regularly inter-spaced short palindromic repeats (CRISPR) adaptive immune system have been engineered to facilitate mammalian genome editing[21,22]. Class II CRISPR nucleases consist of a single large monomeric nuclease with DNA target-site specificity mediated by an RNA molecule (guide RNA). Double-strand DNA cleavage occurs after sequence alignment (heteroduplex formation) between the variable region within the RNA (guide sequence) and the genomic target site. In contrast to engineering new proteins (e.g. ZFN and TALENs), these nucleases only require modification of the guide sequence to direct nuclease activity toward a specific genomic locus. In addition, the monomeric nature of class II CRISPR nucleases does not impose any orientational restraints on target sites. Potential target sites of class II CRISPR nucleases are only limited by the requirement of a protospacer adjacent motif (PAM), located either up- or downstream of the genomic target site on the strand that is not engaged in heteroduplex formation with the guide sequence (protospacer). However, most class II CRISPR nucleases have relatively permissive PAM requirements and many variants with alternate PAMs have since been validated in mammalian systems. Due to their superior properties, we will focus our discussion on two distinct types of class II CRISPR nucleases that have been adapted for mammalian genome editing to date.

CRISPR associated nuclease 9 (Cas9) is a monomeric nuclease first derived from *Streptococcus pyogenes* (SpCas9) and human codon optimized[23]. Cas9 is guided by a synthetic single-guide RNA (sgRNA) of approximately 100-nucleotides (nt) in length[24], containing a 17–20 nt guide sequence that recognizes the target locus. The RuvC-like and HNH nuclease domains independently initiate cleavage on both strands 3 bp upstream of the PAM to generate a blunt-ended DSB (**Figure 2A**). SpCas9, the most widely used class II CRISPR nuclease, primarily recognizes the relatively permissive NGG PAM with limited activity toward NAG PAMs. Orthologs and variants of SpCas9 with alternative PAM specificities have since been published and provide an opportunity to bypass restrictions imposed by the PAM preference of conventional SpCas9[25–34].

An interesting alternative to Cas9 is the more recently described CRISPR from *Prevotella* and *Francisella* 1 (Cpf1)[35]. In addition to Cpf1 from *F. Novicida* (FnCpf1)[35,36], orthologs have been adapted from *Acidaminococcus sp.* (AsCpf1) and *Lachnospiraceae bacterium* (LbCpf1)[37–39]. There are major differences between Cas9 and Cpf1 at the molecular level (**Figure 2**). Cpf1 is guided by a shorter CRISPR RNA (~40 nt) and contains a guide sequence of up to 24 nt of which the 18 nt proximal to the PAM contribute most to binding and cleavage activity[40]. In addition, the Cpf1 PAM is located immediately upstream of the protospacer and is T-rich. Although the exact nick positions have not been defined for all Cpf1 orthologues, DNA cleavage by Cpf1 results in a 5' staggered cut that is located away from the PAM (**Figure 2B**). As a consequence, small insertions or deletions (indels) generated by NHEJ-mediated repair are more likely to maintain critical target site residues, in contrast to Cas9 where indels frequently prevent re-cleavage. The additional cleavage cycles of Cpf1 were speculated to increase the probability for HDR[35]. However, a direct experimental comparison between LbCpf1 and SpCas9 in mice did not reveal a significant increase in HDR mediated donor integration when initiated by LbCpf1[41]. Whereas a more recent study in zebra fish attributed enhanced HDR by LbCpf1, among other things, to its PAM distal cleavage[42].

SPECIFICITY AND CLEAVAGE EFFICIENCY OF CRISPR-DERIVED NUCLEASE VARIANTS

The specificity of designer nuclease-mediated cleavage is an important consideration since off-target cleavage can result in unintended disruption of genomic elements. Genomic cleavage by ZFN or TALEN pairs is inherently specific since it is exceedingly unlikely that two off-target sites are in the required proximity and orientation to support FokI dimerization. By contrast, the monomeric nature of type II CRISPR nucleases has raised concerns regarding off-target cleavage activity. Indeed, initial reports demonstrated substantial off-target indel generation by wild-type SpCas9[43–46]. Algorithms have since been developed that predict cleavage activity at off-target sites for type II CRISPR nucleases[43], which allows the researcher to select highly specific target sites. For particularly sensitive applications an in vitro analysis of off-target cleavage can be obtained via GUIDE-Seq[47].

In addition, there have been efforts to improve the intrinsic specificity of wild-type Cas9 by directed engineering of SpCas9[26,27,48]. These engineered variants display single base sensitivity at many target sites, but often sacrifice on-target cleavage efficiency when compared to wild-type SpCas9 using standard expression protocols[49]. The most recent engineered SpCas9 variant, xCas9, has the most permissive PAM to date and is reported to be superior to SpCas9 in terms of specificity and on-target cleavage activity[32]. However, before this variant is set to replace conventional SpCas9 it needs broader characterization.

Alternatively, the inherent specificity of FokI-based nucleases has been emulated by mutagenic inactivation of the RuvC like nuclease domain of SpCas9, thereby creating a nicking variant[25]. While generating DNA nick's in close proximity on opposite genomic strands can initiate DSB repair machinery, the efficiency is generally lower compared to a DSB generated by a monomeric nuclease[21,25]. Instead, Cas9 nickase variants are now increasingly used to stimulate donor integration using a single genomic DNA nick[50–53], which significantly reduces off and on-target indel generation since single DNA nicks are far less mutagenic compared to

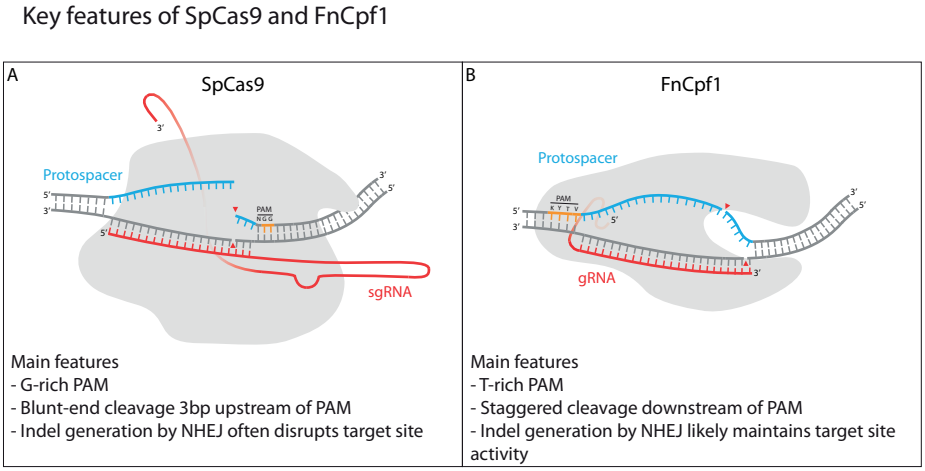

Figure 2. Key features of SpCas9 and LbCpf1.
Schematic representation of SpCas9 (**A**) and LbCpf1 (**B**). Ribonucleoprotein heteroduplexed with target DNA. DNA is indicated with grey lines, unless specified otherwise (PAM and protospacer). Red lines are RNAs. Light grey shape at the back represents protein structure. DNA strand cleavage is indicated using red arrow heads.

DSBs[50–52].

In addition to engineering of class II CRISPR nucleases, significant improvements in both specificity and on-target cleavage activity can be achieved by modification of the guide RNA. A truncated sgRNA of 17nt significantly enhances cleavage specificity of Cas9[43,46,54], often without reducing on-target activity[54,55]. Chemical modifications or even DNA substitutions of select sgRNA residues enhances specificity[56–59], while terminal modifications that prevent RNA degradation lead to enhanced cleavage activity[60]. A combination of extensive chemical modifications throughout the sgRNA sequence further enhances Cas9 cleavage dynamics[61]. Similar modifications of the Cpf1 guide RNA have also been shown to be effective[62,63]. Chemically modified guide RNAs are widely available from commercial suppliers and are especially effective in combination with mRNA or ribonucleoprotein delivery of Cas9 or Cpf1, which we will discuss in a later section.

In general, most nuclease targeting approaches deal with a trade-off between on-target editing efficiency versus on-target specificity. In the interest of maximizing the efficiency of generating a new model system, we recommend a preference for established monomeric type II CRISPR nucleases (**Table 1**), which display the highest on-target cleavage activity. The increased off-target proclivity of monomeric nucleases is mainly a concern in the context of therapeutic *in vivo* gene correction. For research applications, careful selection of target sites will often provide sufficient specificity.

SELECTING A GENOMIC TARGET SITE

While HDR mediated donor integration is maximally stimulated by a DSB at the intended integration site, additional considerations should be taken into account when selecting

Table 1. List of widely available monomeric type II CRISPR nucleases.

Monomeric type II CRISPR nucleases	PAM	cDNA length	Reference	Addgene #
● SpCas9 (*S. pyogenes*)	NGG	4,1kb	Ran et al. 2013	62988
● SpCas9-HF1	NGG	4,1kb	Kleinstiver et al. 2016	72247
● eSpCas9	NGG	4,1kb	Slaymaker et al. 2016	71814
SpCas9n(D10A)*	NGG	4,1kb	Ran et al. 2013	62987
SaCas9 (*S. aureus*)	NNGRRT	3,2kb	Ran et al. 2015	61591
SaCas9 KKH	NNNRRT	3,3kb	Kleinstiver et al. 2015	70708
CjCas9 (*C. jejuni*)	NNNNRYA	2,9kb	Kim et al. 2017	89754
FnCas9 (*F. novicida*)	YG	4,9kb	Hirano et al. 2016	68705
NmCas9 (*N. meningitidis*)	NNNNGAT	3,2kb	Hou et al. 2013	47868
● xCas9**	NG	4,1kb	Hu et al. 2018	108382
● LbCpf1 (*Lachnospiraceae bact.*)	TTTN	3,7kb	Zetsche et al. 2015, Dong et al. 2016, Kim et al. 2017	84751
FnCpf1 (*F. novicida*)	KYTV	3,9kb	Zetsche et al. 2015, Tu et al. 2017	69973
AsCpf1 (*Acidaminococcus sp.*)	TTTN	3,9kb	Zetsche et al. 2015, Yamano et al. 2016, Kim et al. 2017	84750

● Recommended nuclease
● Recommended only if specificity is a special concern
● Superior targeting scope, editing efficiency and specificity relative to spCas9. Not yet broadly characterized.
* Monomeric or dual nickase
** Varying activity towards NG, GAA and GAT PAMs

a genomic target site. As for target site specificity, algorithms have been developed that predict site specific cleavage activity of SpCas9 based on the nucleotide composition of the protospacer and PAM[40,64,65]. Many tools are now available that implement these algorithms to score potential nuclease target sites in a selected stretch of DNA. For conventional monomeric cleavage we recommend the free CRISPR design tool offered by the Benching platform. Among others, it predicts site specific activity of SpCas9 based on algorithms by Doench et al. (2016); allows selection of various genomes to predict specificity scores; supports a variety of PAMs including Cpf1 and allows the export of DNA oligo's suitable for ligation into commonly used expression plasmids. For a more complete overview of CRISPR design tools we suggest a review by Cui et al. (2018)[66].

In practice, the researcher will want to use a CRISPR design tool to select a nuclease target site based on the following criteria; (i) cleavage proximity to the intended integration site; (ii) predicted on-target activity; (iii) absence of exonic off-targets with high cleavage probability and (iv) overlap with the intended integration site. The latter is preferable since a target site that overlaps with the intended integration site will be disrupted during template integration, which prevents re-cleavage without having to introduce additional point modifications in the template. In addition, although cleavage near the intended integration site is preferable, a distal target with a high on-target score may be preferred over a proximal target site with a poor on-target score. Furthermore, while a general off-target score is helpful as an overall indicator of target site specificity, predicted off-targets should be examined on an individual basis to identify off-targets that are particularly detrimental in the context of the research application. These critical sites should be screened in selected clones to confirm the absence of indels. In **Figure 3**, we summarize how the above criteria can be used to interpret the quality of nuclease target sites in proximity to the genomic site of integration.

In general, once CRISPR machinery becomes active within a cell, both alleles will be cleaved. Since NHEJ is dominant over HDR this often leads to the generation of indels within alleles that are not modified by HDR. Generated DSBs within an exonic region therefore often result in a heterozygous null allele in addition to the correctly modified allele. If a heterozygous

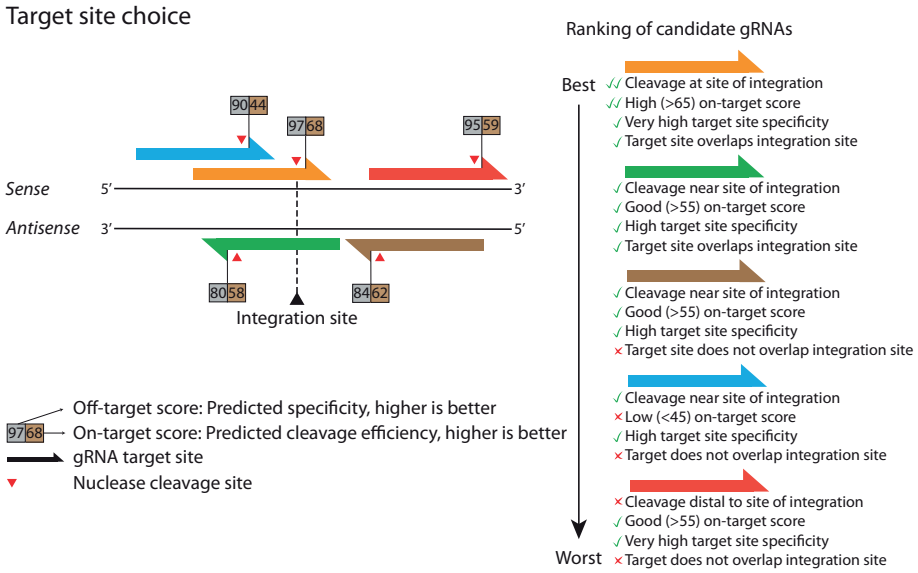

Figure 3. Nuclease target site choice.
Schematic representation of a dsDNA with 5 candidate gRNA (coloured arrows). To ensure optimal HDR of a donor template at the hypothetical integration site, the possible gRNAs are ranked with respect to their cleavage dynamics (on and off-target scores), as well as in relation to their location and orientation towards the intended integration site.

null allele is detrimental to the application of the modified lineage, the modification can be introduced using a DNA nick instead of a DSB[50,52], which we will discuss in a later section. Alternatively, a DSB can be induced within the nearest intron or 3' UTR, where indels are less likely to interfere with expression or protein function. However, positional divergence between the cleavage site and the intended integration site creates an internal region of homology between the genome and donor. This promotes undesired recombination outcomes and reduces the effective probability of generating a correctly modified allele (**Figure 4A**)[67]. Internal homology also occurs when two modifications are simultaneously introduced that have intervening sequences that are unmodified, for instance when generating floxed alleles with two LoxP sites. The probability that the modification located distal to the DSB is not incorporated increases with the extent of internal homology[68]. There are two ways in which internal homology can be prevented from participating in HDR. One strategy disrupts internal homology between the donor and genome by recoding in the corresponding region of the donor (**Figure 4B**)[69]. Alternatively, the internal homology region can be excised from the genome by introducing two DSBs (**Figure 4C**)[70], which is a proven strategy when replacing a genomic sequence[71,72]. However, this does increase the incidence of heterozygous null modifications by promoting the excision and inversion of alleles[67]. In summary, we advocate a preference for recoding as a strategy to minimize small regions of internal homology, whereas excision might be best when dealing with extensive internal homology during genomic sequence replacement.

The positional divergence between the genomic integration site and the nuclease target site

has to be compatible with the type of donor template that is used, since the donor needs to be capable of bridging the gap between those sites. In addition, short homology arms demand cleavage in close proximity to the intended integration site[53,73], while larger homology arms are more tolerant to distal cleavage[67]. As a rule of thumb, we suggest to limit nuclease positional divergence to less than 10% of homology arm length before taking steps to counteract internal homology.

At a glance

- Monomeric type II CRISPR nucleases display the highest on-target activity and provide sufficient specificity for research applications.
- Exploring target sites for multiple monomeric Cas9 as well as Cpf1 variants increases the probability of identifying a high-quality target site.
- Cleavage proximity to the integration site and predicted on-target activity are the main parameters that researchers should use when selecting a nuclease target site to initiate HDR.
- We recommend DNA cleavage to be initiated within a distance corresponding to 10% of homology arm length with respect to the integration site.
- Internal homology between the genome and donor should be minimized, and if extensive, excised from the genome.

SELECTION STRATEGIES

Due to the relatively low success rate of accurate HDR-mediated donor integration, the end result is often a mono-allelic modification, particularly when the locus is inactive and at closed chromatin conformation[74,75]. Therefore, it is important to decide in advance whether a homozygous modification is necessary. Furthermore, if a heterozygous modification is sufficient, the researcher has to consider whether perturbation of the 'secondary' non-recombined allele is detrimental and thus if 'functional loss-of-heterozygosity' needs to be prevented at all costs. Ultimately, the selection method used to identify desired clones will largely dictate the genome editing strategy as a whole. In the following paragraphs, we will discuss a variety of selection approaches and the context in which they are useful.

Direct selection for precise genetic modifications

In some cases, the desired modification conveys a phenotype that can be directly selected for. A clear example is the genomic integration of a fluorescent protein sequence that allows enrichment of correctly targeted cells via fluorescence activated cell sorting (FACS)[76].

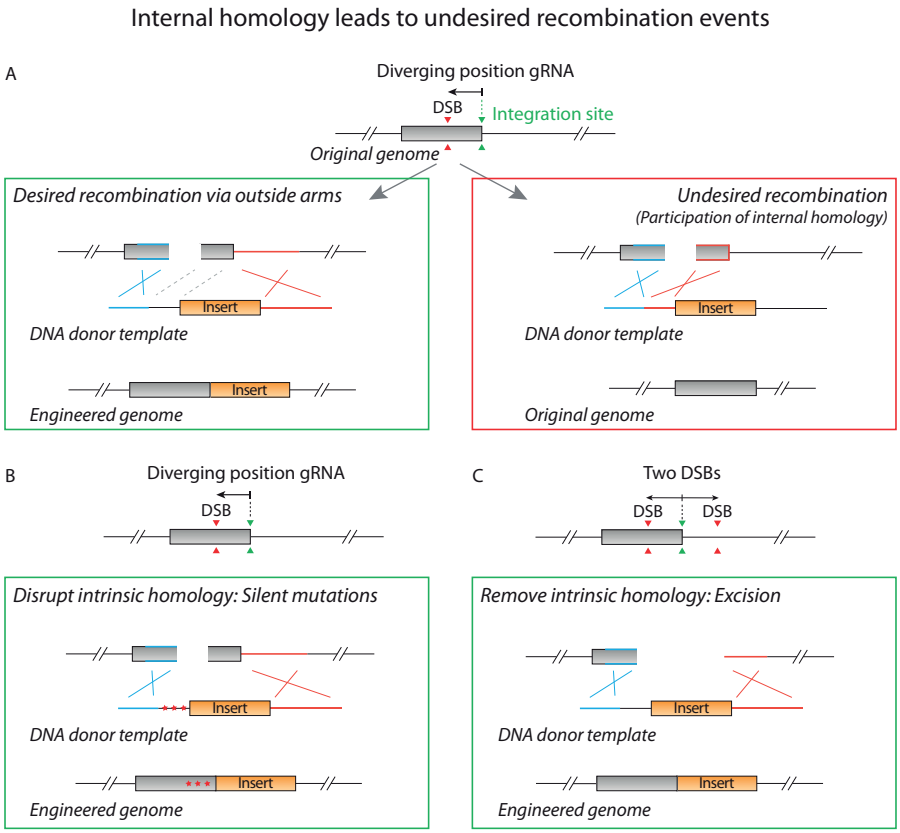

Figure 4. Internal homology increases the risk of undesired recombination events.
(**A**) Positional divergence between DNA cleavage (DSB, indicated with red arrow heads) and the intended integration site (green arrow heads) creates the possibility for an alternative mode of recombination wherein an internal homology region participates. In the green panel, the internal homology region is indicated (dashed grey lines), but HDR is mediated via the intended homology arms at the extremities of the donor template (indicated in blue and red). Alternatively, the internal homology region (red) participates with the upstream homology arm (blue) in HDR, thereby failing to integrate the insert from the donor template (red panel). Since the size of internal homology is proportional to the probability of undesired recombination events, there are two widely used preventive strategies that minimize the extent of internal homology. (**B**) Internal recombination can be prevented by introducing (silent) mutations (red stars) in the internal homology region of the donor template (recoding). (**C**) Alternatively, in case of extensive internal homology, the region can be excised from the genome using dual targeting of the nuclease to introduce two DSBs that flank the internal homology sequence.

Providing that the fluorescent protein, e.g. fused to a protein of interest, will be expressed at detectable levels in the cell type of choice and that these cells are compatible with FACS. Alternatively, modifications that allow immunogenic detection, such as small epitope tags, could offer similar opportunities for FACS-based enrichment. Another class of modifications that allow direct selection are those that convey a selective advantage over the parental lineage by means of modifying culture conditions. This strategy is frequently used in the generation of oncogenic model systems since many oncogenic driver mutations activate signalling pathways that promote growth factor independency. As a result, omitting growth factors from

the culture conditions enables enrichment of correctly modified cells[22,77]. However, this mode of phenotypic selection risks co-selection for orthogonal oncogenic mutations that arise instead or in addition to the desired modification.

Although direct selection for the desired modification allows donor integration without additional modification of the genome, experimental settings are not always compatible with this mode of selection and may therefore require the co-integration of a genetic selection element.

Genetic selection elements

Genetic selection elements commonly drive the expression of a protein that conveys drug resistance or allows fluorescent detection to support subsequent enrichment strategies. The protein that is expressed by the selection element should be non-invasive and able to provide a selectable phenotype in the targeted cells. Expression of the selection element can either be controlled by its own independent transcriptional regulatory elements or alternatively by endogenous regulatory elements.

Independent genetic selection elements are under transcriptional control of a dedicated promoter with ubiquitous activity so that it is expressed in virtually all cell types. In addition, the cDNA that encodes the selection marker is followed by a strong PolyA transcription terminator. As a result, the cassette will function as an independent transcriptional entity. In cases where the intended genomic modification is located within an exon, the selection cassette is frequently integrated within the nearest intron[78]. However, in case the last exon is targeted, e.g. to generate C-terminal fusion proteins, the element is commonly integrated within the endogenous 3'UTR of the gene of interest[79]. The independent selection cassette should be integrated in close proximity to the intended genetic modification in order to minimize internal homology between the genome and donor. However, caution should be taken with respect to disruption or relocation of regulatory elements. An RNA motif prediction tool such as RegRNA 2.0[80] can be used to determine the least invasive integration site. In addition, DNA sequences of candidate integration sites can be compared between mammalian species in order to avoid conserved regions.

The integration of an exogenous polyA transcriptional terminator upstream of the last coding exon can prematurely terminate transcription of the targeted allele[81]. To prevent truncated transcription, the independent selection cassette can be integrated in the opposite transcriptional orientation with respect to the gene of interest, thereby escaping polyadenylation signal recognition by the polymerase that transcribes the targeted allele. However, integration of a strong exogenous promoter in the vicinity of endogenous regulatory elements may influence the expression level and pattern of the modified allele[16,82,83]. In addition, some selection cassettes contain cryptic splice sites which may interfere with splicing of the targeted allele [83,84]. In order to minimize potential interference with endogenous expression it is good practice to remove the cassette once clones have been selected. Often this is achieved by flanking the selection cassette with either LoxP or FRT recombinase sites, allowing removal of the intervening sequence upon transient expression of the appropriate recombinase[85]. This process leaves only a single recombinase site of about 30 bp in length behind, in contrast to the average size of selection cassettes of ~2 kb. Unwanted DNA sequences that are practical leftovers from the editing procedure are often referred to as a scar sequence. However,

although minimal in size and widely considered intrinsically inert, the localization of the scar sequence might still interfere with expression of the modified allele[86]. Scarless removal of a selection cassette can be achieved via nuclease mediated excision followed by MMEJ-based repair of appropriately designed microhomology[87] or by using the piggyBac transposase[88].

For genomic modification strategies that include a selection cassette, we recommend insertion of the cassette within a non-conserved region in-between the 5' splice donor site and the downstream branch point (**Figure 5**). Insertion in-between the branch point and the 3' splice acceptor site is not advisable since it will extend the branch sequence beyond the consensus length. When a selection cassette will be included within the endogenous 3'UTR of the locus of interest, a less invasive location can usually be found ~50–100nt downstream of the endogenous stop codon.

As an alternative to independent expression of a selection cassette, a genetic selection element may be positioned under the transcriptional control of the endogenous allele of interest. This type of selection element does not include a promoter and polyA transcription terminator, and instead expression reflects the level and pattern of the gene of interest. The selection element is either co-integrated with an internal ribosome entry site (IRES) into the endogenous 3'UTR to become expressed as a bicistronic message[79,89], or as a C-terminal fusion protein interspaced by a ribosome skipping 2A peptide[90]. It is important to realize that the stringency for selection depends in both scenarios on the activity of the endogenous promoter. Both methodologies have been successfully used in multiple studies. However, insertion of an IRES sequence into the endogenous 3'UTR may influence expression levels[91], presumably by altering mRNA stability, while C-terminal 2A peptide fusion leaves the endogenous 3'UTR intact. On the other hand, the relative positioning of an IRES within the 3'UTR is flexible while C-terminal 2A peptide fusion requires integration immediately upstream of the endogenous stop codon. Furthermore, while the translational efficiency of an IRES might substantially deviate from the expression levels of the upstream gene, the newest generation of 2A fusion peptides generate near equimolar protein ratios. Therefore, 2A peptide reporters are more suitable as a readout of expression levels[90]. On the other hand, a downside of the 2A peptides is the addition of a 19–22 amino acid peptide at the C-terminus of the upstream protein, which can potentially interfere with normal protein function.

Sampling-based selection

Direct selection for correct template integration is convenient via the simultaneous integration of a genomic selection element. However, this is not always necessary or even preferable. Foremost, using a genomic selection element requires construction of a larger donor even if the desired modification is only a single base substitution. Moreover, scarless removal of a selection cassette remains laborious to engineer, often requiring negative selection strategies. Sampling-based selection is an alternative strategy to identify desired clones. Although broadly applicable, this approach is especially helpful when generating delicate disease models that require solitary integration of their respective mutation. Sampling-based selection generally involves enrichment for cells that obtained transient expression of the designer nuclease. A common strategy relies on FACS-based enrichment of transfected cells via co-expression of 2A-GFP[92] or the use of fluorescently labelled tracrRNA[93]. Alternatively, if the cell line is not compatible with FACS, transient puromycin selection can be used instead[94]. When integrating

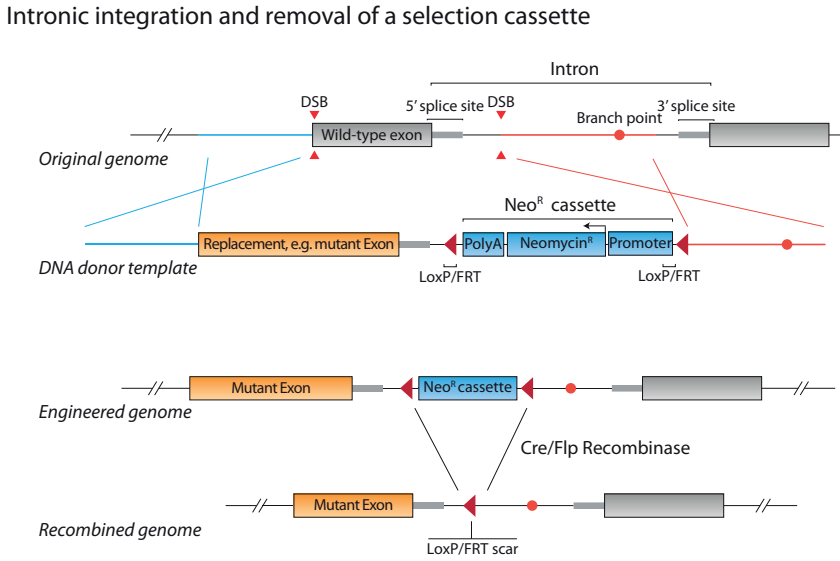

Figure 5. Intronic integration and removal of a selection cassette.
Schematic representation of HDR via a large DNA donor template that includes an autonomous selection cassette (in the opposite transcriptional orientation) to provide neomycin resistance. The selection cassette is integrated in the intron downstream of the integration site. Ideally the positioning of the cassette is in close proximity to the intended modification (mutant exon) to minimize internal homology. However, it is essential that sequences and relative locations of important regulatory elements for correct splicing remain intact (such as the 5' splice donor site and the 3' branch point). After clonal selection, the cassette is ideally removed from the genome in order to exclude undesired influence of the selection cassette on the expression levels of the endogenous gene. Multiple strategies exist for removal, for instance via Cre/Flp mediated recombination of LoxP or Frt sites that flank the cassette (red triangles). The minimal left-over sequence, in this case a single recombination site of ~30nt, is often referred to as a scar sequence. Scar-free removal strategies are available (see text).

epitope tags and other small modifications, the frequency of correctly modified clones can be estimated within the bulk population using TIDER, an adaptation of the popular TIDE algorithm which decomposes Sanger sequencing data generated from multiple alleles[95,96]. This will provide the researcher with an impression of the number of clones that need to be screened in order to obtain a correctly modified clone. In the next section we will discuss the use of TIDER or PCR-based strategies to determine the zygosity state of the modified alleles within individual clones.

We recommend sampling-based selection for modifications that are compatible with ssDNA donor design since these can often be integrated with relatively high efficiency. We advise against sampling-based selection when: (i) integrating large DNA donor templates that often suffer from low integration efficiencies; (ii) when working with model systems that are

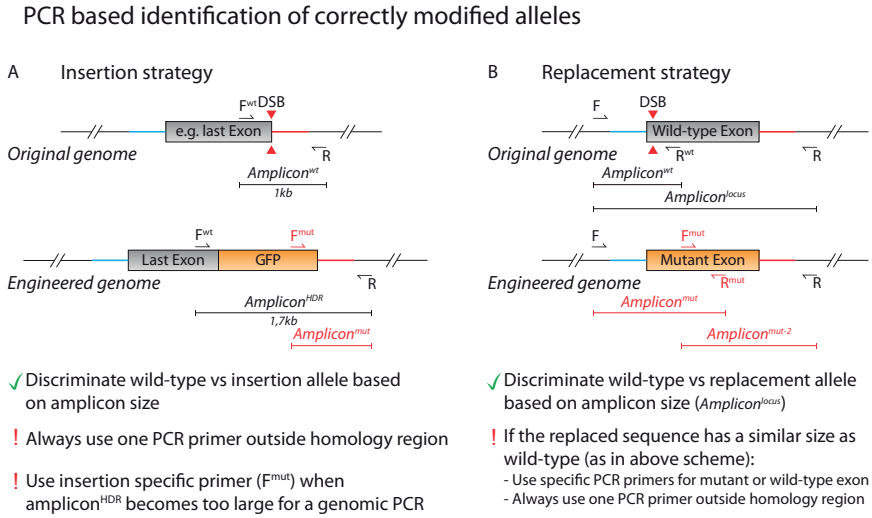

Figure 6. PCR-based identification of correctly modified alleles.
PCR-based assays can be employed to expedite screening of clones for correctly modified alleles (**A**). For insertion strategies, zygosity can be determined by discrimination between PCR amplicon sizes spanning the integration site. Subsequently, sequence integrity can be confirmed by sequencing of the amplicons. (**B**) Discrimination based on size is not always possible when replacing DNA sequences with modified versions. Sequence specific primers can be used to generate amplicons that are specific for WT or modified alleles.

relatively laborious to maintain and scale and (iii) when the projected editing efficiency is low.

Screening clones using PCR-based strategies

Once clones are obtained, they have to be screened to confirm correct editing and determine the zygosity of the modified alleles. A straightforward strategy involves the design of primer pairs that are able to discriminate between non-integrated (*wild-type*) and correctly modified alleles. For insertion strategies, this requires a PCR that spans the genomic integration site with at least one primer annealing to endogenous DNA sequences outside the homology arm regions (**Figure 6A**). This approach prevents false positive amplicons in cases where the donor template randomly integrated into the genome. The generated PCR amplicon allows discrimination of wild-type and insertion alleles based on product size. If a clone generates amplicons corresponding to both wild-type and insertion alleles this indicates heterozygosity, whereas the absence of a wild-type amplicon indicates homozygosity. If the integrated sequence is so large that a corresponding amplicon would preclude efficient genomic PCR amplification, a secondary primer can be designed which anneals only to the integrated DNA sequence.

If a genomic sequence is to be replaced, a PCR spanning the corresponding region often allows discrimination between wild-type and replacement alleles based on product size. In cases where both amplicons are of similar size (wild-type and mutant), primer sets should be designed that amplify either wild-type or mutant specific amplicons (**Figure 6B**).

While a single primer set is often able to identify zygosity, we recommend the design of

redundant primer sets since genomic PCR's can be challenging. In addition, PCR amplicons should span the entire modified sequence so that the integrity of correctly modified alleles can be confirmed via DNA sequencing of the amplicons. The absence of indels within the non-recombined wild-type allele can be analyzed by decomposing the Sanger sequencing data using TIDE, or alternatively by subcloning the amplicon into cloning vectors prior to individual Sanger sequencing of multiple clones representing single alleles.

At a glance

- Genomic modifications that do not allow direct selection may require co-introduction of a genetic selection element, expressed either as an independent transcriptional entity or under control of an endogenous promoter.
- Removal of a genetic selection element is crucial to minimize potential artefacts.
- Sampling-based selection is a broadly applicable alternative to genomic selection cassettes and is recommended for modifications that are compatible with ssDNA donor design.
- A single genomic PCR is often able to discriminate between wild-type and modified alleles based on amplicon size.

DONOR COMPOSITION

DNA donor templates can consist of synthesized single-stranded oligodeoxyribonucleotide (ssODN) donors, larger ssDNA fragments, plasmid- or viral-based donor vehicles, and PCR amplified double-stranded (ds)DNA donors. Each donor type offers distinct advantages and has a unique demand for the extent and distribution of homology. In general, the donor type that is best suited for the introduction of a particular modification depends on the size of the modification, but also on the selection strategy that can be used.

ssDNA donors

Efficient ssDNA donor integration via HDR pathways can be stimulated by a DSB or DNA nick(s)[53,72]. The compact nature of ssDNA donors results in a relatively high concentration of donor molecules within each cell, which is thought to enhance the probability of alignment between the donor and target locus[52]. Indeed, precise editing efficiency is generally higher when mediated by ssDNA donors as compared to plasmid-based donor vectors[21]. Moreover, editing efficiency increases proportionally with donor concentration[97].

Commercially synthesized ssODN donors allow efficient integration of modifications up to ~60 nt during synthesis-dependent strand annealing (SDSA) mediated repair of Cas9 induced DSBs[53]. The proposed mechanism of SDSA is relevant for this discussion. It involves: (i) 5' end resection of the cleaved genomic strands and subsequent base pairing with the 3'

arm of the ssODN; (ii) extension of the genomic sequence using the ssODN as a template and (iii) capture of the opposite genomic strand by the newly synthesized homology[6]. Many studies have contributed to optimal design parameters for ssODN donors in conjunction with blunt-end DNA cleavage, which we summarized in **Figure 7A**. Work by Richardson *et al.* initially suggested that ssODN polarity (i.e. ssODN in sense or antisense orientation) should be complementary to the strand that is not heteroduplexed with Cas9[52]. However, this finding has not been consistent with subsequent studies[42,98,99]. Paix *et al.* propose an alternative model where ssODN polarity should be adjusted such that base pairing between the 3' arm of the ssODN and the genomic strand is not interrupted by the intended modifications[69]. As a consequence, optimal ssODN polarity depends on the relative position of the generated DSB in relation to the integration site. If the DSB is generated downstream of the intended integration site then a sense ssODN should be preferred, whereas cleavage upstream of the integration site favours an antisense ssODN. The polarity rule by Paix *et al.* is in agreement with the performance of ssODNs in the study by Richardson *et al.* and with other published work[52,98,99]. In addition to polarity, the length and distribution of homology should be considered. Richardson *et al.* proposed that the 5' arm has a greater demand for homology[52]. This asymmetric distribution of homology has been confirmed in an independent study by Liang *et al.*[98]. In addition, while in a study by Guo *et al.* an asymmetric ssODN underperformed, we note that the asymmetric ssODN had an unfavourable polarity according to Paix et al. while the symmetric ssODN had the correct polarity, which may explain the underperformance of the asymmetric ssODN[99]. We therefore recommend ssODN polarity according to Paix *et al.* with an asymmetric distribution of homology of 30–36 nt at the 3' and 67–91 nt at the 5' of the ssODN according to Richardson *et al.* Finally, the stability of the ssODN, and thus the editing efficiency, is significantly enhanced by phosphorothioate (PS) modifications of the last two nucleotide bonds at both the 3' and 5' end[98], which can be included during commercial synthesis. Collectively, these design rules have been established using Cas9 mediated cleavage although they will likely translate to Cpf1 mediated cleavage as well.

We recommend the use of ssODNs for the precise generation of modifications ranging from single nucleotide insertions or deletions to small epitope tags and multi-codon deletions. When a single ssODN is used to introduce two or more modifications that are spaced apart, the intervening region should be recoded using silent mutations[69]. As a consequence, the entire region between the proximal and distal modifications is likely treated as a single region of heterology[53]. Although this might negatively impact overall integration efficiency, it will favour simultaneous incorporation of all modifications since internal homology is prevented[53,69].

If a single point mutation is desired, we strongly encourage the researcher to explore whether a base-editor is applicable. Base-editors trigger nucleotide-conversion after being targeted to specific genomic loci based on their fusion to catalytically-dead or nickase Cas9. As a result, base-editors can efficiently mediate any single nucleotide substitution without genomic cleavage[100–102].

Since base-editors do not rely on cleavage, no indel mutations are introduced within the secondary allele, keeping its coding sequence intact and preventing 'functional loss-of-heterozygosity'. As such, base-editors are optimal for introducing heterozygous point mutations, like oncogenic mutations. Similarly, two or more nucleotide substitutions can

be integrated without compromising the secondary allele by stimulating ssODN mediated editing via a DNA nick[52,53]. Although polarity of the ssODN with respect to the generated nick determines the preferred HDR pathway, it has little influence on editing efficiency. Moreover, while optimal ssODN composition for this mode of nick editing has not been determined, an ssODN with 77 nt homology arms was integrated at roughly half the efficiency when stimulated by a DNA nick as compared to a DSB[53].

Commercial ssDNA is now available up to 2 kb, which allows highly efficient generation of modifications that previously required construction of a dedicated donor vector[71,103,104]. Precise genome editing by long ssDNA donors is likely mediated by the single-strand annealing pathway instead of SDSA. As such, the optimal design parameters for long ssDNA donors are likely to be different from ssODN design and have yet to be fully determined. Nevertheless, efficient editing is achieved with homology arms of 50–300 nt with no clear preference for a particular polarity of the ssDNA (**Figure 7B**). We highly recommend long ssDNA donors for modifications that are too large for ssODN synthesis. The only exceptions are current size restrictions and sequence complexities that are rejected by commercial suppliers, such as high GC content.

PCR-generated dsDNA donors

Commercial synthesis of long ssDNA can be expensive and when performed 'in-house' requires construction of a vector with an appropriately located T7 promoter[103]. A PCR generated dsDNA donor is a cheap alternative which is especially useful for medium sized insertions that allow direct selection, e.g. fluorescent knock-in alleles. Homology arms up to 80 nt (or even longer via a nested PCR) can be appended to the desired insertion as overhangs in the PCR primers (**Figure 7C**)[105–107]. The integration efficiency observed for PCR-generated donors is similar to that of traditional donor vectors[108].

Plasmid or viral donor vectors

Modifications that are too large for ssDNA synthesis require construction of a viral or plasmid-based donor vector using molecular cloning techniques. Since a substantial part of these vectors consists of backbone elements such as bacterial selection cassettes or viral packaging sequences, the effective donor template concentration per cell is disproportionally reduced compared to ssDNA donors. On the other hand, donor vectors have sufficient capacity to include a genomic selection cassette, making absolute editing efficiency less important.

Traditionally, donor vectors required relatively large homology arms of up to 2 kb in order facilitate efficient HR mediated donor integration by a designer nuclease-generated DSB[67,108]. Homology arm length of donor vectors can be reduced to 0.6–0.9 kb by flanking the donor with nuclease target sites that are identical to the genomic target site (**Figure 7D**). As a consequence, a linear donor supply is liberated concurrent with genomic cleavage[108,109]. The linear nature and relatively long homology arms of the excised donor fragment is thought to stimulate a novel HDR pathway, themed homology-mediated end joining [109]. Currently, no direct negative consequences of in-vivo donor excision have been reported, and since nuclease target sites are easily included as overhangs in the PCR amplification of the homology arms, the construction of this type of dual-cut donor vector does not require extra labor. Moreover, a donor vector that is flanked with nuclease target sites is compatible with a novel strategy

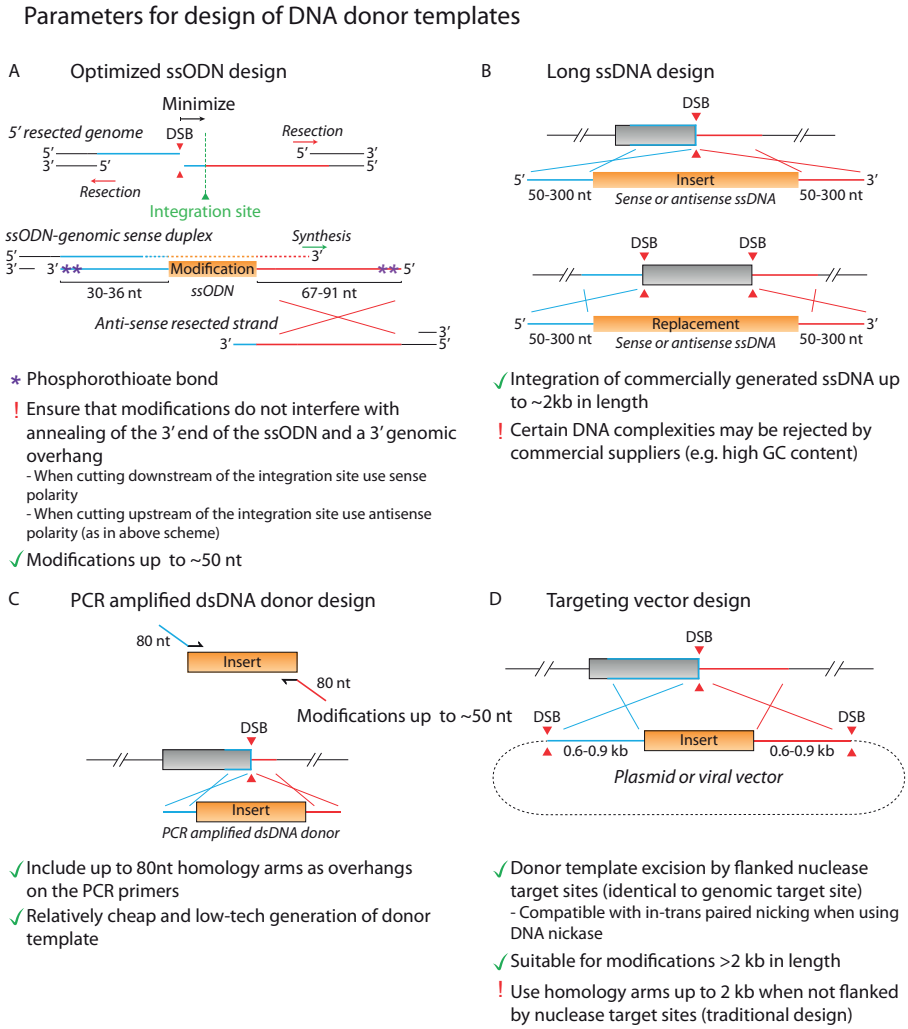

Figure 7. Parameters for donor template design.
(**A**) Schematic representation of ssODN template integration stimulated by a DSB (red arrow heads). Due to 5' DNA end resection by DNA repair pathway associated proteins, an ssODN can be designed to either hybridize in the sense or antisense orientation. Complete hybridization from the 3' end of the ssODN towards the DNA strand extremity (DSB site) is advised. In this example, ssODN hybridization with the antisense genomic resected overhang (red) would lead to mismatches, whereas hybridization with the sense overhang (blue) does not. Furthermore, homology should be distributed in an asymmetric fashion in favour of the 5' homology arm. Phosphorothioate bonds prevent ssODN degradation. (**B**) Schematic representation of HDR using long ssDNA templates. (**C**) Schematic representation of HDR using PCR amplified dsDNA donor. Homology arms up to 80nt can be added to conventional PCR primers as 3' overhangs. (**D**) Schematic representation of HDR using a donor vector. Vectors can be assembled as complex donor templates from multiple sources. Flanking of the template with nuclease target sites identical to the genomic target site allows excision and linearization of the template concurrent with genomic cleavage.

called in trans paired nicking[50], where concurrent nicking of the genome and donor triggers efficient integration without genomic cleavage. However, it remains unclear whether this

strategy can trigger replacement of genomic sequence.
We expect donor vectors flanked with nuclease target sites to develop into the preferred strategy for the integration or substitution of large transgenic elements. Since the homology arms of these vectors are relatively short, vector construction and subsequent genotyping is far more convenient when compared to the use of traditional donor vectors with longer homology arms.

At a glance

- Due to the absence of backbone sequences ssDNA donors result in a high effective donor concentration which improves editing efficiency.
- Modifications up to ~60 nt can be integrated using ssODN donors. Optimized ssODNs are constructed with an asymmetric distribution of homology and a polarity determined by the position of the DSB relative to the intended integration site.
- Modifications up to 1.9 kb can be integrated using commercially available long ssDNA donors.
- PCR generated donors with short homology arms allow cost efficient generation of fluorescent knock-in alleles.
- Modifications too large for ssDNA donor templates require vector construction. By flanking the donor with nuclease target sites, the homology demand can be reduced to 0.6–0.9 kb.

DELIVERY OF HDR COMPONENTS

Efficient delivery of genome editing components into target cells is a crucial step in the process towards generation of genetically modified model systems. The delivery method should be matched to the model system of choice and to the manner in which the designer nuclease and donor are presented to the cell.

In vitro delivery

To date, most publications involving precise CRISPR-mediated genome editing have used established transfection methods including liposomal transfection, electroporation and peptide-mediated cell penetration, to deliver nuclease expression constructs and donor templates into target cells[23,110–113]. Although generally robust and broadly applicable, plasmid delivery has particular drawbacks that should be considered. Foremost, the introduction of high concentrations of foreign DNA into cells can trigger an immune response in certain cell types, which can eventually lead to programmed cell death[114]. In addition, prolonged expression of nucleases from plasmid DNA increases the frequency of indel mutations at

off-target sites[115,116] and along similar lines, prolonged stability of plasmid DNA increases the probability of random plasmid integration into the genome. To circumvent these issues, nucleases can be delivered as pre-assembled ribonucleoprotein complexes (RNPs) or as mRNA molecules along with *in vitro* transcribed or commercially synthesized gRNA[115,117,118]. Messenger RNA is significantly less stable compared to plasmid DNA, resulting in a relatively short but robust spike of nuclease activity. Similarly, RNP delivery circumvents translation, resulting in an immediate spike of nuclease activity followed by a rapid decline due to protein degradation. In each case, nuclease activity is short lived, which reduces the probability of generating off-target indels. Furthermore, the immediate spike in nuclease activity ensures co-presence with initial high concentrations of DNA donor templates prior to their degradation. Indeed, RNP delivery in particular is associated with a significant increase in precise genome editing efficiency[98,119]. In addition, since assembly of RNPs or delivery of mRNA is compatible with chemically modified gRNA, these protocols open up new avenues of maximizing editing efficiency.

Some cell lineages, such as primary cells, remain difficult to transfect with classical transfection methods. Instead, these cells are often virally transduced[120]. However, the cargo restrictions of many viral vectors often prohibit CRISPR mediated genome editing applications. BacMam technology, which employs baculoviral vectors that have the capacity to carry large DNA cargo up to 38 kb in length[121], has recently been used to address viral cargo issues. All the components required to support CRISPR-mediated precise integration of large DNA constructs, including the donor template itself, can be integrated within a single baculoviral genome[122,123]. In addition, transduction in mammalian cells occurs in a transient manner by default, thereby minimizing the risk of viral integration into the host genome. However, since viral transduction is associated with general safety risks, alternative transfection methods are under continuous development[124,125].

While common *in vitro* plasmid delivery methods have been widely applicable in mono-layer cell cultures, transfection of 3D organoid cultures is more challenging. Although both transfection and electroporation can successfully deliver plasmids in organoid structures, the resulting transfection efficiency is generally low[77,110,111]. An optimized electroporation protocol has demonstrated significantly improved transfection efficiency in comparison to liposomal transfection[111]. Nevertheless, cell viability post transfection generally remains low and consequently large quantities of organoid-derived cells are required in order to obtain successfully edited clones. Alternatively, human intestinal organoids have been virally transduced to deliver CRISPR machinery, however this method is not compatible with ssDNA donor delivery[123].

To conclude, delivery of nuclease expression constructs following conventional protocols is convenient for less demanding applications such as heterozygous modifications that allow direct selection. RNP delivery, in particular when assembled with enhanced chemically modified gRNA, supports highly efficient precise editing in conjunction with ssDNA donors[72,98], and more recently in combination with AAV donor transduction[126]. Therefore, we encourage the use of RNP delivery protocols whenever applicable, and especially when generating modifications that depend on a sampling-based selection approach. In this regard, enrichment of an RNP transfected population can be achieved by assembling RNPs with fluorescent tracrRNA[93]. Finally, cell lines that are particularly difficult to transfect can usually

be virally transduced. In this regard, viral-based delivery of genome editing components may be useful as a platform for the precise incorporation of a particular modification across many different cell lines of the same organism.

In vivo delivery

Although significant progress has been made in the development of *in vitro* delivery protocols that target a cellular population in its completeness, *in vivo* delivery is far more challenging. Initial publications demonstrated proof-of-principle *in vivo* HDR-mediated genome editing in adult mice using non-viral hydrodynamic tail vein injections, co-delivering Cas9-sgRNA expression constructs and ssODN donor template into the liver[127,128]. However, among other things due to inferior delivery methods, HDR-mediated gene editing efficiency remained very low. The sporadic introduction of cancer mutations *in vivo* for the rapid development of human cancer models in mice has mainly been supported by locally injected lentiviral transduction[129,130]. Further development of these protocols may benefit from the latest generation of high-capacity adenoviral vectors that are able to carry both the nuclease and gRNA scaffolds in one viral particle[131].

The ultimate clinically-related goal of highly efficient genome editing is to correct disease mutations and phenotypes in living patients in terms of personalized medicine. In contrast to *in vitro* culture systems that allow clonal selection and outgrowth of successfully modified cells, most disease phenotypes for which *in vivo* genome editing is considered a potential clinical break-through require mutational correction in a large fraction of cells that manifest the diseased phenotype. Delivery methods to accommodate this level of precise nuclease mediated editing are currently out of reach. In addition, since many genetic conditions are caused by single point mutations, base editors are a far more likely candidate for clinical translation. Since the scope of our review is to facilitate guidelines for researchers that would like to genetically engineer their preferred model system, we refer to a number of excellent reviews with respect to *in vivo* genome editing for clinical applications[132–134].

At a glance

- Plasmid based nuclease delivery is convenient for less demanding applications such as heterozygous modifications that allow direct selection.
- We encourage the use of RNP delivery protocols in conjunction with chemically modified gRNA, especially when depending on a sampling-based selection approach.
- BacMam technology is recommended for the generation of large genomic modifications in difficult to transfect cell lines, since it allows the delivery of all HDR components in a single construct.
- Clinical applications of CRISPR-mediated precise gene correction are currently out of reach.

COMPLEMENTARY STRATEGIES TO ENHANCE PRECISE EDITING EFFICICIENY

In addition to optimized donor template design, nuclease choice, genomic target site selection and delivery, there are additional complementary strategies that may further enhance CRISPR-mediated HDR efficiency. A major focus has been the development of tools to suppress the competing NHEJ repair pathway. Strategies include depletion or inhibition of the NHEJ pathway proteins KU70, KU80 and DNA ligase IV using either shRNAs[107,135], Adenovirus 4 (Ad4) proteins[135], or molecular inhibition of DNA ligase IV via small molecule inhibitors such as SCR7[107,135–138]. Similar to observations in DNA ligase IV-deficient flies, depletion or inhibition of DNA ligase IV reduced NHEJ activity, while increasing HDR in both mouse and mammalian cell lines[135,136,139]. A similar effect was observed upon the depletion of the KU complex[137]. NHEJ pathway suppression may be of particular interest when generating homozygous mutations, as the Ad4 protein-induced degradation of DNA ligase IV enhanced the net yield of homozygous clones when used in combination with selection markers[135]. However, significant care should be taken when using the SCR7 compound, as it can enhance the number of off-target integrations and induces cell toxicity when used at high concentrations. Also, the sensitivity to NHEJ inhibition seems to be cell type-specific, as improvements in HDR efficiency varied significantly between cell lines and often does not result in a notable beneficial effect[107,108,136]. The search for compounds that enhance HDR continues. One study demonstrated resveratrol to be an even more potent enhancer of HDR-mediated genome editing efficiency when compared to SCR7[138], albeit the molecular mechanism governing its therapeutic properties remain elusive[140]. In addition, two new compounds that enhance Cpf1-mediated HDR have recently been identified[141].

Another interesting approach is cell cycle synchronization in combination with timed Cas9 RNP delivery to focus nuclease activity to the G2/M-phase of the cell cycle when HDR is dominant. Indeed, cell cycle synchronization prior to Cas9 RNP delivery resulted in a significant increase in HDR efficiency in a variety of cell types[8,97,108]. As expected, this also reduced the frequency of NHEJ events[108]. In addition, the minimal concentration of Cas9 RNPs and donor DNA for sufficient HDR was substantially lower[8,97]. However, cell cycle inhibitors by themselves may significantly affect cell viability, thereby decreasing the effective number of targetable cells in the population[8]. In addition, several reports demonstrated that combining NHEJ inhibition and cell cycle synchronization did not further improve HDR efficiency, suggesting that HDR is already the predominant repair pathway during the G2/M-phase[8].

Several reports have investigated the effect of temperature on nuclease mediated HDR. For instance, cold shock treatment at 32 °C for 24–48 h post transfection was shown to enhance Cas9 mediated HDR in human induced pluripotent stem cells[99]. However, a similar protocol turned out to be detrimental to Cas9 induced HDR in many other human cell types[142]. A relative heat shock to 34 °C in zebra fish significantly enhanced Cpf1 mediated HDR but had no effect on Cas9 mediated HDR[42]. Collectively these results suggest that the effect of temperature on HDR rates requires further investigation before it should be generally applied. Although complementary strategies are useful in the context of maximizing precise editing

efficiency, we advise against using these strategies by default. Rather, they should be used in parallel or as a back-up plan when initial genome editing strategies yielded an insufficient number of clones.

At a glance

- Inhibition of NHEJ, either via co-expression of Adenovirus 4 proteins or via small molecule inhibitors of DNA ligase IV, can enhance HDR-mediated genome editing.
- Cell cycle synchronization in the G2/M-phase combined with timed RNP delivery induces nuclease activity in the HDR dominant phase of the cell cycle.
- Complementary strategies should not be used by default but rather in parallel or as a backup strategy.

DISCUSSION

In the last couple of years, CRISPR-mediated genome editing has evolved at a very rapid pace. The expansion of the CRISPR-associated toolkit and our increased understanding of the molecular mechanisms that govern HDR have improved our ability to accurately edit mammalian genomes. Whereas many reviews have shed light on the historical and molecular background of CRISPR technology, up-to-date guidelines with respect to the design of HDR-mediated genome editing strategies were lacking. This review aims to function as a decision-making guide to assist researchers in using state-of-the-art genetics to generate mutant variants of their model system. It should be of special interest to classical cell biologists and biochemists without extensive genetic backgrounds. Especially in 2D cell cultures, introducing disease-related point mutations or protein fusions at endogenous loci is highly efficient. Indeed, solely relying on transient overexpression of (mutant) effector proteins is no longer recommended since scientific standards increasingly demand genetic modifications at endogenous loci. However, we stress the importance of a well thought out genome editing strategy in advance, since the entire process from design to a validated model system may still require a couple of months work. To summarize the current knowledge, opportunities and strategic options available to researchers, we will discuss three different design examples where many aspects discussed in this review will be placed into a real context.

Example 1 (**Figure 8A**): Homozygous loss of phenylalanine at position 508 of the Cystic Fibrosis transmembrane conductance regulator (CFTR) is the most frequent genetic variant that causes Cystic Fibrosis[143]. An accurate human model system will require homozygous deletion of F508 without additional genetic scarring. The small size and homozygous nature of the deletion strongly favours an ssODN donor. A SpCas9 target site is available that cleaves just one nucleotide upstream of the deletion site, favouring an antisense ssODN designed with an asymmetric distribution of homology. Since deletion of F508 will destroy the Cas9 target site, no additional silent mutations are required within the donor. Although the selected

target site has a poor predicted on-target efficiency, better performing target sites cleave further away from the deletion site, likely leading to an overall decrease in performance when working with an ssODN. In addition, no well positioned Cpf1 target sites are available. RNP transfection will maximize editing efficiency, which enhances the isolation of homozygous clones. Since direct selection for F508 CFTR is not available, RNPs will be assembled with chemically stabilized fluorescent tracrRNA in combination with commercially synthesized and chemically stabilized CRISPR-RNA containing the guide sequence. Fluorescent tracrRNA allows FACS-based single cell sorting of transfected cells. In addition, isolating a bulk population for TIDER analysis will give an estimate for the frequency of homozygous clones.

Example 2 (**Figure 8B**): Overexpression of fluorescent fusion proteins illuminates cell biology at the costs of altering protein homeostasis and potentially protein function. In contrast, endogenous tagging of the respective genes is potentially less invasive and probably truer to nature. Fluorescent beta-actin (ACTB) fusions are popular in cell biology[144]. In order to insert mNeongreen (a bright monomeric green fluorophore[145] at its C-terminus in a human cell line, we selected a highly active SpCas9 target site that cleaves within the stop codon of ACTB. The mNeongreen coding sequence will be fused in frame to the C-terminus of hACTB via a 3xGSS flexible linker[144], thereby also disrupting the selected SpCas9 target site. Considering the size of the modification, integration efficiency is maximized by using an ssDNA donor. About 100 nt downstream of the stop codon, the 3' UTR runs into a stretch of sequence complexity which commercial suppliers currently reject. We therefore limited the length of the 3' homology arm of the sense ssDNA donor to 100 nt. By contrast, 5' homology is more flexible which we extended to 200 nt, providing an extra buffer against 5' degradation. The nature of the modifications allows direct selection by FACS and may even permit enrichment for homozygous clones if desired. Correct integration of the template, as well as its zygosity, can easily be determined using a single PCR that spans the integration site. In addition, an additional primer set can be designed with one primer placed on top of the nuclease cleavage site to facilitate identification of heterozygous clones where the secondary allele remained intact.

Example 3 (**Figure 8C**): Patient-derived organoids recapitulate the stem cell driven differentiation hierarchy of self-renewing tissues, among others enabling the study of lineage differentiation[146]. Unfortunately, genetic modification of organoids via sampling-based selection is often prohibited by poor transfection efficiency and laborious clonal expansion. In addition, when modifying a gene that is exclusively expressed in a terminally differentiated cell state, many direct selection strategies are problematic. A C-terminal P2A-CreERT2 fusion to Keratin 20 (KRT20) allows genetic lineage tracing within the enterocyte lineage of human colon organoids[147]. In order to select for this C-terminal fusion, a selection cassette is integrated within the 3' UTR at an unconserved position. The orientation of the selection cassette is not important in this instance since the cassette will be removed using Flp-mediated recombination in an undifferentiated population of cells. Due to the size of the modification (~4 kb) and sequence complexity of the selection cassette, donor vector construction is required. During assembly of the donor vector, both homology arms should by flanked by a copy of the genomic target sequence. This approach will enable both in trans paired nicking as well as linear donor excision concurrent with genomic cleavage. While the

relative position of the selection cassette with respect to CreERT2 creates a limited stretch of internal homology between the endogenous 3'UTR and the donor template, we recommend against introducing point mutations within the start of the 3' UTR in order to avoid disruption of potential regulatory motifs. Instead, we minimize homology by placing the cassette in close proximity to the last exon.

Innovative genome editing technologies will continue to be developed, thereby constantly modifying and changing existing editing procedures and methods. A recent innovation is RNP-donor conjugates that aim to deliver the DNA donor template directly at the site of nuclease activity[148,149]. In addition, assembly of donor vectors by molecular cloning may soon be unnecessary as better ssDNA synthesis protocols are being developed[150]. Ultimately, considering the progression toward nick-mediated editing and base-editors, we anticipate that the future of complex genome editing might not even involve nuclease activity at all.

Figure 8. Designing genome editing strategies: 3 real examples.
(**A**) Schematic work ow of the practical steps and the sequence information for the process of generating F508 CFTR mutant cell lines. Top: The dsDNA sequence of the CFTR gene is presented around the intended modification site. In between the corresponding amino acid sequence is depicted. As a donor template, an asymmetric antisense ssODN is advised (see text). (**B**) Schematic work ow of the practical steps and the sequence information for the process of generating an mNeongreen knock-in at the C-terminus of hACTB in cell lines. Top: The dsDNA sequence of the hACTB gene is presented around its endogenous stop codon. The corresponding amino acid sequence is depicted in between the dsDNA. An ssDNA donor template is depicted below the schematic representation of the hACBT locus. Rationale for strategy design is described in the text. (**C**) Schematic work ow of the practical steps and the sequence information for the process of generating a CreERT2 knock-in in the hKRT20 locus via a P2A fusion at its C-terminus in human colon organoids. Top: A stretch of dsDNA sequence of the 3'UTR of the hKRT20 gene is presented. Below the locus is a schematic representation of the donor plasmid. Rationale for strategy design is described in the text. Yellow arrow indicates gRNA. Cleavage sites (DSB) are indicated with red arrow heads. PAM sequences are underscored.

Genome editing design examples

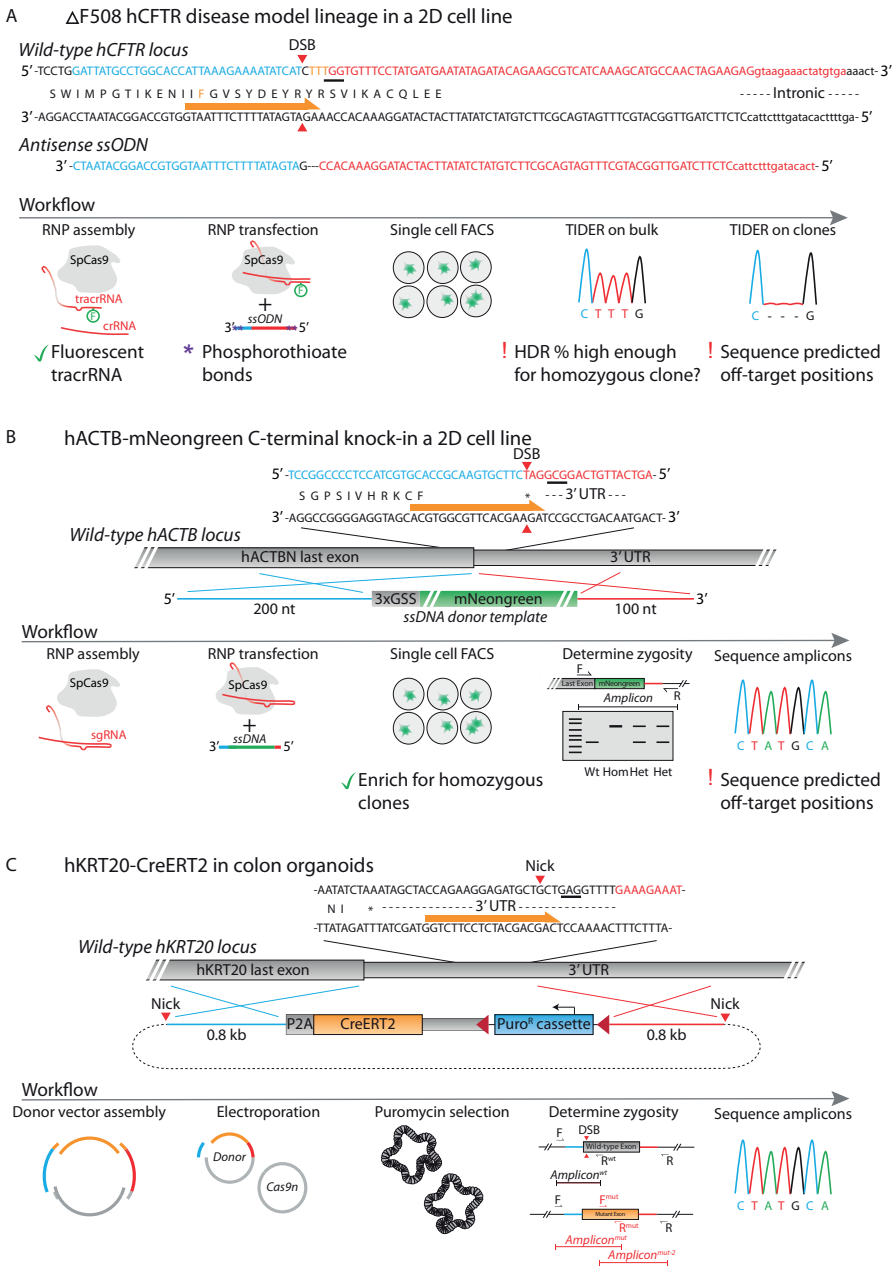

REFERENCES

1. Blasco RB, Karaca E, Ambrogio C, et al. Simple and Rapid InVivo Generation of Chromosomal Rearrangements using CRISPR/Cas9 Technology. *Cell Rep*. 2014. doi:10.1016/j.celrep.2014.10.051
2. Song Y, Yuan L, Wang Y, et al. Efficient dual sgRNA-directed large gene deletion in rabbit with CRISPR/Cas9 system. *Cell Mol Life Sci*. 2016. doi:10.1007/s00018-016-2143-z
3. Wolfs JM, Hamilton TA, Lant JT, et al. Biasing genome-editing events toward precise length deletions with an RNA-guided TevCas9 dual nuclease. *Proc Natl Acad Sci*. 2016. doi:10.1073/pnas.1616343114
4. Chapman JR, Taylor MRG, Boulton SJ. Playing the End Game: DNA Double-Strand Break Repair Pathway Choice. *Mol Cell*. 2012. doi:10.1016/j.molcel.2012.07.029
5. Pfeiffer P, Goedecke W, Obe G. Mechanisms of DNA double-strand break repair and their potential to induce chromosomal aberrations. *Mutagenesis*. 2000.
6. Saleh-Gohari N, Helleday T. Conservative homologous recombination preferentially repairs DNA double-strand breaks in the S phase of the cell cycle un human cells. *Nucleic Acids Res*. 2004. doi:10.1093/nar/gkh703
7. Heyer W-D, Ehmsen KT, Liu J. Regulation of Homologous Recombination in Eukaryotes. *Annu Rev Genet*. 2010. doi:10.1146/annurev-genet-051710-150955
8. Yang D, Scavuzzo MA, Chmielowiec J, Sharp R, Bajic A, Borowiak M. Enrichment of G2/M cell cycle phase in human pluripotent stem cells enhances HDR-mediated gene repair with customizable endonucleases. *Sci Rep*. 2016. doi:10.1038/srep21264
9. Chan F, Hauswirth WW, Wensel TG, Wilson JH. Efficient mutagenesis of the rhodopsin gene in rod photoreceptor neurons in mice. *Nucleic Acids Res*. 2011. doi:10.1093/nar/gkr196
10. Rothkamm K, Kruger I, Thompson LH, Lobrich M. Pathways of DNA Double-Strand Break Repair during the Mammalian Cell Cycle. *Mol Cell Biol*. 2003. doi:10.1128/mcb.23.16.5706-5715.2003
11. Maresca M, Lin VG, Guo N, Yang Y. Obligate ligation-gated recombination (ObLiGaRe): Custom-designed nuclease-mediated targeted integration through nonhomologous end joining. *Genome Res*. 2013. doi:10.1101/gr.145441.112
12. Suzuki K, Tsunekawa Y, Hernandez-Benitez R, et al. In vivo genome editing via CRISPR/Cas9 mediated homology-independent targeted integration. *Nature*. 2016. doi:10.1038/nature20565
13. Nakade S, Tsubota T, Sakane Y, et al. Microhomology-mediated end-joining-dependent integration of donor DNA in cells and animals using TALENs and CRISPR/Cas9. *Nat Commun*. 2014. doi:10.1038/ncomms6560
14. Sakuma T, Nakade S, Sakane Y, Suzuki KIT, Yamamoto T. MMEJ-Assisted gene knock-in using TALENs and CRISPR-Cas9 with the PITCh systems. *Nat Protoc*. 2016. doi:10.1038/nprot.2015.140
15. Yao X, Wang X, Liu J, et al. CRISPR/Cas9 – Mediated Precise Targeted Integration In Vivo Using a Double Cut Donor with Short Homology Arms. *EBioMedicine*. 2017. doi:10.1016/j.ebiom.2017.05.015
16. Müller U. Ten years of gene targeting: Targeted mouse mutants, from vector design to phenotype analysis. *Mech Dev*. 1999. doi:10.1016/S0925-4773(99)00021-0
17. Hasty P, Rivera-Pérez J, Bradley A. The length of homology required for gene targeting in embryonic stem cells. *Mol Cell Biol*. 2015. doi:10.1128/mcb.11.11.5586
18. Storici F, Durham CL, Gordenin DA, Resnick MA. Chromosomal site-specific double-strand breaks are efficiently targeted for repair by oligonucleotides in yeast. *Proc Natl Acad Sci*. 2003. doi:10.1073/pnas.2036296100
19. Urnov FD, Miller JC, Lee YL, et al. Highly efficient endogenous human gene correction using designed zinc-finger nucleases. *Nature*. 2005. doi:10.1038/nature03556
20. Miller JC, Tan S, Qiao G, et al. A TALE nuclease architecture for efficient genome editing. *Nat Biotechnol*. 2011. doi:10.1038/nbt.1755
21. Cong L, Zhang F. Genome engineering using crispr-cas9 system. In: *Chromosomal Mutagenesis: Second Edition*. ; 2014. doi:10.1007/978-1-4939-1862-1_10
22. Drost J, van Jaarsveld RH, Ponsioen B, et al. Sequential cancer mutations in cultured human intestinal stem cells. *Nature*. 2015;521(7550):43-47. doi:10.1038/nature14415
23. Jinek M, East A, Cheng A, Lin S, Ma E, Doudna J. RNA-programmed genome editing in human cells. *Elife*. 2013. doi:10.7554/elife.00471
24. Jinek M, Chylinski K, Fonfara I, Hauer M, Doudna JA, Charpentier E. A programmable dual-RNA-guided DNA endonuclease in adaptive bacterial immunity. *Science (80-)*. 2012. doi:10.1126/science.1225829
25. Ran FA, Hsu PD, Lin C-Y, et al. Double nicking by RNA-guided CRISPR Cas9 for enhanced genome editing specificity. *Cell*. 2013. doi:10.1016/j.cell.2013.08.021
26. Kleinstiver BP, Pattanayak V, Prew MS, et al. High-fidelity CRISPR-Cas9 nucleases with no detectable

genome-wide off-target effects. *Nature*. 2016. doi:10.1038/nature16526
27. Slaymaker IM, Gao L, Zetsche B, Scott DA, Yan WX, Zhang F. Rationally engineered Cas9 nucleases with improved specificity. *Science (80-)*. 2016. doi:10.1126/science.aad5227
28. Guilinger JP, Thompson DB, Liu DR. Fusion of catalytically inactive Cas9 to FokI nuclease improves the specificity of genome modification. *Nat Biotechnol*. 2014. doi:10.1038/nbt.2909
29. Kleinstiver BP, Prew MS, Tsai SQ, et al. Broadening the targeting range of Staphylococcus aureus CRISPR-Cas9 by modifying PAM recognition. *Nat Biotechnol*. 2015. doi:10.1038/nbt.3404
30. Hirano H, Gootenberg JS, Horii T, et al. Structure and Engineering of Francisella novicida Cas9. *Cell*. 2016. doi:10.1016/j.cell.2016.01.039
31. Hou Z, Zhang Y, Propson NE, et al. Efficient genome engineering in human pluripotent stem cells using Cas9 from Neisseria meningitidis. *Proc Natl Acad Sci U S A*. 2013. doi:10.1073/pnas.1313587110
32. Hu JH, Miller SM, Geurts MH, et al. Evolved Cas9 variants with broad PAM compatibility and high DNA specificity. *Nature*. 2018. doi:10.1038/nature26155
33. Ran FA, Cong L, Yan WX, et al. In vivo genome editing using Staphylococcus aureus Cas9. *Nature*. 2015. doi:10.1038/nature14299
34. Kim E, Koo T, Park SW, et al. In vivo genome editing with a small Cas9 orthologue derived from Campylobacter jejuni. *Nat Commun*. 2017. doi:10.1038/ncomms14500
35. Zetsche B, Gootenberg JS, Abudayyeh OO, et al. Cpf1 Is a Single RNA-Guided Endonuclease of a Class 2 CRISPR-Cas System. *Cell*. 2015. doi:10.1016/j.cell.2015.09.038
36. Tu M, Lin L, Cheng Y, et al. A new lease of life': FnCpf1 possesses DNA cleavage activity for genome editing in human cells. *Nucleic Acids Res*. 2017. doi:10.1093/nar/gkx783
37. Dong D, Ren K, Qiu X, et al. The crystal structure of Cpf1 in complex with CRISPR RNA. *Nature*. 2016. doi:10.1038/nature17944
38. Yamano T, Nishimasu H, Zetsche B, et al. Crystal Structure of Cpf1 in Complex with Guide RNA and Target DNA. *Cell*. 2016. doi:10.1016/j.cell.2016.04.003
39. Li B, Zeng C, Dong Y. Design and assessment of engineered CRISPR-Cpf1 and its use for genome editing. *Nat Protoc*. 2018. doi:10.1038/nprot.2018.004
40. Kim HK, Song M, Lee J, et al. In vivo high-throughput profiling of CRISPR-Cpf1 activity. *Nat Methods*. 2017. doi:10.1038/nmeth.4104
41. Zhang Y, Long C, Li H, et al. CRISPR-Cpf1 correction of muscular dystrophy mutations in human cardiomyocytes and mice. *Sci Adv*. 2017. doi:10.1126/sciadv.1602814
42. Moreno-Mateos MA, Fernandez JP, Rouet R, et al. CRISPR-Cpf1 mediates efficient homology-directed repair and temperature-controlled genome editing. *Nat Commun*. 2017. doi:10.1038/s41467-017-01836-2
43. Hsu PD, Scott DA, Weinstein JA, et al. DNA targeting specificity of RNA-guided Cas9 nucleases. *Nat Biotechnol*. 2013. doi:10.1038/nbt.2647
44. Cradick TJ, Fine EJ, Antico CJ, Bao G. CRISPR/Cas9 systems targeting β-globin and CCR5 genes have substantial off-target activity. *Nucleic Acids Res*. 2013;41(20):9584-9592. doi:10.1093/nar/gkt714
45. Mali P, Aach J, Stranges PB, et al. CAS9 transcriptional activators for target specificity screening and paired nickases for cooperative genome engineering. *Nat Biotechnol*. 2013. doi:10.1038/nbt.2675
46. Fu Y, Foden JA, Khayter C, et al. High-frequency off-target mutagenesis induced by CRISPR-Cas nucleases in human cells. *Nat Biotechnol*. 2013. doi:10.1038/nbt.2623
47. Tsai SQ, Zheng Z, Nguyen NT, et al. GUIDE-seq enables genome-wide profiling of off-target cleavage by CRISPR-Cas nucleases. *Nat Biotechnol*. 2015. doi:10.1038/nbt.3117
48. Kulcsár PI, Tálas A, Huszár K, et al. Crossing enhanced and high fidelity SpCas9 nucleases to optimize specificity and cleavage. *Genome Biol*. 2017. doi:10.1186/s13059-017-1318-8
49. Kim S, Bae T, Hwang J, Kim JS. Rescue of high-specificity Cas9 variants using sgRNAs with matched 5' nucleotides. *Genome Biol*. 2017. doi:10.1186/s13059-017-1355-3
50. Chen X, Janssen JM, Liu J, et al. In trans paired nicking triggers seamless genome editing without double-stranded DNA cutting. *Nat Commun*. 2017. doi:10.1038/s41467-017-00687-1
51. Nakajima K, Zhou Y, Tomita A, Hirade Y, Gurumurthy CB, Nakada S. Precise and efficient nucleotide substitution near genomic nick via noncanonical homology-directed repair. *Genome Res*. 2018. doi:10.1101/gr.226027.117
52. Richardson CD, Ray GJ, DeWitt MA, Curie GL, Corn JE. Enhancing homology-directed genome editing by catalytically active and inactive CRISPR-Cas9 using asymmetric donor DNA. *Nat Biotechnol*. 2016. doi:10.1038/nbt.3481
53. Kan Y, Ruis B, Takasugi T, Hendrickson EA. Mechanisms of precise genome editing using oligonucleotide donors. *Genome Res*. 2017. doi:10.1101/gr.214775.116
54. Fu Y, Sander JD, Reyon D, Cascio VM, Joung JK. Improving CRISPR-Cas nuclease specificity using truncated guide RNAs. *Nat Biotechnol*. 2014. doi:10.1038/nbt.2808

55. Singh K, Evens H, Nair N, et al. Efficient In Vivo Liver-Directed Gene Editing Using CRISPR/Cas9. *Mol Ther*. 2018. doi:10.1016/j.ymthe.2018.02.023
56. Ryan DE, Taussig D, Steinfeld I, et al. Improving CRISPR-Cas specificity with chemical modifications in single-guide RNAs. *Nucleic Acids Res*. 2018. doi:10.1093/nar/gkx1199
57. Yin H, Song CQ, Suresh S, et al. Partial DNA-guided Cas9 enables genome editing with reduced off-target activity. *Nat Chem Biol*. 2018. doi:10.1038/nchembio.2559
58. Cromwell CR, Sung K, Park J, et al. Incorporation of bridged nucleic acids into CRISPR RNAs improves Cas9 endonuclease specificity. *Nat Commun*. 2018. doi:10.1038/s41467-018-03927-0
59. Kartje ZJ, Barkau CL, Rohilla KJ, Ageely EA, Gagnon KT. Chimeric Guides Probe and Enhance Cas9 Biochemical Activity. *Biochemistry*. 2018. doi:10.1021/acs.biochem.8b00107
60. Hendel A, Bak RO, Clark JT, et al. Chemically modified guide RNAs enhance CRISPR-Cas genome editing in human primary cells. *Nat Biotechnol*. 2015. doi:10.1038/nbt.3290
61. Yin H, Song C-Q, Suresh S, et al. Structure-guided chemical modification of guide RNA enables potent non-viral in vivo genome editing. *Nat Biotechnol*. 2017. doi:10.1038/nbt.4005
62. McMahon MA, Prakash TP, Cleveland DW, Bennett CF, Rahdar M. Chemically Modified Cpf1-CRISPR RNAs Mediate Efficient Genome Editing in Mammalian Cells. *Mol Ther*. 2018. doi:10.1016/j.ymthe.2018.02.031
63. Wu H, Liu Q, Shi H, et al. Engineering CRISPR/Cpf1 with tRNA promotes genome editing capability in mammalian systems. *Cell Mol Life Sci*. 2018. doi:10.1007/s00018-018-2810-3
64. Doench JG, Fusi N, Sullender M, et al. Optimized sgRNA design to maximize activity and minimize off-target effects of CRISPR-Cas9. *Nat Biotechnol*. 2016. doi:10.1038/nbt.3437
65. Doench JG, Hartenian E, Graham DB, et al. Rational design of highly active sgRNAs for CRISPR-Cas9-mediated gene inactivation. *Nat Biotechnol*. 2014;32(12):1262-1267. doi:10.1038/nbt.3026
66. Cui Y, Xu J, Cheng M, Liao X, Peng S. Review of CRISPR/Cas9 sgRNA Design Tools. *Interdiscip Sci Comput Life Sci*. 2018. doi:10.1007/s12539-018-0298-z
67. Byrne SM, Ortiz L, Mali P, Aach J, Church GM. Multi-kilobase homozygous targeted gene replacement in human induced pluripotent stem cells. *Nucleic Acids Res*. 2015. doi:10.1093/nar/gku1246
68. Vazquez JC, Nogues C, Rucker EB, Piedrahita JA. Factors affecting the efficiency of introducing precise genetic changes in ES cells by homologous recombination: Tag-and-exchange versus the Cre-loxP system. *Transgenic Res*. 1998. doi:10.1023/A:1008888929552
69. Paix A, Folkmann A, Goldman DH, et al. Precision genome editing using synthesis-dependent repair of Cas9-induced DNA breaks. *Proc Natl Acad Sci*. 2017. doi:10.1073/pnas.1711979114
70. Ma Y, Zhang X, Shen B, et al. Generating rats with conditional alleles using CRISPR/Cas9. *Cell Res*. 2014. doi:10.1038/cr.2013.157
71. Miyasaka Y, Uno Y, Yoshimi K, et al. CLICK: One-step generation of conditional knockout mice. *BMC Genomics*. 2018. doi:10.1186/s12864-018-4713-y
72. Quadros RM, Miura H, Harms DW, et al. Easi-CRISPR: A robust method for one-step generation of mice carrying conditional and insertion alleles using long ssDNA donors and CRISPR ribonucleoproteins. *Genome Biol*. 2017. doi:10.1186/s13059-017-1220-4
73. Dewari PS, Southgate B, Mccarten K, et al. An efficient and scalable pipeline for epitope tagging in mammalian stem cells using Cas9 ribonucleoprotein. *Elife*. 2018. doi:10.7554/elife.35069
74. Hockemeyer D, Wang H, Kiani S, et al. Genetic engineering of human pluripotent cells using TALE nucleases. *Nat Biotechnol*. 2011. doi:10.1038/nbt.1927
75. Hockemeyer D, Soldner F, Beard C, et al. Efficient targeting of expressed and silent genes in human ESCs and iPSCs using zinc-finger nucleases. *Nat Biotechnol*. 2009. doi:10.1038/nbt.1562
76. Zhu Z, Verma N, González F, Shi ZD, Huangfu D. A CRISPR/Cas-Mediated Selection-free Knockin Strategy in Human Embryonic Stem Cells. *Stem Cell Reports*. 2015. doi:10.1016/j.stemcr.2015.04.016
77. Matano M, Date S, Shimokawa M, et al. Modeling colorectal cancer using CRISPR-Cas9-mediated engineering of human intestinal organoids. *Nat Med*. 2015. doi:10.1038/nm.3802
78. Schwank G, Koo BK, Sasselli V, et al. Functional repair of CFTR by CRISPR/Cas9 in intestinal stem cell organoids of cystic fibrosis patients. *Cell Stem Cell*. 2013. doi:10.1016/j.stem.2013.11.002
79. Lengner CJ, Camargo FD, Hochedlinger K, et al. Oct4 Expression Is Not Required for Mouse Somatic Stem Cell Self-Renewal. *Cell Stem Cell*. 2007. doi:10.1016/j.stem.2007.07.020
80. Chang TH, Huang HY, Hsu JBK, Weng SL, Horng JT, Huang H Da. An enhanced computational platform for investigating the roles of regulatory RNA and for identifying functional RNA motifs. *BMC Bioinformatics*. 2013. doi:10.1186/1471-2105-14-S2-S4
81. Liu Y, Han X, Yuan J, et al. Biallelic insertion of a transcriptional terminator via the CRISPR/Cas9 system efficiently silences expression of protein-coding and non-coding RNA genes. *J Biol Chem*. 2017. doi:10.1074/jbc.M116.769034

82. Fiering S, Epner E, Robinson K, et al. Targeted deletion of 5'HS2 of the murine β-globin LCR reveals that it is not essential for proper regulation of the β-globin locus. *Genes Dev*. 1995. doi:10.1101/gad.9.18.2203
83. Nagy A, Moens C, Ivanyi E, et al. Dissecting the role of N-myc in development using a single targeting vector to generate a series of alleles. *Curr Biol*. 2004. doi:10.1016/s0960-9822(98)70254-4
84. Jacks T, Shih TS, Schmitt EM, Bronson RT, Bernards A, Weinberg RA. Tumour predisposition in mice heterozygous for a targeted mutation in Nf1. *Nat Genet*. 1994. doi:10.1038/ng0794-353
85. Nagy A. Cre recombinase - Universal reagent for genome tailoring. 2000;109:99-109.
86. Meier ID, Bernreuther C, Tilling T, et al. Short DNA sequences inserted for gene targeting can accidentally interfere with off-target gene expression. *FASEB J*. 2010. doi:10.1096/fj.09-140749
87. Kim S Il, Matsumoto T, Kagawa H, et al. Microhomology-assisted scarless genome editing in human iPSCs. *Nat Commun*. 2018. doi:10.1038/s41467-018-03044-y
88. Yusa K. Seamless genome editing in human pluripotent stem cells using custom endonuclease-based gene targeting and the piggyBac transposon. *Nat Protoc*. 2013. doi:10.1038/nprot2013.126
89. Maruyama M, Ichisaka T, Nakagawa M, Yamanaka S. Differential roles for Sox15 and Sox2 in transcriptional control in mouse embryonic stem cells. *J Biol Chem*. 2005. doi:10.1074/jbc.M501423200
90. Lo CA, Kays I, Emran F, Lin TJ, Cvetkovska V, Chen BE. Quantification of Protein Levels in Single Living Cells. *Cell Rep*. 2015. doi:10.1016/j.celrep.2015.11.048
91. Miquerol L, Langille BL, Nagy A. Embryonic development is disrupted by modest increases in vascular endothelial growth factor gene expression. *Development*. 2000.
92. Duda K, Lonowski LA, Kofoed-Nielsen M, et al. High-efficiency genome editing via 2A-coupled co-expression of fluorescent proteins and zinc finger nucleases or CRISPR/Cas9 nickase pairs. *Nucleic Acids Res*. 2014. doi:10.1093/nar/gku251
93. Seki A, Rutz S. Optimized RNP transfection for highly efficient CRISPR/Cas9-mediated gene knockout in primary T cells. *J Exp Med*. 2018. doi:10.1084/jem.20171626
94. Steyer B, Bu Q, Cory E, et al. Scarless Genome Editing of Human Pluripotent Stem Cells via Transient Puromycin Selection. *Stem Cell Reports*. 2018. doi:10.1016/j.stemcr.2017.12.004
95. Brinkman EK, Kousholt AN, Harmsen T, et al. Easy quantification of template-directed CRISPR/Cas9 editing. *Nucleic Acids Res*. 2018. doi:10.1093/nar/gky164
96. Brinkman EK, Chen T, Amendola M, van Steensel B. Easy quantitative assessment of genome editing by sequence trace decomposition. *Nucleic Acids Res*. 2014. doi:10.1093/nar/gku936
97. Lin S, Staahl BT, Alla RK, Doudna JA. Enhanced homology-directed human genome engineering by controlled timing of CRISPR/Cas9 delivery. *Elife*. 2014. doi:10.7554/eLife.04766
98. Liang X, Potter J, Kumar S, Ravinder N, Chesnut JD. Enhanced CRISPR/Cas9-mediated precise genome editing by improved design and delivery of gRNA, Cas9 nuclease, and donor DNA. *J Biotechnol*. 2017. doi:10.1016/j.jbiotec.2016.11.011
99. Guo Q, Mintier G, Ma-Edmonds M, et al. "Cold shock" increases the frequency of homology directed repair gene editing in induced pluripotent stem cells. *Sci Rep*. 2018. doi:10.1038/s41598-018-20358-5
100. Komor AC, Zhao KT, Packer MS, et al. Improved base excision repair inhibition and bacteriophage Mu Gam protein yields C:G-to-T:A base editors with higher efficiency and product purity. *Sci Adv*. 2017. doi:10.1126/sciadv.aao4774
101. Gaudelli NM, Komor AC, Rees HA, et al. Programmable base editing of T to G C in genomic DNA without DNA cleavage. *Nature*. 2017. doi:10.1038/nature24644
102. Komor AC, Kim YB, Packer MS, Zuris JA, Liu DR. Programmable editing of a target base in genomic DNA without double-stranded DNA cleavage. *Nature*. 2016. doi:10.1038/nature17946
103. Miura H, Quadros RM, Gurumurthy CB, Ohtsuka M. Easi-CRISPR for creating knock-in and conditional knockout mouse models using long ssDNA donors. *Nat Protoc*. 2018. doi:10.1038/nprot.2017.153
104. Miura H, Gurumurthy CB, Sato T, Sato M, Ohtsuka M. CRISPR/Cas9-based generation of knockdown mice by intronic insertion of artificial microRNA using longer single-stranded DNA. *Sci Rep*. 2015. doi:10.1038/srep12799
105. Arbab M, Srinivasan S, Hashimoto T, Geijsen N, Sherwood RI. Cloning-free CRISPR. *Stem Cell Reports*. 2015. doi:10.1016/j.stemcr.2015.09.022
106. Sheridan RM, Bentley DL. Selectable one-step PCR-mediated integration of a degron for rapid depletion of endogenous human proteins. *Biotechniques*. 2016. doi:10.2144/000114378
107. Shy BR, Macdougall MS, Clarke R, Merrill BJ. Co-incident insertion enables high efficiency genome engineering in mouse embryonic stem cells. *Nucleic Acids Res*. 2016. doi:10.1093/nar/gkw685
108. Zhang JP, Li XL, Li GH, et al. Efficient precise knockin with a double cut HDR donor after CRISPR/Cas9-mediated double-stranded DNA cleavage. *Genome Biol*. 2017. doi:10.1186/s13059-017-1164-8
109. Yao X, Wang X, Hu X, et al. Homology-mediated end joining-based targeted integration using CRISPR/Cas9. *Cell Res*. 2017. doi:10.1038/cr.2017.76

110. Schwank G, Clevers H. CRISPR/Cas9-Mediated genome editing of mouse small intestinal organoids. *Methods Mol Biol*. 2016. doi:10.1007/978-1-4939-3603-8_1
111. Fujii M, Matano M, Nanki K, Sato T. Efficient genetic engineering of human intestinal organoids using electroporation. *Nat Protoc*. 2015;10(10):1474-1485. doi:10.1038/nprot.2015.088
112. Zuris JA, Thompson DB, Shu Y, et al. Cationic lipid-mediated delivery of proteins enables efficient protein-based genome editing in vitro and in vivo. *Nat Biotechnol*. 2015. doi:10.1038/nbt.3081
113. Suresh B, Ramakrishna S, Kim H. Cell-Penetrating Peptide-Mediated Delivery of Cas9 Protein and Guide RNA for Genome Editing. *Methods Mol Biol*. 2017;1507:81-94. doi:https://doi.org/10.1007/978-1-4939-6518-2_7
114. Hornung V, Latz E. Intracellular DNA recognition. *Nat Rev Immunol*. 2010. doi:10.1038/nri2690
115. Kim S, Kim D, Cho SW, Kim J, Kim JS. Highly efficient RNA-guided genome editing in human cells via delivery of purified Cas9 ribonucleoproteins. *Genome Res*. 2014. doi:10.1101/gr.171322.113
116. Gaj T, Guo J, Kato Y, Sirk SJ, Barbas CF. Targeted gene knockout by direct delivery of zinc-finger nuclease proteins. *Nat Methods*. 2012. doi:10.1038/nmeth.2030
117. Liang X, Potter J, Kumar S, et al. Rapid and highly efficient mammalian cell engineering via Cas9 protein transfection. *J Biotechnol*. 2015. doi:10.1016/j.jbiotec.2015.04.024
118. Wang H, Yang H, Shivalila CS, et al. One-step generation of mice carrying mutations in multiple genes by CRISPR/cas-mediated genome engineering. *Cell*. 2013. doi:10.1016/j.cell.2013.04.025
119. Wang W, Kutny PM, Byers SL, et al. Delivery of Cas9 Protein into Mouse Zygotes through a Series of Electroporation Dramatically Increases the Efficiency of Model Creation. *J Genet Genomics*. 2016. doi:10.1016/j.jgg.2016.02.004
120. Gong H, Liu M, Klomp J, Merrill BJ, Rehman J, Malik AB. Method for dual viral vector mediated CRISPR-Cas9 gene disruption in primary human endothelial cells. *Sci Rep*. 2017. doi:10.1038/srep42127
121. Cheshenko N, Krougliak N, Eisensmith RC, Krougliak VA. A novel system for the production of fully deleted adenovirus vectors that does not require helper adenovirus. *Gene Ther*. 2001. doi:10.1038/sj.gt.3301459
122. Mansouri M, Bellon-Echeverria I, Rizk A, et al. Highly efficient baculovirus-mediated multigene delivery in primary cells. *Nat Commun*. 2016. doi:10.1038/ncomms11529
123. Hindriksen S, Bramer AJ, Truong MA, et al. Baculoviral delivery of CRISPR/Cas9 facilitates efficient genome editing in human cells. *PLoS One*. 2017;12(6). doi:10.1371/journal.pone.0179514
124. Han X, Liu Z, Jo M chan, et al. CRISPR-Cas9 delivery to hard-to-transfect cells via membrane deformation. *Sci Adv*. 2015. doi:10.1126/sciadv.1500454
125. D'Astolfo DS, Pagliero RJ, Pras A, et al. Efficient intracellular delivery of native proteins. *Cell*. 2015. doi:10.1016/j.cell.2015.03.028
126. Gaj T, Staahl BT, Rodrigues GMC, et al. Targeted gene knock-in by homology-directed genome editing using Cas9 ribonucleoprotein and AAV donor delivery. *Nucleic Acids Res*. 2017. doi:10.1093/nar/gkx154
127. Yin H, Xue W, Chen S, et al. Genome editing with Cas9 in adult mice corrects a disease mutation and phenotype. *Nat Biotechnol*. 2014. doi:10.1038/nbt.2884
128. Xue W, Chen S, Yin H, et al. CRISPR-mediated direct mutation of cancer genes in the mouse liver. *Nature*. 2014. doi:10.1038/nature13589
129. Sanchez-Rivera FJ, Papagiannakopoulos T, Romero R, et al. Rapid modelling of cooperating genetic events in cancer through somatic genome editing. *Nature*. 2014. doi:10.1038/nature13906
130. Roper J, Tammela T, Cetinbas NM, et al. In vivo genome editing and organoid transplantation models of colorectal cancer and metastasis. *Nat Biotechnol*. 2017. doi:10.1038/nbt.3836
131. Ehrke-Schulz E, Schiwon M, Leitner T, et al. CRISPR/Cas9 delivery with one single adenoviral vector devoid of all viral genes. *Sci Rep*. 2017. doi:10.1038/s41598-017-17180-w
132. Lau C-H, Suh Y. In vivo genome editing in animals using AAV-CRISPR system: applications to translational research of human disease. *F1000Research*. 2017. doi:10.12688/f1000research.11243.1
133. Cox DBT, Platt RJ, Zhang F. Therapeutic genome editing: Prospects and challenges. *Nat Med*. 2015. doi:10.1038/nm.3793
134. Savić N, Schwank G. Advances in therapeutic CRISPR/Cas9 genome editing. *Transl Res*. 2016. doi:10.1016/j.trsl.2015.09.008
135. Chu VT, Weber T, Wefers B, et al. Increasing the efficiency of homology-directed repair for CRISPR-Cas9-induced precise gene editing in mammalian cells. *Nat Biotechnol*. 2015. doi:10.1038/nbt.3198
136. Maruyama T, Dougan SK, Truttmann MC, Bilate AM, Ingram JR, Ploegh HL. Increasing the efficiency of precise genome editing with CRISPR-Cas9 by inhibition of nonhomologous end joining. *Nat Biotechnol*. 2015. doi:10.1038/nbt.3190
137. Vartak S V., Raghavan SC. Inhibition of nonhomologous end joining to increase the specificity of CRISPR/Cas9 genome editing. *FEBS J*. 2015. doi:10.1111/febs.13416

138. Li G, Zhang X, Zhong C, et al. Small molecules enhance CRISPR/Cas9-mediated homology-directed genome editing in primary cells. *Sci Rep*. 2017. doi:10.1038/s41598-017-09306-x
139. Hu Z, Shi Z, Guo X, et al. Ligase IV inhibitor SCR7 enhances gene editing directed by CRISPR-Cas9 and ssODN in human cancer cells. *Cell Biosci*. 2018. doi:10.1186/s13578-018-0200-z
140. Kulkarni SS, Cantó C. The molecular targets of resveratrol. *Biochim Biophys Acta - Mol Basis Dis*. 2015. doi:10.1016/j.bbadis.2014.10.005
141. Ma X, Chen X, Jin Y, et al. Small molecules promote CRISPR-Cpf1-mediated genome editing in human pluripotent stem cells. *Nat Commun*. 2018. doi:10.1038/s41467-018-03760-5
142. Xiang G, Zhang X, An C, Cheng C, Wang H. Temperature effect on CRISPR-Cas9 mediated genome editing. *J Genet Genomics*. 2017. doi:10.1016/j.jgg.2017.03.004
143. Bobadilla JL, Macek M, Fine JP, Farrell PM. Cystic fibrosis: A worldwide analysis of CFTR mutations - Correlation with incidence data and application to screening. *Hum Mutat*. 2002. doi:10.1002/humu.10041
144. Nagasaki A, T. Kijima S, Yumoto T, et al. The Position of the GFP Tag on Actin Affects the Filament Formation in Mammalian Cells. *Cell Struct Funct*. 2017. doi:10.1247/csf.17016
145. Cranfill PJ, Sell BR, Baird MA, et al. Quantitative assessment of fluorescent proteins. *Nat Methods*. 2016. doi:10.1038/nmeth.3891
146. Clevers H. Modeling Development and Disease with Organoids. *Cell*. 2016. doi:10.1016/j.cell.2016.05.082
147. Shimokawa M, Ohta Y, Nishikori S, et al. Visualization and targeting of LGR5 + human colon cancer stem cells. *Nature*. 2017. doi:10.1038/nature22081
148. Lee K, Mackley VA, Rao A, et al. Synthetically modified guide RNA and donor DNA are a versatile platform for CRISPR-Cas9 engineering. *Elife*. 2017. doi:10.7554/elife.25312
149. Carlson-Stevermer J, Abdeen AA, Kohlenberg L, et al. Assembly of CRISPR ribonucleoproteins with biotinylated oligonucleotides via an RNA aptamer for precise gene editing. *Nat Commun*. 2017. doi:10.1038/s41467-017-01875-9
150. Veneziano R, Shepherd TR, Ratanalert S, Bellou L, Tao C, Bathe M. In vitro synthesis of gene-length single-stranded DNA. *Sci Rep*. 2018. doi:10.1038/s41598-018-24677-5

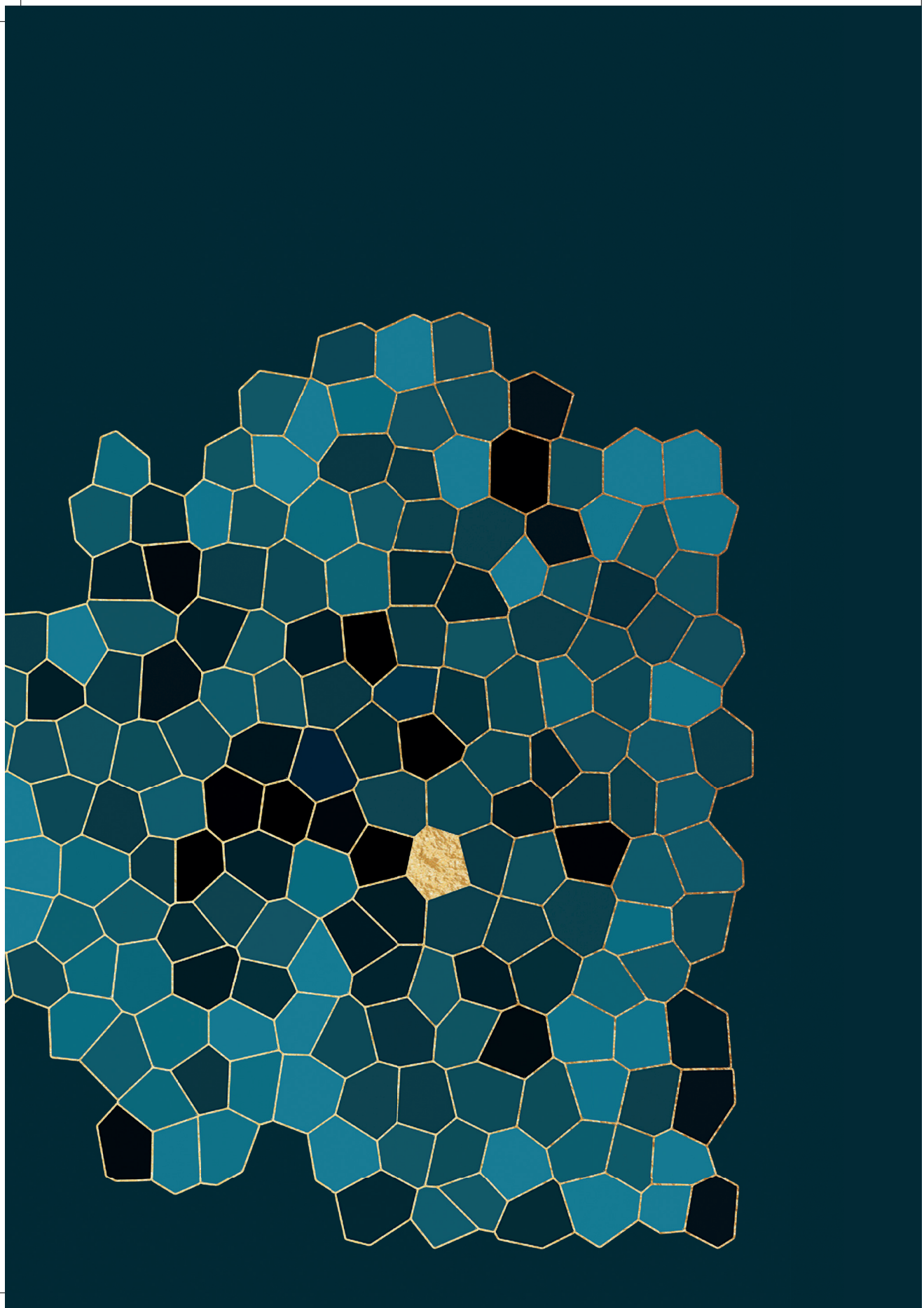

CHAPTER 3

CRISPR-MEDIATED RASGAP DEFICIENCIES IN COLORECTAL CANCER ORGANOIDS REVEAL THAT ONLY LOSS OF NF1 PROMOTES RESISTANCE TO EGFR INHIBITION

Jasmin B. Post, Nizar Hami, Alexander E.E. Mertens, Suraya Elfrink, Johannes L. Bos and Hugo J.G. Snippert

Oncotarget. 2019. 10(14):1440-1457

ABSTRACT

Anti-EGFR therapy is used to treat metastatic colorectal cancer (CRC) patients, for which initial response rates of 10–20% have been achieved. Although the presence of *HER2* amplifications and oncogenic mutations in *KRAS*, *NRAS*, and *BRAF* are associated with EGFR-targeted therapy resistance, for a large population of CRC patients the underlying mechanism of RAS-MEK-ERK hyperactivation is not clear. Loss-of-function mutations in RASGAPs are often speculated in literature to promote CRC growth as being negative regulators of RAS, but direct experimental evidence is lacking. We generated a CRISPR-mediated knock-out panel of all RASGAPs in patient-derived CRC organoids and found that only loss of NF1, but no other RASGAPs e.g. RASA1, results in enhanced RAS-ERK signal amplification and improved tolerance towards limited EGF stimulation. Our data suggests that NF1-deficient CRCs are likely not responsive to anti-EGFR monotherapy and can potentially function as a biomarker for CRC progression.

KEYWORDS

NF1, RASGAP, anti-EGFR therapy resistance, cancer progression, colorectal cancer

INTRODUCTION

Colorectal cancer (CRC) is one of the most common cancers and the third leading cause of worldwide cancer deaths (IARC). The use of monoclonal antibodies (moAbs) targeting the epidermal growth factor receptor (EGFR), such as cetuximab and panitumumab, together with chemotherapy has shown a clinical bene t for the treatment of patients with metastatic CRC (mCRC)[1–3]. The binding of these antibodies to the extracellular domain of the EGFR inhibits downstream activation of the RAS-MEK-ERK signaling pathway, thereby inhibiting cell proliferation and survival[4,5]. Treatment with EGFR targeting moAbs resulted in initial response rates of 10–20% in mCRC patients[1], but it soon became clear that tumors with activating mutations in *KRAS* showed resistance to EGFR inhibition[2,3,6]. Moreover, the treatment of patients with mutant *KRAS* colorectal tumors with EGFR inhibitors seemed to aggravate disease progression[3]. Therefore, these patients are now being excluded from EGFR targeted therapy[7,8].

RAS proteins act as molecular switches that cycle between inactive GDP-bound and active GTP-bound states. Active GTP-bound RAS can stimulate a large variety of downstream signaling cascades, including the mitogen activated protein kinase (MAPK) and phosphatidylinositol-3-kinase (PI3K) pathways, to promote proliferation, migration and survival. The activation of RAS is tightly regulated by guanine nucleotide exchange factors (GEFs) and GTPases activating proteins (GAPs). GEFs accelerate the dissociation of GDP from RAS, whereas GAPs enhance the intrinsic rate of GTP hydrolysis of RAS[9]. Activating mutations in *KRAS* are identified in approximately 35-50% of mCRC patients, resulting in the constitutive downstream activation of MEK and ERK[9,10]. It is thought that *KRAS* oncogenic mutations are early events in cancer progression, potentially even at the onset of tumorigenesis, as they are frequently found in both early and late stages of CRC[10–12]. In agreement with this, genomic studies have highlighted that the MAPK signaling pathway is often aberrantly activated in colorectal tumors[13–16]. However, in contrast to pancreatic cancers, where oncogenic *KRAS* mutations are found in 90% of the cases[17,18], a large population of CRC patients carry tumors that are wild-type for *KRAS*. Indeed, other oncogenic mutations in the MAPK signaling pathway, such as mutations in *NRAS*, *BRAF*, or *HER2* amplifications, have been identified in CRC and are implicated in tumor progression[19–23]. Nevertheless, for at least 25% of mCRC patients the underlying cause of aberrant MAPK pathway activation remains unknown[19–22].

In this regard, RASGAPs that act as negative regulators of RAS signaling are frequently implicated in tumorigenesis. In the human genome, ten functional RASGAP genes have been identified. Genetic analysis of tumor samples only identified a significant number of inactivating mutations in the RASGAPs *neurofibromin* (NF1) and *RASA1* (p120GAP), suggesting that these two RASGAPs can function as tumor suppressors. Moreover, ongoing sequencing efforts of larger patient cohorts may increase the detection of low abundant loss-of-function mutations in several other RASGAPs[24,25].

Loss-of-function mutations in *NF1* are frequently associated with a large variety of cancers, such as melanoma[26–29], leukemia[30–32], glioblastoma[33], and lung cancer[25]. Moreover, multiple studies have linked NF1 activity to RAS and ERK activity[28,29,33–36], including its role in therapy resistance upon targeted inhibition of the MAPK pathway in melanoma[28,29,36,37] and lung

cancer[38]. Inactivating mutations and deletions in the *RASA1* gene have also been detected in a number of cancers, such as lung squamous carcinoma[39], stomach, esophagus[40], leukemia[41], and head and neck[25] cancer, but its role as a tumor suppressor is less well defined.
In line with their molecular function, a suggestive tumor suppressive role for RASGAPs in CRC has been proposed based on association studies[42–46], as well as knock-down experiments in cell lines[47,48]. However, the debate whether indeed all RASGAPs can mediate CRC progression beyond EGF dependence remains ongoing, in particular since the lack of direct loss-of-function data regarding RASGAPs in CRC models.
Here, using CRISPR-mediated knock-out lines in patient-derived CRC organoids that are otherwise wild-type for the RAS pathway, we investigate the role of RASGAPs in CRC progression and in relation to EGFR signaling. Surprisingly, in contrast to widely accepted assumptions, but in line with overall mutation frequencies, we show that only the loss of NF1, but no other RASGAPs, can act as an amplifier of MAPK signaling. As such, NF1-deficiency contributes to CRC progression by minimizing its dependence on EGF-ligand stimulated MAPK signaling.

RESULTS

Low abundant mutation frequencies for RASGAPs in CRC

Strong activating mutations of RAS pathway effectors tend to occur in a mutually exclusive manner, most pronounced for oncogenic mutations in either *RAS* or *BRAF*.
Corresponding with reported activity of NF1 as a tumor suppressor and negative regulator of RAS in lung adenocarcinomas[38], truncating mutations in *NF1* tend to be mutual exclusive with activating mutations in *RAS* and *BRAF* (TCGA) in these tumors (**Figure 1A**). Although the sample size of this lung adenocarcinoma cohort is too small to obtain reliable numbers for low abundant deletion and inactivating mutation frequencies in most other RASGAP genes, inactivating mutations in *RASA1* seem, like NF1, mutual exclusive with other activating mutations of the MAPK signaling pathway (**Figure 1A**).
The mutually exclusivity between loss-of-function mutations in *NF1* and oncogenic mutations in *RAS* and *BRAF* is also observed in melanoma patients (TCGA) (**Figure 1B**). However, a number of melanoma patients do have tumors that present both truncating mutations in *NF1* as well as oncogenic mutations in BRAF. Interestingly, all of the BRAF mutations that show co-occurrence with NF1 truncating mutations, both lung adenocarcinoma and melanoma samples, do not present the V600E hotspot mutation. Indeed, the non-V600E activating mutations in *BRAF* only induce weak oncogenic BRAF activity[49], suggesting that co-occurrence with NF1 loss, is required to obtain sufficient levels of RAS-ERK signaling. The frequency of inactivating alterations in the other RASGAP genes in this cohort of melanoma patients is again infrequent and too low to indicate their potential role in cancer development and progression (**Figure 1B**).
In contrast to lung adenocarcinoma and melanoma patients, the numbers of inactivating mutations in colorectal adenocarcinoma patients are low in all RASGAP genes (TCGA), including NF1 (**Figure 1C**). For CRC, low abundant mutation frequencies of RASGAPs might be the result of tissue-specific mechanisms of MAPK pathway activation and questions whether the loss of RASGAPs can actually play a substantial role in tumor progression of

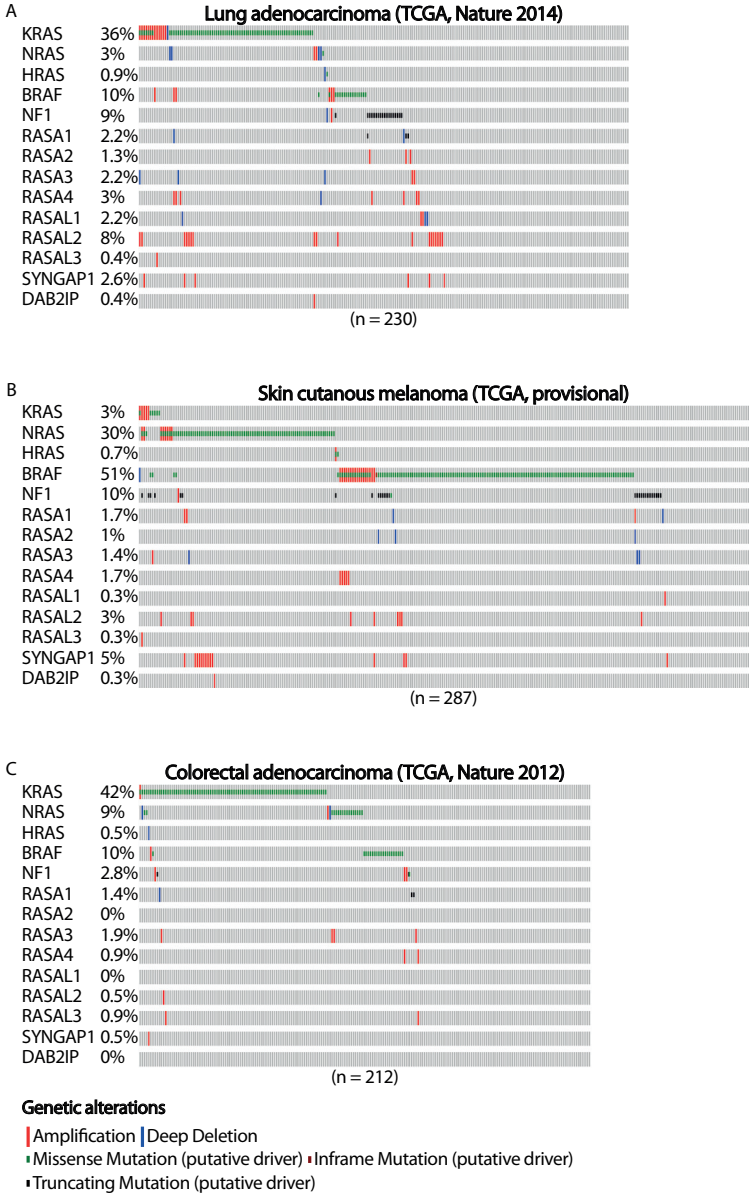

Figure 1. The occurrence of RASGAP and oncogenic mutations in the MAPK signaling pathway in lung adenocarcinoma, melanoma and colorectal adenocarcinoma.
The distribution of driver mutations and copy number alterations in *KRAS*, *NRAS*, *HRAS*, *BRAF*, and *RASGAPs* in (**A**) lung adenocarcinoma (n = 230), (**B**) skin cutaneous melanoma (n = 287) and (**C**) colorectal adenocarcinoma (n = 212) from TCGA datasets are shown. Data were extracted through cBioPortal and presented as OncoPrint. Color coding indicates mutation type: red, homozygous amplification; blue, homozygous deletion; green, missense mutation; brown, inframe putative driver mutation; black, truncating mutation. Left, mutation percentage.

CRCs. Alternatively, other mechanisms affecting RASGAP protein levels, such as post-translational modifications affecting protein stability as well as gene silencing, can also account for decreased RASGAP activity, but this data is not present in sufficient quality and quantity to provide us more insight on functional mutually exclusivity[25,40].
Thus, whereas mutual exclusivity of NF1-loss, in combination with previous experimental data[26,28,29,36,38], support NF1 as a strong oncogenic driver in lung adenocarcinoma and melanoma, the general oncogenic role of RASGAP deficiency in CRC remains inconclusive.

A CRISPR-mediated RASGAP knock-out screen identifies NF1 as the only RASGAP which depletion enables enhanced tumor growth and EGF-independent survival

To circumvent the lack of patient-data regarding loss of RASGAP expression, we set out to test the function of RASGAPs in CRC in an experimental setting. For this we utilize a patient-derived tumor organoid (P18T) with loss-of-function mutations in the WNT (APC) and TP53 pathway, but that is wild-type for the RAS pathway and as such requires EGF-mediated growth factor signaling for growth and survival[50]. With the exception of RASAL3, which shows specific expression in the hematopoietic lineage in mice and humans (**Supplementary Figure 1A**), we identified the other RASGAPs at similar expression levels (**Figure 2A**)[51,52].
To investigate whether loss of RASGAPs enables EGF-independent tumor cell growth and survival in CRCs, we depleted the activity of each RASGAP separately in P18T organoids using CRISPR-induced knock-outs by targeting Cas9 cleavage activity against the conserved arginine finger in the catalytic GAP domain (**Figure 2B**)[53,54]. The generation of knock-outs was confirmed by DNA sequencing analysis of multiple monoclonal RASGAP knock-out organoids (**Supplementary Figure 1B**). Subsequently, the population of RASGAP deficient CRC organoids were intermittently cultured in the absence of EGF signaling activity (EGF depleted growth medium containing afatinib, a small molecule inhibitor that targets the tyrosine kinase receptors EGFR, HER2 and HER4) (**Figure 2B**).
Surprisingly, we found that only the loss of NF1 GAP activity, but not of the other RASGAPs, resulted in a significant organoid growth upon intermittent EGFR inhibition (**Figure 2C**). In contrast to autonomous KRAS mutations, inactive NF1 did not result in complete EGF independence as organoid sizes remained small (but survived) upon continuous EGFR inhibition. However, elevated growth was observed under culture conditions with minimal EGFR stimulation (data not shown).
Since small sized organoids were observed for most conditions, including the negative control, we labelled all living organoids at the end point with calcein green to perform accurate measurements of number and size of organoids. Again, it illustrates that the number of organoids that are significantly larger in size is only observed after loss of NF1 activity in relation to the other RASGAP knock-out organoids (**Figure 2C** and **Supplementary Figure 1C**). Importantly, to exclude the possibility that this observation was influenced by patient specific effects, we performed a similar experiment in which we targeted upstream exons or the GAP domains of *NF1* and *RASA1* in engineered tumor organoids that are also deficient in APC and TP53 (commonly referred to as tumor progression organoid 2 (TPO2))[55]. Reassuring, a similar phenotype was observed in the TPO2 organoids, in which again only the loss of NF1 resulted in an increased outgrowth of large organoids as compared to control (**Supplementary Figures 2A and 2B**).

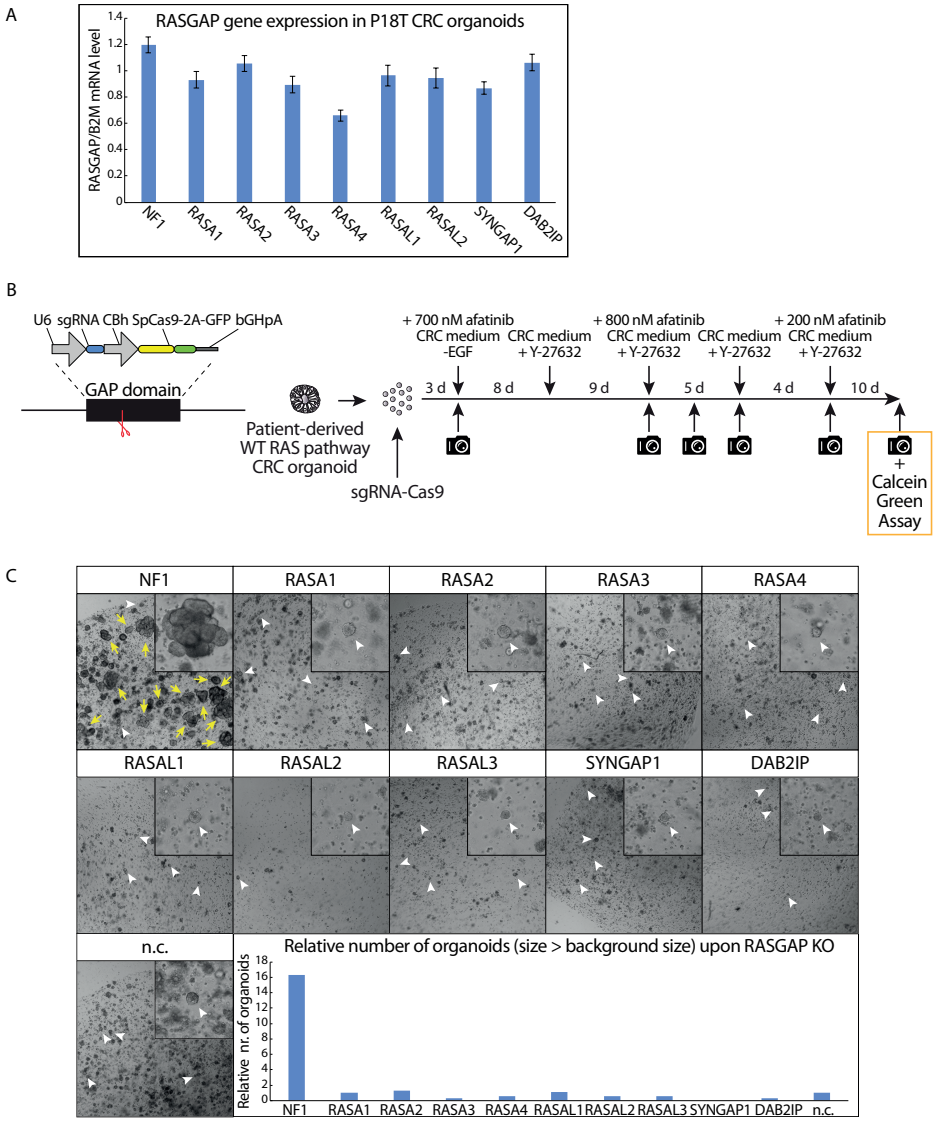

Figure 2. CRISPR screen against RASGAPs in patient-derived CRC organoids reveals increased growth and EGF-independent survival upon loss of NF1 GAP activity.
(**A**) The mRNA expression level of 9 RASGAPs containing an active GAP domain was analyzed in P18T organoids using qPCR. The relative expression of each *RASGAP* gene was normalized to the *B2M* housekeeping gene (representative from n = 3 independent experiments). (**B**) Left; schematic representation of expression plasmid containing both an U6 promoter-driven sgRNA and a CBh promoter-driven SpCas9-2A-GFP was used to target the RASGAP domain. Right; schematic overview of the RASGAP knock-out screen in P18T patient-derived CRC organoids that are wild-type for the RAS signaling pathway. (**C**) P18T CRC organoids in selection medium that have been transfected with indicated sgRNAs and Cas9. White arrow heads indicate representative background organoids. Yellow arrows indicate successful organoids that are significantly larger than background. Bar graph depicts the relative number of organoids with a size larger than background organoids as determined in the negative control. Area of alive RASGAP knock-out organoids was measured using calcein green assay (see Materials and Methods).

Together, these results indicate that only loss of NF1 activity promotes the outgrowth of CRCs upon limited EGFR signaling. The lack of participation by other RASGAPs is surprising, but consistent with the nonredundant and tissue-specific functions of RASGAPs[56].

Generation of NF1 and RASA1 knock-out organoid lines independent of phenotypic selection

As a tumor suppressive role has predominantly been suggested for both NF1 and RASA1[25,40], we continued to investigate both their function in CRC. Since the CRISPR/Cas9-induced truncating mutations in the GAP domain, which lies central in the protein sequence, may have resulted in the generation of dominant-negative versions, we also generated complete *NF1* and *RASA1* knock-out lines in the CRC background of P18T (**Supplementary Figures 3 and 4**). Underscoring the role of NF1 deficiency in CRC progression upon EGFR signal inhibition, all outgrowth clones of NF1 were true knock-outs (10/10), in contrast to only half of the RASA1 clones (7/14). Indeed, our selection method on phenotype could potentially result in the positive selection of undesired off-target mutations, which alone or together with NF1 or RASA1 inactivating mutations may lead to EGF independence and increased cell proliferation. Therefore, additional knock-outs were generated without phenotypic selection, but by means of integration of puromycin selection cassettes via homologous recombination (**Figure 3A**)[57].

Indeed, this strategy led to the successful generation of non-functional *NF1* and *RASA1* genes independent of selection through EGFR inhibition (EGFRi) (**Figures 3B and 3D**). Of note, the puromycin selection cassette was properly integrated into the *NF1* gene body (**Supplementary Figure 5A**), accompanied by the introduction of small indel mutations in the 'secondary' allele (**Figure 3B**). Although the selection cassette was also integrated into the genome of *RASA1* knock-out organoids (**Supplementary Figure 5B**), we could not confirm its exact integration site, probably due to its random genomic integration. Most importantly, we did confirm introduction of small indel mutations at both alleles of the *RASA1* gene (**Figure 3D**). Moreover, Western blot analysis of the different clones showed complete loss of NF1 and RASA1 protein in P18T CRC organoids (**Figures 3C and 3E, and Supplementary Figure 5C**). As we were able to generate multiple RASGAP knock-out clones, we continued working with two different clones of each RASGAP knock-out to exclude clonal effects.

NF1 deficiency, but not RASA1, causes intrinsic EGF-independency

First, we validated whether loss of NF1, but not RASA1, induced intrinsic EGF independence for CRC organoid survival by examining the effect of afatinib (EGFR/HERi) treatment on organoid viability by microscopy. Therefore, 5 days after trypsinization the parental P18T organoids, as well as the NF1 and RASA1 knock-out organoid cultures, were filtered to homogenize their size and subsequently cultured with afatinib or DMSO (control) for 72 hours (**Figure 4A**). In agreement with our RASGAP knock-out screen (**Figure 2**), complete loss of NF1 indeed resulted in a slight increase in EGF independence in terms of cell survival, showing healthy but small organoids after EGFRi treatment. In contrast, the parental P18T, as well as the RASA1 knock-out lines, predominantly died in the presence of EGFR inhibition (**Figure 4B**).

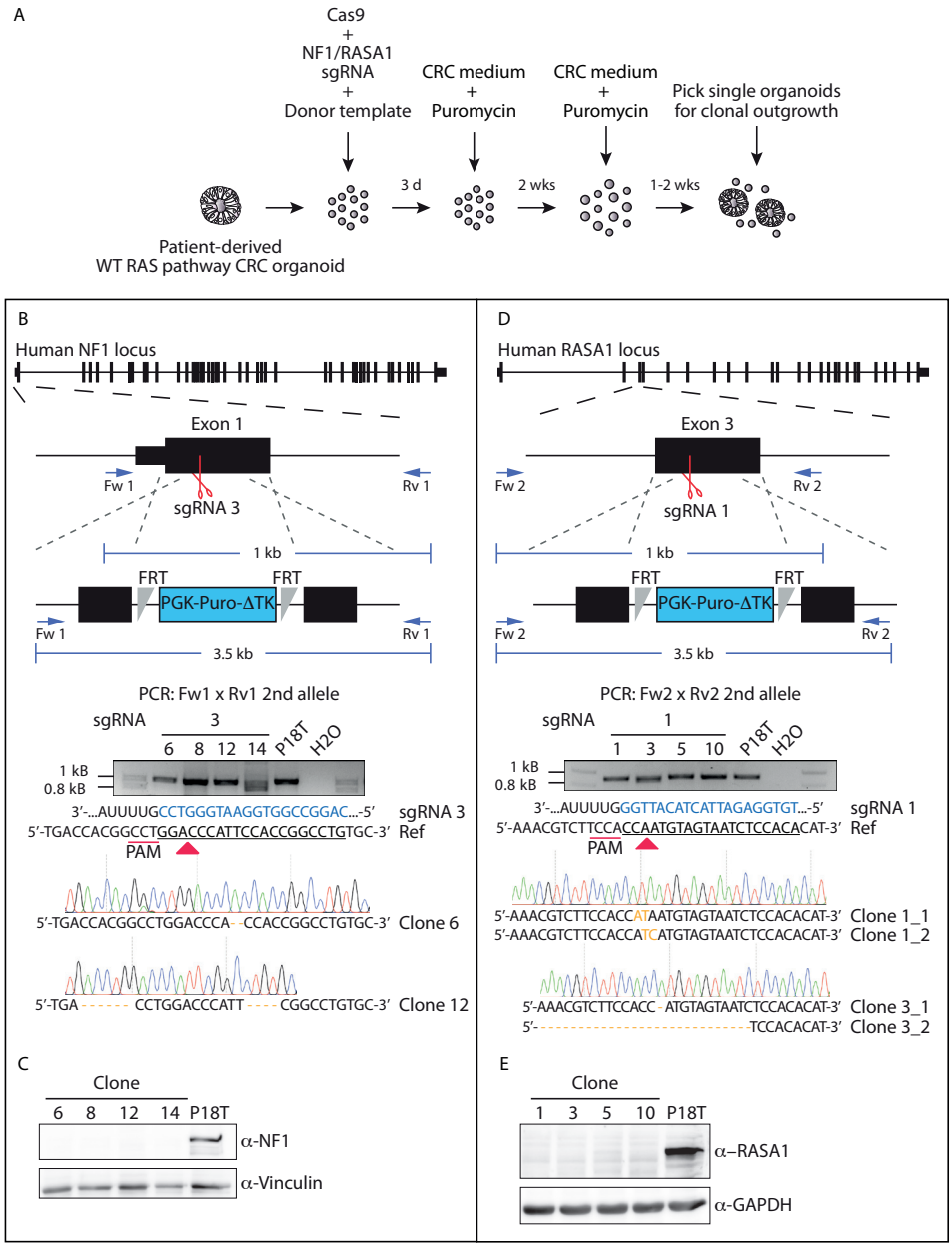

Figure 3. Generation of CRISPR-mediated NF1 and RASA1 knock-out in patient-derived CRC organoids.
(**A**) Selection strategy to generate NF1 and RASA1 knock-out organoids after CRISPR-mediated homologous recombination. (**B, D**) Genetic strategy to target the *NF1* and *RASA1* locus for homologous directed repair via the CRISPR/Cas9. The structure of the *NF1* and *RASA1* gene and the targeted exon is depicted at the top. Black boxes illustrate exons, separated by introns. Red scissors show sgRNA-generated double stranded breaks. Blue arrows illustrate PCR primer pairs. The agarose electrophoresis gel shows the ~1kb PCR product of the allele that was repaired by NHEJ of *NF1* (Clone # 6 and 12) and *RASA1* (Clone # 1 allele 1 and 2, Clone # 2 allele 1 and 2) in selected clones. Sanger sequencing indicate the introduced small indels per clone. Nonmatching bases are shown in orange. Regions of the sgRNA complementary to the protospacer (underlined) are shown in blue. Red arrow heads indicate cleavage sites. (**C, E**) Western blot analysis for NF1 and RASA1 presence in the indicated organoid lines.

Loss of NF1 expression enhances basal RAS-ERK activity in CRC organoids

For both NF1 and RASA1 it has been demonstrated that they can affect RAS and ERK activity in various cell lines[35,38,45]. To investigate the molecular mechanism that underlies increased tumor growth and EGF-independent survival upon loss of NF1 expression, we analyzed the activity of the RAS-MAPK signaling pathway.

Consistent with the phenotypes of our RASGAP knock-out lines, only the loss of NF1 expression in CRC organoids resulted in enhanced ERK activation under basal conditions (**Figure 5A and Supplementary Figure 6A**), which was further verified by quantification (**Supplementary Figure 7A**).

Whereas inhibition of EGF signaling clearly reduced the levels of active (phosphorylated) ERK in all three organoid types (i.e. P18T, NF1 and RASA1 KOs) after 1 hour of afatinib treatment, a substantial reactivation of ERK was observed in alive NF1 knock-out organoids after 72 hours of afatinib treatment (**Figures 5A-B**). Importantly, similar reactivation effects albeit with different kinetics were observed in different NF1 KO clones (**Figure 5B and Supplementary Figure 6A**), explaining their enhanced survival upon EGFR inhibition.

Since the predicted function of NF1 GAP activity is to enhance the intrinsic GTP hydrolysis rate of GTP-bound RAS, we examined the amounts of active, GTP-bound RAS that are present in the absence of NF1. As a positive control, we also analyzed RAS-GTP levels in a P18T organoid line in which an activating mutation in KRAS (G12D) was introduced by CRISPR technology[58]. In comparison with the parental P18T line, loss of NF1 clearly enhanced RAS-GTP levels at basal conditions to similar levels as observed in KRAS mutant P18T organoids. However, whereas a substantial fraction of GTP-bound RAS was detected in oncogenic mutant KRAS organoids after 24 hours of EGFR inhibition, this was not observed in NF1 knock-out organoids (**Figure 5C, Supplementary Figures 6B and 7B**). This discrepancy on RAS-GTP loading may very well be explained by the fact that NF1, in contrast to self-autonomous oncogenic KRAS, acts as an amplifier of RAS-mediated signaling. Therefore, the effect of NF1-loss can only manifest itself in the presence of RAS activating signals, i.e. in the presence of incoming EGF signaling. Indeed, in the RASGAP CRISPR screen we observed that the largest differences in organoid growth and viability were obtained in the presence of minimal EGF signaling.

As expected by the sensitivity of RASA1 knock-out organoids for EGFR signal inhibition, loss of RASA1 did not enhance or sustain RAS-MAPK signaling in case of inhibition, nor under normal growth conditions (**Figure 5C, Supplementary Figures 6A, 6B and 7A, 7B**). Subsequently, we analyzed protein levels of both NF1 and RASA1 in the RASA1 knock-out organoid lines to investigate whether upregulated expression of NF1 acts as a compensation mechanism, but we did not observe any differences in the knock-out lines as compared to wild-type P18T (**Figure 5D**). To explore whether other RASGAPs compensate for the loss of RASA1 activity, we examined the mRNA expression levels of the other RASGAPs in *RASA1* and *NF1* knock-out organoids. In addition to some clonal variability, we detected slight increased expression for most RASGAP genes in the case of NF1 or RASA1 deficiency (**Figure 5E**). However, no clear candidates could be identified which expression level is suggestive for a redundant function to RASA1 deficiency and might have explained a compensatory mechanism that prevents aberrant RAS activation.

Intriguing, while it has been demonstrated that all RASGAPs contain an active GAP domain,

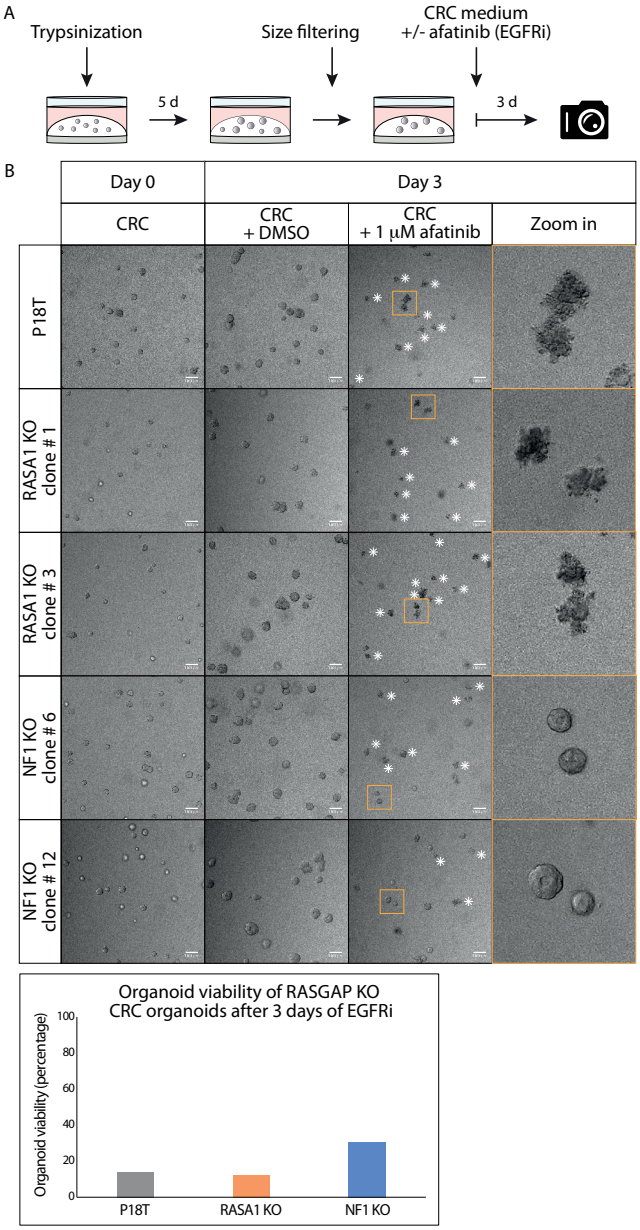

Figure 4. Puromycin selected NF1 knock-out CRC organoids show insensitivity to EGFR inhibition.
(**A**) A schematic overview illustrating the strategy to score sensitivity of NF1 and RASA1 knock-out organoids of similar size treated with colorectal cancer (CRC) medium containing either DMSO or 1 μM afatinib (EGFRi) for 72 hours. (**B**) Representative pictures of the parental patient-derived CRC organoids P18T and P18T RASA1 (clone # 1 and # 3) or NF1 (# 6 and # 12) knock-out organoids prior (day 0) and after 72 hours of DMSO or 1 μM afatinib treatment (Day 3). White asterisks indicate dead organoids. Scale bars, 100 μM. Bar graph depicts the percentage of living organoids (out of 100 organoid counts) based on morphology.

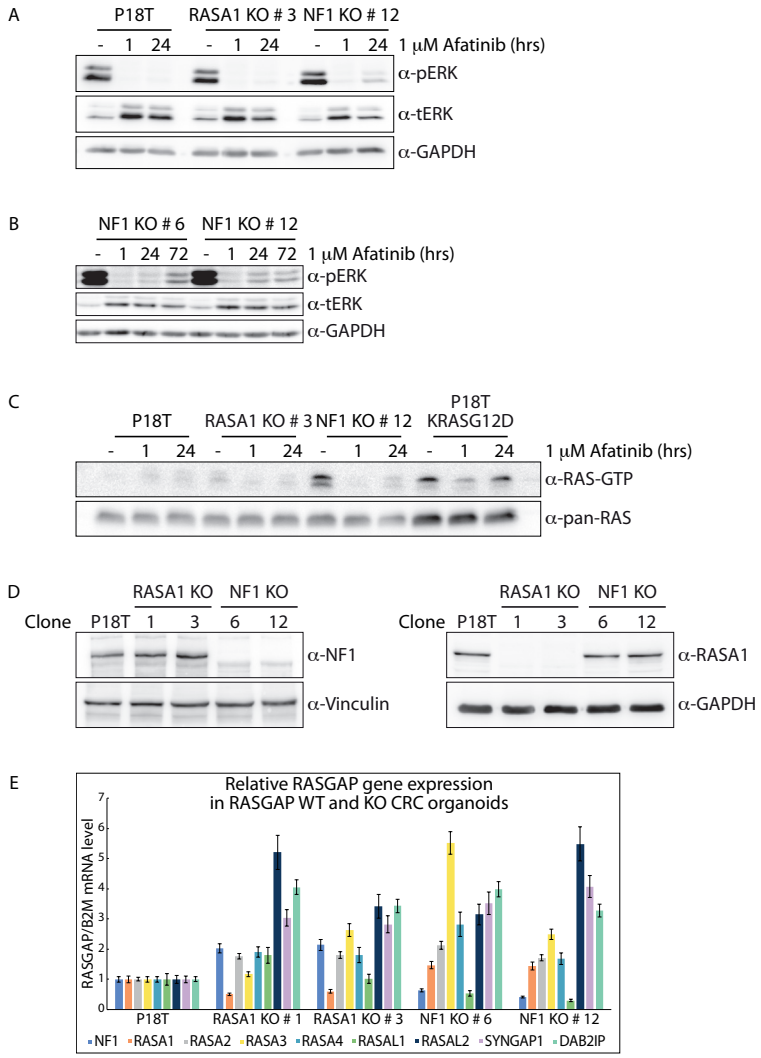

Figure 5. Puromycin selected NF1 knock-out CRC organoids show enhanced RAS and ERK activation.
(**A**) In comparison to P18T and P18T RASA1^{KO} (clone # 3), predominantly P18T NF1^{KO} (clone # 12) organoids show enhanced basal and reactivated ERK phosphorylation levels after 24 hr treatment with CRC medium containing 1 μM afatinib. Representative from n = 3 independent experiments. (**B**) NF1-deficient organoids (clone # 6 and # 12) show residual ERK phosphorylation after treatment with CRC medium containing 1 μM afatinib with varying kinetics. (**C**) Loss of NF1 (clone # 12) leads to elevated levels of RAS activity (GTP-loading) at basal conditions compared to P18T and P18T RASA1^{KO} (clone # 3) CRC organoids. The presence of an oncogenic mutation in *KRAS* (P18T KRAS^{G12D}) leads to elevated and sustained high levels of RAS activity (GTP-loading) at basal and in afatinib-treated conditions, respectively. RAS immunoblots from RAS pull-down assays are shown (RAS-GTP), together with a RAS immunoblot from total cell lysates as loading control. HRAS, KRAS, and NRAS isoforms are detected. Representative from n = 2 independent experiments. (**D**) Immunoblots of P18T, P18T RASA1^{KO} (clone # 1 and 3), P18T NF1^{KO} (clone # 6 and 12) CRC organoids indicate that the loss of RASA1 does not result in elevated protein levels of NF1, and vice versa. Representative from n = 3 independent experiments. (**E**) The relative expression levels of indicated RASGAPs genes that contain an active GAP domain were analyzed in P18T, P18T RASA1^{KO} (clone # 1 and 3), P18T NF1^{KO} (clone # 6 and 12) CRC organoids using RT-PCR. The relative expression of each *RASGAP* gene was normalized to the *B2M* housekeeping gene (representative from n = 3 independent experiments).

our data only identifies NF1 as a bona fide amplifier of RAS-mediated MAPK signaling in patient-derived CRC organoids.

NF1-deficient CRC organoids show enhanced organoid survival and growth upon release of RAS-MAPK pathway inhibition

A recent study showed that NF1 mutations correlated with a poor response to cetuximab-based EGFR inhibition and decreased progression free survival of mCRC patients[46]. Resistance to targeted therapy is often the result of residual RAS-ERK signaling activity[59]. In agreement, we detected enhanced organoid survival and residual ERK activity in NF1-deficient CRC organoids upon long-term EGFR inhibition with afatinib. Therefore, as NF1 loss predominantly amplifies RAS-MAPK signaling activity in unperturbed conditions, we hypothesized that the phenotype of NF1 deficiency might manifest itself most evidently upon the release of EGFR inhibition. In contrast, desired cytotoxicity upon targeted therapy should be achieved upon full RAS-MAPK signal inhibition.

To investigate this, we set up a drug screen to measure the phenotypic response of parental P18T, both RASGAP knock-outs, as well as KRAS mutant P18T organoids, during and after mono- and combinatorial targeted therapies against the RAS-MAPK signaling pathway (**Figure 6A**).

In line with our previous results, NF1 knock-out organoids show some resistance to EGFR-targeted therapy (afatinib) in comparison to wild-type organoids, but not as evident as the resistance observed in KRAS mutant organoids (**Figure 6B and Supplementary Figures 8A-B**). Whereas the observed effects remain subtle for the monotherapies, combined inhibition of MEK (selumetinib) and EGFR/HER (afatinib) resulted in an improved cytotoxic response in NF1 knock-out organoids (**Figure 6B and Supplementary Figures 8A-B**).

Most striking however, when organoids were released from targeted inhibition, a tremendous organoid outgrowth was observed in NF1-deficient organoids that was only matched by KRAS mutant organoids. In contrast, parental $KRAS^{WT}$ and RASA1 knock-out organoids remained small even upon drug withdrawal (**Figure 6C and Supplementary Figure 8**). In contrast to the autonomous $KRAS^{G12D}$ mutation, the phenotype of NF1 deficiency manifests itself predominantly under challenging EGFR signaling conditions, but is not able to rescue complete inhibition of the MAPK signaling pathway. These results are consistent with observations in an *in vitro* and *in vivo* model of NF1-deficient lung adenocarcinoma treated with EGFR and MEK inhibitors[38]. Translating these results to a clinic setting suggests that NF1-deficient mCRC are able to show favorable responses towards targeted inhibition of the RAS-MAPK pathway, but only under strict full inhibitory conditions using combinatorial targeting strategies with ideally a continuous treatment regime.

DISCUSSION

Data analysis of patients with lung adenocarcinoma and melanoma show that of all RASGAPs only inactivating mutations in *NF1* tend to occur in a mutually exclusive manner with activating hotspot mutations in *KRAS*, *NRAS* and *BRAF*. This suggests that the loss of NF1 is sufficient to drive aberrant activity of the RAS-MAPK signaling pathway in the absence of other mutations in the RAS signaling pathway. However, the data is less clear for CRCs, in which

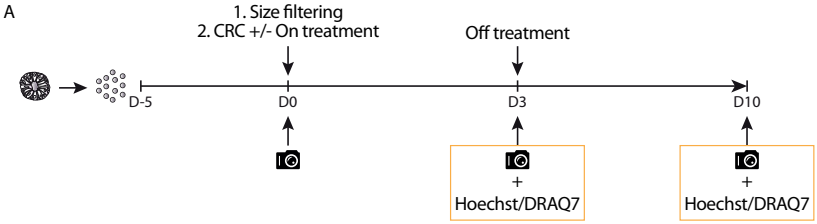

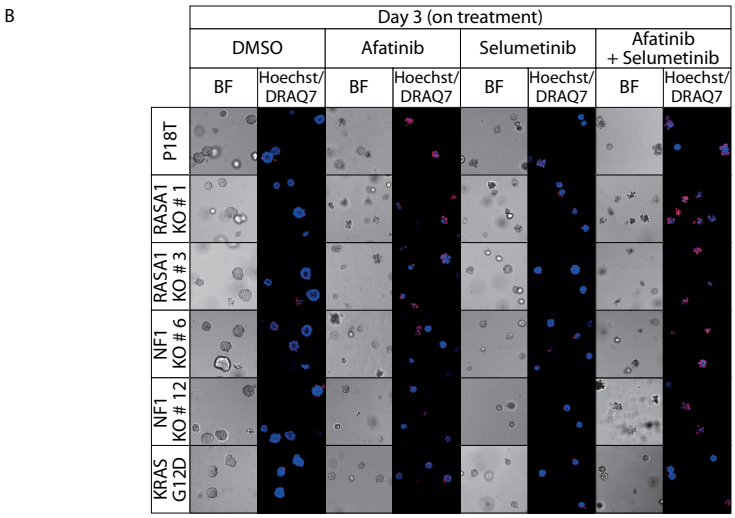

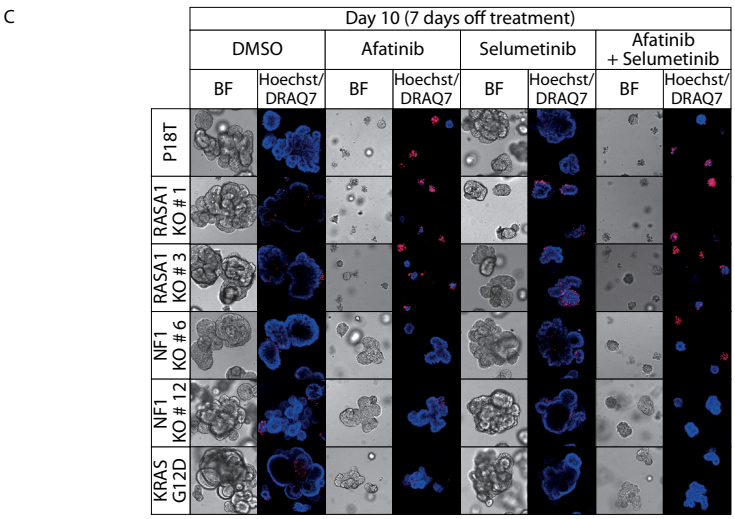

the frequency of loss-of-function mutations in RASGAPs are very low, bringing into question whether the loss of RASGAPs plays an important role in CRC development and progression. Moreover, the identification of RASGAPs in large GWAS studies and RASGAP expression analysis studies has led to their family-wide association with tumorigenesis[39,47,48,60–65], in contrast to mutation frequencies that mainly point to NF1[25].

To end the debate, we set out to investigate the functional relationship between all RASGAPs and tumor growth in the presence and absence of EGFR signaling in colorectal tumors. Therefore, we performed a CRISPR-mediated knock-out screen to study RASGAPs with a functional GAP domain in patient-derived CRC organoids. Surprisingly, of all the potential RASGAPs, we identified that only the loss of NF1 resulted in increased tumor growth and EGF-independent cell survival. Importantly, our observations were made in multiple genetic backgrounds and by multiple genetic strategies. On the biochemical level, loss of NF1 results in enhanced RAS-ERK activation but does require presence of active EGFR signaling to do so. Indeed, in contrast to autonomous $KRAS^{G12D}$, NF1 loss mainly acts as a signal amplifier. As such, NF1 deficient tumors remain vulnerable to targeted inhibition of the MAPK pathway, but only under complete inhibitory conditions. Under normal growth conditions, i.e. presence of EGF signals, NF1 deficiency might be responsible for aberrant MAPK signal activation in CRCs that are wild-type for known MAPK driver genes.

Several studies have shown that the expression of NF1 is altered in a number of sporadic cancers[25,40]. Moreover, loss of NF1 expression has been observed in lung adenocarcinomas and melanomas that are resistant to treatment with EGFR[38] and BRAF[28,29,36,37] inhibitors, respectively. Whereas reports on the frequency of genetic alterations of NF1 in CRC show varying results, a recent study associated mutant NF1 with tumor progression and anti-EGFR therapy resistance[46]. To our knowledge we are the first to present direct loss-of-function data that of all RASGAPs only the loss of NF1 promotes enhanced tumor growth and EGF-independent survival in CRC. Next generation sequencing studies identified that the NF1 gene is altered in approximately 5-6% of colorectal carcinomas[66]. Since loss of NF1 can also be accomplished via mechanisms other than loss-of-function mutations, such as epigenetic gene silencing or aberrant protein stability[33,67], analysis of NF1 protein levels in tumor biopsies may be of importance to correctly stratify the patient population for targeted therapy against the MAPK signaling pathway.

Although enhancing RAS-ERK signaling during normal tumor growth conditions, NF1 deficiencies are not as dominant drivers of MAPK signaling activity as oncogenic versions

Figure 6. Puromycin selected NF1 knock-out CRC organoids show enhanced organoid growth upon release of RAS-MAPK pathway inhibition.

(**A**) A schematic overview illustrating the strategy to score sensitivity and outgrowth of P18T parental, RASGAP knock-out, and oncogenic mutant *KRAS* organoids of similar size during and after treatment with colorectal cancer (CRC) medium containing either DMSO, 1 μM afatinib (EGFRi), 1 μM selumetinib (MEKi), or a combination of 1 μM afatinib and 1 μM selumetinib. Organoid size and frequency of alive organoids was quantified after 72 hr of drug treatment and after 7 days of drug withdrawal by phenotypic analysis. (**B**) Representative zoom-in pictures of the parental patient-derived CRC organoids P18T $KRAS^{WT}$, $KRAS^{G12D}$, and P18T $RASA1^{KO}$ (clone # 1 and # 3) or $NF1^{KO}$ (# 6 and # 12) after 72 hours of DMSO or targeted drug treatment (on treatment). (**C**) Representative zoom-in pictures of the parental patient-derived CRC organoids P18T $KRAS^{WT}$, $KRAS^{G12D}$, and P18T $RASA1^{KO}$ (clone # 1 and # 3) or $NF1^{KO}$ (# 6 and # 12) after 7 days of DMSO or drug withdrawal (off treatment). Hoechst and DRAQ7 was used to visualize nuclei and dead cells, respectively.

of KRAS. As a result, patients with NF1 mutant CRCs are much more likely to respond to combinatorial targeting of the MAPK signaling pathway than RAS mutants in case full inhibition is achieved. In relation to mutational co-occurrence, it is conceivable that loss of NF1 can enhance otherwise weak activating mutations of the MAPK signaling pathway to reach optimal levels of pathway activation for efficient tumor growth[68].

To confirm the role of NF1 as an amplifier of the RAS effector, we also tried to determine the levels of RAS-ERK activation upon minimal perturbation of EGFR signaling with low concentrations of afatinib. In contrast to P18T and RASA1 knock-outs, enhanced levels of active RAS-ERK signaling, comparable to levels of KRAS mutants, was again observed at basal conditions in NF1 knock-out organoids. However, elevated levels of active GTP-bound RAS proteins were challenging to detect under minimal perturbation of EGFR signaling, among others due to drug titration difficulties to achieve reduced but remaining EGFR activity, as well as different distribution of RAS proteins at the membrane under changing EGFR stimulation that can mask the effect of NF1 loss on the membrane pool[69].

Whereas several publications have proposed a tumor suppressor role for RASA1 in CRC[43–45], we did not observe elevated levels of RAS and ERK activity in RASA1 knock-out organoids at basal conditions. Importantly, loss of RASA1 was not sufficient to promote EGF-independent survival. Moreover, the upregulated expression levels of other RASGAPs did not point to a clear candidate that could compensate for its loss. From a molecular perspective, it is not clear whether RASA1 is indeed a negative regulator of RAS in colon, or that the existing pool of NF1 or other RASGAPs is sufficient to compensate its absence. For instance, differences in the RAS binding groove have previously been identified between RASA1 and NF1, which have been attributed to higher RAS binding affinities for NF1[53,54]. Moreover, other studies have demonstrated that RASA1 may have increased activity toward R-RAS compared to other RAS proteins, thereby affecting RalA activity, but not PI3K or MAPK signaling[70,71]. Our data, together with observations that ubiquitous loss of RASA1 in mice does not lead to spontaneous tumor formation, questions whether RASA1 functions as an essential tumor suppressor in the gut[72].

Together, using patient-derived CRC organoids, we reveal that of all RASGAPs with functional GAP domains, only NF1 deficiency promote cell survival and enhanced tumor growth upon challenging EGF signaling conditions in human CRC samples. On the basis of our data, we propose that NF1 protein levels should be determined in CRCs prior initiation of targeted therapy against the MAPK pathway. Patients with NF1-deficient tumors are likely to be unresponsive to anti-EGFR targeted monotherapy. However, on a positive note, we did observe that these tumors, unlike KRAS mutant colorectal tumors, are vulnerable towards combinatorial targeting strategies against the RAS-MAPK pathway.

ACKNOWLEDGEMENTS

This work was funded by a KWF fellowship from the Dutch Cancer Society (UU 2013-6070) (HJGS), general support came from the Netherlands Organization for Scientific Research gravitation program Cancer Genomics Netherlands, the Josephine Nefkens foundation and a 'Sta op tegen Kanker' International Translational Cancer Research Grant (JLB). Stand Up to Cancer is a program administered by the AACR. Furthermore, we thank all members of the

Snippert and Bos laboratories for fruitful discussions and support.

AUTHOR CONTRIBUTIONS

JBP, JLB and HJGS conceived the study. JBP, HJGS designed experiments, and JBP performed most of the experiments. JBP and SE generated clones. AEEM and NH performed drug screens. JBP, AEEM, NH and HJGS analyzed and interpreted the data. JBP and HJGS wrote the manuscript, which was reviewed by all authors.

MATERIALS AND METHODS

Patient-derived organoid culture and maintenance

The patient-derived organoids derived in this study were previously established and characterized (van de Wetering et al., 2015 and Drost et al., 2015). Human CRC and TPO2 (APC-/-, TP53-/-) colon organoids were cultured as described previously (van de Wetering et al., 2015, Drost et al., 2015, Verissimo et al., 2016). Culture medium contained advanced DMEM/F12 medium (Invitrogen) with 1% Penicillin/Streptomycin (P/S, Lonza), 1% Hepes buffer (Invitrogen) and 1% Glutamax (Invitrogen), 20% R-spondin conditioned medium, 10% Noggin conditioned medium, 1x B27 (Invitrogen), 1.25 mM n-Acetyl Cysteine (Sigma-Aldrich), 10 mM Nicotinamide (Sigma-Aldrich), 50 ng/ml EGF (Invitrogen), 500 nM A83-01 (Tocris), 10 μM SB202190 (ApexBio) and 100 μg/ml Primorcin (Invitrogen). Organoids were splitted through Trypsin-EDTA (Sigma-Aldrich) treatment. Culture medium after splitting was supplemented with 10 μM Y-27632 dihydrochloride. For selection of RASGAP knock-out mutants, organoids were grown in culture medium containing 1–2 μM puromycin or lacking EGF and containing 0.2–1.0 μM of afatinib (Selleck Chemicals). The Jurkat cells were cultured in RPMI 1640 medium supplemented with 10% FBS, 1% Penicillin/ Streptomycin (P/S, Lonza) and 1% Glutamax (Invitrogen).

Organoid transfection and genotyping

The transfection protocol of P18T and TPO2 organoids was previously described in detail by Fujii et al. (2015). Three days after transfection, culture media plus Y-27632 was exchanged with selection medium. After puromycin selection, surviving clones were picked and subjected to genotyping to detect the presence of insertions and deletions. For genotyping, genomic DNA was isolated using Viagen Direct PCR (Viagen). The presence of insertions or deletions in RASGAPs was verified by using the PCR product obtained using the following primers:

NF1_fw 5'-GACCCTCTCCTTGCCTCTTC-3',
NF1_rv 5'-GGTGGCTCTGAAGCAGTTTC-3',
RASA1_fw1 5'-GACTCTTCCTTTTCCTCCCG-3',
RASA1_rv1 5'-G CAGTTTGGTGAGAGCCATG-3',
RASA1_fw2 5'-GT TGGGCATTACTGTGCTG-3',
RASA1_rv2 5'-GGTG GTGCAACTGGGTAAAG-3',
NF1_fw GAP domain 5'-GTACACTGTTAAATCTCAGG-3',
NF1_rv GAP domain 5'-AGAGGATGTGATCACAATTC-3',
RASA1_fw GAP domain 5'-GTCTTACAGAGTTAAGTCTG-3',
RASA1_rv GAP domain 5'-GTATTACAGACAGGTGT AAC-3',
RASA2_fw GAP domain 5'-CTTATGCCTTCT AGTATGTC-3',
RASA2_rv GAP domain 5'-TGCTTCTA AAGTGTTCAGTC-3',
RASA3_fw GAP domain 5'-GT GTTGACACAGGACGGTTC-3',
RASA3_rv GAP domain 5'-GGAGTACACAGGGAACATCC-3',
RASA4_fw GAP domain 5'-AGAACACTGGGAGGTG TTTG-3',
RASA4_rv GAP domain 5'-CGAACTCCTG ACCTTAAGTG-3',
RASAL1_fw GAP domain 5'-TGTG CACCTCCAGACAGTTG-3',
RASAL1_rv GAP domain 5'-GACCATGCAGGAAGAGGTTC-3',
RASAL2_fw GAP domain 5'-CAGCATTTCCAGGATG TCTG-3',
RASAL2_rv GAP domain 5'-AGCAGTGTA TGCTGACAAGG-3',
RASAL3_fw GAP domain 5'-GC CTAAGCATCAGCTACAAG-3',
RASAL3_rv GAP domain 5'-GTCTTCAGGTTATTCCGGAG-3',
SYNGAP1_fw GAP domain 5'-CACATCCTGCAGAGT ACAGG-3',
SYNGAP1_rv GAP domain 5'-ACAAGAG GGTGTGGTCACAC-3',
DAB2IP_fw GAP domain 5'-C ACCAGTTCTAGGCTCCTAC-3',
DAB2IP_rv GAP domain 5'-ACTTGCTGGGATCCACTTCG-3'.

Products were sequenced using the following primers:
NF1 exon 1 5'-CTTCCTTTCCTCCAGAGCCTG-3',
RASA1 exon 1 5'-CACAAGCTGCCCTCTCCCTT-3',
RASA1 exon 3 5'-CAAATAAACTTTGAGTGGTA-3',
NF1 GAP domain 5'-GTACACTGTTAAATCTCAGG-3',
RASA1 GAP domain 5'-GTACTTTCAACGCTGCAC-3',
RASA2 GAP domain 5'-CCTTCCCATCAATAGATC-3',
RASA3 GAP domain 5'-GTGTTGACACAGGACGGT TC-3',

RASA4 GAP domain 5'-GAACACTGGAGTCGA AGTC-3',
RASAL1 GAP domain 5'-CTGGAAGAATC ATGACTCC-3',
RASAL2 GAP domain 5'-CCAGTGCG TCATGAAGATAC-3',
RASAL3 GAP domain 5'-GTCT TCAGGTTATTCCGGAG-3',
SYNGAP1 GAP domain 5'-CACGAGATTGGGTTGTGC-3',
DAB2IP GAP domain 5'-CTAGGTCTGGAATCCTAG-3'.
In addition, the CloneJET PCR Cloning Kit was used to confirm indel generation in NF1 knock-outs #1 and #6 and of RASA1 knock-outs #1 and #3.

The presence of the puromycin selection cassette was verified by using the PCR product obtained using primers:

Puro_1_fw 5'-GACCCTCTCCTTGCCTCTTC-3',
Puro_1_rv 5'-GTTGGCGCCTACCGGTGG-3',
Puro_2_fw 5'-ATGGGGACCGAGTACAAGCC-3',
Puro_2_rv 5'-GTCGAAGATGAGGGTGAG-3'.

Vector construction
The CRISPR guide RNA (sgRNAs) were designed by an online CRISPR design tool (http://crispr.mit.edu). The sgRNA guide sequences used can be found in the Supplementary Materials (Supplementary Table 1). The sgRNAs used for the RASGAP knock-out screen were cloned into a plasmid (px458) expressing both sgRNA and hCas9-2A-GFP as previously described (Ran *et al*., 2013).
For CRISPR-mediated homologous recombination the human codon-optimized Cas9 expression plasmid was obtained from Addgene (41815). The sgRNA-GFP plasmid was obtained from Addgene (41819) and used as a template for generating target specific sgRNAs as described in detail by Drost *et al.* (2015). For the generation of the donor template, genomic DNA from P18T organoids was used to PCR amplify the NF1 and RASA1 homology arms using high-fidelity Phusion Polymerase (New England BioLabs). The 5' homology arm of RASA1 spans the region Chr5:87331757-87332526, and the 3' homology arm spans the region Chr5:87332575-87333379. The 5' homology arm of NF1 spans the region Chr17:31094574- 31095323, and the 3' homology arm spans the region Chr17:31095361-31096136. The homology arms were cloned into a pBlueScript plasmid expressing a 3229- bp AATPB:PGKpuroDtk selection cassette (Schwank *et al*., 2013).

Western blot assay and RAS-GTP pull down
Prior to cell lysis, organoids were incubated with 1 mg/ml dispase II (Invitrogen) for 10 minutes at 37° C to digest the BME. Western blot samples for NF1 and RASA1 protein levels were lysed using NETN buffer (50 mM Tris-HCL pH 8.0, 250 mM NaCl, 5 mM EDTA, 0.5% NP-40) containing Complete protease inhibitors (Roche). Western blot samples for phosphorylated ERK were lysed using RIPA buffer (50 mM Tris-HCL pH 8.0, 150 mM NaCl, 0.1% SDS, 0.5% Na-Deoxycholate, 1% NP-40) containing Complete protease inhibitors (Roche). Protein content was quantified using a BCA protein assay kit (PierceTM) and analyzed by Western blotting. Membranes were blocked and probed with antibodies directed against NF1 (RRID:AB_2149790), RASA1 (RRID:AB_303418), Vinculin RRID:AB_477629, a-tubulin (RRID:AB_477579), GAPDH (RRID:AB_2107445), pERK (RRID:AB_331646), and ERK (RRID:AB_390779).
Samples for RAS-GTP isolation were lysed using Ral lysis buffer (50 mM Tris-HCL pH 7.5, 200 mM NaCl, 2 mM MgCl2, 10% glycerol, 1% NP-40) containing Complete protease inhibitors (Roche). Lysates were normalized for protein levels using a BCA protein assay kit (PierceTM) and subsequently GTP-bound RAS was isolated via immunoprecipitation using recombinant RAS binding domain of RAF1 (RAF1-RBD). Protein lysates were run on SDS-PAGE gels and transferred to PVDF membranes (Millipore). Membranes were blocked and probed with antibodies directed against RAS (RRID:AB_397425). Organoid treatments: afatinib (Selleck Chemicals) 1 μM, 1 h and 24 h or DMSO.

RNA isolation, cDNA preparation and qRT–PCR
Organoids were harvested in RLT lysis buffer and RNA was isolated using the Qiagen RNeasy kit (Qiagen) according to the manufacturer's instructions. Extracted RNA was used as a template for cDNA production using iScriptTM cDNA Synthesis Kit (Bio-Rad) according to the manufacturer's protocol. qRT–PCR was performed using FastStart Universal SYBR Green Master mix (Roche) according to the manufacturer's protocol. Results were calculated by using the relative standard curve method. Primer sequences:

B2M_fw 5'-GAGGCTATCCAGCGTACTCCA-3',
B2M_rv 5'-CGGCAGGCATACTCATCTTTT-3',
NF1_fw 5'-GGATCCTACCAGGTTAGAACCATC-3',

NF1_rv 5'-AGCTTTATTCAGTAGGGAGTGGC-3',
RASA1_fw 5'-AATGCAGGATCAAGAACAAG-3',
RASA1_rv 5'-AAGGCATCCTTTGTTTTACG-3',
RASA2_fw 5'-GACTTGTGTAATCACAGTGG-3',
RASA2_rv 5'-TACCCTGAACCTCTGAATTG-3',
RASA3_fw 5'-AAGAGTGTTGAGCAGCCCAT-3',
RASA3_rv 5'-TAGAGAGGCTGGTCCCCTTTG-3',
RASA4_fw 5'-CAGCCGGGACGACGTTATC-3',
RASA4_rv 5'-CCACCCGCTGAAACCCTTAG-3',
RASAL1_fw 5'-CGTGCTGGATGAGGACACTG-3',
RASAL1_rv 5'-TCCCTGCTCAGCGAGATCTT3',
RASAL2_fw 5'-CCCAACTCCATGGACACTGC-3',
RASAL2_rv 5'-GGATGGAAGCCGAAAGCTCG-3',
RASAL3_1_fw 5'-GGATCCAGATCGGATGCCTG-3',
RASAL3_1_rv 5'-TCCCTAGAGCCCAGAGCAC-3',
RASAL3_2_fw 5'-AACAGAACCGGAGACTGCTG-3',
RASAL3_2_rv 5'-GCTCCAACCTGGCCTTTTTC-3',
RASAL3_3_fw 5'-GCTCAAGAGGCTGAAAGAG-3',
RASAL3_3_rv 5'-CAGGTCCAGTTCAGAGAGTG-3',
DAB2IP_fw 5'-CATCATCAGCAGGTTGATGTCC-3',
DAB2IP_rv 5'-AGCGGGCTTTTGTTTCTAATGC-3',
SYNGAP1_fw 5'-ATGCAAAGCTTTAAGGAGTC-3',
SYNGAP1_rv 5'-GTTCCTGATGAAGTTGTTACC-3'

Targeted inhibitors
Afatinib and Selumetinib, were purchased from Selleck Chemicals. These compounds were dissolved in dimethylsulfoxide (DMSO, Sigma-Aldrich) and stored as 10 mM aliquots.

Phenotypic drug screen and calcein green assay
Five days after organoid trypsinization, 1 mg/ml dispase II (Invitrogen) was added to the medium of the organoids and these were incubated for 15 min at 37° C to digest the BME. Subsequently, organoids were mechanically dissociated by pipetting, filtrated using a 40 μm nylon cell strainer (Falcon), resuspended in 75% BME/growth medium (40 organoids/μl) prior plating of two 10 μl drops on NuncTM Lab-TekTM II Chamber SlideTM Systems. After plating culture medium containing either 1 μM of afatinib, 1 μM of selumetinib, a combination of 1 μM of afatinib and 1 μM of selumetinib or DMSO was added. The labtek plates were mounted on an inverted confocal laser scanning microscope (Leica SP8X) and imaged using a 10X objective. For visualization of cell viability, organoids were incubated with 16.2 μM Hoechst 33342 (Life Technologies) and 1.5 μM DRAQ7TM (Cell Signaling #7406) for 30 min at 37° C prior imaging.
For the GAP domain knock-out CRISPR screen, organoids were imaged by an inverted routine microscope (Nikon Eclipse TS100) using a 4X or 10X objective. For calculating organoid count and size, organoids were incubated for 45 minutes with 500 ml culture medium containing 5 μM calcein-green (Invitrogen). For the quantification of the organoid size and count, FIJI analysis software was used.

SUPPLEMENTARY FIGURES

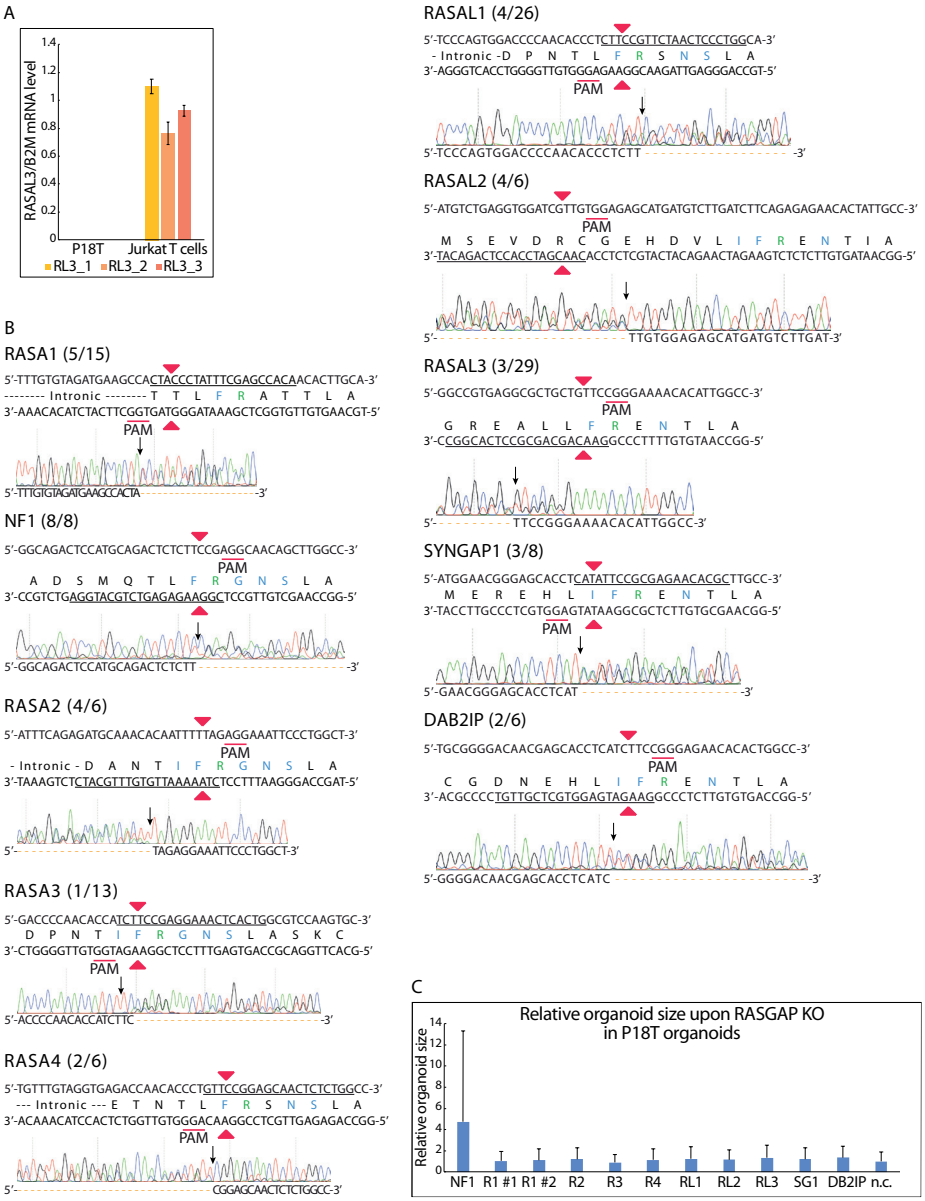

Supplementary Figure 1. CRISPR screen targeting GAP domains reveals increased cell growth upon NF1 loss in patient-derived CRC organoids.
(**A**) The mRNA expression level of RASAL3 was analyzed in P18T organoids and Jurkat T cells using qPCR. The relative expression of *RASAL3* was normalized to the *B2M* housekeeping gene (representative from n = 3 independent experiments). (**B**) Sanger sequencing results (representative of multiple monoclonal organoid lines) indicate the introduction of indels in the GAP domain of each *RASGAP* targeted by the CRISPR machinery. The number of mutant monoclonal organoids per total number of clones sequenced are indicated in brackets. Nonmatching bases are shown in orange. The protospacer is underlined. The catalytic arginine of the finger loop

is depicted in green and the conserved residues in blue. Red and black arrow heads indicate cleavage sites. (C) The bar graph depicts the relative size of organoids (size > background) upon CRISPR-mediated knock-out of indicated RASGAPs in P18T CRC organoids after selection with EGF depletion and afatinib treatment. Organoids size was measured by the calcein green assay (see Materials and Methods).

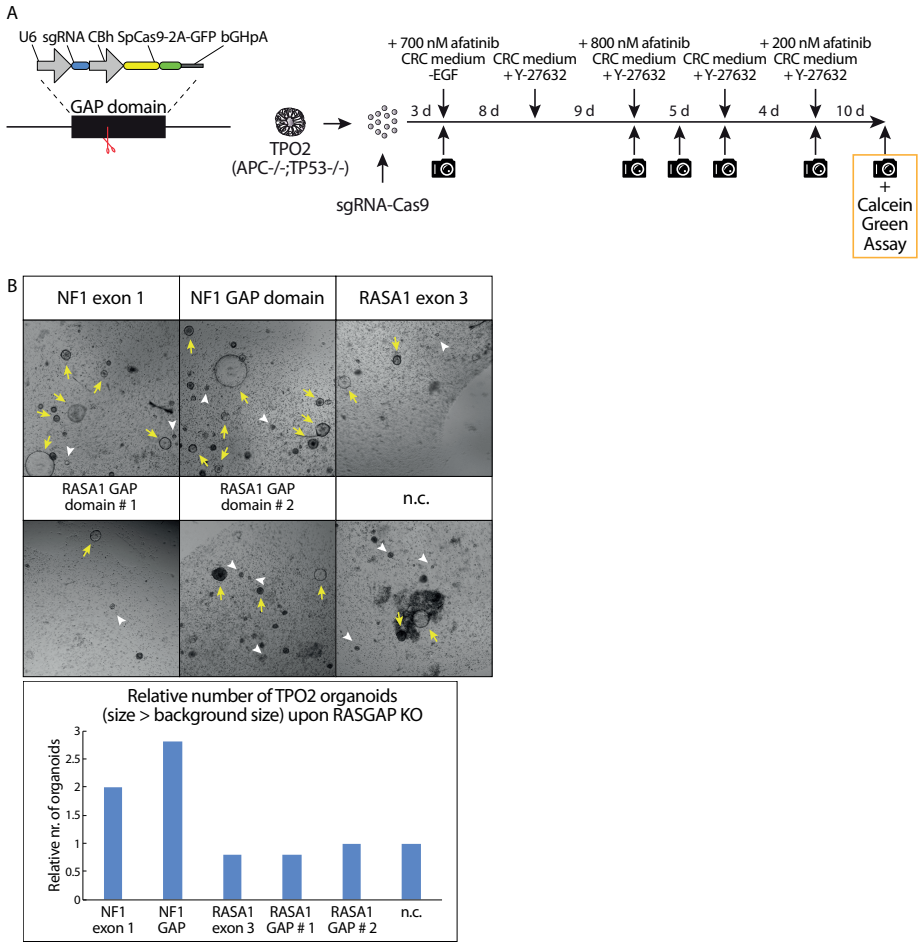

Supplementary Figure 2. CRISPR screen targeting GAP domains reveals increased growth and EGF-independent survival upon NF1 loss in human tumor progression organoids.
(A) A schematic overview of the RASGAP knock-out screen in engineered human colorectal tumor organoids, so-called TPO2 (APC–/–, TP53–/–). An expression plasmid containing both an U6 promoter-driven sgRNA and a CBh promoter-driven SpCas9-2A-GFP was used to target the RASGAP domain. (B) TPO2 organoids in selection medium that have been transfected with indicated sgRNAs and Cas9. White arrow heads indicate representative background organoids. Yellow arrows indicate successful organoids that are significantly larger than background. Bar graph depicts the relative number of organoids with a size larger than background organoids as determined in the negative control. Area of alive RASGAP knock-out organoids was measured using calcein green assay (see Materials and Methods).

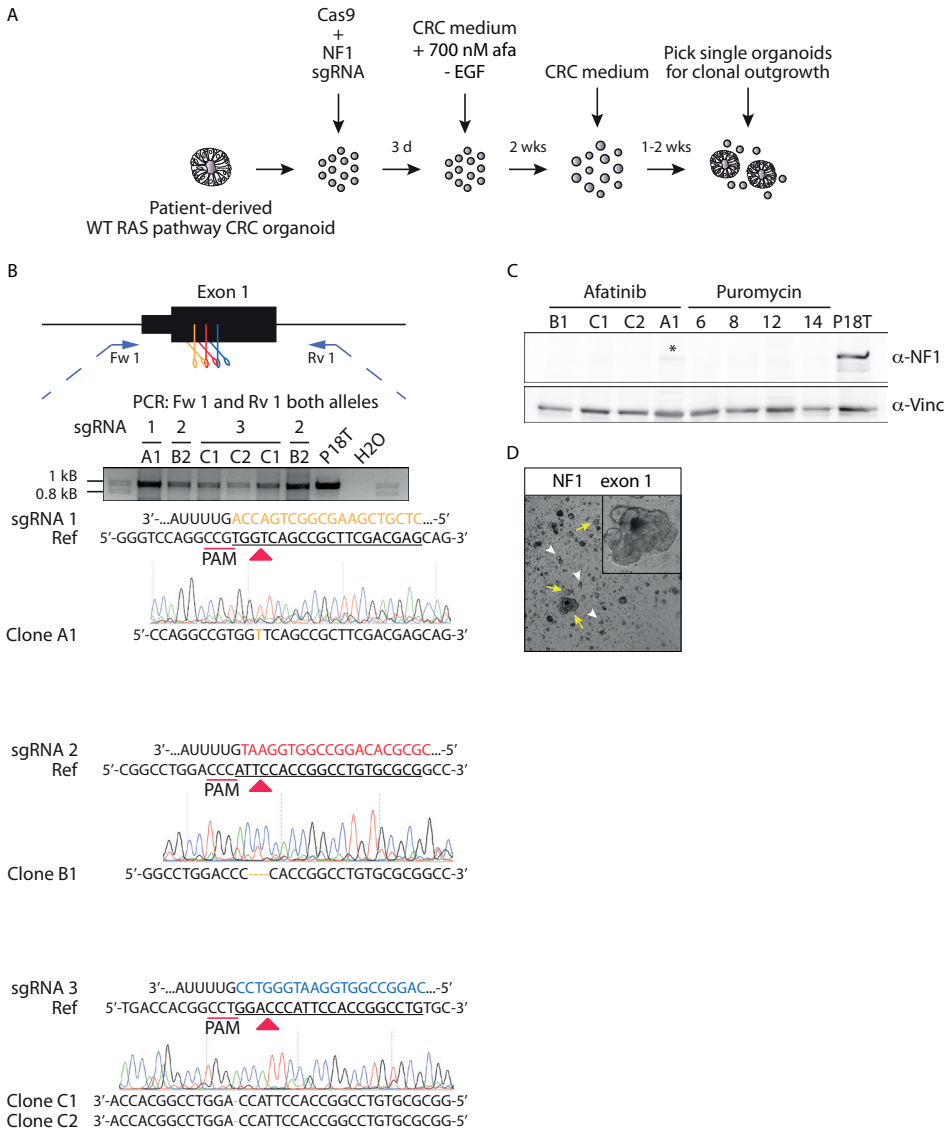

Supplementary Figure 3. Generation of CRISPR-mediated NF1 knock-out in patient-derived CRC organoids using phenotypic selection.

(**A**) Selection strategy to generate NF1 knock-out organoids after CRISPR-induced small indel generation. (**B**) Genetic strategy for CRISPR/Cas9-mediated generation of small indels in exon 1 of *NF1* via non-homologous end-joining. The black box illustrates exon 1, and thin strokes illustrate introns. Scissors show double stranded breaks generated by three different sgRNAs (yellow, red and blue). Blue arrows illustrate PCR primer pairs. The agarose electrophoresis gel shows the PCR product of the targeted exon of *NF1* in selected clones. PCR amplification products were sequenced. Regions of sgRNA 1, 2 and 3 complementary to the protospacer (underlined) are shown in yellow, red and blue, respectively. Red arrow heads indicate cleavage sites and introduced mutations are shown in orange (**C**) Western blot analysis of NF1 expression in the indicated organoid lines. Left 4 clones are selected on phenotype (afatinib presence). For reference, right 4 clones are reproduced from Figure 3C. Asterisks indicate residual NF1 protein presence. (**D**) Representative picture of NF1 knock-out organoids selected by EGF depletion and EGFR inhibition (afatinib).

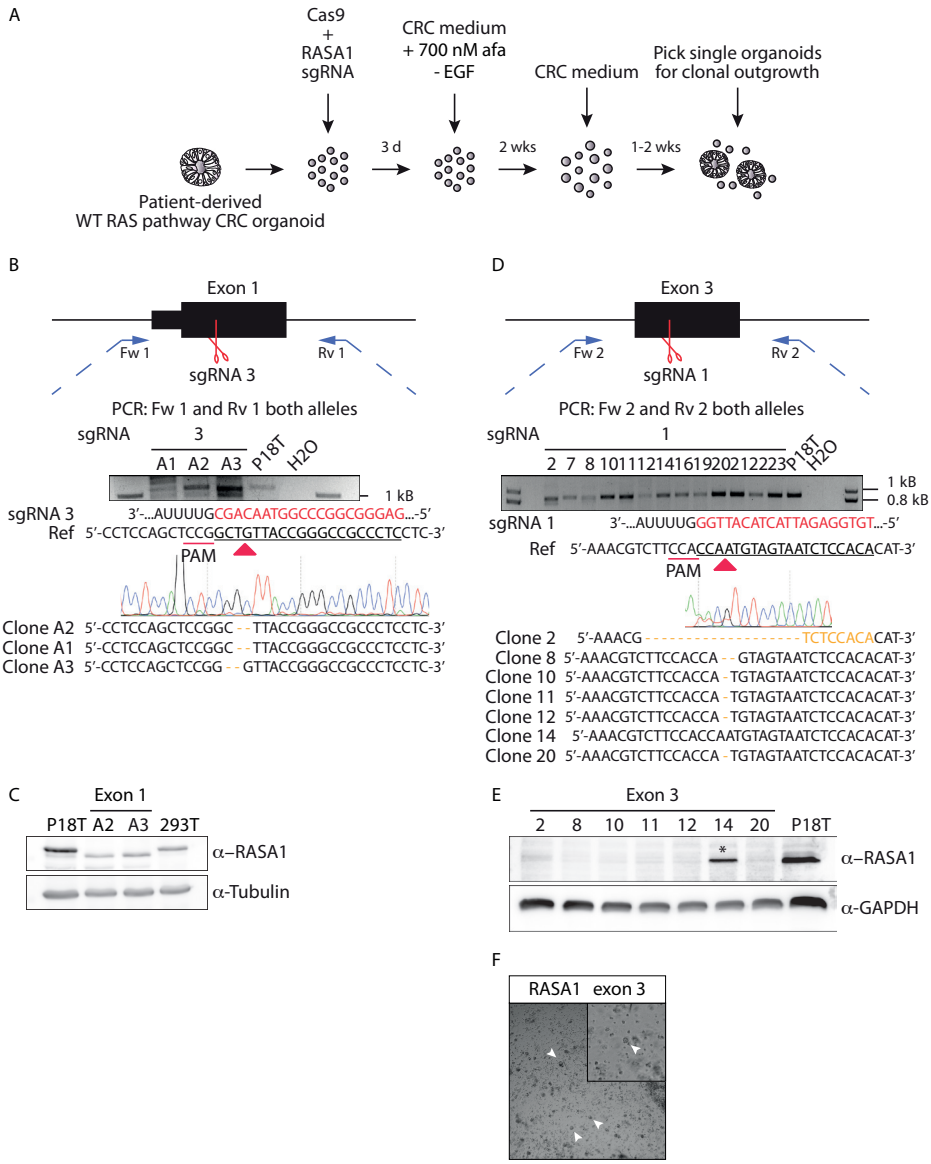

Supplementary Figure 4. Generation of CRISPR-mediated RASA1 knock-out in patient-derived CRC organoids using phenotypic selection.
(**A**) Selection strategy to generate RASA1 knock-out organoids after CRISPR-induced small indel generation. (**B, D**) Genetic strategy for CRISPR/Cas9-mediated generation of small indels in exon 1 and 3 of *RASA1* respectively via non-homologous end-joining. The black boxes illustrate exon 1 and 3 respectively, and thin strokes illustrate introns. Scissors show double stranded breaks generated by different sgRNAs. Blue arrows illustrate PCR primer pairs. The agarose electrophoresis gel shows the PCR product of the targeted exons of *RASA1* in selected clones. PCR amplification products were sequenced. Regions of sgRNAs complementary to the protospacer (underlined) are shown in red. Red arrow heads indicate cleavage sites and introduced mutations are shown in orange. Note that the *RASA1* exon 3 sequence of clone 14 reveals to be wild-type. (**C, E**) Western blot analysis of RASA1 levels in the indicated organoid lines. Note that targeting of exon 1 of *RASA1* results in predominant expression of a truncated isoform due to an alternative start site in exon 1. Asterisks indicate wild-type RASA1 protein presence. In agreement with the wild-type

sequence of clone 14, normal levels of RASA1 is detected. (**F**) Representative picture of RASA1 exon 3 knock-out organoids selected by EGF depletion and EGFR inhibition (afatinib).

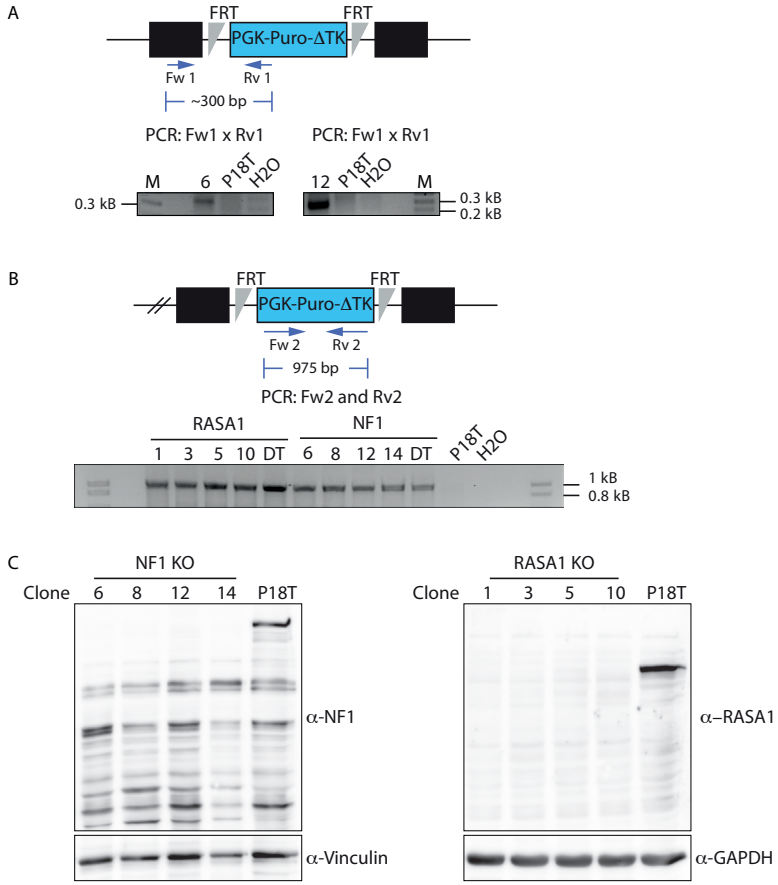

Supplementary Figure 5. Genomic integration of puromycin selection cassette in NF1 and RASA1 knock-out patient-derived CRC organoids.
(**A**) The structure of the targeted exon of *NF1* is depicted at the top. Black box illustrates exon 1, and thin strokes illustrate introns. Blue arrows illustrate PCR primer pairs. The agarose electrophoresis gel shows the ~300 bp PCR product of the integrated puromycin selection cassette at the targeted *NF1* locus in the selected clones (knock-out clones # 6 and 12). (**B**) The structure of the targeted exon of *NF1* and *RASA1* is depicted at the top. The agarose electrophoresis gel shows the ~1 kb PCR product of the integrated puromycin selection cassette in the genome of the selected clones that were targeted for homologous recombination (RASA1 knock-out clones # 1, 3, 5 and 10, and NF1 knock-out clones # 6, 8, 12 and 14). The donor template (DT) was used as a positive control. (**C**) Uncropped images of western blot analysis for NF1 and RASA1 presence in the indicated organoid lines.

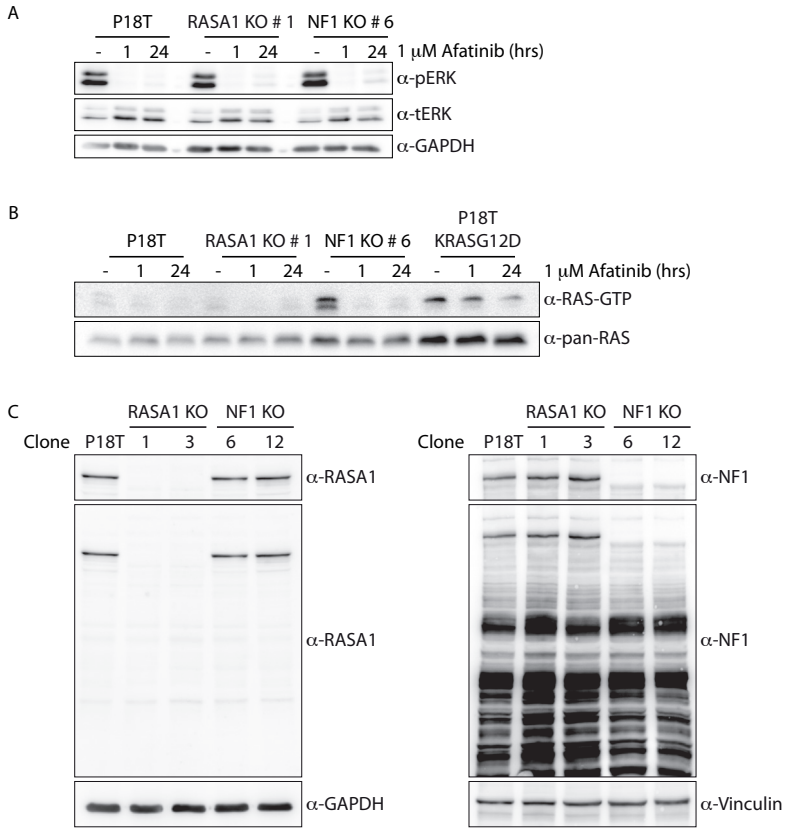

Supplementary Figure 6. Puromycin selected NF1 knock-out CRC organoids show enhanced RAS and ERK activation.

Same as Figure 5, but for different clones. (**A**) In comparison to P18T and P18T RASA1^{KO} (clone # 1), predominantly the P18T NF1^{KO} (clone # 6) shows enhanced basal ERK phosphorylation levels. Representative from n = 3 independent experiments. (**B**) Loss of NF1 (clone # 6) leads to elevated levels of RAS activity (GTP-loading) at basal conditions compared to P18T and P18T RASA1^{KO} (clone # 1) CRC organoids. The presence of an oncogenic mutation in *KRAS* (P18T KRAS^{G12D}) leads to elevated and sustained high levels of RAS activity (GTP-loading) at basal and in afatinib-treated conditions, respectively. RAS immunoblots from RAS pull-down assays are shown (RAS-GTP), together with a RAS immunoblot from total cell lysates as loading control. HRAS, KRAS, and NRAS isoforms are detected. Representative from n = 2 independent experiments. (**C**) Uncropped images of immunoblots of P18T, P18T RASA1^{KO} (clone # 1 and 3), P18T NF1^{KO} (clone # 6 and 12) CRC organoids indicate that the loss of RASA1 does not result in elevated protein levels of NF1, and vice versa. Representative from n = 3 independent experiments.

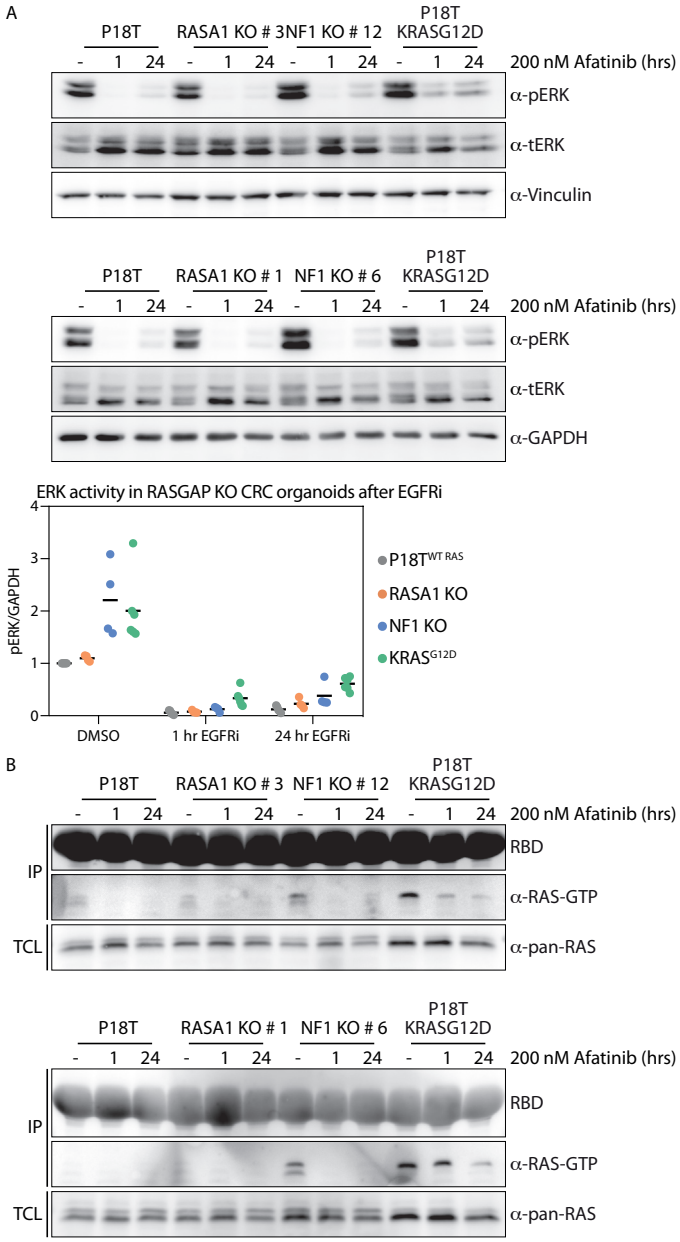

Supplementary Figure 7. Puromycin selected NF1 knock-out CRC organoids show enhanced RAS and ERK activation (low concentration of EGFR inhibition).
Same as Figure 5 and Supplementary Figure 6, but at 200 nM of afatinib treatment. (**A**) In comparison to P18T and P18T RASA1^{KO}, predominantly the P18T NF1^{KO} shows enhanced basal ERK phosphorylation levels. Representative from n = 2 independent experiments. Scatter dot plot depicts ERK phosphorylation levels normalized to GAPDH of P18T parental, RASA1^{KO} and NF1^{KO} organoids (n = 3). (**B**) Loss of NF1 leads to elevated levels of RAS activity (GTP-loading) at basal conditions compared to P18T and P18T RASA1^{KO} CRC organoids. The presence of an oncogenic mutation in *KRAS* (P18T KRAS^{G12D}) leads to elevated and sustained high levels of RAS activity (GTP-loading) at basal and in afatinib-treated conditions, respectively. RAS immunoblots from RAS pull-down assays are shown

(RAS-GTP), together with a RAS immunoblot from total cell lysates as loading control. HRAS, KRAS, and NRAS isoforms are detected. Representative from n = 2 independent experiments.

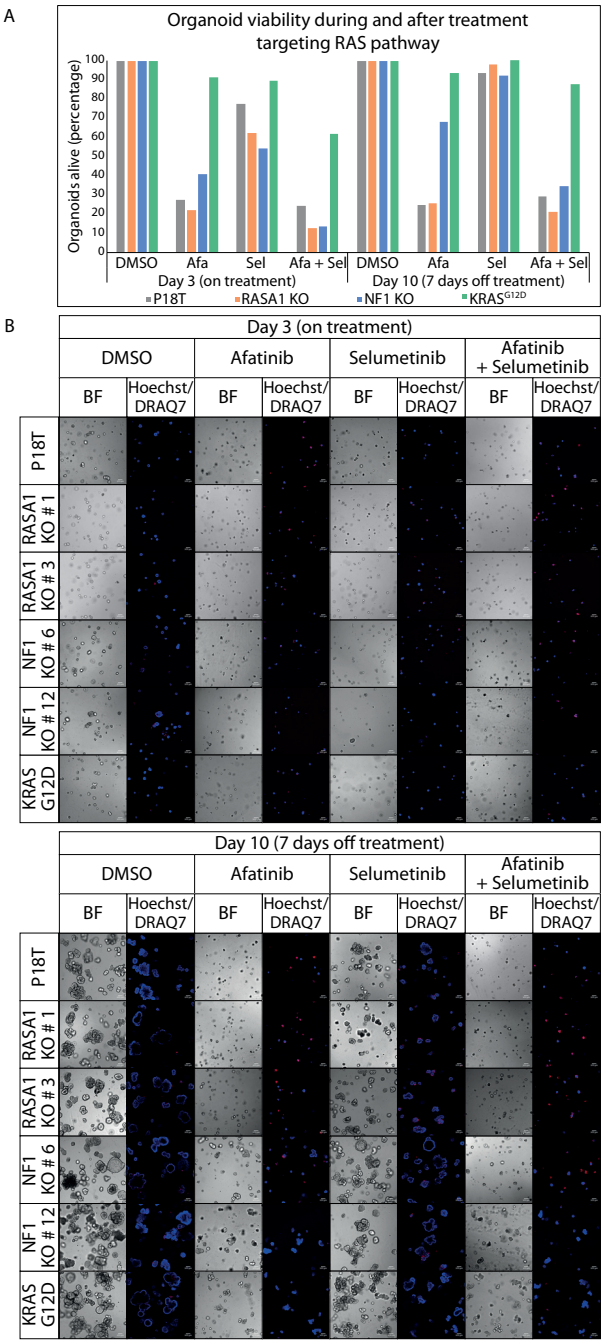

Supplementary Figure 8. Puromycin selected NF1 knock-out CRC organoids show enhanced organoid survival and growth upon release of RAS-MAPK pathway inhibition.
(**A**) Bar graph depicts the frequency of alive organoids after 3-day treatment and 7-day release of treatment with colorectal cancer (CRC) medium containing either DMSO, 1 μM afatinib (EGFRi), 1 μM selumetinib (MEKi), or a combination of 1 μM afatinib and 1 μM selumetinib in P18T parental, RASGAP knock-out, and oncogenic mutant *KRAS* organoids. (**B**) Original pictures of organoids depicted in Figure 6. Scale bars, 100 μM. Hoechst and DRAQ7 was used to visualize nuclei and dead cells, respectively.

SUPPLEMENTARY TABLES

Supplementary Table 1. Target sites of and sgRNA guide sequences used for the generation of knock-out organoids.

Target site	Guide sequence
RASA1 exon 1	GAGGGCGGCCCGGTAACAGC
RASA1 exon 3	TGTGGAGATTACTACATTGG
NF1 exon 1 # 1	CTCGTCGAAGCGGCTGACCA
NF1 exon 1 # 2	CGCGCACAGGCCGGTGGAAT
NF1 exon 1 # 3	CAGGCCGGTGGAATGGGTCC
NF1 GAP domain	TCCATGCAGACTCTCTTCCG
RASA1 GAP domain # 1	CAAGTGTTGTGGCTCGAAAT
RASA1 GAP domain # 2	TGTGGCTCGAAATAGGGTAG
RASA2 GAP domain	GATGCAAACACAATTTTTAG
RASA3 GAP domain	CAGTGAGTTTCCTCGGAAGA
RASA4 GAP domain	CCAGAGAGTTGCTCCGGAAC
RASAL1 GAP domain	CCAGGGAGTTAGAACGGAAG
RASAL2 GAP domain	ATGTCTGAGGTGGATCGTTG
RASAL3 GAP domain	GCCGTGAGGCGCTGCTGTTC
SYNGAP1 GAP domain	GCGTGTTCTCGCGGAATATG
DAB2IP GAP domain	ACAACGAGCACCTCATCTTC

REFERENCES

1. Cunningham D, Humblet Y, Siena S, et al. Cetuximab Monotherapy and Cetuximab plus Irinotecan in Irinotecan-Refractory Metastatic Colorectal Cancer. *N Engl J Med*. 2004;351(4):337-345. doi:10.1056/NEJMoa033025
2. Van Cutsem E, Köhne C-H, Hitre E, et al. Cetuximab and Chemotherapy as Initial Treatment for Metastatic Colorectal Cancer. *N Engl J Med*. 2009;360(14):1408-1417. doi:10.1056/NEJMoa0805019
3. Douillard JY, Siena S, Cassidy J, et al. Randomized, Phase III trial of panitumumab with infusional fluorouracil, leucovorin, and oxaliplatin (FOLFOX4) Versus FOLFOX4 alone as first-line treatment in patients with previously untreated metastatic colorectal cancer: The PRIME study. *J Clin Oncol*. 2010;28(31):4697-4705. doi:10.1200/JCO.2009.27.4860
4. Masui H, Kawamoto T, Sato JD, Wolf B, Sato G, Mendelsohn J. Growth Inhibition of Human Tumor Cells in Athymic Mice by Anti-Epidermal Growth Factor Receptor Monoclonal Antibodies. *Cancer Res*. 1984;44(3):1002-1007.
5. Brand TM, Iida M, Wheeler DL. Molecular mechanisms of resistance to the EGFR monoclonal antibody cetuximab. *Cancer Biol Ther*. 2011;11(9):777-792. doi:10.4161/cbt.11.9.15050
6. Karapetis CS, Khambata-Ford S, Jonker DJ, et al. *K-ras* Mutations and Benefit from Cetuximab in Advanced Colorectal Cancer. *N Engl J Med*. 2008. doi:10.1056/NEJMoa0804385
7. Amgen. EPAR - Summary For The Public: Vectibix (panitumumab). 2015;44(0):1-4. http://www.ema.europa.eu/docs/en_GB/document_library/EPAR_-_Summary_for_the_public/human/000741/WC500047704.pdf%0Ahttp://www.ema.europa.eu/ema/index.jsp?curl=pages/medicines/human/medicines/000741/human_med_001128.jsp&mid=WC0b01ac058001d124.
8. European Medicines Agency. CHMP summary of opinion—erbitux. *http://www ema.europa.eu/docs/en_GB/document_library/Summary_of_opinion/human/000558/WC500155463.pdf*. 2013;1(November):14-15.
9. Cox AD, Der CJ. Ras history: The saga continues. *Small GTPases*. 2010;1(1):2-27. doi:10.4161/sgtp.1.1.12178
10. Bos JL, Fearon ER, Hamilton SR, et al. Prevalence of ras gene mutations in human colorectal cancers. *Nature*. 1987;327(6120):293-297. doi:10.1038/327293a0
11. Yuen ST, Davies H, Chan TL, et al. Similarity of the phenotypic patterns associated with BRAF and KRAS mutations in colorectal neoplasia. *Cancer Res*. 2002;62(22):6451-6455. doi:10.1038/sj.leu.2404688
12. Nash GM, Gimbel M, Cohen AM, et al. KRAS mutation and microsatellite instability: Two genetic markers of early tumor development that influence the prognosis of colorectal cancer. *Ann Surg Oncol*. 2010;17(2):416-424. doi:10.1245/s10434-009-0713-0
13. Misale S, Bozic I, Tong J, et al. Vertical suppression of the EGFR pathway prevents onset of resistance in colorectal cancers. *Nat Commun*. 2015;6:8305. doi:10.1038/ncomms9305
14. Misale S, Yaeger R, Hobor S, et al. Emergence of KRAS mutations and acquired resistance to anti-EGFR therapy in colorectal cancer. *Nature*. 2012;486(7404):532-536. doi:10.1038/nature11156
15. Diaz LA, Sausen M, Fisher GA, Velculescu VE. Insights into therapeutic resistance from whole-genome analyses of circulating tumor DNA. *Oncotarget Oncotarget Oncotarget*. 2013;44(4):1856-1857. doi:10.18632/oncotarget.1486
16. Misale S, Arena S, Lamba S, et al. Blockade of EGFR and MEK Intercepts Heterogeneous Mechanisms of Acquired Resistance to Anti-EGFR Therapies in Colorectal Cancer. *Sci Transl Med*. 2014;6(224):224ra26-224ra26. doi:10.1126/scitranslmed.3007947
17. Almoguera C, Shibata D, Forrester K, Martin J, Arnheim N, Perucho M. Most human carcinomas of the exocrine pancreas contain mutant c-K-ras genes. *Cell*. 1988;53(4):549-554. doi:10.1016/0092-8674(88)90571-5
18. Smit VT, Boot AJ, Smits AM, Fleuren GJ, Cornelisse CJ, Bos JL. KRAS codon 12 mutations occur very frequently in pancreatic adenocarcinomas. *Nucleic Acids Res*. 1988;16(16):7773-7782. https://www.ncbi.nlm.nih.gov/pubmed/3047672.
19. Bardelli A, Siena S. Molecular mechanisms of resistance to cetuximab and panitumumab in colorectal cancer. *J Clin Oncol*. 2010;28(7):1254-1261. doi:10.1200/JCO.2009.24.6116
20. De Roock W, Claes B, Bernasconi D, et al. Effects of KRAS, BRAF, NRAS, and PIK3CA mutations on the efficacy of cetuximab plus chemotherapy in chemotherapy-refractory metastatic colorectal cancer: A retrospective consortium analysis. *Lancet Oncol*. 2010;11(8):753-762. doi:10.1016/S1470-2045(10)70130-3
21. Bertotti A, Papp E, Jones S, et al. The genomic landscape of response to EGFR blockade in colorectal cancer. *Nature*. 2015;526(7572):263-267. doi:10.1038/nature14969
22. Misale S, Di Nicolantonio F, Sartore-Bianchi A, Siena S, Bardelli A. Resistance to Anti-EGFR therapy in colorectal cancer: From heterogeneity to convergent evolution. *Cancer Discov*. 2014;4(11):1269-1280. doi:10.1158/2159-8290.CD-14-0462

23. Medico E, Russo M, Picco G, et al. The molecular landscape of colorectal cancer cell lines unveils clinically actionable kinase targets. *Nat Commun*. 2015;6:7002. doi:10.1038/ncomms8002
24. Davoli T, Xu AW, Mengwasser KE, et al. XCumulative haploinsufficiency and triplosensitivity drive aneuploidy patterns and shape the cancer genome. *Cell*. 2013. doi:10.1016/j.cell.2013.10.011
25. Lawrence MS, Stojanov P, Mermel CH, et al. Discovery and saturation analysis of cancer genes across 21 tumour types. *Nature*. 2014;505:495. https://doi.org/10.1038/nature12912.
26. Krauthammer M, Kong Y, Bacchiocchi A, et al. Exome sequencing identifies recurrent mutations in NF1 and RASopathy genes in sun-exposed melanomas. *Nat Genet*. 2015;47(9):996-1002. doi:10.1038/ng.3361
27. Hodis E, Watson IR, Kryukov G V., et al. A landscape of driver mutations in melanoma. *Cell*. 2012;150(2):251-263. doi:10.1016/j.cell.2012.06.024
28. Nissan MH, Pratilas CA, Jones AM, et al. Loss of NF1 in cutaneous melanoma is associated with RAS activation and MEK dependence. *Cancer Res*. 2014;74(8):2340-2350. doi:10.1158/0008-5472.CAN-13-2625
29. Maertens O, Johnson B, Hollstein P, et al. Elucidating distinct roles for NF1 in melanomagenesis. *Cancer Discov*. 2013;3(3):338-349. doi:10.1158/2159-8290.CD-12-0313
30. Boudry-Labis E, Roche-Lestienne C, Nibourel O, et al. Neurofibromatosis-1 gene deletions and mutations in de novo adult acute myeloid leukemia. *Am J Hematol*. 2013;88(4):306-311. doi:10.1002/ajh.23403
31. Chang T, Krisman K, Theobald EH, et al. Sustained MEK inhibition abrogates myeloproliferative disease in Nf1 mutant mice. *J Clin Invest*. 2013;123(1):335-339. doi:10.1172/JCI63193
32. Mullally A, Ebert BL. NF1 inactivation Revs up Ras in adult acute myelogenous leukemia. *Clin Cancer Res*. 2010;16(16):4074-4076. doi:10.1158/1078-0432.CCR-10-1438
33. McGillicuddy LT, Fromm JA, Hollstein PE, et al. Proteasomal and Genetic Inactivation of the NF1 Tumor Suppressor in Gliomagenesis. *Cancer Cell*. 2009;16(1):44-54. doi:10.1016/j.ccr.2009.05.009
34. Cichowski K, Santiago S, Jardim M, Johnson BW, Jacks T. Dynamic regulation of the Ras pathway via proteolysis of the NF1 tumor suppressor. *Genes Dev*. 2003;17(4):449-454. doi:10.1101/gad.1054703
35. Hiatt KK, Ingram DA, Zhang Y, Bollag G, Clapp DW. Neurofibromin GTPase-activating Protein-related Domains Restore Normal Growth in Nf1-/- Cells. *J Biol Chem*. 2001;276(10):7240-7245. doi:10.1074/jbc.M009202200
36. Whittaker SR, Theurillat JP, Van Allen E, et al. A genome-scale RNA interference screen implicates NF1 loss in resistance to RAF inhibition. *Cancer Discov*. 2013;3(3):350-362. doi:10.1158/2159-8290.CD-12-0470
37. Van Allen EM, Wagle N, Sucker A, et al. The genetic landscape of clinical resistance to RAF inhibition in metastatic melanoma. *Cancer Discov*. 2014;4(1):94-109. doi:10.1158/2159-8290.cd-13-0617
38. de Bruin EC, Cowell C, Warne PH, et al. Reduced NF1 expression confers resistance to EGFR inhibition in lung cancer. *Cancer Discov*. 2014;4(5):606-619. doi:10.1158/2159-8290.CD-13-0741
39. Campbell JD, Alexandrov A, Kim J, et al. Distinct patterns of somatic genome alterations in lung adenocarcinomas and squamous cell carcinomas. *Nat Genet*. 2016;48:607. https://doi.org/10.1038/ng.3564.
40. Wells R, Birnstiel M. Kinetic complexity of chloroplastal deoxyribonucleic acid and mitochondrial deoxyribonucleic acid from higher plants. *Biochem J*. 1969;112(5):777-786. doi:10.1016/j.cell.2013.10.011. Cumulative
41. Zhao Z, Chen C-C, Rillahan CD, et al. Cooperative loss of RAS feedback regulation drives myeloid leukemogenesis. *Nat Genet*. 2015;47(5):539-543. doi:10.1038/ng.3251
42. Grewal T, Koese M, Tebar F, Enrich C. Differential Regulation of RasGAPs in Cancer. *Genes Cancer*. 2011;2(3):288-297. doi:10.1177/1947601911407330
43. Sun D, Yu F, Ma Y, et al. MicroRNA-31 activates the RAS pathway and functions as an oncogenic MicroRNA in human colorectal cancer by repressing RAS p21 GTPase activating protein 1 (RASA1). *J Biol Chem*. 2013;288(13):9508-9518. doi:10.1074/jbc.M112.367763
44. Sun D, Wang C, Long S, et al. C/EBP-beta-activated microRNA-223 promotes tumour growth through targeting RASA1 in human colorectal cancer. *Br J Cancer*. 2015;112(9):1491-1500. doi:10.1038/bjc.2015.107
45. Gong B, Liu WW, Nie WJ, et al. MiR-21/RASA1 axis affects malignancy of colon cancer cells via RAS pathways. *World J Gastroenterol*. 2015;21(5):1488-1497. doi:10.3748/wjg.v21.i5.1488
46. Mei Z, Shao YW, Lin P, et al. SMAD4 and NF1 mutations as potential biomarkers for poor prognosis to cetuximab-based therapy in Chinese metastatic colorectal cancer patients. *BMC Cancer*. 2018;18(1):1-7. doi:10.1186/s12885-018-4298-5
47. Ohta M, Seto M, Ijichi H, et al. Decreased Expression of the RAS-GTPase Activating Protein RASAL1 Is Associated With Colorectal Tumor Progression. *Gastroenterology*. 2009;136(1):206-216. doi:10.1053/j.gastro.2008.09.063
48. Min J, Liu L, Li X, et al. Absence of DAB2IP promotes cancer stem cell like signatures and indicates poor

survival outcome in colorectal cancer. *Sci Rep*. 2015;5:1-12. doi:10.1038/srep16578
49. Wan PT, Wan PT, Garnett MJ, et al. Mechanism of activation of the RAF-ERK signaling pathway by oncogenic mutations of B-RAF. *Cell*. 2004;116(6):855-867. papers2://publication/uuid/6A789316-AB6F-4316-B640-A6CE5046EAE0.
50. Van De Wetering M, Francies HE, Francis JM, et al. Prospective derivation of a living organoid biobank of colorectal cancer patients. *Cell*. 2015;161(4):933-945. doi:10.1016/j.cell.2015.03.053
51. Saito S, Kawamura T, Higuchi M, et al. RASAL3, a novel hematopoietic RasGAP protein, regulates the number and functions of NKT cells. *Eur J Immunol*. 2015;45(5):1512-1523. doi:10.1002/eji.201444977
52. Muro R, Nitta T, Okada T, Ideta H, Tsubata T, Suzuki H. The Ras GTPase-activating protein Rasal3 supports survival of naive T cells supports survival of naive T cells. *PLoS One*. 2015;10(3):1-14. doi:10.1371/journal.pone.0119898
53. Scheffzek K. The Ras-RasGAP Complex: Structural Basis for GTPase Activation and Its Loss in Oncogenic Ras Mutants. *Science (80-)*. 1997;277(5324):333-338. doi:10.1126/science.277.5324.333
54. Ahmadian MR, Kiel C, Stege P, Scheffzek K. Structural fingerprints of the Ras-GTPase activating proteins neurofibromin and p120GAP. *J Mol Biol*. 2003;329(4):699-710. doi:10.1016/S0022-2836(03)00514-X
55. Drost J, van Jaarsveld RH, Ponsioen B, et al. Sequential cancer mutations in cultured human intestinal stem cells. *Nature*. 2015;521(7550):43-47. doi:10.1038/nature14415
56. King PD, Lubeck BA, Lapinski PE. Nonredundant functions for Ras GTPase-activating proteins in tissue homeostasis. *Sci Signal*. 2013;6(264):re1. doi:10.1126/scisignal.2003669
57. Bollen Y, Post J, Koo B-K, Snippert HJG. How to create state-of-the-art genetic model systems: strategies for optimal CRISPR-mediated genome editing. *Nucleic Acids Res*. 2018;46(13):6435-6454. doi:10.1093/nar/gky571
58. Verissimo CS, Overmeer RM, Ponsioen B, et al. Targeting mutant RAS in patient-derived colorectal cancer organoids by combinatorial drug screening. *Elife*. 2016. doi:10.7554/eLife.18489
59. Ahronian LG, Corcoran RB. Effective MAPK Inhibition is critical for therapeutic responses in colorectal cancer with BRAF mutations. *Mol Cell Oncol*. 2016;3(1):1-3. doi:10.1080/23723556.2015.1048405
60. Min J, Zaslavsky A, Fedele G, et al. An oncogene-tumor suppressor cascade drives metastatic prostate cancer by coordinately activating Ras and nuclear factor-B. *Nat Med*. 2010;16(3):286-294. doi:10.1038/nm.2100
61. Arafeh R, Qutob N, Emmanuel R, et al. Recurrent inactivating RASA2 mutations in melanoma. *Nat Genet*. 2015;47(12):1408-1410. doi:10.1038/ng.3427
62. Liu D, Yang C, Bojdani E, Murugan AK, Xing M. Identification of RASAL1 as a major tumor suppressor gene in thyroid cancer. *J Natl Cancer Inst*. 2013;105(21):1617-1627. doi:10.1093/jnci/djt249
63. Calvisi DF, Ladu S, Conner EA, et al. Inactivation of Ras GTPase-activating proteins promotes unrestrained activity of wild-type Ras in human liver cancer. *J Hepatol*. 2011;54(2):311-319. doi:10.1016/j.jhep.2010.06.036
64. Huang Y, Zhao M, Xu H, et al. RASAL2 down-regulation in ovarian cancer promotes epithelial-mesenchymal transition and metastasis. *Oncotarget*. 2014;5(16). doi:10.18632/oncotarget.2244
65. McLaughlin SK, Olsen SN, Dake B, et al. The RasGAP Gene, RASAL2, Is a Tumor and Metastasis Suppressor. *Cancer Cell*. 2013;24(3):365-378. doi:10.1016/j.ccr.2013.08.004
66. Philpott C, Tovell H, Frayling IM, Cooper DN, Upadhyaya M. The NF1 somatic mutational landscape in sporadic human cancers. *Hum Genomics*. 2017;11(1):13. doi:10.1186/s40246-017-0109-3
67. Yap Y-S, McPherson JR, Ong C-K, et al. The NF1 gene revisited – from bench to bedside. *Oncotarget*. 2014. doi:10.18632/oncotarget.2194
68. Stites EC, Trampont PC, Haney LB, Walk SF, Ravichandran KS. Cooperation between Noncanonical Ras Network Mutations. *Cell Rep*. 2015;10(3):307-316. doi:10.1016/j.celrep.2014.12.035
69. Stowe IB, Mercado EL, Stowe TR, et al. A shared molecular mechanism underlies the human rasopathies Legius syndrome and Neurofibromatosis-1. *Genes Dev*. 2012;26(13):1421-1426. doi:10.1101/gad.190876.112
70. Li S, Nakamura S, Hattori S. Activation of R-Ras GTPase by GTPase-activating proteins for ras, gap1(m), and p120GAP [In Process Citation]. *JBiolChem*. 1997;272(31):19328-19332.
71. Sung H, Kanchi KL, Wang X, et al. Inactivation of RASA1 promotes melanoma tumorigenesis via R-Ras activation. *Oncotarget*. 2016;7(17):23885-23896. doi:10.18632/oncotarget.8127
72. Lapinski PE, Kwon S, Lubeck BA, et al. RASA1 maintains the lymphatic vasculature in a quiescent functional state in mice. *J Clin Invest*. 2012;122(2):733-747. doi:10.1172/JCI46116

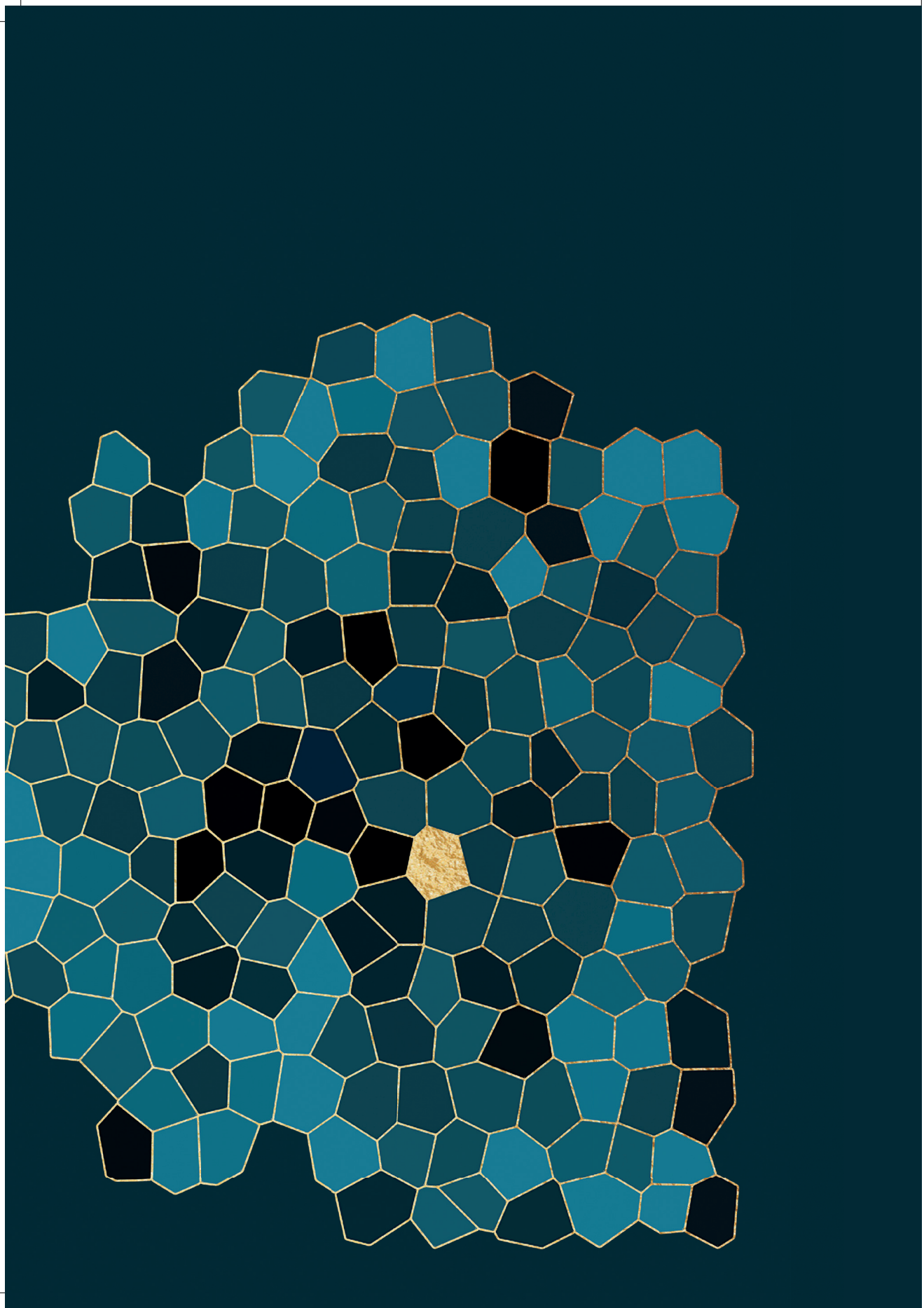

CHAPTER 4

BRAF FUSION GENE PARTNERS INFLUENCE ONCOGENIC BRAF ACTIVITY

Christina S. Stangl*, Jasmin B. Post*,
Markus J. van Roosmalen, Nizar Hami,
Ingrid Verlaan-Klink, Harmjan R. Vos,
Robert M. van Es, Marco J. Koudijs, Emile E. Voest,
Hugo J.G. Snippert and Wigard P. Kloosterman

Under review at Molecular Cancer Research

* These authors contributed equally to this work

ABSTRACT

Fusion genes can be oncogenic drivers in a variety of cancer types and represent potential targets for targeted therapy. The *BRAF* gene is frequently involved in oncogenic gene fusions, with fusion frequencies of 0.2-3% throughout different cancers. However, *BRAF* fusions rarely occur in the same gene configuration, potentially challenging personalized therapy design. In particular, the impact of the wide variety of fusion partners on the oncogenic role of *BRAF* during tumor growth and drug response is unknown. Here, we used patient-derived colorectal cancer organoids to functionally characterize and cross-compare previously identified *BRAF* fusions containing various partner genes (*AGAP3*, *DLG1* and *TRIM24*) with respect to cellular behavior, downstream signaling activation and response to targeted therapies. We demonstrate that 5′ fusion partners mainly promote canonical oncogenic *BRAF* activity by replacing the auto-inhibitory N-terminal region. However, 5' partner choice of BRAF fusions influences their subcellular localization and intracellular signaling capacity, revealing distinct subsets of affected signaling pathways and altered gene expression by phosphoproteomics and RNA sequencing. Presence of the different *BRAF* fusions resulted in varying sensitivities to combinatorial inhibition of MEK and the EGF receptor family. However, all *BRAF* fusions conveyed resistance to targeted monotherapy against the EGF receptor family, suggesting that *BRAF* fusions should be screened alongside other MAPK pathway alterations to identify mCRC patients to exclude from anti-EGFR targeted treatment.

KEYWORDS

CRC, Organoids, Fusion Genes, BRAF, Fusion Partner, Resistance, Signaling

INTRODUCTION

Cancer genomes are often subject to genomic instability which can result in various genomic rearrangements, including translocations[1,2]. Some genomic rearrangements can lead to oncogenic transformation, in particular when tumor suppressor genes are being disrupted or oncogenic fusion genes are created[3]. Fusion genes are chimeric genes resulting in proteins with altered or novel functions. Alternatively, fusions may facilitate the connection of a strong promoter to the coding sequence of a second gene, causing high expression of a protein such as kinases[3,4].

Recent advances in sequencing technologies and bioinformatic solutions have enabled the straightforward identification of novel fusion genes[3,5]. This has revealed that their frequency of occurrence varies between many cancer types, ranging from high frequencies in breast cancer (14,7%) to low frequencies in uveal melanoma (0,16%)[3], but also highlighted the vast diversity of fusion partners (>10,800 unique fusion configurations, Quiver Fusion Database). Oncogenic fusion proteins frequently interfere with signaling pathways that regulate cellular differentiation and proliferation and therefore are excellent targets for personalized cancer therapy. Fusions that involve the *BRAF* oncogene are mutually exclusive with other oncogenic mutations in the MAPK pathway (e.g. $BRAF^{V600E}$), suggesting that *BRAF* fusion genes promote constitutive MAPK signaling[6]. Indeed, previous studies have shown that loss of the auto-inhibitory N-terminal domain of BRAF promotes BRAF kinase activity independent of upstream RAS signaling activity resulting in enhanced downstream MAPK signaling[7,8]. Furthermore, specific *BRAF* fusion genes have been implicated in acquired resistance to targeted therapies[9,10]. For example, the *AGAP3-BRAF* fusion has been reported to induce resistance to the BRAF inhibitor vemurafenib in a $BRAF^{V600E}$-mutated melanoma patient that was previously responsive to treatment[9]. Hence, *BRAF* fusion genes may represent an important and understudied mode to activate oncogenic MAPK signaling.

BRAF fusion genes have been identified in multiple cancers with a wide variety of 5' fusion partners (> 60 different partners published, some of which have only been described once)[6,11]. The large variety of *BRAF* fusion partners complicates straightforward discrimination between oncogenic effects that are shared versus actions that are influenced or even determined by the unique fusion partner. Therefore, in contrast to common *BRAF* hotspot mutations, this high diversity of fusion gene configurations impedes the clinical interpretation of *BRAF* fusion genes in relation to their oncogenic potential and treatment responses.

To explore cellular and molecular effects of different BRAF fusion configurations that have recently been identified in colorectal cancers (e.g. *AGAP3-BRAF*, *DLG1-BRAF* and *TRIM24-BRAF*)[6], we employed patient-derived colorectal cancer organoids (CRC PDOs) that are representative patient models[12]. We here show that expression of different *BRAF* fusions in CRC PDOs renders overall resistance to targeted inhibition of the MAPK pathway, similar as the common $BRAF^{V600E}$ mutation. However, notable differences in signaling activity and sensitivity towards MAPK targeting drugs were observed between the different *BRAF* oncogenes, e.g. *BRAF* fusions and $BRAF^{V600E}$. Based on quantitative phosphoproteomics and RNA sequencing, we show that 5′ fusion partners mainly promote canonical oncogenic *BRAF* activity by replacing the auto-inhibitory N-terminal region, but also impose unique features

that can influence, amongst others, strength of downstream pathway activation.

RESULTS

Establishment of inducible BRAF fusion gene expression in colorectal cancer organoids

In a recent RNA sequencing screen of primary colon tumors we identified *BRAF* fusion genes containing different 5' partner genes[6]. To characterize and cross-compare the influence of the 5' partner between different *BRAF* fusions, we used CRC PDOs (P18T line) with a mutational background characteristic for *BRAF* fusion-positive CRC tumors, i.e. non-functional APC and TP53, and KRAS wild-type[6,13]. We employed this platform (**Figure 1A**) to stably integrate a panel of *BRAF* fusion genes (*AGAP3-BRAF*, *DLG1-BRAF* and *TRIM24-BRAF*) as well as a wild-type *BRAF* ($BRAF^{WT}$), a truncated *BRAF* gene containing only the kinase domain ($BRAF^{Kinase}$) and a *BRAF* gene with the canonical V600E mutation ($BRAF^{V600E}$) (**Figure 1B**). *BRAF* (fusion) gene expression was under the control of doxycycline (dox) inducible Tet-On activity to ensure controlled and selective construct expression (**Figure 1C**).

We confirmed selective mRNA expression of all BRAF variants upon dox administration (**Figure 2A**). Furthermore, the presence of the various BRAF proteins was visualized by immunoblot staining against the C-terminal HA-tag (**Figure 2B**). In the absence of dox, no BRAF (fusion) mRNA or protein was detected, demonstrating tight control of gene expression by tetracycline-responsive promoters.

5' partner choice affects subcellular localization and intracellular signaling capacity of BRAF fusion proteins

Whereas various studies have shown that BRAF fusions promote MAPK pathway activation by effectuating loss of the auto-inhibitory N-terminal domain of BRAF[6,14], specific effects imposed by the 5′ partner on the fusion protein have not been studied yet. Indeed, the 5′ fusion partners of BRAF, e.g. AGAP3[15], DLG1[16], or TRIM24[17] manifest distinct biological functions in their original conformation and a potential carry-over towards the fusion is likely. First we characterized the effects of fusion gene expression during normal culture conditions on MAPK pathway activation, which is implicated in cellular growth and proliferation[18]. Normal culture conditions of CRC PDOs include epidermal growth factors (EGF) that induce baseline levels of MAPK pathway activity. Only the expression of *DLG1-BRAF* resulted in enhanced pERK levels, while the other BRAF fusions as well as the well-known oncogenic mutant $BRAF^{V600E}$ did not deviate from baseline pERK levels under normal culture conditions (**Figure 2C**). In agreement with previous literature[19], none of the BRAF (fusion) proteins had an effect on AKT activity (**Supplementary Figure 1**). Importantly, BRAF (fusion) protein levels vary between organoid lines (**Figure 2B**), potentially influencing observed phenotypes. Reassuring, the expression levels of the BRAF fusions do not correlate with the levels of ERK phosphorylation, which indicates that there is a specific influence of the 5′ fusion partner on the downstream MAPK pathway activation (**Supplementary Figure 2**).

We hypothesized that the 5′ fusion partners can redirect the subcellular localization of the BRAF fusion proteins, thereby affecting the efficiency by which the BRAF kinase domain can activate downstream MEK. Therefore, we visualized the intracellular localization of the

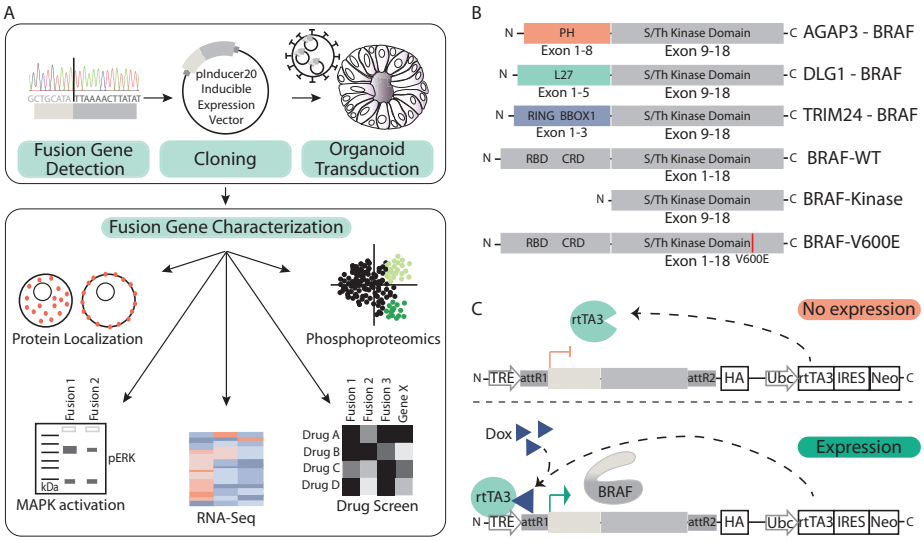

Figure 1. Overview of experimental set-up for characterization of *BRAF* (fusion) genes.
(**A**) Schematic overview of the fusion gene expression platform and workflow. Fusion genes are identified by sequencing and fusion breakpoints are validated by PCR and sequencing. (Fusion) gene constructs are cloned into the inducible expression vector pInducer20. The pInducer20 constructs are stably integrated into CRC organoids by means of lentiviral transduction. Thereafter, *BRAF* (fusion) genes are characterized through analysis of localization, MAPK pathway activation, phosphoproteomics, RNA sequencing and drug screenings. (**B**) Schematic overview of the investigated *BRAF* fusion genes. BRAF fusions and their respective 5' partners (*AGAP3*, *DLG1*, *TRIM24*) and BRAF variants (*BRAF-WT*, *BRAF-Kinase*, *BRAF-V600E*) are depicted with their retained functional domains. PH: Pleckstrin Homology, L27: L27 protein interaction module, RING: zinc finger domain ring type, BBOX1: B-box-type zinc finger domain, RBD: Ras-binding domain, CRD: Cysteine-rich domain, S/Th Kinase Domain: Serine/Threonine Kinase Domaine. (**C**) Depiction of the inducible pInducer20 vector cassette. cDNA of a BRAF (fusion) transcript (flanked by attR1/R2 sites) with an HA-tag linked to the C-terminus. The expression of the BRAF (fusion) transcript is under the control of a tetracycline-responsive element (TRE) which is activated upon interaction with dox-bound reverse tetracycline-controlled transactivator 3 (rtTA3). The rtTA3 expression is under the control of a constitutively active Ubc promoter but can only interact with the TRE upon dox binding.

BRAF variants by using immunofluorescent staining against the C-terminal HA-tag. Indeed, we observed differences in the cellular localization of the different BRAF fusions (**Figure 2D**). The $BRAF^{WT}$, $BRAF^{Kinase}$ and $BRAF^{V600E}$ proteins exhibited, as expected, a diffuse localization pattern throughout the cytoplasm[20]. Whereas a similar localization pattern was observed for the AGAP3-BRAF and TRIM24-BRAF fusion proteins, DLG1-BRAF fusions were primarily localized to the plasma membrane. This is most likely due to the retained L27 domain of DLG1 in the DLG1-BRAF fusion, which triggers native DLG1 localization likewise to the apical plasma membrane[21].

Phosphoproteomics reveals that BRAF fusions and $BRAF^{V600E}$ induce similar signaling pathways in HEK293 cells

Based on the observed differences between the BRAF fusions with respect to ERK activation, we aimed to characterize the type and extent of unique intracellular signaling pathways that are specifically activated by a BRAF fusion, in comparison to $BRAF^{V600E}$ and $BRAF^{WT}$.

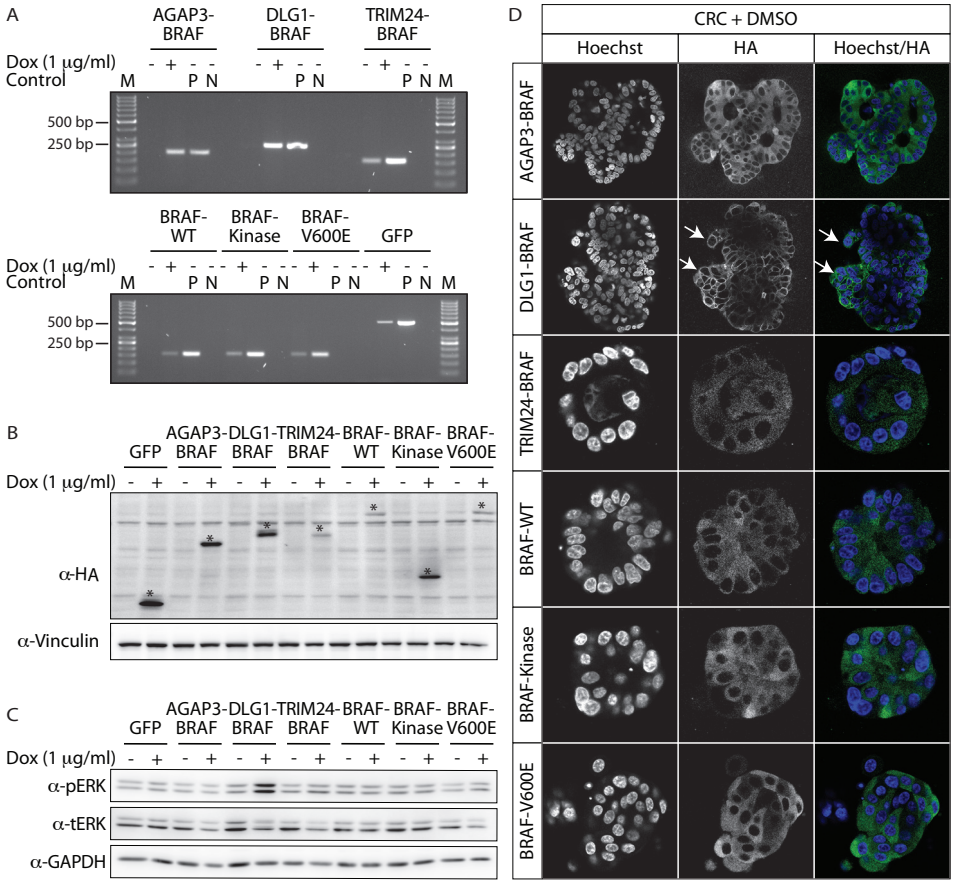

Figure 2. *BRAF* (fusion) gene expression, MAPK pathway activation, and localization in P18T CRC organoids. (**A**) Breakpoint-PCR verifying the expression of the BRAF (fusion) transcripts in P18T CRC organoids upon dox administration. Respective breakpoint primers are used on uninduced (-), induced (+; 1 µg/ml dox for 24h), positive (respective pInducer20-plasmid; P) and negative control (water; N). (**B**) Immunoblotting for HA-tagged BRAF (fusion) proteins verifying the protein expression in P18T CRC organoids at the expected height and upon dox administration (1 µg/ml for 24h). Correct BRAF (fusion) protein bands are highlighted with an asterisk. Vinculin was used as loading control. (**C**) Organoids expressing *BRAF* genes were not induced (-) or induced (+) with dox (1 µg/ml) for 24h and immunoblotted for phosphorylated ERK (pERK) and total ERK (tERK). GAPDH was used as loading control. (**D**) P18T CRC organoids expressing BRAF constructs were stained for the HA-tag to visualize the protein localization (HA-tag = green) and the nucleus (Hoechst = blue). White arrows are pointing to the protein localization at the plasma membrane.

To identify all downstream phosphosites that are regulated by a BRAF fusion, we performed an unbiased SILAC-based phosphoproteomics screen (**Supplementary Figure 3A**). Since organoids are not a suitable platform to scale to sufficient protein quantities required for phosphoproteomic screens, and organoid growth kinetics may potentially be affected in SILAC medium, we opted to use HEK293 cells instead. HEK293 cells are a well-characterized cell system with an unperturbed MAPK pathway[22], a major prerequisite to not mask potential BRAF (fusion)-induced effects on MAPK signaling, and are compatible with growth

in both types of SILAC media which is not trivial for most well-known cancer cell lines. Like our organoid lines, we confirmed inducible *BRAF* fusion gene expression by mRNA and Western Blot analysis (**Supplementary Figures 4A-B**). In contrast to P18T organoids, weak BRAF fusion gene expression was detected in the uninduced state (- dox) of HEK293 cells (**Supplementary Figures 4A-B and 5**), presumably due to supplemented FBS in HEK293 culture medium[23]. Importantly however, except for *GFP* and *BRAF^{WT}* expressing cells, a strong increase in pERK levels was detected in HEK293 cells upon expression of all oncogenic *BRAF* variants (**Supplementary Figure 4C**). Whereas a significant increase in ERK phosphorylation during unperturbed culture conditions was only observed upon *DLG1-BRAF* expression in our CRC PDOs (**Figure 2C**), this was not the case in HEK293 cells. Presumably, this discrepancy may be the result of technical differences between the 2D and 3D models, such as different integration and expression efficiencies of the fusion proteins, or may be attributed to the inherent biological differences between the two model systems. In support of the latter, the distinctive localization patterns of BRAF fusion proteins observed in organoids (**Figure 2D**) was absent in unpolarized HEK293 cells (**Supplementary Figure 5**)[24]. Moreover, the MAPK signaling pathway is already active in organoids prior induction of the fusion variants, while largely inactive in HEK293 cells, potentially masking their effects during normal growth conditions. As a result, we now reveal phosphorylation targets of the different oncogenic BRAF variants as a result of intrinsic capacity, rather than induced by differences in subcellular localization.

To identify targets directly downstream of BRAF (fusion) protein signaling by phosphoproteomic analysis, we measured the earliest time-point of BRAF (fusion) protein expression upon dox-mediated induction. Time-course measurements of HA-tagged protein expression and ERK phosphorylation in the *GFP* and *DLG1-BRAF* expressing cell lines identified 4 hours as the minimal duration of dox exposure for protein expression and robust downstream MAPK pathway activation (**Supplementary Figures 6A-B**). Same kinetics were confirmed in the remaining *BRAF* fusion cell lines (**Supplementary Figure 6C**).

In general, we observed that expression of BRAF fusions, BRAF^{V600E} and BRAF^{Kinase} mainly induced an increase in protein phosphorylation in 4 hours (**Figure 3A, Supplementary Figure 6D, Supplementary Figure 3B, and Table 1**). BRAF^{WT} expression only resulted in one significantly downregulated phosphosite belonging to the BRAF protein itself, indicative of a negative feedback response induced by BRAF overexpression (**Figure 3A**). In contrast to BRAF^{V600E} and BRAF fusions, the presence of BRAF^{Kinase} resulted in a rather low number of upregulated phosphosites (**Supplementary Figure 3B and Table 1**).

To explore kinase activities responsible for the deregulated targets within the phosphoproteomics data, we used Kinase-Substrate Enrichment Analysis (KSEA)[24]. With the exception of GFP, we noticed that all BRAF variants showed a significant activation of kinases involved in the MAPK signaling pathway, including MEK1/2, ERK1/2, and Raf (**Figure 3B, Supplementary Figure 3C and Supplementary Table 1**). In addition, BRAF fusions and BRAF^{V600E} also showed significant activation of kinases involved in cell cycle progression and DNA damage response, such as CDK1, CDK2, Aurora kinase B and CHEK1 (**Figure 3B and Supplementary Table 1**).

Next, we explored phosphotargets that are common to all BRAF fusions, versus unique targets per BRAF variant. We identified 289 phosphosites and 298 proteins that are shared as substrate

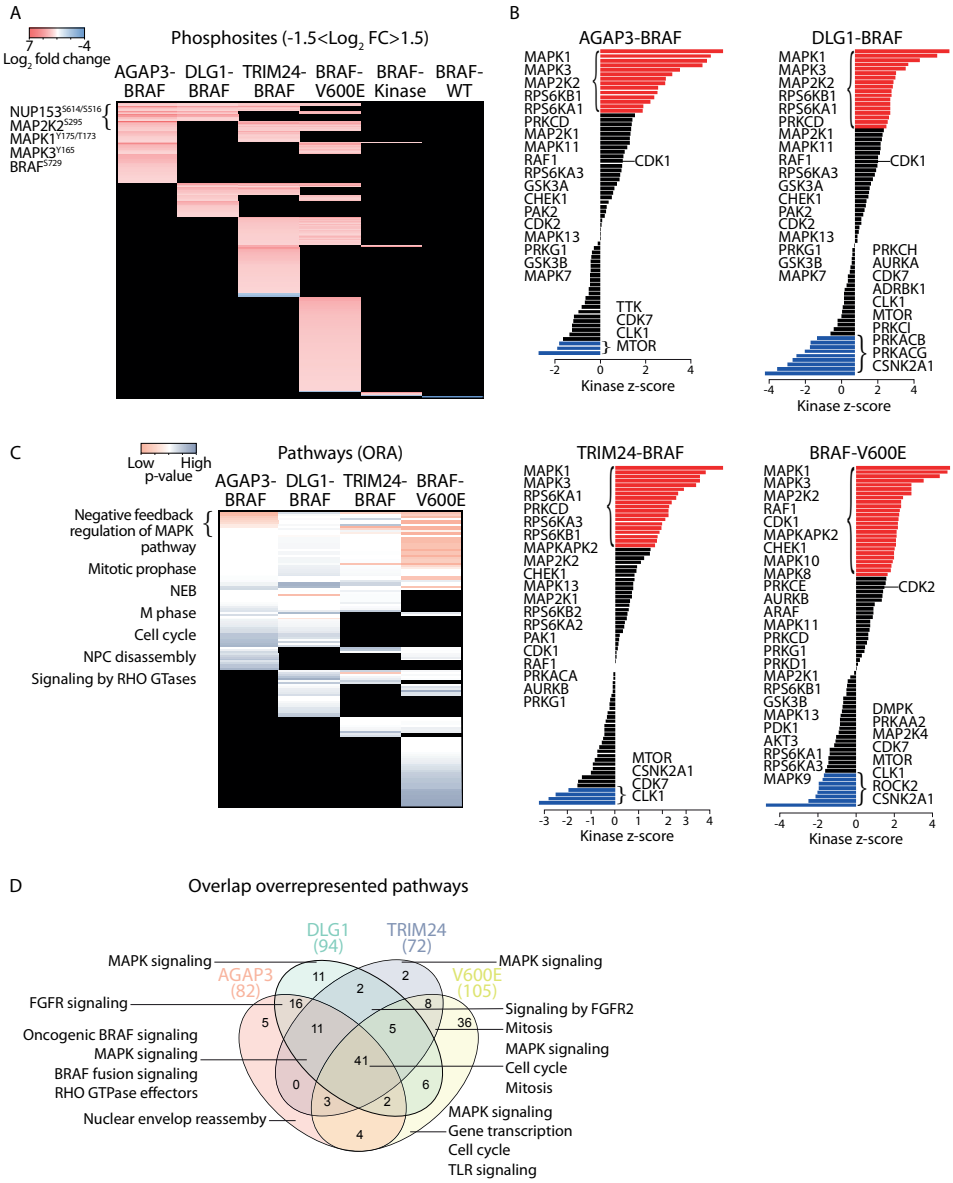

Figure 3. Phosphoproteomics screen in HEK293 cells reveals that BRAF fusions and BRAF^{V600E} activate similar signaling pathways.

(**A**) Heatmap of ratio changes of significantly affected (-1.5<Log2 fold change (FC)>1.5, *p*-value<0.05) phosphosites induced upon *BRAF* (*fusion*) gene expression in HEK293 cells. Phosphosites in the MAPK signaling pathway that are shared between *BRAF fusion* and *BRAF^{V600E}* expressing cells are indicated at the upper left (**B**) Kinase-Substrate Enrichment Analysis results showing kinase activity scores of *BRAF fusion* and *BRAF^{V600E}* expressing HEK293 cells. (**C**) Overrepresentation analysis of significantly enriched pathways (heatmap of *p*-values) upon *BRAF* (*fusion*) gene and *BRAF^{V600E}* expression in HEK293 cells. Heatmap shows that the majority of highly enriched pathways are shared among oncogenic BRAF^{V600E} and fusion variants (most significant common pathways are indicated upper left). (**D**) Venn diagram depicting the overlap of overrepresented pathways between oncogenic *BRAF* variants (*fusion* genes and *BRAF^{V600E}*) in HEK293 cells.

Table 1. Summary of phosphoproteomics screen in BRAF (fusion) expressing HEK293 cells.

	Phosphosites/proteins (detected in fw and rv experiments)	Significant phosphosites/proteins (Log2 1.5 FC)	Upregulated phosphosites/proteins (Log2 1.5 FC)	Downregulated phosphosites/proteins (Log2 1.5 FC)
AGAP3-BRAF	5765/2456	100/87	100/87	0/0
DLG1-BRAF	6180/2526	65/61	65/61	0/0
TRIM24-BRAF	6914/2801	150/135	145/131	5/5
$BRAF^{V600E}$	7159/2843	202/178	202/177	1/1
$BRAF^{Kinase}$	4390/2001	8/7	7/6	1/1
$BRAF^{WT}$	6626/2656	6/1	0/0	6/1
GFP	6740/2705	0/0	0/0	0/0

(direct or indirect) by all BRAF fusions, $BRAF^{V600E}$, and $BRAF^{Kinase}$ (**Supplementary Figure 3D**). As indicated already, most of the overlapping targets include members of the MAPK signaling pathway, such as ERK1/2 (MAPK3/1), BRAF, and MEK2 (MAP2K2). Moreover, these phosphotargets turned out to be most strongly upregulated (**Figure 3A and Supplementary Figure 3B**). Besides shared downstream targets, we found that each BRAF fusion also induced the phosphorylation of a unique set of substrates (**Figure 3A and Supplementary Figure 3B**). Intriguingly however, the degree by which these unique phosphosites are phosphorylated was generally lower when compared to the fold change of shared phosphosites (**Supplementary Figure 3B**).

Next, when analyzing which pathways are represented by the set of downstream phosphotargets (Overrepresentation Enrichment Analysis (ORA, Webgestalt[25]), we noticed a high degree of overlap between the different *BRAF* fusion and *$BRAF^{V600E}$* expressing cells (**Figure 3C**). In particular, the pathways mainly converged on MAPK signaling pathway regulation and cell cycle progression (**Figures 3C-D**).

Together, from a protein intrinsic point of view, these data indicate that the different BRAF fusions have largely similar substrates as $BRAF^{V600E}$ and activate similar signaling pathways, mainly involving MAPK pathway activation and cell cycle progression. To improve our understanding of the global impact of *BRAF* (fusion) genes, and to complement the phosphoproteomic analysis, we performed RNA sequencing (**Methods**) on CRC PDOs. Unlike the phosphoproteomic screen on HEK293 cells, we observe various activation levels of the MAPK pathway in CRC PDOs by the BRAF (fusion) variants and $BRAF^{V600E}$ when compared to the $BRAF^{Kinase}$, $BRAF^{WT}$ and GFP expressing lines (**Supplementary Figure 7**). Western Blot analysis confirmed that dox-induced expression of $BRAF^{V600E}$, AGAP3-BRAF and DLG1-BRAF in CRC PDOs indeed resulted in increased MEK-ERK phosphorylation and confirmed varying degrees of MAPK pathway activation between oncogenic BRAF variants (**Supplementary Figure 7A**).

As previously stated, it is possible that baseline levels of MAPK pathway activity during normal culture conditions of CRC PDOs (**Figure 2C**) masks BRAF oncogene-specific effects on the MAPK pathway, but are picked up in unpolarized HEK293 cells with a largely inactive MAPK pathway. Based on gene expression analysis (**Methods**) of organoids expressing fusion genes, we indirectly confirmed the activation of MAPK signaling by BRAF fusions, specifically for the *DLG1-BRAF* fusion. The DLG1-BRAF fusion induced a large amount of differentially expressed genes in CRC PDOs that were mainly involved in the cell cycle and

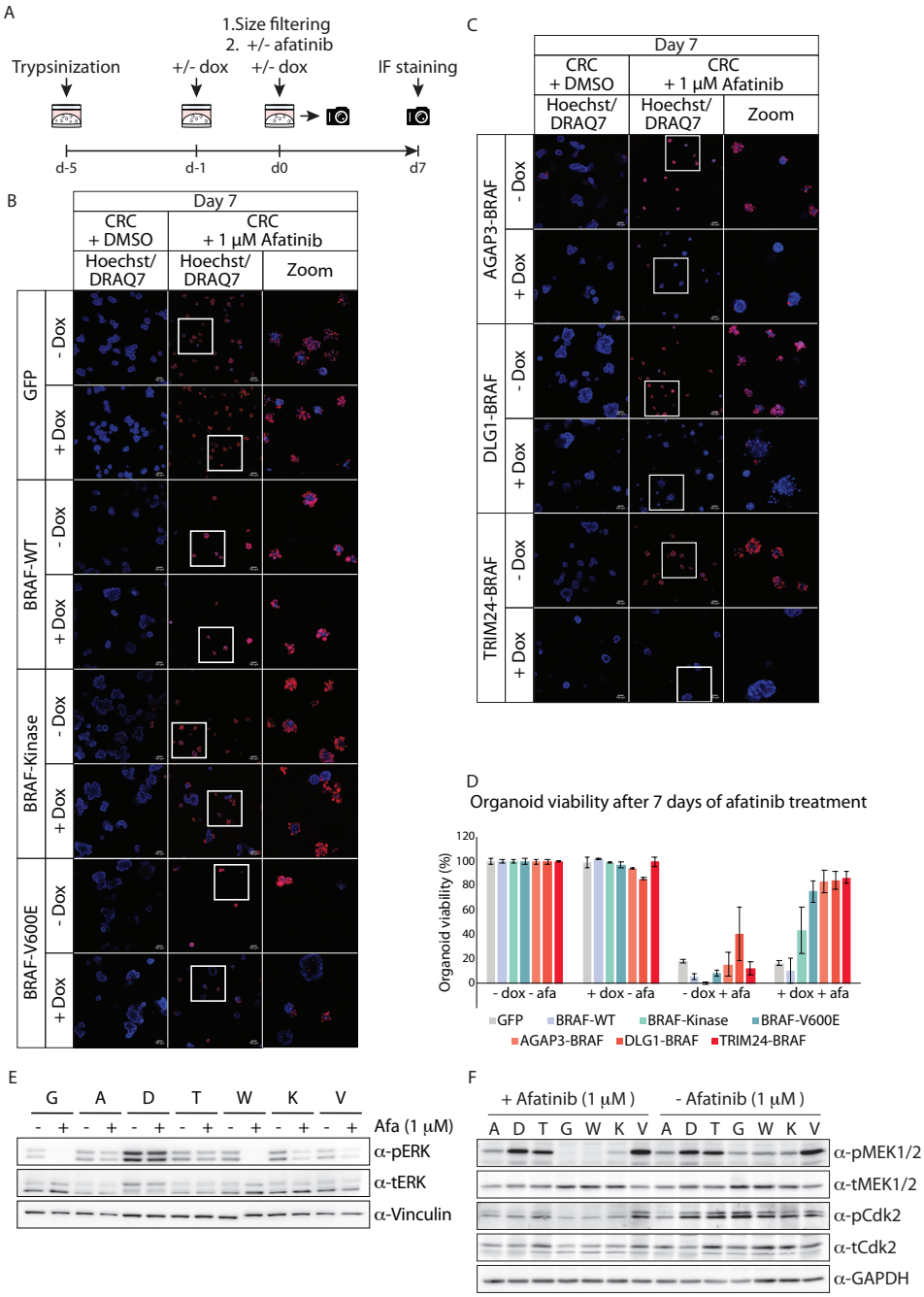

signaling by Rho GTPases (**Supplementary Figures 7B-D and Supplementary Tables 2 and 3**)[26,27]. Indeed, MAPK pathway activation promotes cell proliferation[28] and migration[28,29], which corresponds to the strong effects of DLG1-BRAF on ERK activation. Furthermore, we confirmed that the expression of genes implicated in cell cycle regulation, such as *CHEK1*, *CHEK2* and *CCNB2* was similarly regulated in organoids expressing *DLG1-BRAF* and in a tumor sample positive for the *DLG1-BRAF* fusion, corroborating the validity of these findings (**Methods, Supplementary Figures 8A-B**).

BRAF fusion genes confer resistance to targeted EGFR inhibition

Besides *KRAS*, oncogenic mutations in *BRAF* (e.g. V600E) have been associated with resistance to anti-EGFR targeted therapy in metastatic CRC (mCRC)[30,31]. BRAF fusions may also influence the sensitivity of tumor cells to anti-EGFR targeted therapy due to constitutive activation of downstream MAPK signaling. Therefore, we challenged the CRC PDOs with a pan-HER inhibitor (afatinib) for 7 days and scored viability by microscopy (Figure 4A). Consistent with previous patient-derived CRC studies[32], most of the *GFP* and $BRAF^{WT}$ expressing organoids died upon EGFR-inhibition, while the majority of $BRAF^{V600E}$ mutant organoids showed resistance to similar treatment (**Figure 4B and Supplementary Figure 9A**). In addition, we observed that expression of all *BRAF* fusion variants provided resistance to afatinib (**Figure 4C, Figure 4D and Supplementary Figure 9A**). Interestingly, $BRAF^{Kinase}$ organoids exhibited an intermediate phenotype to anti-EGFR targeted treatment compared to the *BRAF* fusion organoids, showing few large surviving organoids together with significant cell death (**Figure 4B, 4D and Supplementary Figures 9A-B**). As $BRAF^{Kinase}$ expression is comparable to expression of BRAF fusions (**Figure 2B**), these data suggest that a protein domain at the N-terminal side of the BRAF kinase domain is important to maximize BRAF activity.

Previous studies have shown that constitutive MAPK pathway activation plays an essential role in anti-EGFR therapy resistance in mCRC[32,33]. To validate that *BRAF* fusion genes can promote MAPK pathway signaling independent of external EGF stimulation, we investigated ERK and AKT activity upon afatinib treatment. In accordance to the observed phenotypes, the afatinib-sensitive lines (*GFP* and $BRAF^{WT}$) failed to phosphorylate ERK upon EGFR

Figure 4. *BRAF* (fusion) genes confer resistance to EGFR inhibition.
(**A**) Schematic overview of the phenotypic screening method to measure organoid viability after afatinib treatment. (**B**) P18T CRC organoids with (+ dox (1 μg/ml)) or without (- dox) induced expression of *GFP*, $BRAF^{WT}$, $BRAF^{Kinase}$, or $BRAF^{V600E}$ were treated with DMSO or afatinib (1 μM) for 7 days and stained for nuclei (Hoechst = blue) and dead cells (DRAQ7 = red). White squares represent zoomed-in areas. (**C**) P18T CRC organoids with (+ dox (1 μg/ml)) or without (- dox) induced expression of *AGAP3-BRAF*, *DLG1-BRAF* or *TRIM24-BRAF* fusion genes were treated with DMSO or afatinib (1 μM) for 7 days and stained for nuclei (Hoechst = blue) and dead cells (DRAQ7 = red). White squares represent zoomed-in areas. (**D**) Bar graph depicts the percentage of viable organoids after 7 days of DMSO or afatinib (1 μM) treatment in the presence or absence of dox (1 μg/ml) (from 2 independent experiments). (**E**) BRAF (fusion) protein expressing organoids were treated with DMSO (-) or 1 μM afatinib (+) for 24h and immunoblotted for phosphorylated ERK (pERK) and total ERK (tERK). Vinculin was used as loading control. (**F**) Same as in (E), immunoblotted for phosphorylated MEK (pMEK) and CDK2 (pCDK2), and total MEK (tMEK) and CDK2 (tCDK2). GAPDH was used as a loading control. A, AGAP3-BRAF; D, DLG1-BRAF; T, TRIM24-BRAF; G, GFP; W, BRAF-WT; K, BRAF-Kinase, V, BRAF-V600E.

inhibition whilst afatinib-resistant lines (*BRAF fusions*, $BRAF^{V600E}$ and $BRAF^{Kinase}$) were able to sustain ERK phosphorylation (**Figure 4E**). Along similar lines, we confirmed sustained phosphorylation by *BRAF* fusions and $BRAF^{V600E}$ of additional targets identified with the phosphoproteomics screen, like pMEK and pCDK2 (**Figure 4F**). Intriguingly, this was especially apparent during EGFR inhibition as common targets of the MAPK pathway seem already activated to significant levels during normal growth conditions (**Figure 2C**). Additionally, no influence of BRAF fusions on pAKT levels was observed (**Supplementary Figure 10**). Intriguingly, although $BRAF^{V600E}$ and $BRAF^{Kinase}$ expressing organoids were able to sustain ERK phosphorylation, the degree of ERK phosphorylation was affected by EGFR inhibition. This is concordant with two recent studies which show that *KRAS* mutant lung cancer cells still require upstream receptor signaling for tumor growth and survival[30,34]. Dependency on continuous upstream signaling input at the receptor level, however, was not observed in organoids expressing the *BRAF* fusion genes. Furthermore, the *DLG1-BRAF* fusion consistently showed stronger ERK phosphorylation, both at unperturbed (**Figure 2C**) and afatinib-treated conditions (**Figure 4E**), pointing towards an enhanced capacity to activate the downstream MAPK pathway, possibly due to its localization at the plasma membrane.

BRAF fusions elicit differential sensitivities to combinatorial targeting of EGFR and MEK

To identify drugs that could be used for the treatment of mCRC patients with *BRAF* fusion genes, we tested a panel of MAPK pathway targeting agents in a drug screen (**Figure 5A**). Previously, a synergistic effect was observed with dual inhibition of the MAPK pathway on *BRAF* and *RAS* mutant CRC cells[32,35]. Therefore, we investigated whether a similar effect could be achieved with combinatorial targeting of the MAPK pathway. Organoids expressing $BRAF^{WT}$ or *GFP* were highly sensitive to afatinib (pan-HERi) treatment in this drug screen assay, while $BRAF^{V600E}$, $BRAF^{Kinase}$ and *BRAF* fusion expressing organoids showed resistance, with $BRAF^{V600E}$, *DLG1-BRAF* and *TRIM-BRAF* mutant organoids showing resistance at even high concentrations (**Figure 5B and Supplementary Figure 11A**). MEK inhibition (selumetinib) had a similar inhibitory effect on $BRAF^{WT}$, $BRAF^{V600E}$, $BRAF^{Kinase}$ and *BRAF* fusion expressing organoids, which was slightly lower compared to its inhibitory effect on the control *GFP* expressing line (**Figure 5C and Supplementary Figure 11A**). Combining selumetinib with afatinib resulted in an additive effect on $BRAF^{Kinase}$ and *AGAP3-BRAF* expressing organoids that already exhibited higher sensitivity to afatinib compared to organoids with the other *BRAF* fusions (**Figure 5D and Supplementary Figure 11**A). We observed only a minor additive effect of this combinatorial treatment on highly afatinib-resistant *DLG1-BRAF* and *TRIM-BRAF* fusions, as well as $BRAF^{V600E}$ mutants, compared to afatinib or selumetinib alone. We conclude that, unlike mutant *KRAS*, the combination of pan-HER and MEK inhibition only has an additive effect in some, i.e. *AGAP3-BRAF* and $BRAF^{Kinase}$, but not all oncogenic *BRAF* expressing CRC organoids.

Next, we tested whether combining a MEK inhibitor with an ERK inhibitor has additive or synergistic effect. All oncogenic *BRAF* variants showed approximately similar sensitivity to the specific ERK1/2-inhibitor SCH772984[36], which was comparable to the control *GFP* expressing organoids (**Figure 5E and Supplementary Figure 11A**). Combinatorial targeting of MEK (selumetinib) and ERK (SCH772984) improved overall sensitivity, without major differences between the lines (**Figure 5F and Supplementary Figure 11A**).

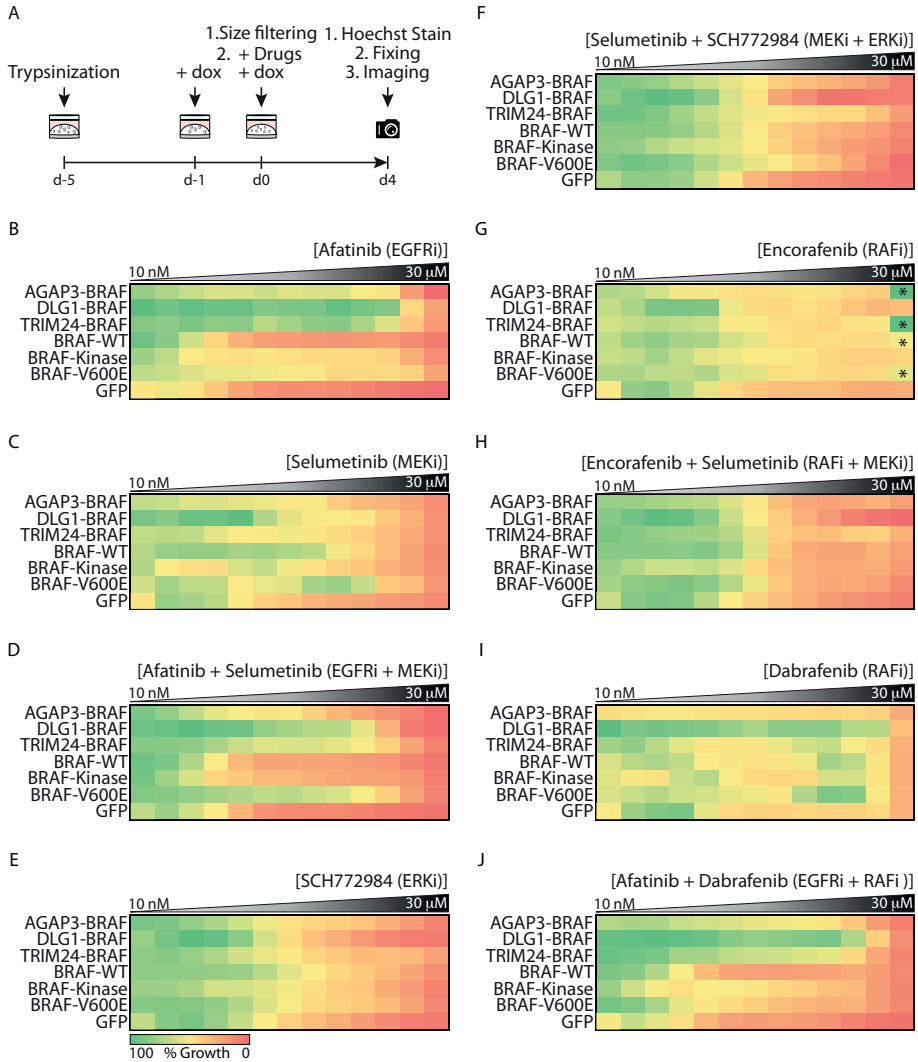

Figure 5. Differential sensitivities of *BRAF* (fusion) genes to targeted BRAF and ERK inhibition.
(**A**) Schematic overview of the drug screening method. In short, a 4-day drug screen is started on 5 days old organoids in which fusion genes are expressed 24 h prior to the start of the screen. (**B**) Heatmap of drug response (growth) to afatinib, (**C**) selumetinib, (**D**) afatinib plus selumetinib, (**E**) SCH772984, (**F**) SCH772984 plus selumetinib, (**G**) encorafenib, (**H**) encorafenib plus selumetinib, (**I**) dabrafenib, and (**J**) dabrafenib plus afatinib. Asterisks indicate analysis artefacts due to organoid swelling at high concentrations of encorafenib (**Suppl. Fig. 11B**).

Finally, organoids were exposed to the selective, ATP-competitive BRAF inhibitor encorafenib or dabrafenib[37]. Similar to what has been reported previously[35], organoid growth was barely affected by the abrogation of *BRAF* kinase activity by encorafenib or dabrafenib, independent of whether oncogenic BRAF variants were present or not (**Figure 5G, 5I and Supplementary Figure 11A**). Surprisingly, combinatorial targeting of the MAPK pathway that includes BRAF

inhibition, either combined with pan-HER or with MEK inhibitors, did not reveal significant improvements over pan-HER or MEK inhibition alone (**Figure 5H, 5J and Supplementary Figure 11A**).

Together, screening drug sensitivities across multiple oncogenic *BRAF* lines revealed intertumoral differences against the pan-HER inhibitor afatinib. *AGAP3-BRAF* expressing organoids behaved overall similarly as drug sensitive $BRAF^{WT}$ and the $BRAF^{Kinase}$ mutants to combined EGFR and MEK inhibition, while *DLG1*- and *TRIM24-BRAF* fusions approximated resistance phenotypes of the $BRAF^{V600E}$ mutant. In contrast, ERK or BRAF inhibition, alone or in combination, gave similar responses between all the lines, irrespective of oncogenic *BRAF* variants, $BRAF^{WT}$ or normal control (*GFP*).

DISCUSSION

BRAF fusions are recurrent events throughout various cancer types and form oncogenic drivers[11]. Thus far, few studies have addressed the effect of *BRAF* fusion expression on intracellular signaling and cellular processes[14,38]. Moreover, while some results have been obtained for *ALK* and *BRAF* fusions[39,40], the possible effects induced by specific 5' fusion partners of *BRAF* have not been thoroughly investigated in a clinically relevant model system. It is generally assumed that the loss of the N-terminal domain is responsible for enhanced oncogenic *BRAF* activity[14]. Whereas this is consistent with our findings showing enhanced MAPK pathway activation upon *BRAF* fusion gene expression, we systematically investigated the influence of 5' partner genes on BRAF activity.

As opposed to previous studies describing fusion gene characterization in cell lines, we here used a patient-derived organoid model that is the closest representative of human colorectal tumors that is compatible with biochemical analysis of signaling pathway alterations by BRAF fusions. Using the organoid system, we observed that subcellular localization of the BRAF fusion protein, as well as the level of MAPK pathway activation were affected by the 5´partner. A distinct localization of DLG1-BRAF proteins was detected at the plasma membrane, possibly responsible for the enhanced activation of the MAPK pathway in unperturbed as well as in drug-treated conditions as compared to AGAP3-BRAF, TRIM24-BRAF and the canonical $BRAF^{V600E}$ mutation. Wild-type BRAF is usually expressed throughout the cytoplasm and gets recruited to the plasma membrane through activated Ras[41]. Previous studies showed that localization of the BRAF protein to the plasma membrane potentiates BRAF signaling through proximity to downstream effectors[42]. Mediated by its L27 domain, DLG1 is known to localize to junctions at the plasma membrane[21]. Exactly this domain is retained in the DLG1-BRAF fusion and is likely to promote its plasma membrane localization independent of active RAS. Redirected subcellular localization showcases how the 5` fusion partners can influence functionality of oncogenic BRAF. In concordance with previous studies, the unique localization of DLG1-BRAF at the plasma membrane was lost in unpolarized 2D HEK293 cells and underscores the advantage of using 3D tumor organoid models for assessing functional effects of oncogenes[43].

We performed an unbiased phosphoproteomic screen to identify proteins that are differentially phosphorylated by each of the different *BRAF* (fusion) genes. We observed that BRAF fusion signaling mainly converges on the same signaling targets and pathways (e.g. MAPK) as the

oncogenic $BRAF^{V600E}$ mutant, with very few BRAF fusion-specific targets. On the other hand, whole transcriptome expression analysis identified shared as well as fusion-specific effects. Intriguingly, most of the deregulated genes that all BRAF fusions have in common are presumably beyond the traditional effects of MAPK pathway activity. ERK activity levels (with the exception of enhanced levels in DLG1-BRAF) were similar between all lines, which may be attributed to the already default active MAPK signaling pathway due to EGF presence at normal culture conditions. The expression of the *DLG1-BRAF* fusion uniquely affected a subset of genes which mainly converged on the cell cycle. Similarly, cell cycle related genes were deregulated in a *DLG1-BRAF* fusion-positive CRC patient, substantiating this observation. Together, this data shows that *BRAF* fusion genes commonly impact gene sets involved in cell proliferation and migration and that specific *BRAF* fusions can affect unique and distinct sets of genes.

In clinical practice, mCRC patients are treated with anti-EGFR targeting monoclonal antibodies, given that the patient does not harbor oncogenic *KRAS* or *NRAS* mutations[44,45]. In addition, oncogenic mutations in *BRAF* (e.g. V600E) are also associated with anti-EGFR therapy resistance in CRC[46]. Here we observed that all *BRAF* fusion genes tested were able to confer resistance to targeted inhibition of EGFR with the small-molecule inhibitor afatinib. Our data highlight that *BRAF* fusions active the MAPK pathway to equal or even more pronounced levels than oncogenic $BRAF^{V600E}$, both at unperturbed and afatinib-treated growth conditions. Furthermore, sustained activity of the downstream MAPK signaling pathway in the presence of afatinib is in concordance with resistance mechanisms observed in patients that are insensitive to EGFR-targeting agents[47]. These findings emphasize the clinical relevance of this study that suggest to include *BRAF* fusions to genetic screening programs for CRC patients to assist personalized therapy design.

In conclusion, we show in a patient-relevant model system that 5' fusion partners can impose a unique influence on the oncogenic effects of BRAF, among others by redirecting its subcellular localization. Nevertheless, all *BRAF* fusion genes showed insensitivity towards targeted inhibition of EGFR family members. Therefore, we provide a strong incentive to include *BRAF* fusion genes to genetic screening programs for CRC patients amenable for anti-EGFR therapy.

ACKNOWLEDGEMENTS

This work is part of the Oncode Institute, which is partly financed by the Dutch Cancer Society, and was funded by the gravitation program CancerGenomiCs.nl from the Netherlands Organization for Scientific Research (NWO), by a grant from the Dutch Cancer Society (UU 2013-6070), by a 'Sta op tegen Kanker' International Translational Cancer Research Grant, by a ERC starting grant (H.J.G.S), and a Dutch Cancer Society grant (WPK). Stand Up to Cancer is a program administered by the AACR. Furthermore, we thank all members of the Kloosterman, Voest, Snippert and Bos laboratories for fruitful discussions and support. We thank the Proteomics facility (UMCU) and Macrogen (Korea) for their help with the Phosphoproteomics and RNA sequencing experiments. We thank Glen Monroe and Hans Bos for critical reading of the manuscript and Francis Blokzijl for providing a script for the RNA sequencing analysis. We thank Robert Coebergh, Jan Ijzermans, Anieta Sieuwerts and

John Martens for collaborations that led up to this work.

AUTHOR CONTRIBUTIONS

CS, MJK, WPK and EEV conceived the study. CS, JBP, HJGS and WPK designed experiments, and CS and JBP performed and analyzed most of the experiments. IV performed viral transductions. NH analyzed drug screens. HV and RE performed phosphoproteomics and JBP and HV analyzed data. CS and MJR analyzed RNA Sequencing. CS, JBP, HJGS and WPK interpreted the data. CS and JBP wrote the manuscript, which was edited by EEV, HJGS and WPK and reviewed by all authors.

MATERIALS AND METHODS

BRAF (fusion) gene cloning

To ensure controlled and selective expression, *BRAF* (fusion) genes were introduced into the pInducer20 vector[48], which encompasses a "Tet-on" system, where gene expression is only activated by the addition of dox (Figure 1C). In addition, a C-terminal HA-tag was linked different BRAF (fusion) genes to facilitate protein quantification and *in situ* detection by immunohistochemistry. *BRAF* (fusion) genes were cloned into the vector pInducer20[48] by using the Gateway Cloning System (Invitrogen). In brief, patient RNA[6] was reverse-transcribed with the High Capacity cDNA RT Kit (Applied Biosciences). BRAF (fusion) constructs were amplified from cDNA with the Phusion Polymerase (Biolabs) utilizing forward and reverse primers with the respective 3' or 5' attB overhang (List of Primers, Supplementary Table 4). PCR products were run on a 1% agarose gel, the expected bands excised and gel purified with the Wizard SV Gel and PCR clean-up system (Promega). *TRIM24-BRAF* was ordered from Twist Bioscience with the appropriate attB overhangs. Entry-vectors (attL) were generated by combining the attP donor-vector pDonr201 (150 ng) with the purified attB-PCR products (100 fmol) and mixed with BP clonase II. The mixture was incubated for 60 mins at 25° C and the reaction was stopped with Proteinase K for 10 mins at 37° C. DH5α- library efficient cells (Invitrogen) were transformed with 1 ul of the BP reactions according to manufacturer's protocol and plated on kanamycin-LB agar plates (50 μg/ml). Bacteria were grown overnight at 37° C and single colonies were picked the next day for growing a 3 ml LB culture for a mini-prep. Plasmid DNA was extracted with the QIAPrep Spin Miniprep Kit (Qiagen) and correct insertion of fusion gene into the pDonr201 (now pEntry-vector) was verified by Sanger Sequencing. Generation of an expression-vector is achieved by combining the attR destination-vector pInducer20 (150 ng) with pEntry (150 ng, attL) and mixed with LR clonase II. The mixture was incubated for 60 mins at 25° C and the reaction was stopped with Proteinase K for 10 mins at 37° C. DH5-alpha library efficient cells were transformed with 1 ul of the LR reaction and plated on ampicillin LB agar plates (50 μg/ml). Bacteria were grown overnight at 37° C and single colonies were picked the next day for growing a 3 ml LB culture for a mini-prep. Plasmid DNA was extracted with the Qiagen MiniPrep Kit and correct insertion of fusion gene into the pInducer20 (now expression-vector) was verified by Sanger Sequencing.

Patient-derived CRC organoid and HEK293 culture and maintenance

The P18T patient-derived organoids were previously established and characterized[13,49]. P18T CRC organoids were cultured as described previously[13,32]. Culture medium contained advanced DMEM/F12 medium (Invitrogen) with 1% Penicillin/Streptomycin (P/S, Lonza), 1% Hepes buffer (Invitrogen) and 1% Glutamax (Invitrogen), 10% R-spondin conditioned medium, 10% Noggin conditioned medium, 1x B27 (Invitrogen), 1.25 mM n-Acetyl Cysteine (Sigma-Aldrich), 10 mM Nicotinamide (Sigma-Aldrich), 50 ng/ml EGF (Invitrogen), 500 nM A83-01 (Tocris), and 10 μM SB202190 (ApexBio). Organoids were split through Trypsin-EDTA (Sigma-Aldrich) treatment. Culture medium after splitting was supplemented with 10 μM Y-27632 dihydrochloride. For selection of organoids stably expressing *BRAF* (fusion) genes, organoids were grown in culture medium containing 400 μg/ml G418 (Santa Cruz).

HEK293 cells were cultured in DMEM medium (Lonza) supplemented with 10% FBS, 1% Penicillin/Streptomycin (P/S, Lonza) and 1% Glutamax (Invitrogen). For selection of HEK293 cells stably expressing *BRAF* (fusion) genes, HEK293 cells were grown in culture medium containing 400 μg/ml G418 (Santa Cruz).

P18T organoid lines were confirmed mycoplasm-negative with the mycoplasm PCR ELISA kit (Roche; last test was performed 12/9/2019) and organoids were kept in culture for 10 passages until final experiments were performed. HEK293 were kept in culture for 16 passages until final experiments were performed.

Lentiviral organoid and HEK293 transduction

Each *BRAF* (fusion) gene construct was stably integrated into the genome of patient-derived P18T organoids or HEK293 cells utilizing lentiviral transduction resulting in polyclonal *BRAF* (fusion) gene expressing lines. The P18T organoid line, which is deficient in the WNT and TP53 pathway, is derived from a non-hypermutated colorectal tumor. Furthermore, it is wild-type for the RAS signaling pathway and therefore dependent on EGF-mediated growth factor signaling for growth and survival[13]. For virus production, HEK293T cells were transfected with pHDM.Hgpm2 (1 μg), Rev (1 μg), Tat (1 μg), HDM.G (2 μg) and the respective pInducer20-construct plasmid (5 μg) using the Xtreme Gene transfection reagent (Roche). Medium was refreshed the following day. On day 3 medium was collected, sterile filtered (45 μM) and concentrated in a Ultracentrifuge at 35.000 rpm for 2.5 h at 4° C. Virus from one 10 cm dish of HEK 293T cells was resuspended in 250 μl infection medium (CRC medium + 10 μM Y-27632 + Polybrene (Millipore) and used for the transduction of one well of a 24-well plate of P18T organoids. Pre-infection, organoids were trypsinized to small clumps of single cells, pelleted in a 15 ml tube and resuspended in 15 μl infection medium per virus infection. Resuspended virus was added to the cells and cells were spin-infected at 600 rpm for 1 hour at room temperature. Thereafter, organoid-virus mixture was incubated at 37° C for 2 hours and spun down at 1400 rpm for 5 mins at 4° C. Supernatant was carefully removed and organoids were plated in 40 μl Matrigel (Corning

Life Sciences BV) and supplemented with CRC medium plus 10 µM Y-27632. Three days after infection, selection with G418 (400 µg/ml) (Corning Life Sciences BV) was started and organoids were kept under antibiotic pressure for 1 month.

Reverse Transcription and Breakpoint PCR
To confirm selective fusion gene expression upon dox treatment, organoids were cultured with dox (1 µg/ml) or vehicle (ddH_20) for 24 hours and RNA was extracted with the RNAeasy MiniKit (Qiagen) according to the manufacturer's protocol. 500 ng of DNA-free RNA was reverse transcribed into cDNA using the High Capacity cDNA RT Kit (Thermofisher). Breakpoint PCR was performed with AmpliTaqGold (Applied Biosystems) utilizing specific breakpoint primers for each *BRAF* fusion gene or primers targeting the junction between *BRAF* and the HA-tag (Supplementary Table 4). PCR products were loaded and visualized on an 2% agarose gel.

RT-qPCR
To assess differences in *BRAF* (fusion) gene expression levels, 500 ng DNA-free RNA was transcribed into cDNA as described above. Thereafter, RT-qPCR was performed with the Power-up SYBR green assay (Applied Biosystems) on a CFX cycler (Bio-Rad). All reactions were performed in triplicate and in a total volume of 10 µl comprising 5 µl 2x MM, Primer (final 5 µM) and 1 µl cDNA (approx. 10 ng). Expression levels were normalized to glucose-6-phosphatase isomerase (GPI) housekeeping gene expression and fold change was calculated with respect to the expression levels of induced $BRAF^{WT}$ expressing organoids (= set to 1).

Western blot assay
Prior to cell lysis, organoids were incubated with 1 mg/ml dispase II (Invitrogen) for 10 minutes at 37°C to digest the BME. HEK293 cells were washed with PBS prior to cell lysis. Western blot samples for were lysed using RIPA buffer (50 mM Tris-HCL pH 8.0, 150 mM NaCl, 0.1% SDS, 0.5% Na-Deoxycholate, 1% NP-40) containing Complete protease inhibitors (Roche). Protein content was quantified using a BCA protein assay kit (Pierce™) and analyzed by Western blotting. Membranes were blocked and probed with antibodies directed against HA (RRID:AB_631618), Vinculin (RRID:AB_477629), GAPDH (RRID:AB_2107445), beta-catenin (RRID:AB_397555), pERK (RRID:AB_331646), ERK (RRID:AB_390779), pMEK (RRID:AB_331648), MEK (RRID:AB_823567), pCDK2 (AB_2078685), tCDK2 (RRID:AB_631215), pAKT (RRID: AB_2315049) and AKT (RRID: AB_1147620).
Organoid treatments: dox (MP Biomedicals) 1 µg/ml, 24 h or dd H_20. Dox 1 µg/ml 24 h followed by treatment with afatinib (Selleck Chemicals) 1 µM, 24 h or DMSO.

Phenotypic drug screen
Four days after organoid trypsinization, 1 µg/ml dox or ddH2O was added to the organoid cultures. After 24 hours, 1 mg/ml dispase II (Invitrogen) was added to the medium of the organoids and these were incubated for 15 min at 37° C to digest the BME. Subsequently, organoids were mechanically dissociated by pipetting, filtrated using a 40 µm nylon cell strainer (Falcon), resuspended in 75% BME/growth medium (40 organoids/ml) and plated as two 10 µl drops on Nunc™ Lab-Tek™ II Chamber Slide™ Systems. After plating, culture medium containing either 1 µg/ml dox or ddH2O, together with 1 µM of afatinib or DMSO was added. The labtek plates were mounted on an inverted confocal laser scanning microscope (Leica SP8X) and imaged using a 10X objective. For visualization of cell viability, organoids were incubated with 16.2 mM Hoechst 33342 (Life Technologies) and 1.5 mM DRAQ7™ (Cell Signaling #7406) for 30 min at 37° C prior imaging. For calculating organoid viability and size, organoids were scored by morphology and analyzed by automated brightfield morphometry using Organoseg[50].

Immunofluorescence
For immunofluorescence, organoids and HEK293 cells were washed in PBS, fixed and permeabilized with 4% PFA (Aurion) containing 0.25% glutaraldehyde (Sigma), and blocked with PBS containing 0.3% Triton X-100 (Sigma), 1 mg/ml BSA (Sigma Aldrich), 5% NGS (Life Technologies), and incubated with antibodies at 4°C overnight.
For immunofluorescence of HEK293 cell cultures, cells were washed in PBS, fixed with 4% PFA, permeabilized with PBS containing 0.2% Triton X-100, blocked in PBS containing 3% NGS, 2% BSA and 50 mM ammonium chloride, and incubated with antibodies directed against HA (RRID:AB_390929) at 4°C overnight. Hoechst 33342 was added together with secondary antibodies to stain for DNA.
Images were captured with a Leica SP8X microscope using a 40X objective. Post-acquisition analyses of phenotypes were performed manually using ImageJ.
Treatments: Culture medium containing 1 µg/ml dox or ddH2O for 24 h.

Drug screen and viability assessment
Five days after organoid trypsinization to single cells, 1 mg/ml dispase II (Invitrogen) was added to the medium of the organoids and these were incubated for 15 min at 37° C to digest the BME. Subsequently, organoids were

mechanically dissociated from the BME by subtle pipetting, filtrated using a 40 µm nylon cell strainer (Falcon), resuspended in 2% BME/growth medium (15–20,000 organoids/ml) prior plating of 40 µl (Multi-dropTM Combi Reagent Dispenser) on BME pre-coated 384-well plates. The drugs and their combinations were added 3 hrs after plating the organoids by using the Tecan D300e Digital Dispenser. Drugs were dispensed in a non-randomized manner and DMSO end concentration was 0.6% in all wells. 96 hrs after adding the drugs organoids were fixed with 4% PFA (Merck) and stained with Hoechst (Invitrogen). Organoids were screened by automated microscopy of whole wells (CX5 High Content Screening (HCS) platform (Thermo Scientific), equipped with an Olympus UPLFLN U Plan Fluorite 4x Microscope Objective). Organoid size was measured by integrating Hoechst signal and contrast using Columbus Cellular imaging and analyses (Perkin Elmer). Relative survival was determined by normalization of the results to controls (average of all 5 nM drug concentrations = 100% alive) and 20 µM Navitoclax (= 0% alive), which induces maximal killing within 96 hours after treatment. Multiple identical drug combinations were averaged.

Targeted inhibitors
Afatinib, Selumetinib, Encorafenib and Navitoclax were purchased from Selleck Chemicals. SCH772984 was obtained from MedChem Express. Dabrafenib was obtained from Bio-Connect. These compounds were dissolved in dimethylsulfoxide (DMSO, Sigma-Aldrich) and stored as 10 mM aliquots.

Curve fitting and drug sensitivity
Dose-response curves were generated using GraphPad software by performing nonlinear regression (curve fit), assuming a standard Hill equation (chosen method: log(inhibitor) vs. Response, constrain top=100).

RNA Sequencing
Organoids were treated with dox (1 µg/ml) or ddH_20 for 24 hours and RNA was extracted with the RNAeasy MiniKit (Qiagen) according to the manufacturer's protocol. 1 µg of total RNA was shipped to Macrogen (Korea). RNA-libraries were prepared for sequencing with the Illumina TruSeq Stranded Total RNA (+ Ribo-Zero HMR) Kit and sequenced on the NovaSeq platform (2x100bp, 60M reads per sample). Data were processed with our in-house RNA analysis pipeline (https://github.com/UMCUGenetics/RNASeq, v.2.4.0, default settings) by utilizing STAR (v.2.4.2a) to map the reads. Samples were normalized for sequencing depth based on the sum of the read counts over all genes for each sample. Expressed genes were selected by excluding all genes where ≥ 3 samples had less than 10 reads. Principal Component Analysis (PCA), Euclidean Distance-based clustering and Differential Expression (DGEA) calculations were performed with the DESeq2 package[51]. P-adjusted ($p_{adjusted}$) was calculated by multiplying the *p*-value with the number of genes (=expressed genes) tested. Unsupervised hierarchical clustering was performed on 300 intermediately expressed genes (mean gene expression > 100 and max gene expression 500). DGEA was performed on induced BRAF fusion lines vs. all other lines or each induced line vs. controls (= all uninduced lines and induced GFP line). Geneset overrepresentation analysis was performed on Webgestalt[25], with the settings set to Reactome pathway analysis and the reference gene set as all protein-coding genes. The top 50 up- and downregulated genes upon *DLG1-BRAF* fusion gene expression were based on the DGEA analysis between the *DLG1-BRAF* expressing organoid line and the control lines ($p_{adjusted}$ <0.05). The cohort of CRC patients (n=233) was selected from a cohort of primary CRC patients[6] by excluding all patients with a mutation in *KRAS* or $BRAF^{V600E}$.

Mass spectrometry sample preparation and enrichment of phosphopeptides
For SILAC labeling, HEK293 cells were cultured in high-glucose (10% dialyzed FBS (BioWest)) DMEM (Thermo) lacking lysine and arginine supplemented with Lys-0/Arg-0 or Lys-8/Arg-10 (Silantes). After 4 hours of doxycycline or ddH2O administration, cells were lysed in 8 M Urea, 1M Ammonium-BiCarbonate (ABC) containing 10 mM Tris(2-carboxyethyl)phosphine hydrochloride (TCEP) and 40mM 2-chloro-acetamide supplemented with protease inhibitors (Roche, complete EDTA-free) and 1% (v/v) phosphatase inhibitor cocktails 2 and 3 (Sigma, Cat. No. P5726 and Cat. No. P0044). After ultra-sonication, cell lysates were mixed 1:1 and proteins (20 mg total) were overnight in solution digested with trypsin (1:50) (Worthington). Peptides were desalted using SepPack columns (Waters) and eluted in 80% acetonitrile (ACN), 0.1% Formic Acid (FA) (buffer B) after which TFA was added to 1%. To enrich phosphopeptides for, 50 mg titanium dioxide (TiO2) beads (Sachtopore-NP, 5 µM, 300 Å, Zirchrom) were washed with 5% NH3 and equilibrated 3 times with 6% TFA in 80% ACN after which the phospho-peptides were allowed to bind at 37 ˚C for 5 minutes on a shaker. After centrifugation, remaining phospho-peptides were enriched from the supernatant sequentially. After loading the beads on an in-house made C8 stage-tip (Empore, 3M) they were washed 3 times with 1% TFA in 80% ACN. Peptides were eluted with 200 µl 5% NH3 into 40µl 20% FA followed by elution with 5 µl buffer B. Peptides were loaded on in-house made C18 stage-tips and divided with high PH elution into three fractions (100 mM NH3/FA PH=10 in 5%, 10% or 50% ACN).

LC-MS/MS analysis
After elution from the stage tips, acetonitrile was removed using a SpeedVac and the remaining peptide solution

was diluted with buffer A (0.1% FA) before loading. Peptides were separated on a 30 cm pico-tip column (75µm ID, New Objective) in-house packed with 1.9 µm aquapur gold C-18 material (dr. Maisch) using 240 gradient (7% to 80% ACN 0.1% FA), delivered by an easy-nLC 1000 (Thermo), and electro-sprayed directly into an Orbitrap Fusion Tribrid Mass Spectrometer (Thermo Scientific). The latter was set in data dependent Top speed mode with a cycle time of 1 second, in which the full scan over the 400-1500 mass range was performed at a resolution of 240000. Most intense ions (intensity threshold of 5000 ions) were isolated by the quadrupole and fragmented with an HCD collision energy of 30%. The maximum injection time of the ion trap was set to 50 milliseconds with injection of ions for all available parallelizable time.

Mass spectrometry data analysis

Raw files were analyzed with the Maxquant software version 1.6.1.0[52] with phosphorylation of serine threonine and tyrosine as well as oxidation of methionine set as variable modifications, and carbamidomethylation of cysteine set as fixed modification. The Human protein database of Uniprot was searched with both the peptide as well as the protein false discovery rate set to 1%. The SILAC quantification algorithm was used in combination with the 'match between runs' tool (option set at two minutes). Peptides were filtered for reverse hits and standard contaminants.

The mass spectrometry proteomics data have been deposited to the ProteomeXchange Consortium via the PRIDE partner repository (Perez-Riverol et al., 2019) with the dataset identifiers PXD013461.

Resulting phosphorylation sites were analyzed in Perseus software (Version 1.5) using MaxQuant normalized H/L ratios. Reverse hits, common contaminants, and sites with localization probability below 0.75 were deleted. Furthermore, identified phosphopeptides were log2-transformed and accounted for quantification only if they were present in both forward and reverse (label-swap) experiments. *p*-values were calculated in a Student's *t*-test (*p*-value < 0.05, S0=0) with Perseus 1.5 software. Subsequently, phosphoproteomics data were normalized to relative protein expression and ratios were deemed significantly changed if they were <-1.5 or >1.5 fold. Kinase activity scores were calculated using Kinase-Substrate Enrichment Analysis (KSEA) analysis[24] in which we used both PhosphoSitePlus and NetworKIN databases. The NetworKIN cutoff score was set to 5, the *p*-value cutoff was set to 0.05, and the substrate count cutoff was to 5. Geneset overrepresentation analysis was performed on Webgestalt[25], with the settings set to Reactome pathway analysis and the reference gene set as all protein-coding genes.

SUPPLEMENTARY FIGURES

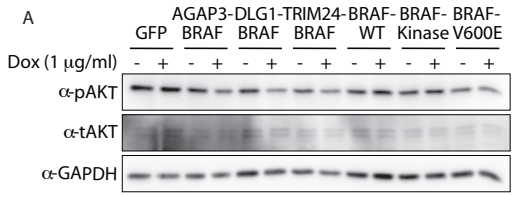

Supplementary Figure 1. Impact of BRAF (fusion) gene expression on phosphorylation of AKT.
(**A**) BRAF (fusion) expressing organoids were not induced (-) or induced (+) with dox (1 µg/ml) for 24h and immuno–blotted for phosphorylated AKT (pAKT) and total AKT (tAKT). GAPDH was used as loading control.

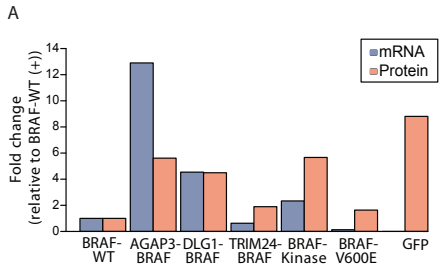

Supplementary Figure 2. *BRAF* (*fusion*) gene mRNA and protein expression levels.
(**A**) Quantification of BRAF (fusion) expression on mRNA and protein levels. mRNA was quantified with qRT-PCR. Protein was quantified with western blot. mRNA and protein levels were normalized to expression levels of induced $BRAF^{WT}$ expressing P18T organoids (set to 1).

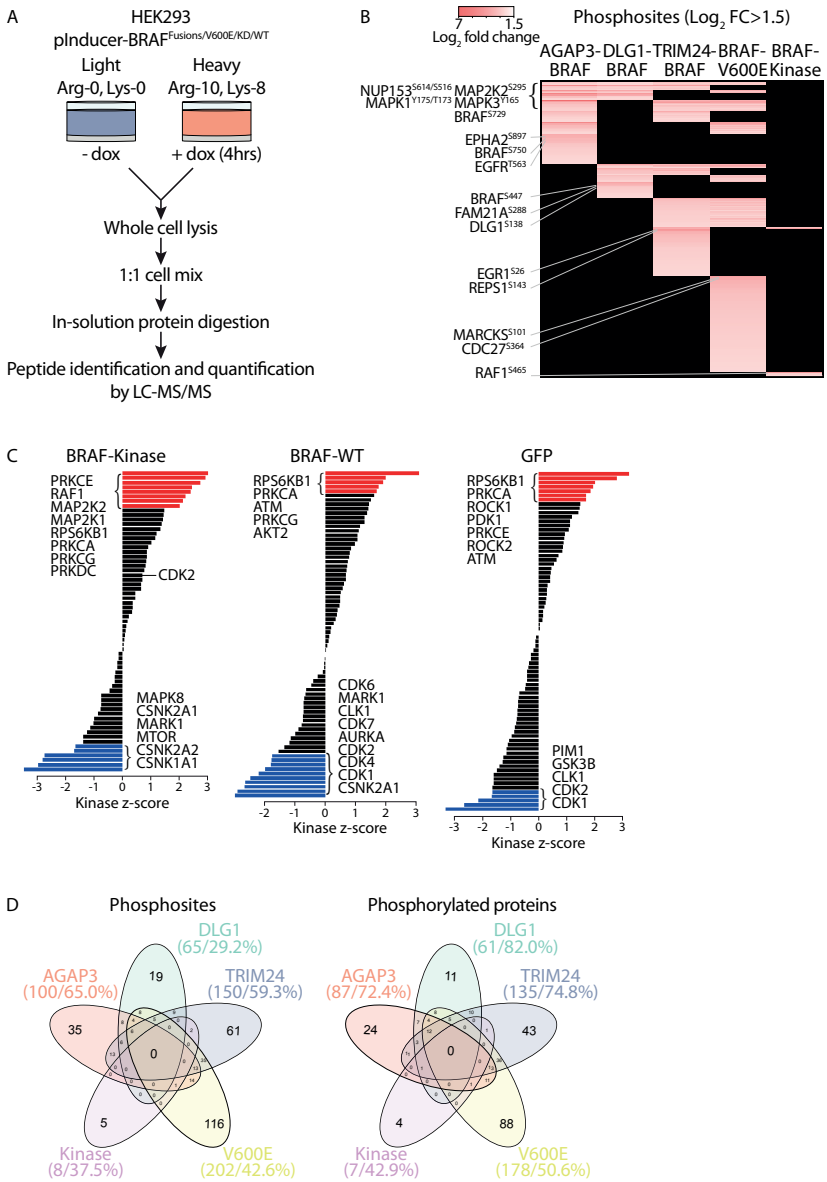

Supplementary Figure 3. Phosphoproteomics screen in HEK293 cells reveals that BRAF fusions and BRAF^{V600E} activate similar signaling pathways.
(**A**) Schematic overview of the SILAC-based phosphoproteomics screen performed on *BRAF* (*fusion*) expressing HEK293 cells. (**B**) Heatmap of ratio changes of significantly upregulated (Log_2 FC>1.5, p-value<0.05) phosphosites induced upon *BRAF* (*fusion*) gene expression in HEK293 cells. Phosphosites in the MAPK signaling pathway that are shared between *BRAF fusion* and *BRAF^{V600E}* expressing cells are indicated at the upper left. *BRAF* (*fusion*)-specific phosphotargets (highest ratio changes) are indicated with grey lines. (**C**) Kinase-Substrate Enrichment Analysis results showing kinase activity scores of *BRAF^{Kinase}*, *BRAF^{WT}*, and *GFP* expressing HEK293 cells. (**D**) Venn diagram depicting the overlap of specific phosphosites and phosphorylated proteins (-1.5<Log_2 FC>1.5, p-value<0.05) between *BRAF fusion*, *BRAF^{V600E}*, and *BRAF^{Kinase}* in HEK293 cells. Between brackets is indicated the percentage of overlapping phosphosites/proteins between *BRAF fusion*, *BRAF^{V600E}*, and *BRAF^{Kinase}* expressing cells.

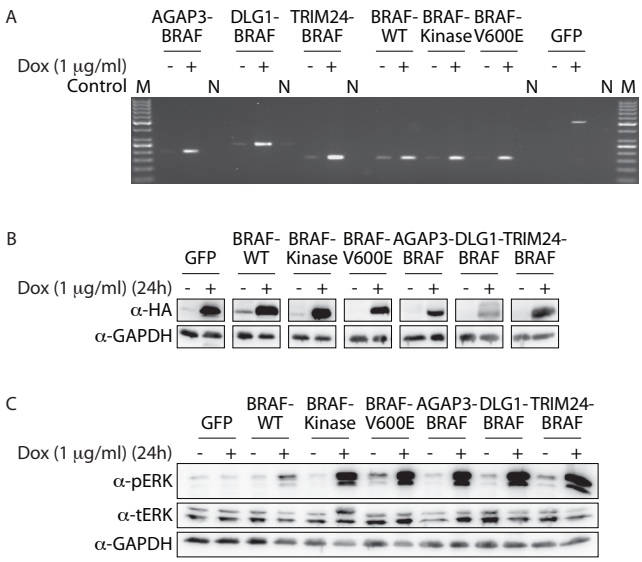

Supplementary Figure 4. *BRAF* (*fusion*) gene expression and MAPK pathway activation in HEK293 cells.
(**A**) Breakpoint-PCR verifying the expression of the BRAF (fusion) transcripts in HEK293 cells upon dox administration. Respective breakpoint primers are used on uninduced (-), induced (+;1 μg/ml dox for 24h), positive (respective pInducer20-plasmid; P) and negative control (water; N). (**B**) Immunoblotting for HA-tagged BRAF (fusion) proteins in HEK293 cells verifying the protein expression at the expected height and upon dox administration (1 μg/ml for 24h). GAPDH was used as loading control. (**C**) HEK293 cells were not induced (-) or induced (+) with dox (1 μg/ml) for 24h and immunoblotted for phosphorylated ERK (pERK) and total ERK (tERK). GAPDH was used as loading control.

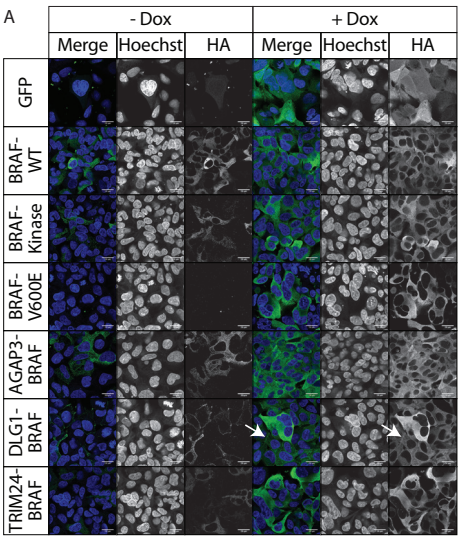

Supplementary Figure 5. BRAF (fusion) protein localization in HEK293 cells.
HEK293 cells transduced with *GFP*, *BRAF*^{WT}, *BRAF*^{Kinase}, *BRAF*^{V600E}, *AGAP3-BRAF*, *DLG1-BRAF* or *TRIM24-BRAF* were not induced (- dox) or induced (+ dox (1 μg/ml for 24h)) and stained for the HA-tag to visualize the protein localization (HA-tag = green) and the nucleus (Hoechst = blue). White arrows indicate localization to the plasma membrane.

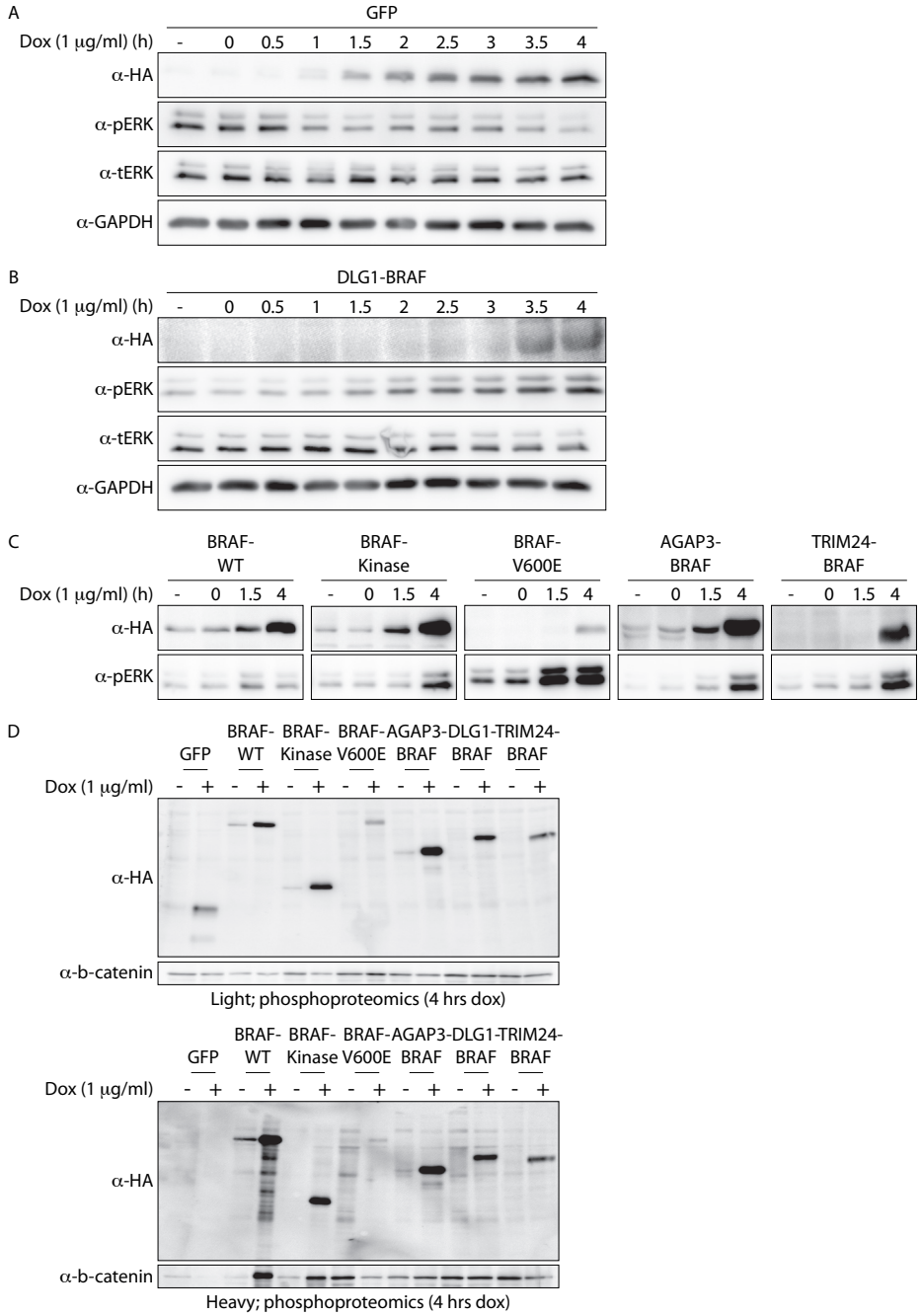

Supplementary Figure 6. Establishment of optimal duration of dox induction for BRAF (fusion) protein expression.

(**A**) *GFP*- and (**B**) *DLG1-BRAF*-transduced HEK293 cells were induced with dox (1 μg/ml) for up to 4 hours and immunoblotted for protein expression (HA-tag), pERK and tERK. GAPDH was used as loading control. (**C**) $BRAF^{WT}$, $BRAF^{Kinase}$, $BRAF^{V600E}$, *AGAP3-BRAF*, or *TRIM24-BRAF*-transduced HEK293 cells were induced with dox (1 μg/ml) for up to 4 hours and immunoblotted for protein expression (HA-tag) and pERK. (**D**) Verification of BRAF (fusion)

protein expression immunoblotting upon dox induction (1 µg/ml) for 4 hours from the lysates of the phosphoproteomics experiment (light and heavy labeled cells). Blots were probed for of protein expression (HA-tag) and beta-catenin was used as loading control.

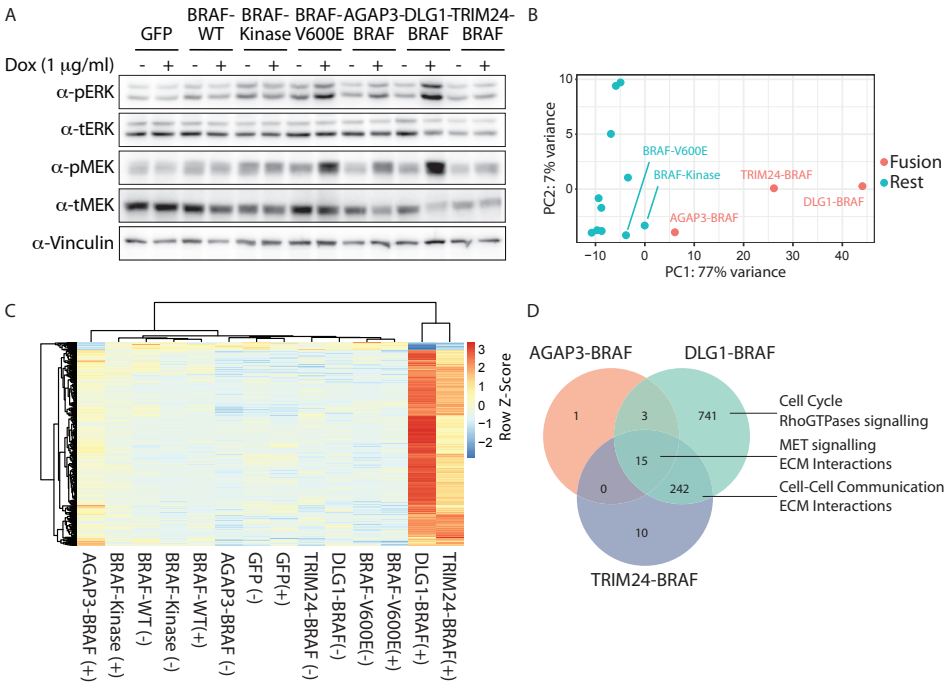

Supplementary Figure 7. Transcriptomic analysis of *BRAF* (*fusion*) gene expressing P18T CRC organoid lines. (**A**) Immunoblotting for phosphotargets pERK and pMEK of *BRAF* (fusion) genes that were identified by phosphoproteomics shows upregulated levels of MAPK signaling in $BRAF^{V600E}$, *AGAP3-BRAF* and *DLG1-BRAF* upon dox administration (1 µg/ml for 24h). Vinculin was used as loading control. (**B**) Principal Component Analysis of gene expression levels for *BRAF* (*fusion*) gene and *GFP* expressing lines (- dox and + dox (1 µg/ml, 24h)). (**C**) Unsupervised clustering of 300 randomly chosen genes with intermediate gene expression (mean read-counts > 100 and maximal read-count < 500). (**D**) Overlap of the significantly differentially expressed genes ($p_{adjusted}$ <0.05) between the *AGAP3-BRAF*, *DLG1-BRAF* or *TRIM24-BRAF* expressing organoid lines and the control lines (uninduced lines and induced *GFP* line). Gene set overrepresentation analysis revealed pathways enriched for genes involved in specific cellular functions.

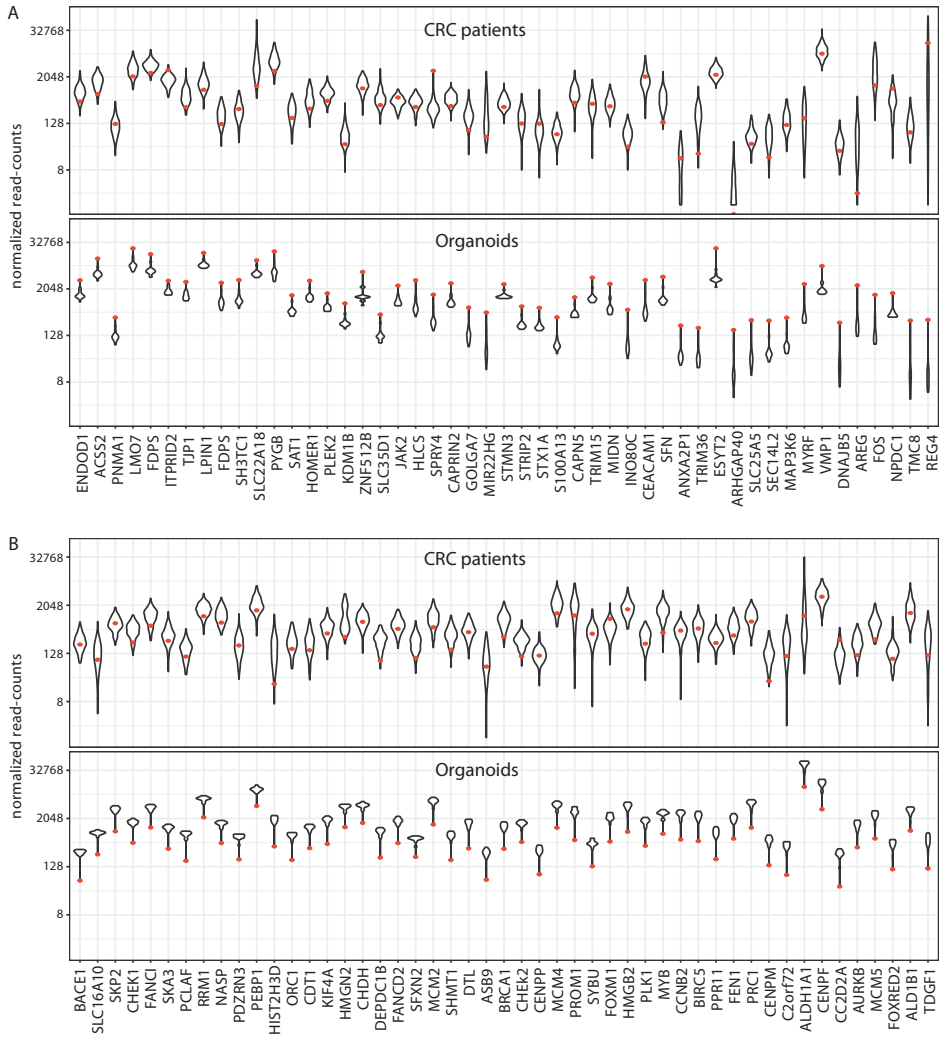

Supplementary Figure 8. Expression of most differentially expressed genes in *DLG1-BRAF* expressing P18T organoids and CRC patients.
Expression levels of Top 50 upregulated (**A**) and Top 50 downregulated (**B**) genes upon *DLG1-BRAF* expression in CRC organoids and in CRC patients (n=233) wild-type for *KRAS* and *BRAF*. Violin-plots depicts overall distribution of expression and red dot indicates expression levels in the *DLG1-BRAF*-positive CRC patient or the *DLG1-BRAF* expressing organoid line.

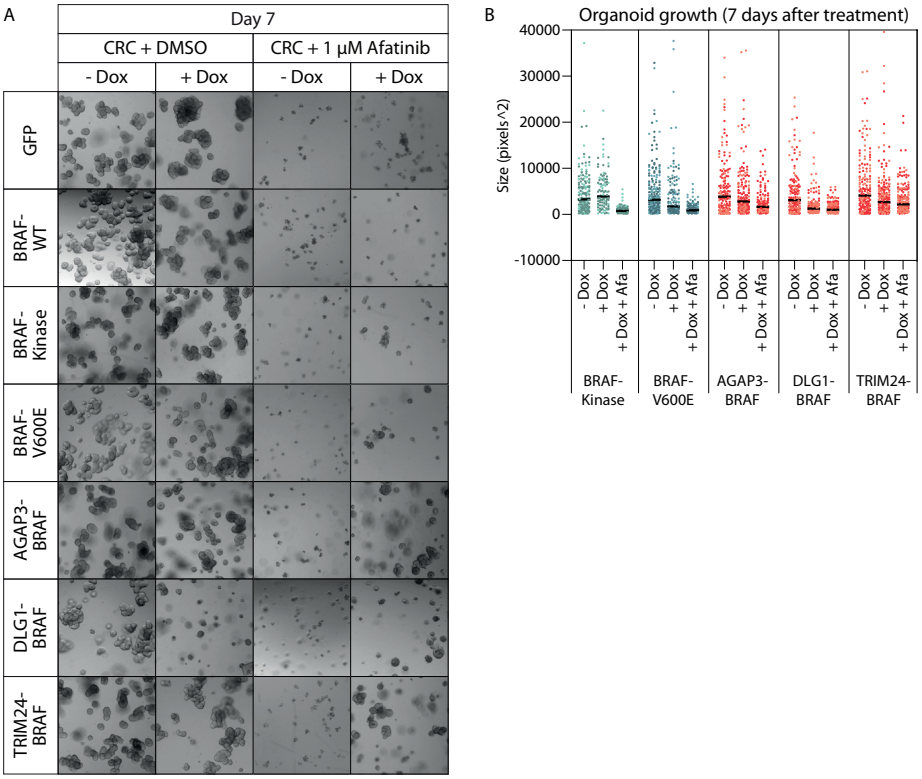

Supplementary Figure 9. *BRAF* (*fusion*) genes confer resistance to EGFR inhibition.
(**A**) Representative bright field pictures of P18T CRC organoids with (+ dox (1 μg/ml)) or without (- dox) induced expression of *GFP* or *BRAF* (*fusion*) genes that were treated with DMSO or afatinib (1 μM) for 7 days. (**B**) Quantitative analysis of organoid growth in $BRAF^{Kinase}$, $BRAF^{V600E}$ or *BRAF fusion* lines treated with or without doxycycline (+ dox (1 μg/ml)) and afatinib (1 μM) for 7 days. Each dot represents one organoid. Colours represent the different biological replicates. Data from 3 8-wells Lab-Tek chambered coverglass is shown per condition.

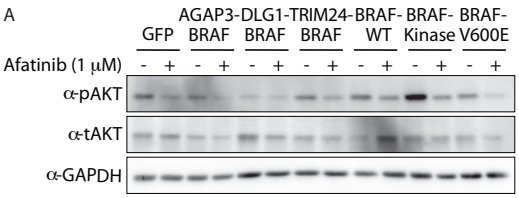

Supplementary Figure 10. Impact of afatinib exposure on pAKT levels in *BRAF* (*fusion*) gene expressing CRC organoids.
(**A**) BRAF (fusion) protein expressing organoids were treated with DMSO (-) or 1 μM afatinib (+) for 24h and immunoblotted for phosphorylated AKT (pAKT) and total AKT (tAKT). GAPDH was used as loading control.

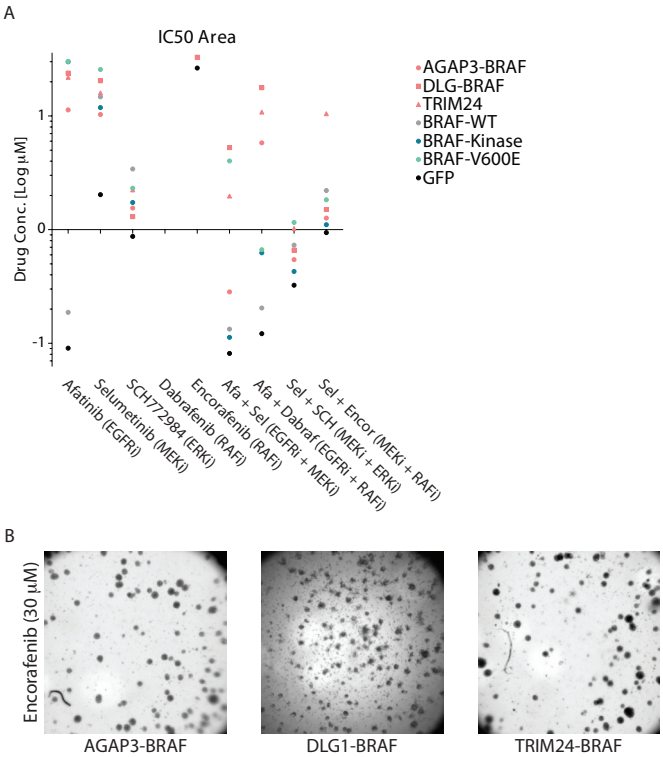

Supplementary Figure 11. Differential sensitivities of *BRAF* (*fusion*) genes to combinatorial targeting of EGFR and MEK.
(**A**) IC50 values for organoid growth (area) of *BRAF* (*fusion*) and *GFP* expressing organoids treated with afatinib (EGFRi), selumetinib (MEKi), SCH772984 (ERKi), encorafenib (RAFi) and dabrafenib (RAFi) in a mono- or combinatorial fashion. (**B**) Representative pictures of *BRAF fusion* expressing organoids treated with 30 µM encorafenib, showing organoid swelling in *AGAP3-BRAF* and *TRIM24-BRAF* lines.

SUPPLEMENTARY TABLES

Supplementary Table 1.
KSEA kinase scores and kinase-substrate links identified in phosphoproteomic screen (provided separately due to size)

Supplementary Table 2.
Differential Gene Expression Analysis on *BRAF* (*fusion*) gene expressing organoid lines (provided separately due to size)

Supplementary Table 3.
Z-scores of significantly differential expressed genes (provided separately due to size)

Supplementary Table 4. List of *BRAF* (*fusion*) gene and *GFP*-specific primers used for breakpoint PCR, HA-tag spanning PCR and gateway cloning.

Construct	**Breakpoint fwd 5'->3'**	**Breakpoint rev 5'->3'**
AGAP3-BRAF	AGCGCCTTCAGCGACTACT	GCAGACAAACCTGTGGTTGA
DLG1-BRAF	ACACTGCCAAGCAGCCTTAG	GCAGACAAACCTGTGGTTGA
TRIM24-BRAF	CTGTGAGGACAACGCAGAAG	GCAGACAAACCTGTGGTTGA
BRAF-WT		
BRAF-Kinase		
BRAF-V600E		
GFP	CCTGAAGTTCATCTGCACCA	CTTTGCTCAGGGCGGACT
Construct	**HA-tag rev 5'->3'**	**HA-tag rev 5'->3'**
AGAP3-BRAF	TGCTTGTGCTTCTCCAAAAA	TGGGACGTCGTATGGGTATT
DLG1-BRAF	TGCTTGTGCTTCTCCAAAAA	TGGGACGTCGTATGGGTATT
TRIM24-BRAF	TGCTTGTGCTTCTCCAAAAA	TGGGACGTCGTATGGGTATT
BRAF-WT	TGCTTGTGCTTCTCCAAAAA	TGGGACGTCGTATGGGTATT
BRAF-Kinase	TGCTTGTGCTTCTCCAAAAA	TGGGACGTCGTATGGGTATT
BRAF-V600E	TGCTTGTGCTTCTCCAAAAA	TGGGACGTCGTATGGGTATT
GFP		
Construct	**AttR1 5'->3'**	
AGAP3-BRAF	GGGGACAAGTTTGTACAAAAAAGCAGGCTTTGCCACCATGGTGCTTGTGGGCACGCAG	
DLG1-BRAF	GGGGACAAGTTTGTACAAAAAAGCAGGCTTTGCCACCATGCCGGTCCGGAAGCAAG	
TRIM24-BRAF	GGGGACAAGTTTGTACAAAAAAGCAGGCTTTGCCACCATGGAGGTGGCGGTGGAG	
BRAF-WT	GGGGACAAGTTTGTACAAAAAAGCAGGCTTTGCCACCATGGCGGCGCTGAGCGGTG	
BRAF-Kinase	GGGGACAAGTTTGTACAAAAAAGCAGGCTTTGCCACCATGGACTTGATTAGAGACC	
BRAF-V600E	GGGGACAAGTTTGTACAAAAAAGCAGGCTTTGCCACCATGGCGGCGCTGAGCGGTG	
GFP	GGGGACAAGTTTGTACAAAAAAGCAGGCTTTGCCACCATGGTGAGCAAGGGCGAGG	
Construct	**AttR2 5'->3'**	
AGAP3-BRAF	GGGGACCACTTTGTACAAGAAAGCTGGGTTGTGGACAGGAAACGCACCATATC	
DLG1-BRAF	GGGGACCACTTTGTACAAGAAAGCTGGGTTGTGGACAGGAAACGCACCATATC	
TRIM24-BRAF	GGGGACCACTTTGTACAAGAAAGCTGGGTTGTGGACAGGAAACGCACCATATC	
BRAF-WT	GGGGACCACTTTGTACAAGAAAGCTGGGTTGTGGACAGGAAACGCACCATATC	
BRAF-Kinase	GGGGACCACTTTGTACAAGAAAGCTGGGTTGTGGACAGGAAACGCACCATATC	
BRAF-V600E	GGGGACCACTTTGTACAAGAAAGCTGGGTTGTGGACAGGAAACGCACCATATC	
GFP	GGGGACCACTTTGTACAAGAAAGCTGGGTTCTTGTACAGCTCGTCCATG	

red = attR1 site
blue = attR2 site
_ = Gene specific

REFERENCES

1. Gu W, Zhang F, Lupski JR. Mechanisms for human genomic rearrangements. *Pathogenetics*. 2008;1(1):4. doi:10.1186/1755-8417-1-4
2. Macintyre G, Ylstra B, Brenton JD. Sequencing Structural Variants in Cancer for Precision Therapeutics. *Trends Genet*. 2016. doi:10.1016/j.tig.2016.07.002
3. Mertens F, Johansson B, Fioretos T, Mitelman F. The emerging complexity of gene fusions in cancer. *Nat Rev Cancer*. 2015. doi:10.1038/nrc3947
4. Mitelman F, Johansson B, Mertens F. The impact of translocations and gene fusions on cancer causation. *Nat Rev Cancer*. 2007. doi:10.1038/nrc2091
5. Parker BC, Zhang W. Fusion genes in solid tumors: An emerging target for cancer diagnosis and treatment. *Chin J Cancer*. 2013. doi:10.5732/cjc.013.10178
6. Kloosterman WP, Coebergh Van Den Braak RRJ, Pieterse M, et al. A systematic analysis of oncogenic gene fusions in primary colon cancer. *Cancer Res*. 2017;77(14):3814-3822. doi:10.1158/0008-5472.CAN-16-3563
7. Chong H, Guan KL. Regulation of Raf through phosphorylation and N terminus-C terminus interaction. *J Biol Chem*. 2003;278(38):36269-36276. doi:10.1074/jbc.M212803200
8. Heidecker G, Huleihel M, Cleveland JL, et al. Mutational activation of c-raf-1 and definition of the minimal transforming sequence. *Mol Cell Biol*. 2015;10(6):2503-2512. doi:10.1128/mcb.10.6.2503
9. Kulkarni A, Al-Hraishawi H, Simhadri S, et al. BRAF fusion as a novel mechanism of acquired resistance to vemurafenib in BRAFV600E mutant melanoma. *Clin Cancer Res*. 2017. doi:10.1158/1078-0432.CCR-16-0758
10. Schrock AB, Zhu VW, Hsieh WS, et al. Receptor Tyrosine Kinase Fusions and BRAF Kinase Fusions are Rare but Actionable Resistance Mechanisms to EGFR Tyrosine Kinase Inhibitors. *J Thorac Oncol*. 2018;13(9):1312-1323. doi:10.1016/j.jtho.2018.05.027
11. Ross JS, Wang K, Chmielecki J, et al. The distribution of BRAF gene fusions in solid tumors and response to targeted therapy. *Int J Cancer*. 2016. doi:10.1002/ijc.29825
12. Drost J, Clevers H. Organoids in cancer research. *Nat Rev Cancer*. 2018. doi:10.1038/s41568-018-0007-6
13. Van De Wetering M, Francies HE, Francis JM, et al. Prospective derivation of a living organoid biobank of colorectal cancer patients. *Cell*. 2015. doi:10.1016/j.cell.2015.03.053
14. Lu H, Villafane N, Dogruluk T, et al. Engineering and functional characterization of fusion genes identifies novel oncogenic drivers of cancer. *Cancer Res*. 2017. doi:10.1158/0008-5472.CAN-16-2745
15. Oku Y, Huganir RL. AGAP3 and Arf6 Regulate Trafficking of AMPA Receptors and Synaptic Plasticity. *J Neurosci*. 2013. doi:10.1523/jneurosci.0341-13.2013
16. Humbert PO, Grzeschik NA, Brumby AM, Galea R, Elsum I, Richardson HE. Control of tumourigenesis by the Scribble/Dlg/Lgl polarity module. *Oncogene*. 2008. doi:10.1038/onc.2008.341
17. Herquel B, Ouararhni K, Davidson I. The TIF1α-related TRIM cofactors couple chromatin modifications to transcriptional regulation, signaling and tumor suppression. *Transcription*. 2011. doi:10.4161/trns.2.5.17725
18. Kim EK, Choi EJ. Pathological roles of MAPK signaling pathways in human diseases. *Biochim Biophys Acta - Mol Basis Dis*. 2010. doi:10.1016/j.bbadis.2009.12.009
19. Chen B, Tardell C, Higgins B, Packman K, Boylan JF, Niu H. BRAFV600E negatively regulates the AKT pathway in melanoma cell lines. *PLoS One*. 2012. doi:10.1371/journal.pone.0042598
20. Abd Elmageed ZY, Moore RF, Tsumagari K, et al. Prognostic Role of BRAF V600E Cellular Localization in Melanoma. *J Am Coll Surg*. 2018. doi:10.1016/j.jamcollsurg.2017.12.040
21. Hanada T, Takeuchi A, Sondarva G, Chishti AH. Protein 4.1-mediated Membrane Targeting of Human Discs Large in Epithelial Cells. *J Biol Chem*. 2003. doi:10.1074/jbc.M305209200
22. Zhou F, Dong C, Davis JE, Wu WH, Surrao K, Wu G. The mechanism and function of mitogen-activated protein kinase activation by ARF1. *Cell Signal*. 2015. doi:10.1016/j.cellsig.2015.06.007
23. Meyer-Ficca ML, Meyer RG, Kaiser H, Brack AR, Kandolf R, Küpper JH. Comparative analysis of inducible expression systems in transient transfection studies. *Anal Biochem*. 2004. doi:10.1016/j.ab.2004.07.011
24. Wiredja DD, Koyutürk M, Chance MR. The KSEA App: a web-based tool for kinase activity inference from quantitative phosphoproteomics. *Bioinformatics*. 2017. doi:10.1093/bioinformatics/btx415
25. Wang J, Vasaikar S, Shi Z, Greer M, Zhang B. WebGestalt 2017: A more comprehensive, powerful, flexible and interactive gene set enrichment analysis toolkit. *Nucleic Acids Res*. 2017. doi:10.1093/nar/gkx356
26. Williams GH, Stoeber K. The cell cycle and cancer. *J Pathol*. 2012;226(2):352-364. doi:10.1002/path.3022
27. Jansen S, Gosens R, Wieland T, Schmidt M. Paving the Rho in cancer metastasis: Rho GTPases and

beyond. *Pharmacol Ther*. 2018. doi:10.1016/j.pharmthera.2017.09.002
28. Vial E, Sahai E, Marshall CJ. ERK-MAPK signaling coordinately regulates activity of Rac1 and RhoA for tumor cell motility. *Cancer Cell*. 2003. doi:10.1016/S1535-6108(03)00162-4
29. Downward J. Targeting RAS signalling pathways in cancer therapy. *Nat Rev Cancer*. 2003. doi:10.1038/nrc969
30. Moll HP, Pranz K, Musteanu M, et al. Afatinib restrains K-RAS-driven lung tumorigenesis. *Sci Transl Med*. 2018;10(44):1-13. doi:10.1126/scitranslmed.aao2301
31. De Roock W, Claes B, Bernasconi D, et al. Effects of KRAS, BRAF, NRAS, and PIK3CA mutations on the efficacy of cetuximab plus chemotherapy in chemotherapy-refractory metastatic colorectal cancer: A retrospective consortium analysis. *Lancet Oncol*. 2010. doi:10.1016/S1470-2045(10)70130-3
32. Verissimo CS, Overmeer RM, Ponsioen B, et al. Targeting mutant RAS in patient-derived colorectal cancer organoids by combinatorial drug screening. *Elife*. 2016. doi:10.7554/elife.18489
33. Misale S, Bozic I, Tong J, et al. Vertical suppression of the EGFR pathway prevents onset of resistance in colorectal cancers. *Nat Commun*. 2015;6:8305. doi:10.1038/ncomms9305
34. Kruspig B, Monteverde T, Neidler S, et al. The ERBB network facilitates KRAS-driven lung tumorigenesis. *Sci Transl Med*. 2018. doi:10.1126/scitranslmed.aao2565
35. Prahallad A, Sun C, Huang S, et al. Unresponsiveness of colon cancer to BRAF(V600E) inhibition through feedback activation of EGFR. *Nature*. 2012. doi:10.1038/nature10868
36. Morris EJ, Jha S, Restaino CR, et al. Discovery of a novel ERK inhibitor with activity in models of acquired resistance to BRAF and MEK inhibitors. *Cancer Discov*. 2013. doi:10.1158/2159-8290.CD-13-0070
37. Sun J, Zager JS, Eroglu Z. Encorafenib/binimetinib for the treatment of BRAF-mutant advanced, unresectable, or metastatic melanoma: Design, development, and potential place in therapy. *Onco Targets Ther*. 2018. doi:10.2147/OTT.S171693
38. Tomić TT, Olausson J, Wilzén A, et al. A new fusion mediating MAPK pathway activation in pilocytic astrocytoma. *PLoS One*. 2017. doi:10.1371/journal.pone.0175638
39. Childress MA, Himmelberg SM, Chen H, Deng W, Davies MA, Lovly CM. ALK Fusion Partners Impact Response to ALK Inhibition: Differential Effects on Sensitivity, Cellular Phenotypes, and Biochemical Properties. *Mol Cancer Res*. 2018. doi:10.1158/1541-7786.mcr-18-0171
40. Turner JA, Bemis JGT, Bagby SM, et al. BRAF fusions identified in melanomas have variable treatment responses and phenotypes. *Oncogene*. 2019. doi:10.1038/s41388-018-0514-7
41. Lavoie H, Therrien M. Regulation of RAF protein kinases in ERK signalling. *Nat Rev Mol Cell Biol*. 2015;16(5):281-298. doi:10.1038/nrm3979
42. Harding A, Tian T, Westbury E, Frische E, Hancock JF. Subcellular localization determines MAP kinase signal output. *Curr Biol*. 2005;15(9):869-873. doi:10.1016/j.cub.2005.04.020
43. van Beest M, Robben JH, Savelkoul PJM, et al. Polarisation, key to good localisation. *Biochim Biophys Acta - Biomembr*. 2006;1758(8):1126-1133. doi:10.1016/j.bbamem.2006.03.007
44. Van Cutsem E, Cervantes A, Adam R, et al. ESMO consensus guidelines for the management of patients with metastatic colorectal cancer. *Ann Oncol*. 2016;27(8):1386-1422. doi:10.1093/annonc/mdw235
45. Sepulveda AR, Hamilton SR, Allegra CJ, et al. Molecular biomarkers for the evaluation of colorectal cancer: Guideline from the American society for clinical pathology, college of American pathologists, association for molecular pathology, and American society of clinical oncology. *Arch Pathol Lab Med*. 2017. doi:10.5858/arpa.2016-0554-CP
46. van Brummelen EMJ, de Boer A, Beijnen JH, Schellens JHM. BRAF Mutations as Predictive Biomarker for Response to Anti-EGFR Monoclonal Antibodies . *Oncologist*. 2017;22(7):864-872. doi:10.1634/theoncologist.2017-0031
47. Zhao B, Wang L, Qiu H, et al. Mechanisms of resistance to anti-EGFR therapy in colorectal cancer. 2017;8(3):3980-4000. www.impactjournals.com/oncotarget.
48. Meerbrey KL, Hu G, Kessler JD, et al. The pINDUCER lentiviral toolkit for inducible RNA interference in vitro and in vivo. *Proc Natl Acad Sci*. 2011. doi:10.1073/pnas.1019736108
49. Drost J, van Jaarsveld RH, Ponsioen B, et al. Sequential cancer mutations in cultured human intestinal stem cells. *Nature*. 2015;521(7550):43-47. doi:10.1038/nature14415
50. Borten MA, Bajikar SS, Sasaki N, Clevers H, Janes KA. Automated brightfield morphometry of 3D organoid populations by OrganoSeg. *Sci Rep*. 2018;8(1):5319. doi:10.1038/s41598-017-18815-8
51. Love MI, Huber W, Anders S. Moderated estimation of fold change and dispersion for RNA-seq data with DESeq2. *Genome Biol*. 2014. doi:10.1186/s13059-014-0550-8
52. Cox J, Mann M. MaxQuant enables high peptide identification rates, individualized p.p.b.-range mass accuracies and proteome-wide protein quantification. *Nat Biotechnol*. 2008. doi:10.1038/nbt.1511

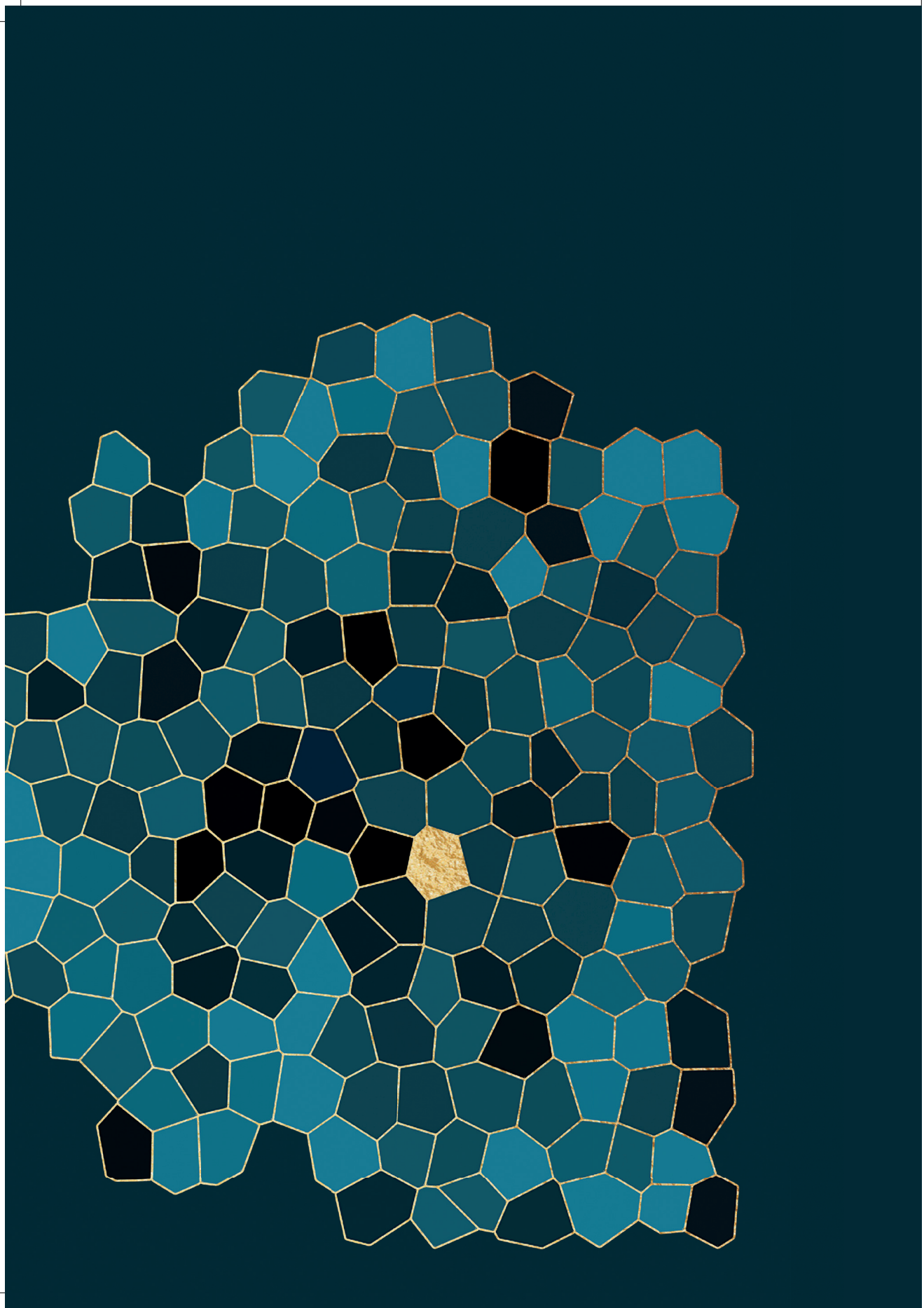

CHAPTER 5

CANCER MODELING IN COLORECTAL ORGANOIDS REVEALS INTRINSIC DIFFERENCES BETWEEN ONCOGENIC *RAS* AND *BRAF* VARIANTS ON TUMOR PROGRESSION AND THERAPY RESISTANCE

Jasmin B. Post, Nizar Hami, Jeroen Lohuis, Marieke van de Ven, Renske de Korte-Grimmerink, Christina S. Stangl, Ellen Stelloo, Ingrid Verlaan, Jacco van Rheenen and Hugo J.G. Snippert

To be submitted

ABSTRACT

Colorectal cancers (CRCs) with oncogenic mutations in *KRAS*, *NRAS* and *BRAF* are associated with resistance to anti-EGFR targeted therapy. Consequently, all RAS mutant CRC patients are being excluded from this therapy. Yet, intertumoral heterogeneity in drug response has been reported for CRCs with various RAS mutations. However, it is poorly understood to what extent such differences are derived from different genetic backgrounds in tumors, or intrinsic differences between the various oncogenic mutations within the EGFR-RAS pathway. Therefore, using CRISPR technology we generated an isogenic panel of patient-derived CRC organoids (APC, TP53 mutant) with frequent RAS pathway mutations, i.e. $KRAS^{G12D}$, $KRAS^{G13D}$, $NRAS^{G12D}$ and $BRAF^{V600E}$. Moreover, true heterozygosity of the mutations was ensured to prevent malignant transformation by allelic imbalance. As expected, we found that all RAS pathway mutants promoted ERK activation and tumor growth. However, we noticed different potentials. $KRAS^{G12D}$ and $BRAF^{V600E}$ mutations, but not $KRAS^{G13D}$ and $NRAS^{G12D}$, conferred robust resistance to anti-EGFR therapy and showed sustained RAS-MEK-ERK signaling activity. Moreover, different clones with independent acquisition of the same mutation revealed that the oncogene-driven phenotypes were independent of karyotype evolution. However, different patient-derived and engineered CRC organoids with identical oncogenic RAS and BRAF variants showed differences in drug response, indicating that intertumoral heterogeneity is fueled by mutation-specific effects as well as mutational background. To optimize personalized cancer treatment of CRC patients, our data suggest that the exact point mutation in the EGFR signaling pathway should be taken into account. Accurate genotype-phenotype correlations will facilitate future decision-making of therapeutic strategy, followed by tailored-made adjustments based on personalized drug response data.

KEYWORDS

BRAF and RAS oncogenes, Anti-EGFR therapy resistance, Colorectal Cancer, Organoids, Intertumoral heterogeneity, Personalized medicine

INTRODUCTION

The EGFR-RAS signaling pathway stimulates cellular proliferation during development, homeostasis and regeneration[1,2]. Consequently, aberrant activation of the signaling cascade by oncogenic mutations is frequently detected in cancers[3]. In metastatic colorectal cancer (mCRC), most abundant are mutations in RAS proteins or downstream kinase BRAF and to lesser extent at the receptor level[4,5]. KRAS, NRAS and HRAS are three RAS isoforms that propagate upstream EGFR signaling activity towards downstream RAF kinases[6]. Despite their ubiquitous expression pattern[7,8] and high similarity in amino acid sequence (80%)[9–11], the prevalence of oncogenic mutations across RAS isoforms are not equally distributed between different cancers[12]. Colorectal cancer is one of the most extreme cases, with mutations in *KRAS* being detected in 35-50% of the cases[13], including even distribution across all tumorigenic stages[14]. In contrast, mutations in *NRAS* are only identified in 3-5% of mCRC patients and predominantly in malignant CRCs[13–15], while HRAS mutations are virtual absent[12]. Moreover, the relative mutation frequency at hotspot locations differs between RAS isoforms, with G12 and G13 mutations most often detected in KRAS (combined 90%) and Q61 mutations frequently found in NRAS (57%)[16].

These observations suggest that oncogenic variants of *RAS* isoforms are not equal during CRC development, including codon-specific influences. Indeed, mouse studies have demonstrated that the endogenous expression of $KRAS^{G12D}$, but not $NRAS^{G12D}$, promotes progression of intestinal neoplasia[17]. An increasing amount of observations seem at odds with the almost uniform classification of CRC tumors with a mutant EGFR signaling pathway. Accurate patient stratification based on RAS mutations is clinically relevant given that anti-EGFR targeted therapy has shown beneficial effects in mCRC patients without oncogenic RAS mutations[18,19]. However, just like oncogenic RAS variants being associated with different tumor phenotypes, various clinical studies demonstrated differences in therapeutic outcome for mCRC patients with different oncogenic RAS variants. For instance, they reported that mCRCs with *KRAS* codon 13 mutations are more often associated with a poorer prognosis compared to those with *KRAS* codon 12 mutations[20–22]. Paradoxically, patients with *KRAS* codon 13 mutations are reported to benefit from treatment with EGFR inhibitors[20–22], in contrast to resistant *KRAS* codon 12 mutant tumors.

Unfortunately, the cause and consequences of potential differences between these oncogenic variants are poorly understood. In particular, intrinsic differences in tumorigenic potential between mutant variants is challenging to dissect, considering the immense different mutational backgrounds per human tumor[5]. Moreover, *NRAS* mutations are more often detected in tumors of the left colon, whereas *KRAS* mutant tumors are most frequently found in right colon[14,23], creating the possibility that these are two different tumor subtypes of different epigenetic make-up and cellular composition. The situation is even more extreme for oncogenic mutations in *BRAF* (mostly V600E) that are detected in approximately 11% of CRC cases[4]. In contrast to RAS mutations, BRAF mutations are common in tumors with a hypermutation phenotype (microsatellite instable)[24], show co-occurrence with WNT pathway mutations in *RNF43* rather than in *APC*[4,5] and show different metastatic behavior[16,23].

To optimize personalized cancer treatment of CRC patients, we set out to improve our

understanding of genotype-phenotype correlations and investigate the intrinsic similarities and differences between a series of common mutations in the EGFR signaling pathway. Patient-derived CRC organoids (CRC PDOs) are 3-dimensional 'mini-organs' that are established from primary tumor tissue, either obtained from biopsies or surgical resected material. CRC PDOs maintain the histopathological features of the native tumor, including high concordance between somatic mutations, transcriptome and drug response between matched primary tumors and derived organoid cultures[25–27]. Importantly, PDOs are compatible with CRISPR/Cas9-mediated introduction of cancer mutations[28,29], and were used to generate a series of isogenic lines with various oncogenic RAS pathway mutations to reveal their similarities and differences.

RESULTS

CRC PDOs with different MAPK pathway mutations display varying sensitivities to MAPK pathway inhibition

To document the intertumoral heterogeneity in drug response between CRCs with an oncogenic mutant MAPK signaling pathway, we performed a drug screen targeting various effectors in the MAPK pathway (**Figures 1A and B**). Specifically, we applied this screen on a panel of CRC PDOs that are either wild-type or mutant for *KRAS*, *NRAS* or *BRAF* without displaying any other MAPK pathway mutations detected by Sanger sequencing (**Supplementary Figure 1A**).

In line with observations from the clinic, we observed that CRC PDOs with activating mutations in *RAS* and *BRAF* exhibited resistance to the pan-HER inhibitor afatinib[18,30,31]. The strongest sensitivity to EGFR inhibition was observed in two out of the four *RAS*/*BRAF*^{WT} CRC PDOs (P18T and B2-071) (**Figure 1C and Supplementary Figure 1B**). We noticed limited response to EGFR inhibition in the two remaining *RAS*/*BRAF*^{WT} CRC PDOs (B2-054 and B2-074). Potentially, these CRCs have MAPK pathway alterations that are either unknown, or were not identified by Sanger sequencing [29,32–34], but are in agreement with clinical observation of CRC patients enrolled in anti-EGFR therapy that show no response[35].

In concordance with previous clinical and experimental observations, MAPK pathway inhibition downstream of RAS and BRAF with only the MEK inhibitor selumetinib was largely ineffective in the panel CRC PDOs[36–38] (**Figure 1D and Supplementary Figure 1B**). However, upon combinatorial treatment with both EGFR and MEK inhibitors, an improved

Figure 1. Differential drug sensitivities of *RAS* and *BRAF* mutant CRC PDOs to targeted MAPK pathway inhibition.

(**A**) Schematic overview of the drug screening method. In short, a 3-day drug screen was initiated on 5 days old CRC PDOs expressing different *RAS* and *BRAF* mutations. (**B**) Representative bright field pictures of CRC PDOs (P18T) treated with increasing drug concentrations. (**C - I**) Heat maps of dose-response measurements (cell viability) in CRC PDO lines to (**C**) afatinib, (**D**) selumetinib, (**E**) afatinib plus selumetinib, (**F**) SCH772984, (**G**) SCH772984 plus selumetinib, (**H**) vemurafenib and (**I**) vemurafenib plus afatinib. Organoids were treated (72 hr) with vehicle (DMSO) or inhibitors targeting the EGFR-RAS-ERK pathway (5 nM – 30 μM range, in 14 logarithmic intervals). Red represents maximal cell death and green represents maximal viability. Drug names and their nominal targets are indicated above, the MAPK pathway mutant status per line at the left and the corresponding PDO line at the right. Average of 2 technical replicates.

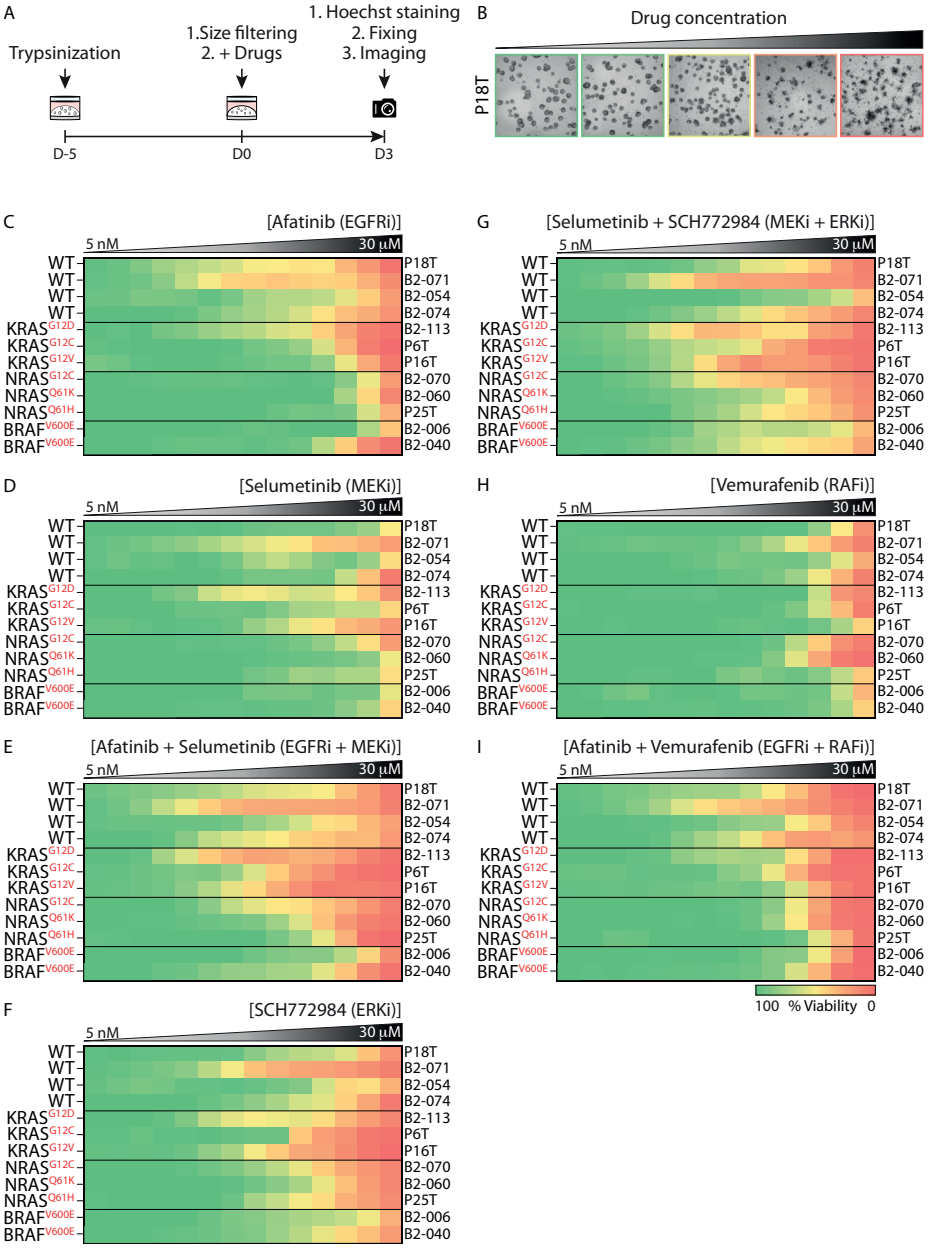

drug response was predominantly detected in *K*- and *NRAS* mutant PDOs (**Figure 1E and Supplementary Figure 1B**).

Treatment with the ERK inhibitor SCH772984 showed the strongest effect on *KRAS* mutant and *RAS*/*BRAF*^{WT} CRC organoids, albeit at varying sensitivities (**Figure 1F and Supplementary Figure 1B**). Combinatorial treatment with ERK and MEK inhibitors induced an additive effect in most CRC organoids, irrespective of the mutational background, while variability in response between CRC PDOs remained largely unaffected (**Figure 1G and Supplementary Figure 1B**).

BRAF inhibition with vemurafenib, largely ineffective in most CRC PDOs including organoids mutant for *BRAF*, corresponds with previous observations in CRC cell lines and clinical studies[39–42] (**Figure 1H and Supplementary Figure 1B**). Strikingly, also a minor additive response was observed when EGFR and BRAF inhibitors were co-administered in CRC PDOs (**Figure 1I and Supplementary Figure 1B**), recapitulating observations from the clinic about insufficient response rates in *BRAF* mutant patients[43].

Remarkedly, differential drug sensitivities were observed between CRC PDOs with similarly affected oncogenes. In particular the *NRAS*^{G12C} mutant showed higher sensitivity to most drugs than the other *NRAS* mutants, either due to the type of point mutation or other tumor intrinsic properties. Similar type of deviation in drug response was observed between KRAS mutants, confirming previous reports on CRC organoid biobanks with various RAS mutants[26,44–46]. Overall, *BRAF* mutant CRC PDOs showed a very resistant phenotype to MAPK pathway inhibition. However, the nature of their primary tumors (e.g. sessile serrated adenomas) instead of their mutational status, could very well be responsible for the observed phenotype.

Generation of endogenous oncogenic RAS and BRAF knock-in variants in CRC PDOs

To exclude the impact of genetic background, epigenetics and cellular composition on drug response when comparing various oncogenic mutations in the MAPK pathway, we set out to generate a panel of isogenic CRC PDOs harboring different RAS pathway mutations (RPMs). Apart from a non-functional APC and TP53 pathway, CRC PDO P18T has a genetically wild-type MAPK signaling pathway and shows sensitivity towards EGF-mediated tumor growth[25].

Figure 2. Generation of oncogenic *BRAF* and *RAS* knock-in variants in CRC PDOs.
(**A**) Genetic strategy to target *KRAS*, *NRAS* and *BRAF* locus for homologous directed repair using CRISPR/Cas9 technology. Red and blue lines indicate oncogenic missense and silent mutations, respectively. Black boxes illustrate exons, separated by introns. Red scissor shows sgRNA-generated double stranded break. Black arrows illustrate PCR primer pairs that were used for the identification of knock-in clones. (**B**) Puromycin selection strategy to generate *RAS* and *BRAF* mutant CRC PDOs after CRISPR-mediated homologous recombination. (**C**) Per mutation the agarose electrophoresis gels showing the ~1kb PCR product of the knock-in allele in 3 monoclonal lines per mutations. Sanger sequencing confirms presence of both knock-in and WT alleles. DNA sequences show introduction of missense (red) and silent (blue) mutations. The mRNA expression levels of wild-type and mutant alleles was analyzed using qPCR. The relative expression of each allele was normalized to the *B2M* housekeeping gene (representative from n = 3 independent experiments). (**D**) Western blot analysis shows enhanced RAS activity (GTP-loading) in *RAS* mutant CRC PDOs compared to P18T organoids. KRAS and NRAS immunoblots from RAS pull-down assays (RAS-GTP) and total lysates (loading control) are shown for *KRAS* and *NRAS* mutant organoids, respectively. Representative from n=2 independent experiments.

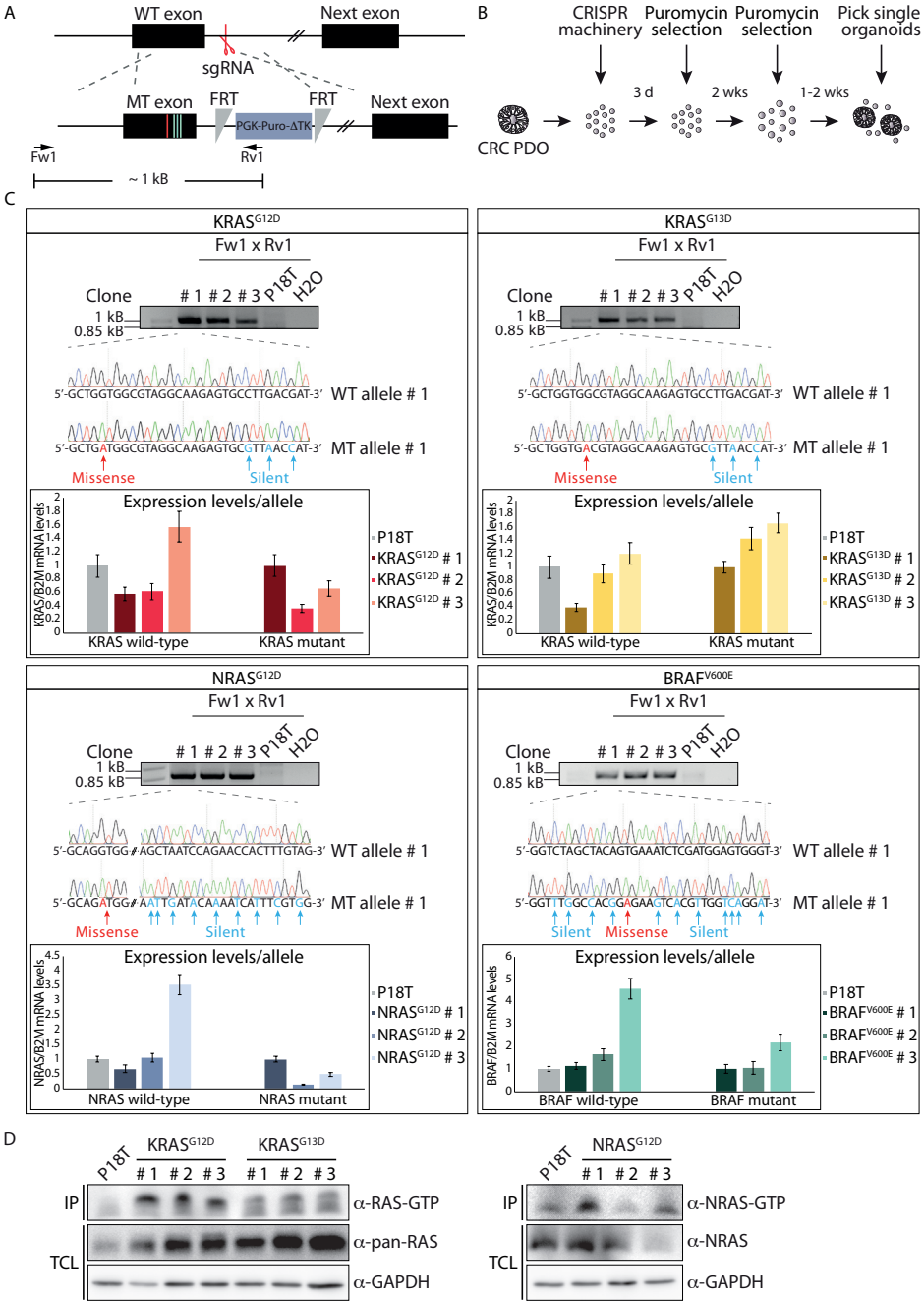

Therefore, we isolated CRC PDO P18T to introduce different oncogenic mutations in *KRAS*, *NRAS* and *BRAF* via homologous recombination (HR) using the CRISPR technology (**Figure 2A**). Importantly, the donor template contained a puromycin selection cassette to enable selection independent of using the attributed mutant phenotype for selection like previously applied growth factor depletion regimens (e.g. EGF) (**Figures 2A and 2B**)[47,48]. Next, we targeted CRISPR/Cas9 to the intronic region directly downstream of the exon of interest. Although this position is not optimal in relation to the distant upstream location of the point mutations, introducing a small intronic indel mutation in the non-recombined allele will have minimal to no impact on its integrity. Maintaining the expression of the wild-type allele is essential as it avoids allelic imbalance, a phenomenon that has been described during progression to malignancy where mutant KRAS gains the upper hand over wild-type[49–52] (**Figure 2A**).
The generation of oncogenic mutations in *KRAS, NRAS* and *BRAF* were confirmed by DNA sequencing analysis of three independent monoclonal lines (**Figure 2C**), confirming the presence of both mutant and wild-type alleles. Additional DNA sequence analyses of the intronic regions targeted by Cas9 confirmed the generation of indels in the allele that was not subjected to HR (**Supplementary Figures 2A and 2B**). In agreement, both wild-type and mutant alleles were shown to be expressed at near equal ratios in the isogenic RPM lines as demonstrated by qPCR analysis using allele-specific primers (**Figure 2C**). Subsequent RAS-GTP pull down assays with the RAS binding domain (RBD) of RAF confirmed presence of oncogenic RAS proteins, including overall correlation between increased active RAS-GTP loading levels and mRNA expression of the mutant allele (**Figure 2D**). Moreover, we observed increased protein levels of total RAS in *RAS* mutant organoids, indicative of positive feedback regulation induced by oncogenic *RAS* proteins as previously reported[53–55].

$BRAF^{V600E}$ and $KRAS^{G12D}$ knock-in CRC PDOs show resistance to pan-HER inhibition

To maintain clonal diversity, we continued with three independent clones per oncogenic mutation and investigated their effect on EGF-dependent tumor growth.
Therefore, we monitored organoid number, size, and viability at different time points after organoid plating and drug administration (**Supplementary Figure 3A**). Under normal growth conditions, we observed no significant differences between parental P18T and oncogenic RPM lines (**Figure 3A**). However, significant differences were observed when we challenged

Figure 3. $KRAS^{G12D}$ and $BRAF^{V600E}$ knock-in mutations promote organoid survival and growth.
(**A**) Quantitative analysis of organoid size and number in isogenic RPM lines during normal culture conditions (DMSO) at different time points after organoid plating. Size and number of viable organoids were measured by uptake of fluorescent calcein green (see methods). Each dot represents one organoid[76]. Data from 1 8-well Lab-Tek chambered coverglass is shown. (**B**) Representative fluorescent pictures of parental P18T, or $KRAS^{G12D}$, $KRAS^{G13D}$, $NRAS^{G12D}$ and $BRAF^{V600E}$ knock-in organoids (clones # 1) after 7 days of DMSO or afatinib treatment (1 μM). Scale bars, 100 μM. Hoechst (blue) and DRAQ7 (red) was used to visualize nuclei and dead cells, respectively. (**C**) Representative bright field pictures of parental P18T, or $KRAS^{G12D}$, $KRAS^{G13D}$, $NRAS^{G12D}$ and $BRAF^{V600E}$ knock-in organoids (clones # 1) 7 days after release of afatinib treatment (day 14). Representative zoom-in panels show fluorescent calcein green signal in living cells. Asterisks indicate autofluorescence of dead material (**Suppl. Fig 3C**). (**D**) Quantitative analysis of organoid growth and viability in isogenic RPM lines prior (day 0), during (day 7) and after (day 14) treatment with afatinib (1 μM). Size and number of viable organoids were measured by uptake of fluorescent calcein green (see methods). Each dot represents one organoid[76]. Data from 1 8-well Lab-Tek chambered coverglass is shown.

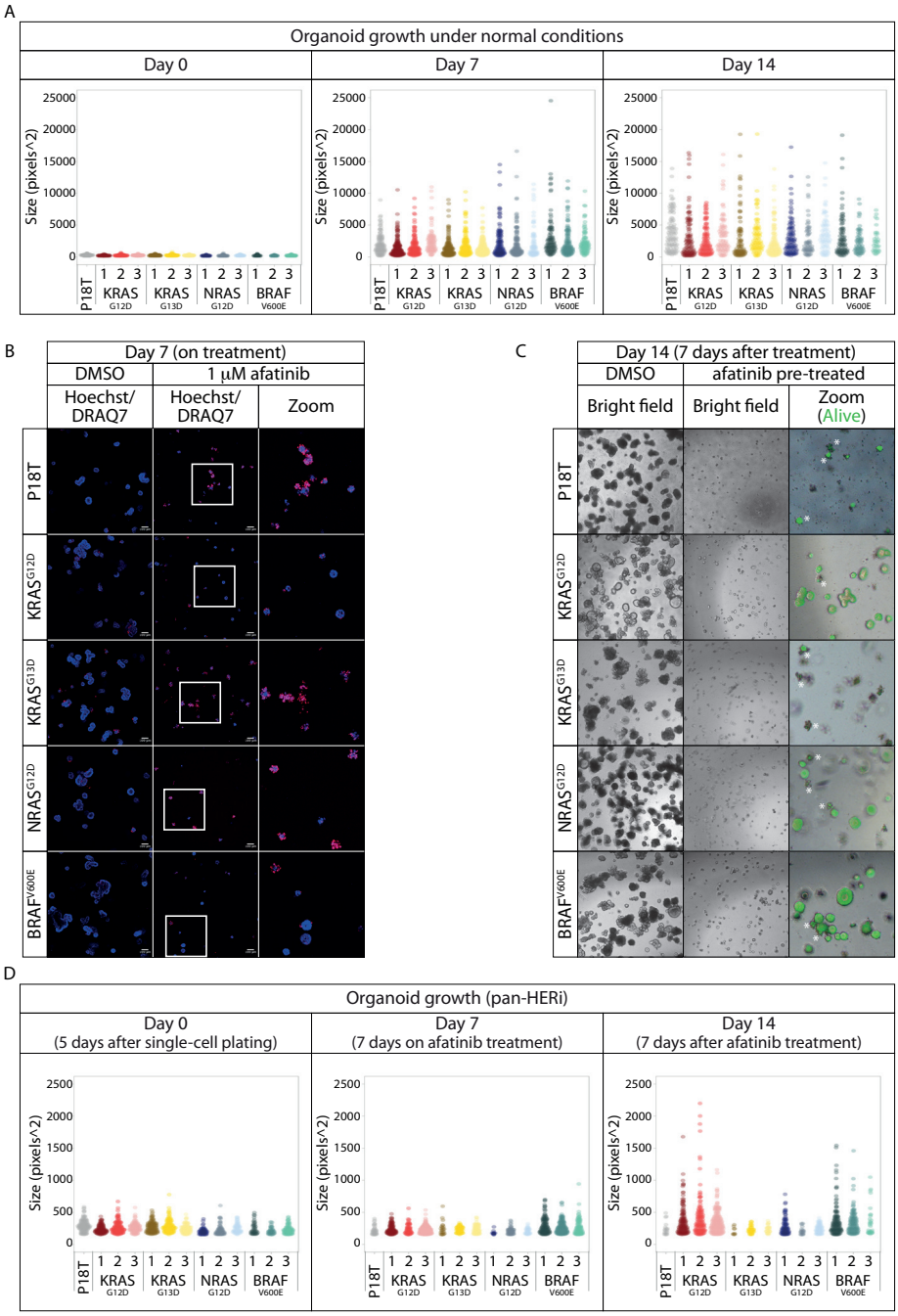

the RPM organoids with the pan-HER inhibitor afatinib to block all EGF-stimulated receptor signaling. Whereas all oncogenic RPM organoids had a survival benefit compared to parental P18T organoids upon short-term (3 days) afatinib treatment, organoids expressing *KRAS*^{G12D} and *BRAF*^{V600E} oncogenes showed most resistance to afatinib that became most prevalent during long-term (7 days) treatment (**Figure 3B and Supplementary Figure 3B**). In particular, relapse after drug treatment showed a striking growth of both *KRAS*^{G12D} and *BRAF*^{V600E} mutant organoids, while the others were significantly depleted in number or showed growth arrest (**Figures 3C-D and Supplementary Figure 3C**). While overall phenotypes per mutation showed resemblance, we did observe interclonal heterogeneity, in particular for NRAS. Presumably epigenetic and/or transcriptional differences between the cells-of-origin of the mutant clones can still affect phenotype[26,45]. For example, the most resistant NRAS^{G12D} clone (#1) correlates with highest expression level and GTP-loading of the mutant protein.
Remarkedly, regardless of oncogenic RAS pathway mutations, we observed that growth remains dependent on additional HER-mediated signaling input (**Figures 3B and D**). Although the HER receptor family is upregulated in the RPM organoids (**Supplementary Figure 3D**), we noticed that EGFR signaling was mostly responsible for this (**Supplementary Figure 3E**).

BRAF^{V600E} *and KRAS*^{G12D} *knock-in CRC PDOs show residual MAPK pathway activation upon pan-HER inhibition*

Previous studies have indicated that the lack of sensitivity towards MAPK pathway inhibition in *RAS* and *BRAF* mutant CRCs is caused by residual levels of ERK activity[41,56,57]. To investigate the molecular mechanism underlying resistance to pan-HER inhibition as observed in *KRAS*^{G12D} and *BRAF*^{V600E} RPM organoids, we analyzed MAPK signaling activity using biochemistry. As expected, introduction of the oncogenic mutations in RPM organoids resulted in increased ERK activation under normal culture conditions (**Figure 4A and Supplementary Figure 4A**). In line with the sensitive phenotypes during pan-HER inhibition, we noticed complete loss of MEK and ERK activity in P18T organoids as well as in *KRAS*^{G13D} and *NRAS*^{G12D} RPM organoids. In contrast, residual MEK and ERK activity was observed in RPM organoids expressing *KRAS*^{G12D} and *BRAF*^{V600E}, albeit with different kinetics (**Figure 4A and Supplementary Figure 4A**).

Figure 4. *KRAS*^{G12D} and *BRAF*^{V600E} RPM lines show residual MAPK pathway activity in the presence of pan-HER inhibition.
(**A**) Organoids expressing oncogenic *KRAS* (G12D and G13D), *NRAS* (G12D) and *BRAF* (V600E) variants show enhanced basal ERK phosphorylation levels compared to P18T organoids. Pan-HER inhibition (1 μM afatinib) shows sustained ERK and MEK phosphorylation in *KRAS*^{G12D} and *BRAF*^{V600E} organoids compared to P18T, *KRAS*^{G13D} and *NRAS*^{G12D} organoids. Top panels are representative biochemistry experiments on clones # 1 from n=3. Bottom scatter plot depicts ERK phosphorylation levels normalized to GAPDH for all clones ($n \geq 4$). Baseline of P18T (DMSO) is set at 1. (**B**) Top panels depict biochemistry on RAS activity (GTP-loading) in unperturbed culture conditions and pan-HER inhibition (1 μM afatinib) for *KRAS* (G12D and G13D) and *NRAS* (G12D) mutant clones # 1 and 2 compared to P18T CRC organoids. RAS immunoblots from RAS pull-down assay are shown (RAS-GTP), together with a RAS immunoblot from total cell lysates as loading control. HRAS, KRAS, and NRAS isoforms are detected in mutant KRAS pull-down assays. NRAS isoforms are detected in mutant NRAS pull-down assays. Representative from n = 3 independent experiments. Scatter plots below depict RAS-GTP levels normalized to GAPDH for all clones ($n \geq 3$). Baseline of P18T (DMSO) is set at 1.

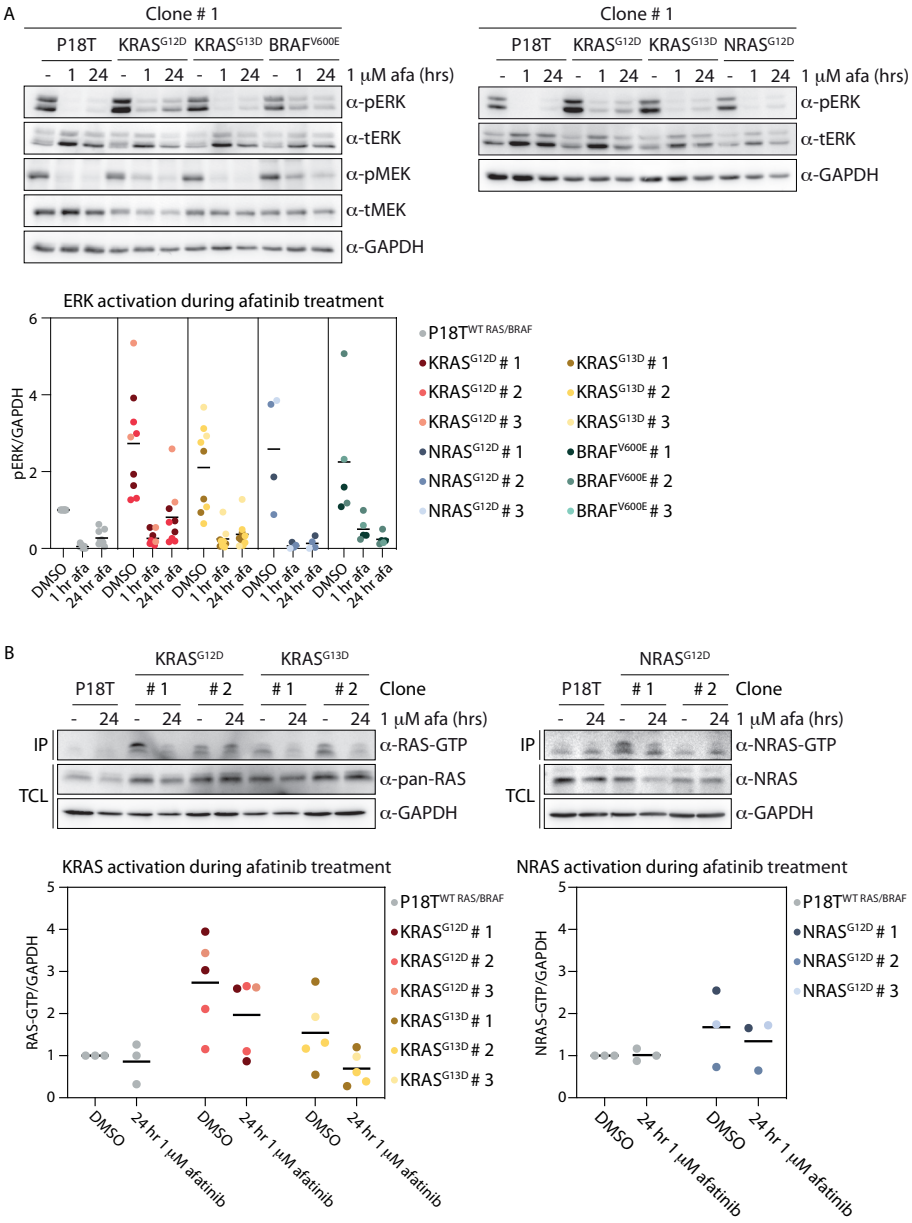

Initially, all organoids with oncogenic *RAS* variants displayed a fast and full inhibition of ERK phosphorylation upon pan-HER inhibition. Subsequently, over the course of 24 hours most reactivation of ERK was observed in the presence of mutant $KRAS^{G12D}$. Unlike oncogenic RAS variants, the drug response of $BRAF^{V600E}$ mutant organoids towards pan-HER inhibition displayed slower kinetics of downstream pathway inhibition (**Figure 4A and Supplementary Figure 4A**). Moreover, even after 72 hours we noticed no strong reactivation of ERK as consistently observed in $KRAS^{G12D}$ organoids, but minimal levels that remained stable over time (**Supplementary Figure 4B**).

The level of active RAS-GTP was elevated in almost all *RAS* mutant RPM organoids in unperturbed culture conditions (**Figure 4B and Supplementary Figures 4C-D**) with the exception of $NRAS^{G12D}$ # 2, which is consistent with the limited expression levels of the mutant allele. Subsequently, an overall decrease in RAS-GTP loading was observed for all mutant lines in the absence of upstream EGFR signaling input, although the degree of reduction varied per mutation (least in $KRAS^{G12D}$, most in $KRAS^{G13D}$) and per clone.

Interclonal variability on karyotype and transcriptome

All RPM clones were created from the same polyclonal P18T organoid culture. As a result, clonal RPM lines can originate from different subclones present in the parental culture and might underly interclonal variability. To interrogate the clonal origin of the RPM lines, we determined DNA copy number alterations (CNAs) of the RPM organoids to determine clonal-specific karyotypes. Overall, a high degree of similarity in the pattern of CNAs was observed across all isogenic RPM organoid lines and the parental P18T organoids (**Figure 5A**). Moreover, amplification of the *BRAF* allele as indicated in the CNA plots, corresponds with the detection of two wild-type alleles with independent Cas9-created indels in $BRAF^{V600E}$ # 1 (**Supplementary Figure 2B**). Notably, RPM clones with the highest passage numbers (clone #1) showed most clone specific deviations from the average karyotype, indicative of ongoing clonal evolution as previously reported[26]. Moreover, across the different mutants, certain clones displayed a higher degree of CNA resemblance than to others. In particular, a gain of chromosome 2 in half of the clones and (sub)chromosomal loss of chromosome 4 in most but not all. The observed deviations in karyotypes confirms that the lines originated from different clonal populations that were present in the bulk P18T culture. In particular, $NRAS^{G12D}$ # 1 that is the most phenotypic outlier of the $NRAS^{G12D}$ mutants also displays

Figure 5. Karyotype and gene expression profiles of RPM lines.
(**A**) DNA copy number alterations of monoclonal RPM lines (clones # 1-3) and parental (P) P18T organoids. Centromeric regions (thin black line in chromosomes) are excluded due to repetitive nature of DNA sequence. Dashed lines indicate the genetic location of *BRAF*, *KRAS* and *NRAS loci*. Colors per (sub)chromosome indicate CNA according to legend. (**B**) Principle Component Analysis of gene expression levels for monoclonal RPM lines and parental P18T organoids (bulk and monoclonal lines # 1-3) during unperturbed growth conditions (DMSO) and pan-HER inhibition (1 μM afatinib for 24 hr). Left panel indicates treatment. Right panel indicates clone identities. Hue at background corresponds to treatment. (**C**) Heatmap of significantly downregulated genes ($p_{adjusted}$ <0.05; $\log_2$ fold change (FC) ≤-2) after afatinib treatment in all RPM lines and parental P18T organoids gives uniform EGFR target genes (**D**) As in (C), but EGFR signature genes as determined in P18T organoids that sustain expression levels in all RPM lines. (**E**) As in (D), but EGFR signature genes as determined in P18T organoids with only sustained expression levels in resistant $KRAS^{G12D}$ and $BRAF^{V600E}$ clones. RAS-ERK pathway related genes are depicted in bold. Cell cycle-related genes are marked in bold, red font.

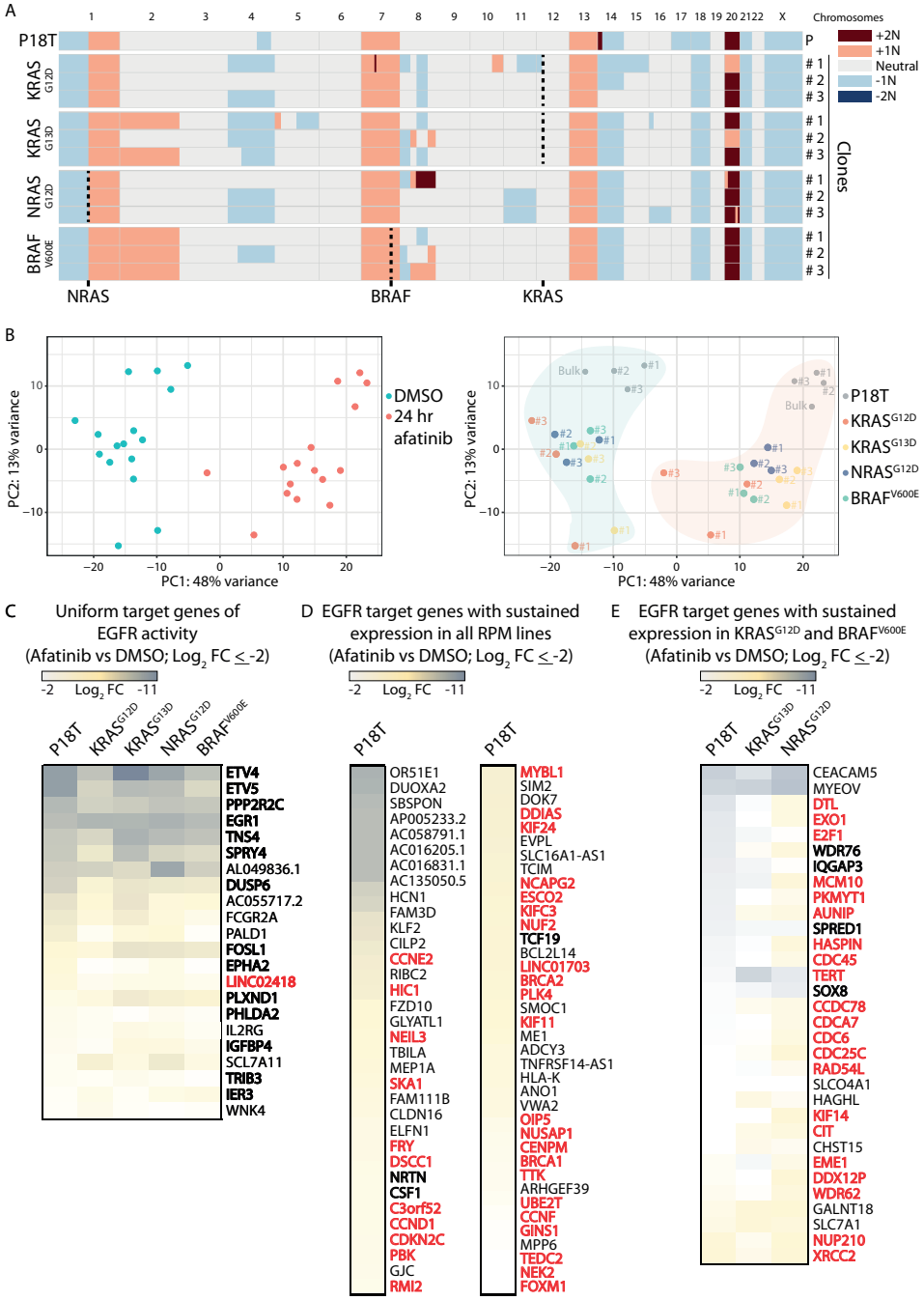

most genomic alterations, potentially supporting the concept that clonal origin may underly interclonal variability. Nevertheless, overall phenotypic response towards EGF-independent growth conditions seems primarily dictated by the specific RAS pathway mutation and independent of clonal deviations.

Next, we performed RNA sequencing analysis to investigate the degree of clonal variability on the transcriptional level, both during normal growth conditions as well as during pan-HER targeted therapy. To measure the variance in global gene expression between all RPM lines, we performed Principle Component Analysis (PCA, Methods). Based on the first two principle components, the largest differences in gene expression were observed between DMSO and afatinib treated conditions and between wild-type and mutant RAS pathway organoids (**Figure 5B**). Moreover, during normal growth conditions we noticed somewhat random clustering between all RPM clones, but a tendency to cluster per mutation/phenotype during EGF-deprived signaling with $KRAS^{G12D}$ and $BRAF^{V600E}$ clustering towards the center of the PC1 axis.

Subsequently, we determined the transcriptional signature mediated by EGFR signaling in CRC organoids in relation to RAS/RAF oncogene-mediated transcriptional activity. Using the parental P18T organoids, we determined 266 target genes which expression is downstream of EGFR signaling activity in CRC organoids with a wild-type MAPK pathway (**Supplementary Figure 5A and Supplementary Table 1**). Intriguingly, this EGFR gene signature with many known targets of the MAPK pathway remains to a large extent dependent on upstream EGFR signaling activity in the RPM mutants (**Figure 5C, Supplementary Figure 5A and Supplementary Table 1**), in agreement with the significant reduction in ERK activity upon afatinib treatment. Target genes of the EGFR signature that are least affected in the RPM mutants relate to cell cycle pathways, which is most dramatic for $KRAS^{G12D}$ and $BRAF^{V600E}$ RPM lines and in line with the observed phenotypes (**Figure 5D-E, Supplementary Figure 5B and Supplementary Tables 1-3**). Moreover, when directly comparing differential gene expression between afatinib-resistant (i.e. $KRAS^{G12D}$ and $BRAF^{V600E}$) and -sensitive clones (i.e. $KRAS^{G13D}$ and $NRAS^{G12D}$) independently analyzed from the EGFR gene signature, we again observed lower expression of cell cycle-related genes in sensitive organoids during treatment (**Supplementary Figures 5B-C**).

Intertumoral heterogeneity between MAPK oncogenic mutations during drug responses

To improve the characterization of drug response phenotypes in relation to KRAS, NRAS and BRAF oncogenes, we performed a drug screen on the RPM organoids with various targeted inhibitors against the MAPK pathway (**Figure 6A**).

Confirming previous observations, $KRAS^{G12D}$ and $BRAF^{V600E}$ RPM organoids showed resistance to pan-HER inhibition with afatinib, with $NRAS^{G12D}$ mutants being an intermediate and $KRAS^{G13D}$ phenocopying the parental P18T line (**Figure 6B and Supplementary Figure 6A**).

While MEK inhibition alone showed limited effect, intertumoral variability was as expected (**Figure 6C and Supplementary Figure 6A**). Moreover, combined inhibition of MEK and EGFR showed high sensitivity for P18T, $KRAS^{G13D}$ and $NRAS^{G12D}$ mutant organoids, with a pronounced additive effect on $NRAS^{G12D}$ organoids (**Figure 6D and Supplementary Figure 6A**). Monotherapy against ERK with SCH772984 showed a similar pattern as MEK inhibition,

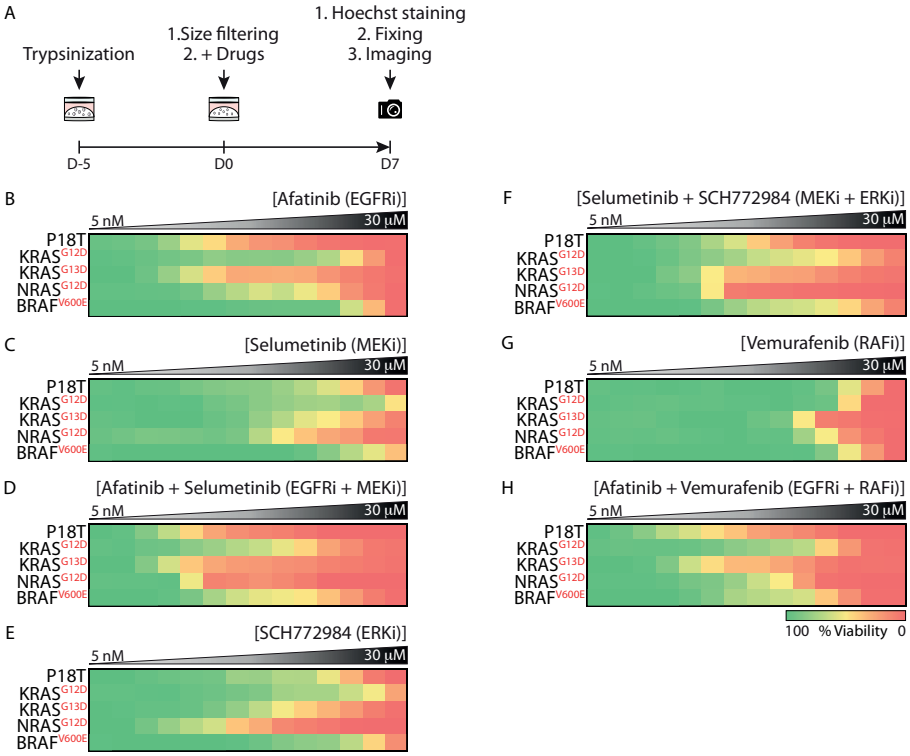

Figure 6. Differential drug sensitivities of oncogenic *RAS* and *BRAF* knock-in CRC PDOs to targeted MAPK pathway inhibition.
(**A**) Schematic overview of the drug screening method. In short, a 7-day drug screen was initiated on 5 days old P18T and RPM organoids expressing different *RAS* and *BRAF* mutations. (**B** - **H**) Heat maps of dose-response measurements (cell viability) in CRC PDO lines to (**B**) afatinib, (**C**) selumetinib, (**D**) afatinib plus selumetinib, (**E**) SCH772984, (**F**) SCH772984 plus selumetinib, (**G**) vemurafenib and (**H**) vemurafenib plus afatinib. Organoids were treated (7 days) with vehicle (DMSO) or inhibitors targeting the EGFR-RAS-ERK pathway (5 nM – 30 µM range, in 14 logarithmic intervals). Red represents maximal cell death and green represents maximal viability. Drug names and their nominal targets are indicated above and the MAPK pathway mutant status per line at the left. Average of 2 technical replicates.

albeit with overall lower IC50s (**Figure 6E and Supplementary Figure 6A**), while intertumoral variability in drug response upon combining MEK and ERK inhibitors resembled pathway inhibition via pan-HER and MEK inhibition (**Figure 6F and Supplementary Figure 6A**). General insensitivity towards BRAF inhibition with vemurafenib was observed in all RPM organoids, including $BRAF^{V600E}$ (**Figure 6G and Supplementary Figure 6A**), with minimal additive effects upon its combination with dominant pan-HER inhibition (**Figure 6H and Supplementary Figure 6A**). Together, the data confirm earlier observations that $KRAS^{G12D}$ and $BRAF^{V600E}$ impose a more resistant phenotype towards EGF-independent growth conditions than $KRAS^{G13D}$ and $NRAS^{G12D}$. In addition, unique targetable vulnerabilities per mutation type were not identified within the MAPK pathway.

Next, we decided to focus on multiple patient-derived $BRAF^{V600E}$ mutants (CRC PDOs and $BRAF^{V600E}$ RPMs) in order to keep the oncogenic mutation a constant, while varying between separate tumors. The 3-day drug response phenotypes of *$BRAF^{V600E}$* RPM lines showed overall high resemblance to the other *BRAF* mutant CRC PDOs. Yet, intertumoral heterogeneity was observed between the lines where B2-040 showed most sensitive phenotypes. This confirms the widely supported notion that differences beyond the oncogenic mutation, among others differences in (epi)genetic landscape, cellular composition and transcriptional levels, will additionally impact tumor cell intrinsic drug sensitivities (**Supplementary Figures 6B-I**).

In vivo tumor growth and response to anti-EGFR therapy

To characterize the similarities and differences of the RPM lines in vivo, we xenografted the RPM organoids in mice to analyze growth dynamics (**Figure 7A**). As expected, tumors from isogenic RPM organoids displayed faster growth rates as compared to the parental P18T organoids (**Figure 7B**). Moreover, we observed that *$KRAS^{G13D}$* mutant tumors showed the fastest growth rates compared to other RPM tumors, resembling elevated tumor growth dynamics of mCRC patients with *$KRAS^{G13D}$* mutations[20–22]. More surprising to us was that $KRAS^{G12D}$ showed slowest growth kinetics of the RPM lines, since endogenous expression of $KRAS^{G12D}$, but not $NRAS^{G12D}$, promotes cancer progression in murine colonic epithelium after loss of APC expression[17].

Multiple studies have been published reporting the accuracy of tumor-derived organoids in predicting patient responses to therapy[27,58,59]. To verify whether our observed intertumoral differences in drug responses between the RPM lines are also observed *in vivo*, we applied afatinib treatment for 28 days. Consistent with results from *in vitro* experiments, a significant decrease in growth rate was observed in P18T, *$KRAS^{G13D}$* and *$NRAS^{G12D}$* mutant tumors upon afatinib treatment (**Figure 7-C-E**). In comparison, *$BRAF^{V600E}$* and *$KRAS^{G12D}$* mutant tumors were most resistant, showing only a marginal reduction in tumor growth compared to vehicle (**Figure 7F-G**). Although overall *in vitro* responses were more dramatic, presumably due to a mismatch between achieved drug concentrations *in vivo*, the overall pattern of intertumoral differences between the RPM clones remained present.

$KRAS^{G13D}$ mutant tumors are an interesting outlier, considering its malignant nature during unperturbed growth conditions in mice. Yet, sensitivity to anti-EGFR therapy remains, so suppressed growth rates could be established towards the range of vehicle-treated parental P18T tumors (**Figure 7D**). This corresponds to observations from the clinic, showing that patients with *$KRAS^{G13D}$* mutant CRCs benefit from cetuximab treatment, but are inferior to the

Figure 7. *In vivo* growth dynamics of RPM organoids.
(**A**) A schematic overview illustrating in vivo examination of xenografted RAS pathway mutant (RPM) CRC PDOs in mice. In short, CRC PDOs were subcutaneously injected in mice. Above 50 mm^3, growth of tumors was analyzed for 35 days. Above 200 mm^3, tumors were treated with either vehicle or afatinib (20 mg/kg via oral gavage, 5 days on/2 days off) for 28 days. (**B**) Graph displays the mean percentage change in tumor volume relative to initial tumor volume (50 mm^3) of xenografts from indicated RPM organoids monitored over the experimental period. Error bars represent standard deviation. n = 5 per group. **** $p < 0.0001$, 2-way ANOVA Dunnett's multiple comparisons test. (**C**) Graphs display the mean percentage change in tumor volume relative to initial tumor volume (200 mm^3) of xenografts from P18T treated with vehicle or afatinib. (**D**) like (C) but for $KRAS^{G13D}$ (**E**) $NRAS^{G12D}$, (**F**) $KRAS^{G12D}$ and (**G**) $BRAF^{V600E}$. Error bars represent standard deviation. n = 5 per group. $p > 0.05$; * $p < 0.05$; ** $p < 0.01$; **** $p < 0.0001$; n.s., not significant. For multiple comparison per time point 2-way ANOVA (Bonferroni's multiple comparisons test) was used. For overall *in vivo* response Welch's *t*-test was used.

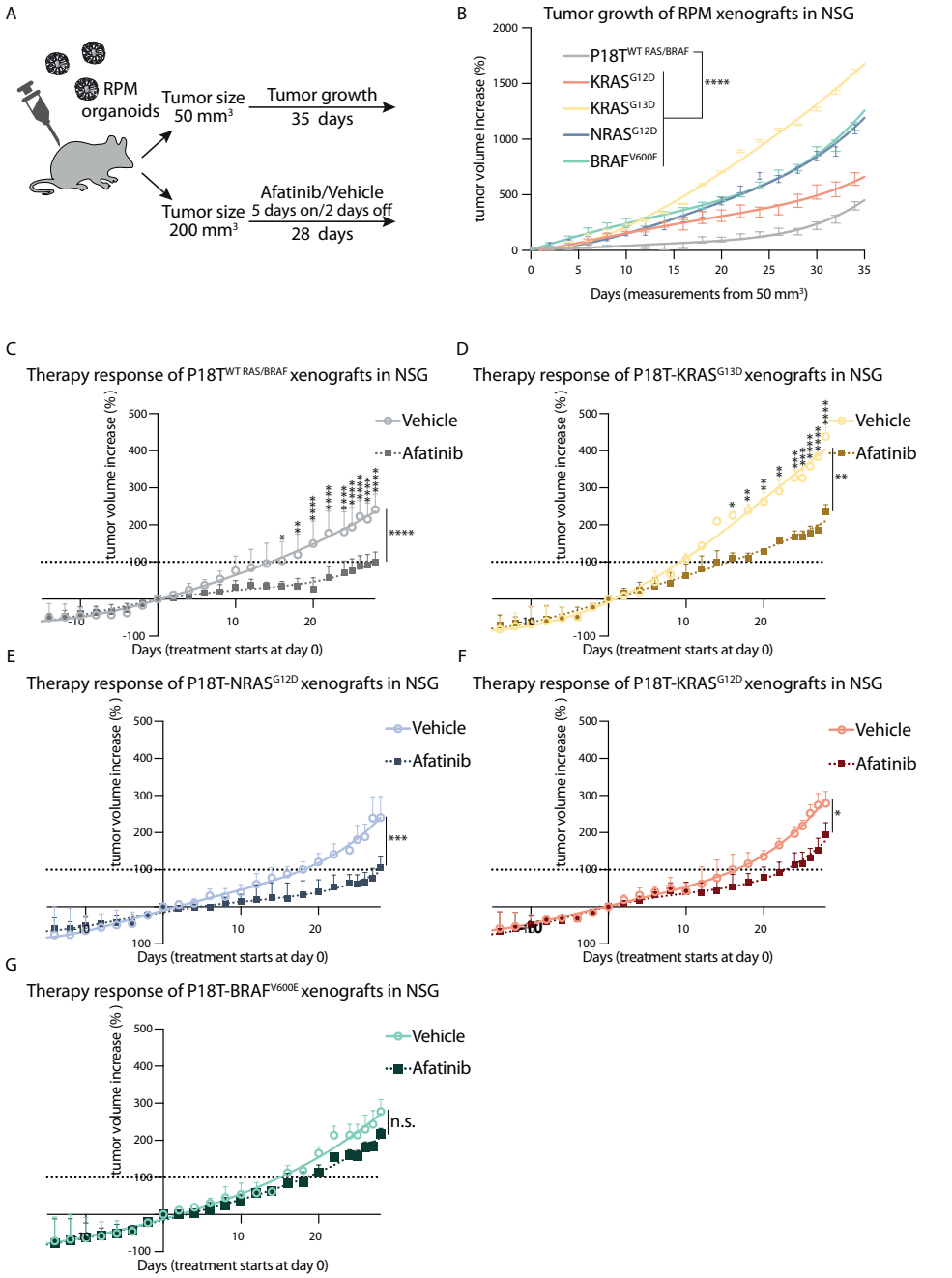

response of CRC patients with *RAS*^{WT} tumors[20,22,60].

DISCUSSION

Despite the overlapping functions of RAS and BRAF oncogenes, data analyses of CRC patients and cell lines suggest that mutation variants of oncogenic RAS and BRAF proteins are associated with different tumor types and involved in distinct tumorigenic pathways[17,23,61,62]. Moreover, CRCs with oncogenic *RAS* variants can react differently to EGFR inhibition[20–22,63,64]. Nevertheless, stratification of patient cohorts per mutation is significantly hampered by limited statistical power due to small sample sizes. Therefore, mCRC patients with any activating mutation in *RAS* are currently being excluded from anti-EGFR targeted therapy[65]. Moreover, from a practical point of view it is very challenging to dissect similarities and differences between various oncogenic RAS and BRAF variants using patient-derived material. Foremost, because intertumoral heterogeneity is to a large extent influenced by differences in genetic landscape of the tumor, epigenetics, cellular composition, tumor location, stroma infiltration, and more[4,23,24,62,66].

Therefore, to address the influence of a single RAS pathway mutation on tumor progression and anti-EGFR therapy resistance, we generated a panel of isogenic CRC PDO lines with endogenous expression of a variety of oncogenic *BRAF* and *RAS* mutations. Confirming the oncogenic role of MAPK pathway mutations, we observed that activating mutations in *BRAF* (i.e. V600E), *KRAS* (i.e. G12D and G13D) and *NRAS* (i.e. G12D) enhanced downstream MAPK pathway activity. In the presence of exogenous EGF levels during normal culture conditions, growth analysis and RNA sequencing did not reveal significant differences between the RPM lines. In contrast, under more challenging conditions as EGF-independent growth due to pan-HER inhibition, we noticed apparent differences between the RPM mutants where KRAS^{G12D} and BRAF^{V600E} showed most resistant phenotypes. Same differential sensitivity towards pan-HER inhibition was also observed *in vivo*.

During normal growth conditions *in vivo* where EGF supply is limited but not absent, *KRAS*^{G13D} RPM lines displayed enhanced tumor growth over the other RPM tumors. This corresponds to the malignant nature of *KRAS*^{G13D} mutant CRCs in patients that is likely caused by the high level of intrinsic GDP-to-GTP exchange rates of KRAS^{G13D} mutant proteins, resulting in guanine nucleotide exchange factor (GEF) independent RAS auto-activation[20,22,60,67,68]. The codon-specific effects of KRAS^{G13D} mutants are likely masked in *ex vivo* culture conditions with EGF concentrations that saturate EGFR phosphorylation and downstream pathway activation. The structural differences between KRAS^{G12D} and KRAS^{G13D} proteins might explain their distinct response to pan-HER inhibition[68,69], as KRAS^{G13D}, but not KRAS^{G12D}, retain sensitivity to GAP-mediated GTP hydrolysis as demonstrated by *in vitro* GTP hydrolysis experiments[67,68].

The high prevalence of codon 12 and 61 mutations in *KRAS* and *NRAS*, respectively, suggests that the transforming capacity differs per oncogenic mutation and RAS isoform[6] (COSMIC database). We observed that *NRAS*^{G12D} were 'weaker' mutants than *KRAS*^{G12D} in terms of EGF-independent growth phenotypes of our RPM lines. In contrast, a NRAS^{Q61} mutant CRC PDO showed most resemblance to KRAS^{G12D}. It has been reported that *NRAS* codon 61 mutants are more efficient inducers of downstream MAPK signaling than *NRAS* codon 12[70]. Due to

different expression levels, we observed fewer active RAS proteins in $NRAS^{G12D}$ RPM organoids compared to $KRAS^{G12D}$ RPM organoids. A possible explanation for the preference of codon 61 mutations over codon 12 in *NRAS* is that lower expression levels require compensation by a potent mutation in order to achieve sufficient MAPK activation and transformative capacity. For *KRAS*, codon 61 mutations might create too much oncogenic potency, as $KRAS^{Q61}$ mutations appear more active than $KRAS^{G12D}$ mutations *in vitro*, and result in growth arrest of primary lung fibroblast[50,71].

Although $KRAS^{G12D}$ and $BRAF^{V600E}$ RPM organoids showed resistance to pan-HER inhibition, a strong reduction in ERK activation and cell proliferation was observed. This indicates that upstream receptor activation is important to elevate levels of ERK activity, despite presence of MAPK pathway activating mutations. Conceptually, this parallels other observations in *RAS* mutant cancer cells, showing that the capacity of RAS and RAF oncogenes to activate downstream MAPK signaling is not maximal[72,73]. Moreover, the residual levels of RAS-ERK activity in *RAS* mutant organoids during drug screens did correlate with observed phenotypes, where ERK phosphorylation levels were significantly higher in afatinib-resistant ($KRAS^{G12D}$) clones compared to afatinib-sensitive ($KRAS^{G13D}$ and $NRAS^{G12D}$) clones. In contrast, $BRAF^{V600E}$ mutant clones showed a different drug response than the oncogenic *RAS* variants, with slower kinetics and an incomplete inhibition but stable suppression over time. Considering that both the $KRAS^{G12D}$ and $BRAF^{V600E}$ mutant organoids manifest similar resistance phenotypes, we speculate that both drug response kinetics, i.e. either suppressed and sustained over time or initially eliminated with subsequent minimal reactivation, effectuate low ERK activity levels that are sufficient to support organoid survival, but not growth. Intriguing, while the minimal levels of ERK activity in $BRAF^{V600E}$ and $KRAS^{G13D}$ mutant organoids seem comparable, their phenotypes deviate significantly. Most likely, minimal differences in ERK activity levels at the lower range might have different phenotypic outcomes. Future methodologies for sensitive quantifications of signaling activities at the single cell level and in real-time will prove instrumental for full understanding how pathway activity levels in tumors correlate with drug response phenotypes (manuscript in preparation), among others to discriminate between heterogeneities of signaling activities between cells and fluctuating activity levels over time.

Together, we show that oncogenic knock-in mutations in the MAPK pathway in CRC PDOs resemble phenotypes observed in the clinic and can be used to understand mutation-specific oncogene signaling in CRC. Furthermore, we observed differential sensitivities to MAPK pathway inhibition between RAS pathway mutations, supportive of the notion that mCRC patients with $NRAS^{G12D}$ and $KRAS^{G13D}$ mutations, which are currently being excluded from anti-EGFR targeted therapy, might actually benefit from anti-EGFR therapy. Further investigation will be required to determine whether the current stratification of mCRC patients based on overall *RAS* mutant status should be reconsidered and include codon- and isoform-specific variations. Indeed, in addition to intrinsic differences between various mutations as revealed with the RPM organoids, cross-comparison of different CRC PDOs with identical $BRAF^{V600E}$ mutation displayed intertumoral heterogeneity beyond the exact mutation type, like genetic landscape, epigenetics, cellular composition, tumor location and stroma infiltration. How all these multiple variables, including mutation type, act in concert in establishing a (drug response) phenotype is challenging to dissect as tumors have often adapted in multiple possible scenarios to accomplice sufficient MAPK activity. Future decision-making for

therapeutic strategy should use the most optimal genotype-phenotype correlations to assist in overall patient stratification to narrow down on potential therapeutic options, after which tailored-made adjustments can be made based on personalized drug response data.

ACKNOWLEDGEMENTS

This work is part of the Oncode Institute, which is partly financed by the Dutch Cancer Society, and was funded by the gravitation program CancerGenomiCs.nl from the Netherlands Organization for Scientific Research (NWO), by a grant from the Dutch Cancer Society (UU 2013-6070), by a 'Sta op tegen Kanker' International Translational Cancer Research Grant, and ERC starting grant (H.J.G.S). Stand Up to Cancer is a program administered by the AACR. Furthermore, we thank all members of the Snippert, Gloerich and De Rooij laboratories for fruitful discussions and support. We thank Utrecht Sequencing Facility for providing sequencing service and data. Utrecht Sequencing Facility is subsidized by the University Medical Center Utrecht, Hubrecht Institute,Utrecht University and The Netherlands X-omics Initiative (NWO). We thank the UMCU Bioinformatics Expertise Core (UBEC) facility for their help with the analysis of RNA sequencing results. Last, we would like to thank the people from the Preclinical Intervention Unit of the Mouse Clinic for Cancer and Ageing (MCCA) at the NKI for performing the intervention studies.

AUTHOR CONTRIBUTIONS

JBP and HJGS conceived the study. JBP, HJGS designed experiments, and JBP performed most of the experiments. JBP generated clones. NH performed drug screens. JBP and NH analyzed and interpreted the data. IV cultured and characterized CRC PDOs by targeted genome sequencing. JL, MV and RK performed in vivo mouse experiments, which was analyzed and interpreted by JBP. CS performed RNA sequencing analysis. JBP and CS analyzed and interpreted the data. ES performed and analyzed CNA experiments, which was interpreted by JBP and HJGS. JBP and HJGS wrote the manuscript, which was reviewed by all authors.

MATERIALS AND METHODS

Patient-derived organoid culture and maintenance

The patient-derived P6T, P16T, P18T and P25T organoids used in this study were previously established and characterized[25]. Other patient-derived organoids described in this study were established and characterized by the Hubrecht Organoid Technology (hub4organoids.eu). Human CRC organoids were cultured as described previously[25,44]. Culture medium contained advanced DMEM/F12 medium (Invitrogen) with 1% Penicillin/Streptomycin (P/S, Lonza), 1% Hepes buffer (Invitrogen) and 1% Glutamax (Invitrogen), 10% R-spondin conditioned medium, 10% Noggin conditioned medium, 1x B27 (Invitrogen), 1.25 mM n-Acetyl Cysteine (Sigma-Aldrich), 10 mM Nicotinamide (Sigma-Aldrich), 50 ng/ml EGF (Invitrogen), 500 nM A83-01 (Tocris), 10 mM SB202190 (ApexBio) and 100 mg/ml Primorcin (Invitrogen). Organoids were splitted through Trypsin-EDTA (Sigma-Aldrich) treatment. Culture medium after splitting was supplemented with 10 mM Y-27632 dihydrochloride. For selection of RAS pathway mutants, organoids were grown in culture medium containing 1-2 mM puromycin.

Organoid transfection and genotyping

The transfection protocol of P18T organoids was previously described in detail by Fujii *et* al. (2015). Three days after transfection, culture media plus Y-27632 was exchanged with selection medium. After puromycin selection, surviving clones were picked and subjected to genotyping to detect the presence of homologous recombination.
For genotyping, genomic DNA was isolated using Viagen Direct PCR (Viagen). The presence of oncogenic and silent mutations in exons and insertions or deletions in introns of *BRAF*, *KRAS* and *NRAS* was verified by using the PCR product obtained using the following primers:
$KRAS^{G12D/G13D}$ exon fw 5'-GGCTCATTGCAACCTCGG-3',
$KRAS^{G12D/G13D}$ exon rv 5'-GTTGGCGCCTACCGGTGG-3',
$KRAS^{G12D/G13D}$ exon silent mutations fw 5'-GAGACGGAGTCTTGCTCTAT-3',
$KRAS^{G12D/G13D}$ exon silent mutations rv 5'-GCTGTATGGTTAACGCACTC-3',
$KRAS^{G12D/G13D}$ intron fw 5'-CCGCAGAACAGCAGTCTG-3',
$KRAS^{G12D/G13D}$ intron rv 5'-TGATGTCACAATACCAAG-3',
$NRAS^{G12D}$ exon fw 5'-CCGACTGATTACGTAGCG-3',
$NRAS^{G12D}$ exon rv 5'-GTTGGCGCCTACCGGTGG-3',
$NRAS^{G12D}$ exon silent mutations rv 5'-GGGATCATATTCATCCACG-3',
$NRAS^{G12D}$ intron fw 5'-CCGACTGATTACGTAGCG-3',
$NRAS^{G12D}$ intron rv 5'-CTCATGAATGAACTCAACAC-3',
$BRAF^{V600E}$ exon fw 5'- GGAGAGCAGGATACCACAGC-3',
$BRAF^{V600E}$ exon rv 5'-GTTGGCGCCTACCGGTGG-3',
$BRAF^{V600E}$ exon silent mutations rv 5'-AACGTGACTTCTCCGTGGCC-3',
$BRAF^{V600E}$ intron fw 5'-CTTCATAATGCTTGCTCTG-3',
$BRAF^{V600E}$ intron rv 5'-CCTGCCTTAAATTGCATAC-3'.

Products were sequenced using the following primers:
$KRAS^{G12D/G13D}$_exon 5'-CACCGATACACGTCTGCAGTCAAC-3',
$NRAS^{G12D}$ exon 5'-CCAAATGGAAGGTCACAC-3',
$BRAF^{V600E}$ exon 5'-CTTCATAATGCTTGCTCTG-3',

In addition, the CloneJET PCR Cloning Kit was used to confirm indel generation in introns of the allele of *BRAF*, *KRAS* and *NRAS* knock-ins #1 that was subject to NHEJ.

Vector contruction

The CRISPR guide RNA (sgRNAs) were designed by an online CRISPR design tool (http://crispr.mit.edu). The sgRNA guide sequences used can be found in the supplementary data (Supplementary Table 4). For CRISPR-mediated homologous recombination the human codon-optimized Cas9 expression plasmid was obtained from Addgene (41815). The sgRNA-GFP plasmid was obtained from Addgene (41819) and used as a template for generating target specific sgRNAs as described in detail by Drost *et al.* (2015). For the generation of the donor template, genomic DNA from P18T organoids was used to PCR amplify the *NRAS*, *KRAS* and *BRAF* 3' homology arms using high-fidelity Phusion Polymerase (New England BioLabs). The 5' homology arm of *KRAS* spans the region Chr12:25245385-25245994, the 3' homology arm spans the region Chr12:25244479-25245229. The 5' homology arm of *NRAS* spans the region Chr1:114716161-114716768, the 3' homology arm spans the region Chr1:114715261-114716010. The 5' homology arm of *BRAF* spans the region Chr7:140753392-140753973, the 3' homology arm spans the region Chr7:140752465-140753206. Gene block fragments (idtDNA) were used to generate 5' homology arms containing

silent and oncogenic mutations. The gene block fragments and homology arms were cloned into a pBlueScript plasmid expressing a 3229-bp AATPB:PGKpuroDtk selection cassette (Schwank *et al*., 2013).

Western blot assay and RAS-GTP pull down

Prior to cell lysis, organoids were incubated with 1 mg/ml dispase II (Invitrogen) for 10 minutes at 37° C to digest the BME. Western blot samples for phosphorylated ERK and MEK were lysed using RIPA buffer (50 mM Tris-HCL pH 8.0, 150 mM NaCl, 0.1% SDS, 0.5% Na-Deoxycholate, 1% NP-40) containing Complete protease inhibitors (Roche). Protein content was quantified using a BCA protein assay kit (Pierce™) and analyzed by Western blotting. Membranes were blocked and probed with antibodies directed against pMEK (RRID:AB_331648), MEK (RRID:AB_823567), pERK (RRID:AB_331646), ERK (RRID:AB_390779) and GAPDH (RRID:AB_2107445). Samples for RAS-GTP isolation were lysed using Ral lysis buffer (50 mM Tris-HCL pH 7.5, 200 mM NaCl, 2 mM MgCl2, 10% glycerol, 1% NP-40) containing Complete protease inhibitors (Roche). Lysates were normalized for protein levels using a BCA protein assay kit (Pierce™) and subsequently GTP-bound RAS was isolated via immunoprecipitation using recombinant RAS binding domain of RAF1 (RAF1-RBD). Protein lysates were run on SDS-PAGE gels and transferred to PVDF membranes (Millipore). Membranes were blocked and probed with antibodies directed against RAS (RRID:AB_397425) and NRAS (RRID:AB_628041). Organoid treatments: afatinib (Selleck Chemicals) 1 μM, 1 h and 24 h or DMSO.

RNA isolation, cDNA preparation and qRT–PCR

Organoids were harvested in RLT lysis buffer and RNA was isolated using the Qiagen RNeasy kit (Qiagen) according to the manufacturer's instructions. Extracted RNA was used as a template for cDNA production using iScript™ cDNA Synthesis Kit (Bio-Rad) according to the manufacturer's protocol. qRT–PCR was performed using FastStart Universal SYBR Green Master mix (Roche) according to the manufacturer's protocol. Results were calculated by using the relative standard curve method. Primer sequences:
B2M_fw 5'-GAGGCTATCCAGCGTACTCCA-3',
B2M_rv 5'-CGGCAGGCATACTCATCTTTT-3',
KRAS wild-type fw 5'-GCAAGAGTGCCTTGACGATAC-3',
KRAS wild-type rv 5'-CTGCTGTGTCGAGAATATC-3',
KRAS mutant fw 5'-GCAAGAGTGCGTTAACCATAC-3',
KRAS mutant rv 5'-CTGCTGTGTCGAGAATATC-3',
NRAS wild-type fw 5'-TCCAGCTAATCCAGAACCAC-3',
NRAS wild-type rv 5'-CCAGCTGTATCCAGTATGTC-3',
NRAS mutant fw 5'-GCGCACTGACAATCCAATTG-3',
NRAS mutant rv 5'-CCAGCTGTATCCAGTATGTC-3',
BRAF wild-type fw 5'-ATCTCGATGGAGTGGGTC-3',
BRAF wild-type rv 5'-CTGGTCCCTGTTGTTGATG-3',
BRAF mutant fw 5'-CACGGAGAAGTCACGTTG-3',
BRAF mutant rv 5'-GGTAACTGTCCAGTCATC-3',
EGFR fw 5'-AGTGCCTGAATACATAAACC-3',
EGFR rv 5'-GTAGTGTGGGTCTCTGC-3',
HER2 fw 5'-TGTGACTGCCTGTCCCTACAA-3',
HER2 rv 5'-CCAGACCATAGCACACTCGG-3',
HER3 fw 5'-ATACACACCTCAAAGGTACTC-3',
HER3 rv 5'-ATCTTCTTCTTCAGTACCCAG-3'.

Phenotypic drug screen and Calcein Green Assay

Five days after organoid trypsinization, 1 mg/ml dispase II (Invitrogen) was added to the medium of the organoids and these were incubated for 15 min at 37° C to digest the BME. Subsequently, organoids were mechanically dissociated by pipetting, filtrated using a 40 mm nylon cell strainer (Falcon), resuspended in 75% BME/growth medium (40 organoids/μl) prior plating of two 10 μl drops on Nunc™ Lab-Tek™ II Chamber Slide™ Systems. After plating culture medium containing either 1 μM of afatinib, 1 μM of erlotinib or DMSO was added. The labtek plates were mounted on an inverted confocal laser scanning microscope (Leica SP8X) and imaged using a 10X objective. For visualization of cell viability, organoids were incubated with 16.2 μM Hoechst 33342 (Life Technologies) and 1.5 μM DRAQ7™ (Cell Signaling #7406) for 30 min at 37° C prior imaging. For calculating organoid viability, the morphology of 100 organoids was scored after 3 and 7 days of 1 μM afatinib (pan-HERi) treatment.
For organoid viability and growth analysis, organoids were imaged by an inverted routine microscope (Nikon Eclipse TS100) using a 4X objective. For calculating organoid count and size, organoids were incubated for 20 minutes with 500 ml culture medium containing 5 μM calcein-green (Invitrogen). For the quantification of the organoid size and count, FIJI analysis software was used and presented as dot plots[76].

Drug screen and viability assessment

Five days after organoid trypsinization to single cells, 1 mg/ml dispase II (Invitrogen) was added to the medium of the organoids and these were incubated for 15 min at 37° C to digest the BME. Subsequently, organoids were mechanically dissociated from the BME by subtle pipetting, filtrated using a 40 µm nylon cell strainer (Falcon), resuspended in 2% BME/growth medium (15–20,000 organoids/ml) prior plating of 30 µl (72 hrs drug screen) or 50 µl (7 days drugscreen) (Multi-dropTM Combi Reagent Dispenser) on BME pre-coated 384-well plates. The drugs and their combinations were added 3 hrs after plating the organoids by using the Tecan D300e Digital Dispenser. Drugs were dispensed in a non-randomized manner and DMSO end concentration was 0.9% in all wells. 72 hrs or 7 days after adding the drugs organoids were fixed with 4% PFA (Merck) and stained with Hoechst (Invitrogen). Organoids were screened by automated microscopy of whole wells (CX5 High Content Screening (HCS) platform (Thermo Scientific), equipped with an Olympus UPLFLN U Plan Fluorite 4x Microscope Objective). Organoid roundness was measured by integrating Hoechst signal and contrast using Columbus Cellular imaging and analyses (Perkin Elmer). Relative survival was determined by normalization of the results to DMSO (= 100% alive) and 20 µM Navitoclax (= 0% alive), which induces maximal killing within 72 hours after treatment. Multiple identical drug combinations were averaged.

Targeted inhibitors

Afatinib, Selumetinib, Vemurafenib, Erlotinib and Navitoclax were purchased from Selleck Chemicals. SCH772984 was obtained from MedChem Express. These compounds were dissolved in dimethylsulfoxide (DMSO, Sigma-Aldrich) and stored as 10 mM aliquots.

Curve fitting and drug sensitivity

Dose-response curves were generated using GraphPad software by performing nonlinear regression (curve fit), assuming a standard Hill equation (chosen method: log(inhibitor) vs. Response, constrain top=100).

RNA seq

Organoids were treated with DMSO or afatinib (1 µM) for 24 hours and organoids were lysed in RLT lysis+ buffer containing 1% beta-mercaptoethanol. RNA was extracted with the QiaSymphony SP kit (Qiagen) according to the manufacturer's protocol. RNA-libraries were prepared for sequencing with the Illumina Truseq Stranded mRNA polyA kit and sequenced on the NextSeq500 platform (1x75bp, 20M reads per sample). Data were processed by the UBEC facility Illumina analysis pipeline (https://github.com/UMCUGenetics/RNASeq) by utilizing STAR (v2.4.2a) to map the reads. Samples were normalized for sequencing depth based on the sum of the read counts over all genes for each sample. Expressed genes were selected by excluding all genes where ≥ 3 samples had less than 10 reads. Principal Component Analysis (PCA), Euclidean Distance-based clustering and Differential Expression (DGEA) calculations were performed with the DESeq2 package[74]. P-adjusted ($p_{adjusted}$) was calculated by multiplying the p-value with the number of genes (=expressed genes) tested. Unsupervised hierarchical clustering was performed on all differentially expressed genes.

DGEA was performed on untreated parental P18T lines vs. untreated $KRAS^{G12D}$, $KRAS^{G13D}$, $NRAS^{G12D}$ and $BRAF^{V600E}$ mutant lines, on treated parental P18T lines vs. treated $KRAS^{G12D}$, $KRAS^{G13D}$, $NRAS^{G12D}$ and $BRAF^{V600E}$ mutant lines, on untreated vs treated lines per mutation, or on treated $KRAS^{G12D}$ and $BRAF^{V600E}$ vs $KRAS^{G13D}$ and $NRAS^{G12D}$ mutant lines. For subsequent analysis, we set a cut-off threshold of a $\log_2$ 2 fold change of genes that were differentially expressed in all three (mutant) or four (P18T) monoclonal lines.

CNAs

Genomic DNA was extracted from the parental P18T and RAS pathway mutant organoid lines using the QIAamp DNA Micro Kit (Qiagen) according to the manufacturer's protocol. Approximately 100 ng genomic DNA of each sample was used for DNA library preparation (TruSeq Nano DNA library preparation kit, Illumina). Subsequently, libraries were sequenced on an Illumina NextSeq500 using 75-bp single-end sequencing. Raw sequencing data was aligned to human reference genome hg19/GRCh37 using Burrows-Wheeler Aligner mapping tool (BWA-MEM; Version 0.7.5a). Further data processing procedures are fully described at: https://github.com/UMCUGenetics/IAP. DNA copy number profiles were generated using Ginkgo as described by Garvin et al. (2015)[75] (pipeline available at: https://github.com/robertaboukhalil/ginkgo). The reads were binned into 1 Mb variable-length intervals and data was segmented to obtain copy number estimates across the genome. Copy number values deviating >0.6 from the average ploidy were considered to indicate deletions or amplifications. R package ggplot2 was used to generate a heatmap for visualization.

Organoid xenograft experiments

Approval for this study was obtained by the local animal experimental committee at The Netherlands Cancer Institute

(IVD-NKI; OZP 80102; WP8520). Parental P18T and RAS pathway mutant knock-in patient-derived organoids were transplanted subcutaneous as single cells at a density of 3x10^5 organoids in 100 µl 50% Matrigel/medium with 10% collagen type I (BD Bio- sciences) mixture into NSG-B2m mice (JAX stock no: 010636).
Tumor growth dynamics were analyzed for 35 days in mice with established tumors of 50 mm^3. Mice with established tumors (average volume of 200 mm^3) were treated with afatinib (20 mg/kg; five days on, two days off) or vehicle for four weeks. After two weeks recovery from the drug treatment, mice were sacrificed.
Tumor volumes were evaluated three times per week by caliper and the approximate volume of the mass was calculated using the formula Dxd2/2, where D is the major tumor axis and d is the minor tumor axis. For in vivo dosing, afatinib was dissolved in 1.8% hydroxypropyl-b-cyclodextrin (Sigma), 5% of a 10% acetic acid stock and aqueous natrosol (0,5%). All agents were administered via oral gavage. We used 5 mice per group that were randomly assigned to the different treatment groups before the start of the experiment. We determined outliers with the following rule: If a number is less than Q1-1.5xIQR or greater than Q3+1.5xIQ, then it is considered to be an outlier, with IQR being the interquartile range, equal to the difference between the third quartile (Q3) and first quartile (Q1). Mice that showed outliers in more than 40% of the total number of measurements were excluded from analysis.

Statistical analysis
GraphPad Prism 8.1.1 was used for statistical analysis. All values are given as means $\pm$ SD, as indicated in figure legends. Comparison between two groups were made by Welch's *t*-test. For comparison of more than two groups, we used 2-way ANOVA with subsequent Dunnett's or Bonferroni's multiple comparison test.

SUPPLEMENTARY FIGURES

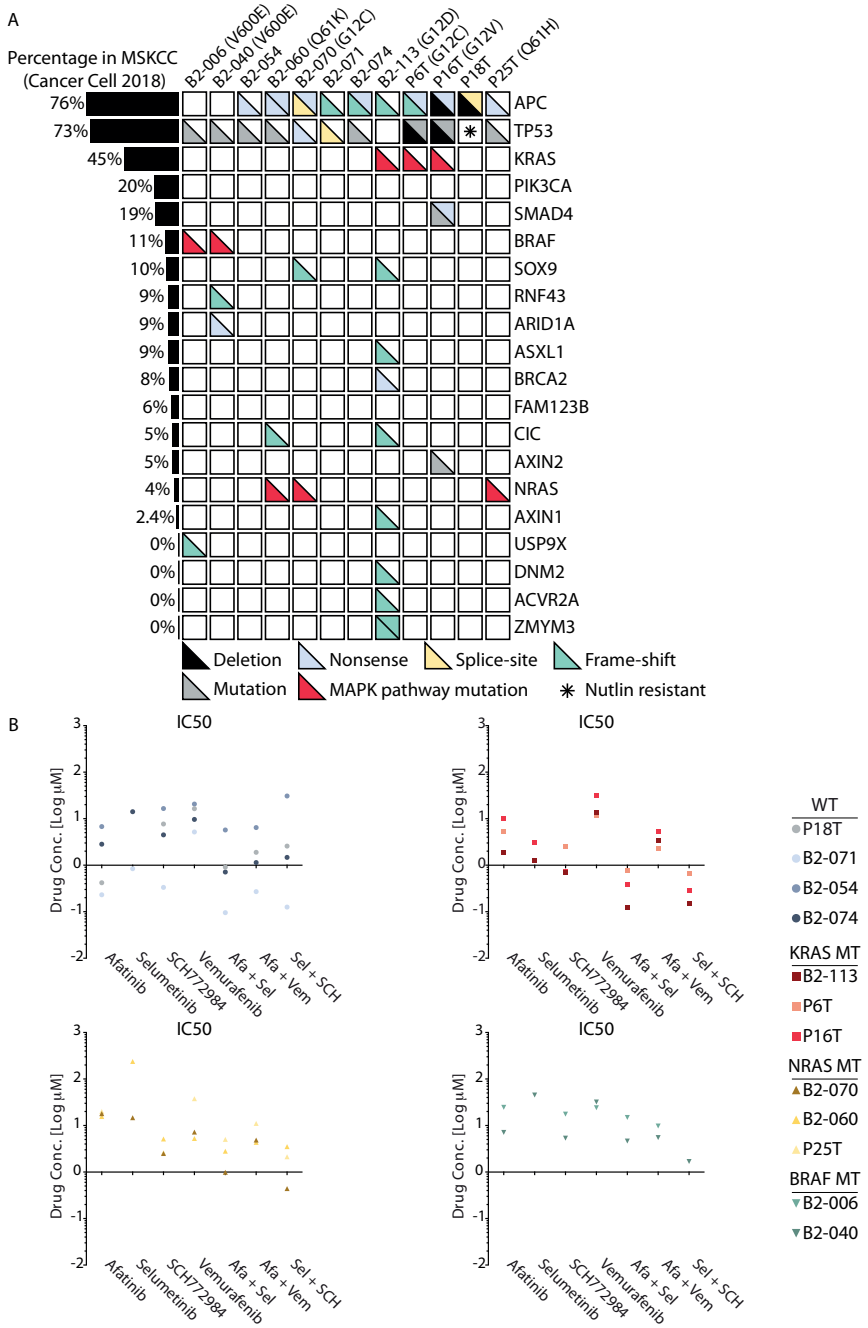

Supplementary Figure 1. Overview of common cancer mutations in selected CRC PDOs with oncogenic mutant MAPK signaling.

(**A**) Overview of common cancer mutations identified in the selected CRC PDOs with oncogenic mutations in the

MAPK pathway. Each box (per half) represents both alleles and indicates a deletion, missense mutation, nonsense mutation, splice-site mutation or a frame-shift alteration according to legend. MAPK pathway mutations are marked in red. The asterisk in P18T indicates a non-functional TP53 pathway (e.g. Nutlin-3 resistant). Genetic alterations in the panel of CRC PDOs are compared to the frequency of mutations as reported in clinical samples (cBioPortal) and are indicated on the left. CRC PDOs identities is indicated at the top, gene names on the right. (**B**) IC50 values derived from dose-response measurements of CRC PDOs treated with afatinib, selumetinib, SCH772984 and vemurafenib in a mono- or combinatorial fashion (see **Fig. 1**). Panels are subdivided per MAPK mutation in the CRC PDO lines. Line identity is indicated in the legend.

Supplementary Figure 2. Intronic indel mutations during generation of oncogenic *BRAF* and *RAS* knock-in variants in CRC PDOs.

(**A**) Genetic strategy to identify the introduction of indel mutations in the introns of *KRAS*, *NRAS* and *BRAF* alleles as a result of Cas9 targeting. In the absence of homologous recombination, double strand breaks are repaired by NHEJ. Black arrows illustrate PCR primer pairs, which amplify genomic loci from both alleles that can be discriminated based on size. The smaller product that includes Cas9-targeted location (orange) was sent for Sanger sequencing (**B**) Per mutation the gRNA target site is shown, as well as the agarose electrophoresis gels showing the PCR product of the allele that was repaired by NHEJ (all data from clones # 1). Sanger sequencing indicates the introduction of small indel mutations in the intronic region. Nonmatching bases are shown in orange. Regions of the sgRNA complementary to the protospacer (underlined) are shown in blue. Red arrow heads indicate Cas9 cleavage sites. Of note, Sanger sequencing of clone # 1 of *BRAF*^{V600E} mutant CRC PDOs shows the presence of multiple 'normal' alleles (>2N). +Puro indicates the monoclonal line that contains the puromycin selection cassette. ΔPuro indicates derivative of the mono-

clonal lines #1 in which the puromycin selection cassette was removed via FLP-FRT recombination.

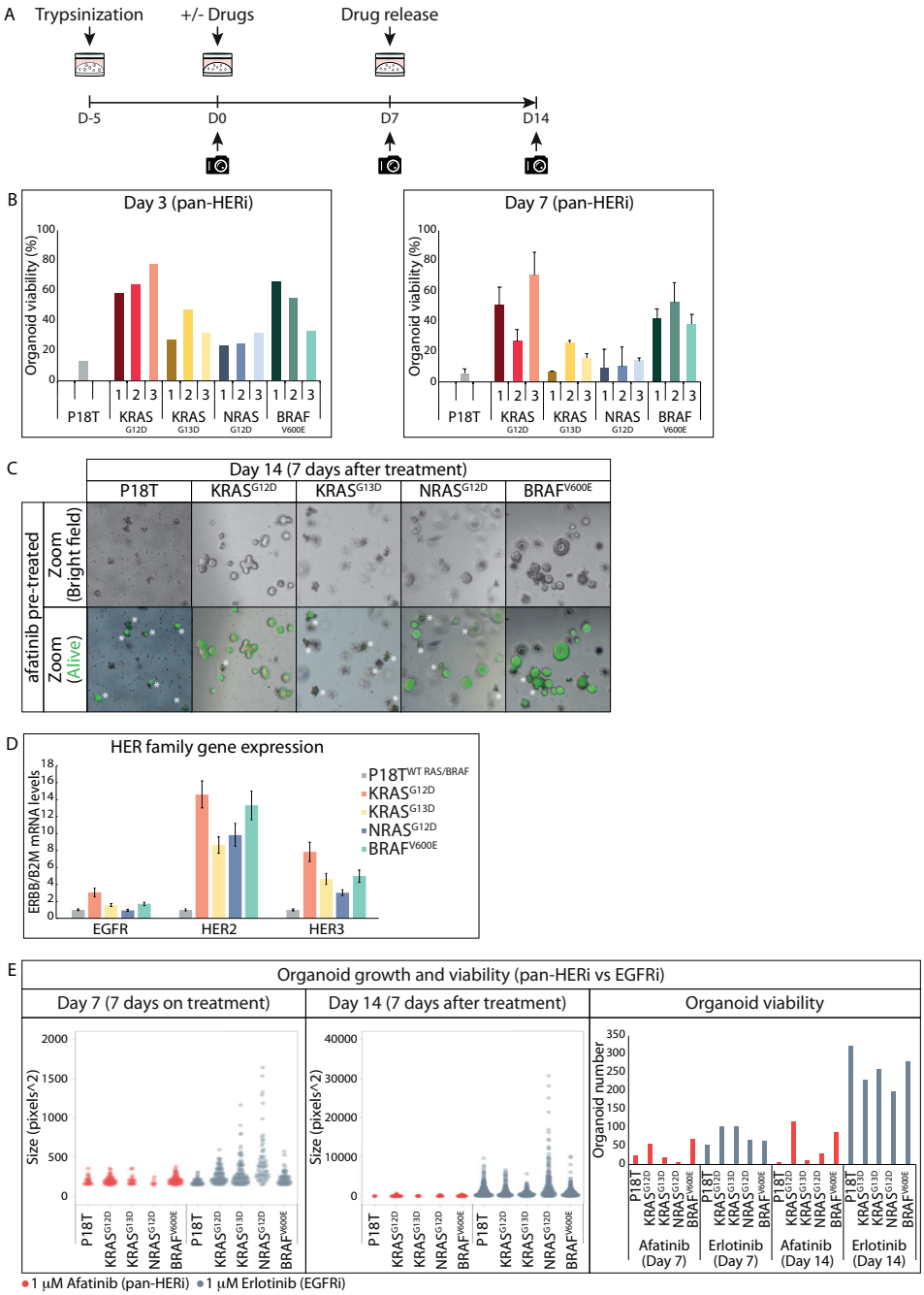

Supplementary Figure 3. *KRAS*^{G12D} and *BRAF*^{V600E} knock-in mutations promote organoid survival in the absence of EGFR signaling activity.
(**A**) Schematic overview of the strategy to score viability and growth of parental P18T and *KRAS*^{G12D}, *KRAS*^{G13D}, *NRAS*^{G12D} and *BRAF*^{V600E} knock-in organoids. Growth from single cells ensures homogeneous size distribution during the experiment. Organoid size and viability were quantified after 3 and 7 days of drug treatment and 7 days after drug withdrawal using the selective uptake of fluorescent calcein green by viable cells. (**B**) Bar graphs depict the percentage of viable organoids after 3 and 7 days of pan-HER inhibition (1 μM afatinib). (**C**) Representative zoom-in panels of parental P18T, or *KRAS*^{G12D}, *KRAS*^{G13D}, *NRAS*^{G12D} and *BRAF*^{V600E} knock-in organoids (clones # 1) 7 days after release of afatinib treatment (day 14). Upper panel shows bright field pictures, lower panel shows overlay with fluorescent calcein green signal in living cells. Asterisks indicate autofluorescence of dead material. (**D**) mRNA expression levels of EGFR, HER2 and HER3 in parental P18T and *KRAS*^{G12D}, *KRAS*^{G13D}, *NRAS*^{G12D} and *BRAF*^{V600E} knock-in organoids measured by qPCR analysis, normalized over housekeeping gene *B2M* (n=3). (**E**) Quantitative analysis of organoid size and viability of isogenic RPM lines during (day 7) and after (day 14) treatment with pan-HER inhibition (1 μM afatinib, red dots) or EGFR selective inhibition (1 μM erlotinib, grey dots). Size and number of viable organoids were measured by selective uptake of fluorescent calcein green by viable cells (see methods). Each dot represents one organoid[76]. Data from 1 8-well Lab-Tek chambered coverglass is shown.

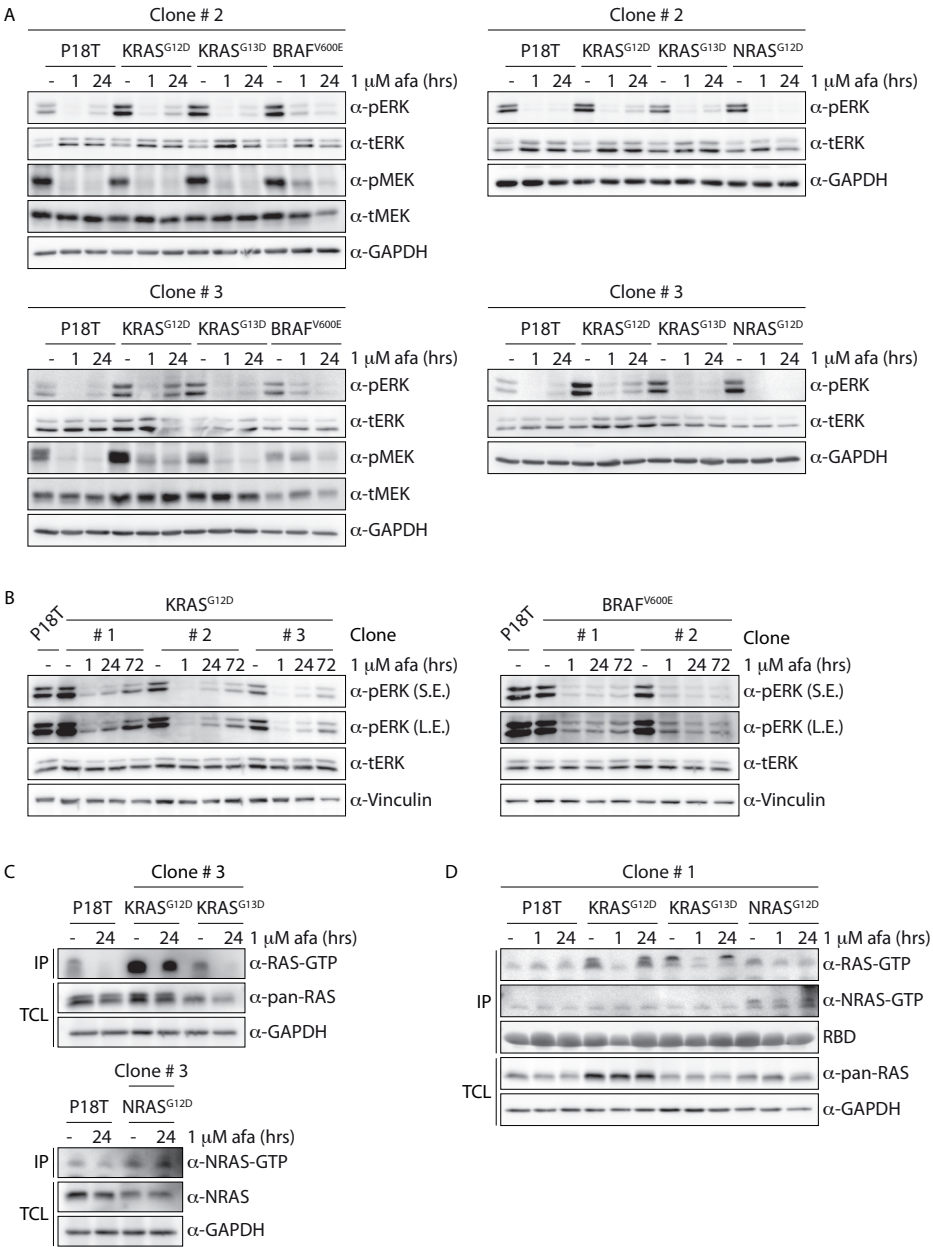

Supplementary Figure 4. *KRAS*^{G12D} and *BRAF*^{V600E} RPM lines show residual MAPK pathway activity in the presence of pan-HER inhibition.

(**A**) Organoids expressing oncogenic *KRAS* (G12D and G13D), *NRAS* (G12D) and *BRAF* (V600E) variants show enhanced basal ERK phosphorylation levels compared to P18T organoids. Pan-HER inhibition (1 μM afatinib) shows sustained ERK and MEK phosphorylation in *KRAS*^{G12D} and *BRAF*^{V600E} organoids compared to P18T, *KRAS*^{G13D} and *NRAS*^{G12D} organoids. Top panels are representative biochemistry experiments on clones # 2 from n=3. Bottom panels are representative biochemistry experiments on clones # 3 from n=3. (**B**) *KRAS*^{G12D} organoids show ERK reactivation upon prolonged pan-HER inhibition (72 hours of 1 μM afatinib), whereas low levels of ERK phosphorylation remain stable in *BRAF*^{V600E} organoids. Left panel (KRAS^{G12D}) are biochemistry experiments on clones # 1-3 from n=1. Right

panel (BRAF^{V600E}) are biochemistry experiments on clones # 1-2 from n=1. S.E., short exposure. L.E. long exposure. (**C**) Biochemistry on RAS activity (GTP-loading) in unperturbed culture conditions and pan-HER inhibition (afatinib 1 μM) for *KRAS* (G12D and G13D) and *NRAS* (G12D) mutant clones # 3 compared to P18T CRC organoids. RAS immunoblots from RAS pull-down assay are shown (RAS-GTP), together with a RAS immunoblot from total cell lysates as loading control. HRAS, KRAS, and NRAS isoforms are detected in mutant KRAS pull-down assays. NRAS isoforms are detected in mutant NRAS pull-down assays. Representative from n = 3 independent experiments. (**D**) as in B but for clones # 1.

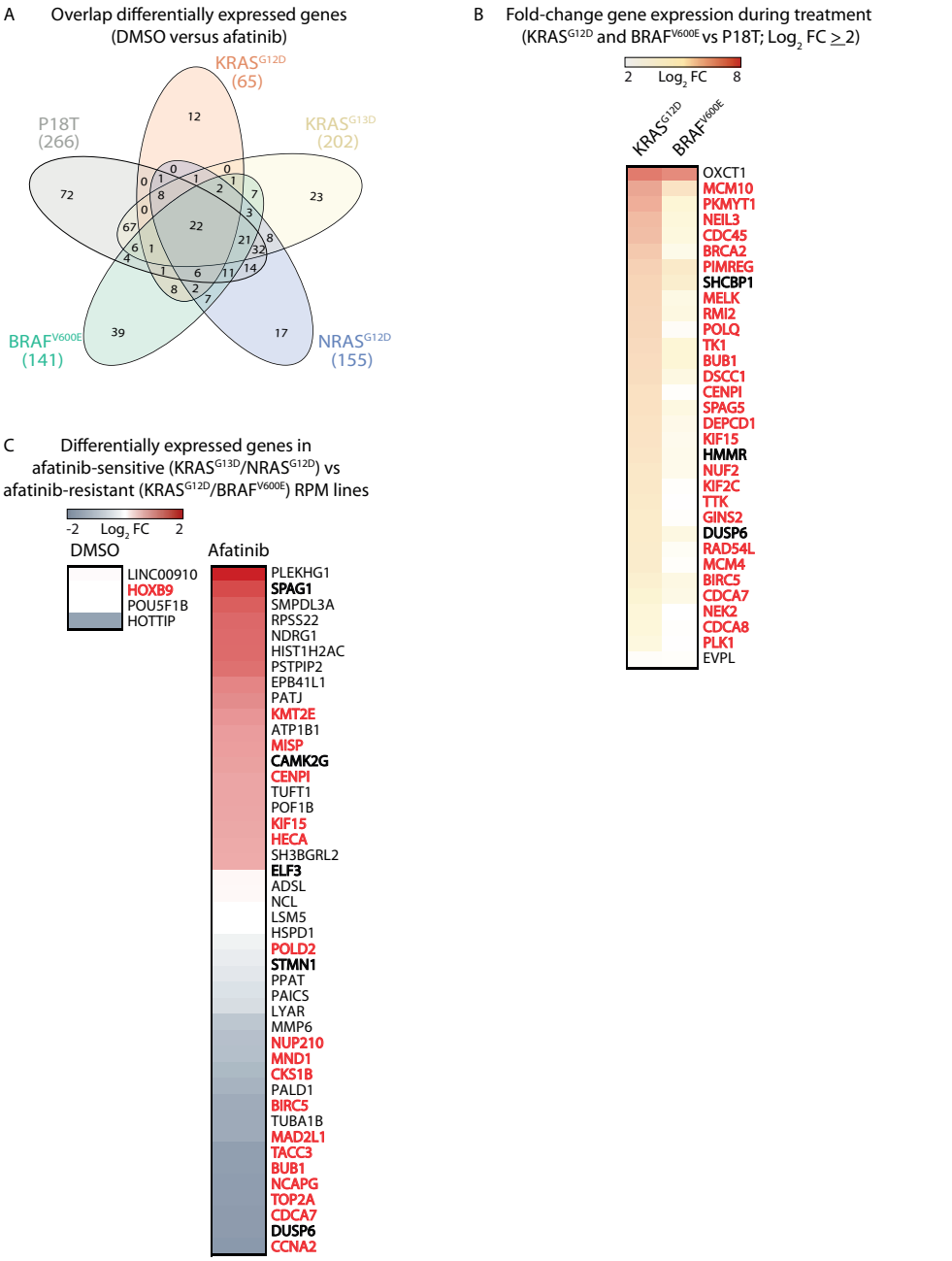

Supplementary Figure 5. Gene expression profiles of RPM lines during unperturbed and EGF-independent growth.

(**A**) Overlap of significantly downregulated genes ($p_{adjusted}$ <0.05; log_2 fold change (FC) ≤-2) upon pan-HER inhibition (1 μM afatinib) treatment versus DMSO in parental P18T (average of bulk and clones # 1-3) and *KRAS*^{G12D}, *KRAS*^{G13D}, *NRAS*^{G12D} and *BRAF*^{V600E} knock-in organoids (average of clones # 1-3). The EGFR gene signature in P18T of 266 genes includes 22 genes that are uniform targets in all lines. (**B**) Heatmaps of the genes (not-restricted to EGFR gene signature in P18T) with significantly higher expression ($p_{adjusted}$ <0.05; log_2 fold change (FC) ≥2) in KRAS^{G12D} and BRAF^{V600E} RPM lines when compared to parental P18T lines in treated (afatinib) conditions. (**C**) Heatmaps of the genes (not-restricted to EGFR gene signature in P18T) with differential expression ($p_{adjusted}$ <0.05; log_2 fold change (FC) ≥2) in afatinib-sensitive (*KRAS*^{G13D} and *NRAS*^{G12D}) versus afatinib-resistant (*KRAS*^{G12D} and *BRAF*^{V600E}) RPM lines during unperturbed (DMSO) and treated (1 μM afatinib) conditions. RAS-ERK pathway genes are depicted in bold. Cell cycle-related genes are marked in bold, red font.

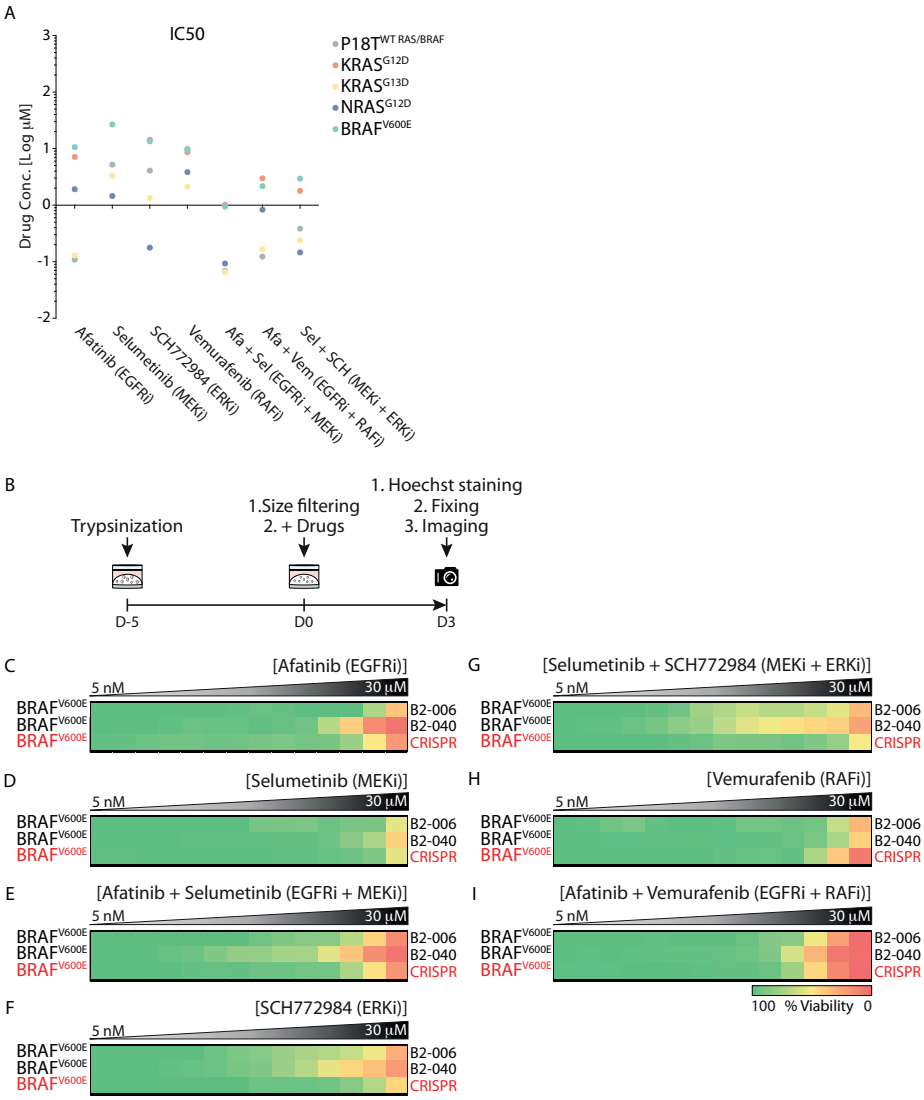

Supplementary Figure 6. Differential drug sensitivities of engineered RPM lines and patient-derived *BRAF*^{V600E} CRC PDOs to targeted MAPK pathway inhibition.
(**A**) IC50 values derived from dose-response measurements of RPM organoids treated with afatinib, selumetinib, SCH772984 and vemurafenib in a mono- or combinatorial fashion (see Fig. 6). Line identity is indicated in the legend. (**B**) Schematic overview of the 3 day drug screening method to compare CRC PDO lines with identical oncogenic *BRAF* mutation. (**C**) Heatmaps of drug response (viability) to afatinib, (**D**) selumetinib, (**E**) afatinib plus selumetinib, (**F**) SCH772984, (**G**) SCH772984 plus selumetinib, (**H**) vemurafenib and (**I**) vemurafenib plus afatinib. Organoids were treated (72 hr) with vehicle (DMSO) or inhibitors targeting the EGFR-RAS-ERK pathway (5 nM – 30 μM range, in 14 logarithmic intervals). Red represents maximal cell death and green represents maximal viability. Drug names and their nominal targets are indicated above, the MAPK mutant status per line at the left and the corresponding PDO line at the right. RPM organoids are indicated in red font. Average of 2 technical replicates.

SUPPLEMENTARY TABLES

Supplementary Table 1. Differential Gene Expression Analysis on P18T and RPM organoid lines (afatinib versus DMSO treatment; provided separately due to size)

Supplementary Table 2. Differential Gene Expression Analysis in unperturbed P18T and RPM organoid lines (RPM versus P18T organoids; provided separately due to size)

Supplementary Table 3. Differential Gene Expression Analysis in afatinib-treated P18T and RPM organoid lines (RPM versus P18T organoids; provided separately due to size)

Supplementary Table 4. Target sites of and sgRNA guide sequences used for the generation of knock-in organoids.

Target site	Guide sequence
KRAS intron	AATATGCATATTACTGGTGC
NRAS intron	GTCTCTCACTTGTCGGATCA
BRAF intron	TAGTAACTCAGCAGCATCTC

REFERENCES

1. Malumbres M, Barbacid M. RAS oncogenes: the first 30 years. *Nat Rev Cancer*. 2003;3:459. https://doi.org/10.1038/nrc1097.
2. Downward J. Targeting RAS signalling pathways in cancer therapy. *Nat Rev Cancer*. 2003. doi:10.1038/nrc969
3. Roskoski R. The ErbB/HER family of protein-tyrosine kinases and cancer. *Pharmacol Res*. 2014. doi:10.1016/j.phrs.2013.11.002
4. Yaeger R, Chatila WK, Lipsyc MD, et al. Clinical Sequencing Defines the Genomic Landscape of Metastatic Colorectal Cancer. *Cancer Cell*. 2018. doi:10.1016/j.ccell.2017.12.004
5. Muzny DM, Bainbridge MN, Chang K, et al. Comprehensive molecular characterization of human colon and rectal cancer. *Nature*. 2012;487(7407):330-337. doi:10.1038/nature11252
6. Cox AD, Der CJ. Ras history: The saga continues. *Small GTPases*. 2010;1(1):2-27. doi:10.4161/sgtp.1.1.12178
7. Fiorucci G, Hall A. All three human ras genes are expressed in a wide range of tissues. *BBA - Gene Struct Expr*. 1988;950(1):81-83. doi:10.1016/0167-4781(88)90076-0
8. Leon J, Guerrero I, Pellicer A. Differential expression of the ras gene family in mice. *Mol Cell Biol*. 2015;7(4):1535-1540. doi:10.1128/mcb.7.4.1535
9. Hobbs GA, Der CJ, Rossman KL. RAS isoforms and mutations in cancer at a glance. *J Cell Sci*. 2016;129(7):1287-1292. doi:10.1242/jcs.182873
10. Johnson CW, Reid D, Parker JA, et al. The small GTPases K-Ras, N-Ras, and H-Ras have distinct biochemical properties determined by allosteric effects. *J Biol Chem*. 2017;292(31):12981-12993. doi:10.1074/jbc.M117.778886
11. Castellano E, Santos E. Functional specificity of Ras isoforms: So similar but so different. *Genes and Cancer*. 2011;2(3):216-231. doi:10.1177/1947601911408081
12. Cox AD, Fesik SW, Kimmelman AC, Luo J, Der CJ. Drugging the undruggable RAS: Mission Possible? *Nat Rev Drug Discov*. 2014;13(11):828-851. doi:10.1038/nrd4389
13. De Roock W, Claes B, Bernasconi D, et al. Effects of KRAS, BRAF, NRAS, and PIK3CA mutations on the efficacy of cetuximab plus chemotherapy in chemotherapy-refractory metastatic colorectal cancer: A retrospective consortium analysis. *Lancet Oncol*. 2010. doi:10.1016/S1470-2045(10)70130-3
14. Ogura T, Kakuta M, Yatsuoka T, et al. Clinicopathological characteristics and prognostic impact of colorectal cancers with NRAS mutations. *Oncol Rep*. 2014;32(1):50-56. doi:10.3892/or.2014.3165
15. Cercek A, Braghiroli MI, Chou JF, et al. Clinical features and outcomes of patients with colorectal cancers harboring NRAS mutations. *Clin Cancer Res*. 2017;23(16):4753-4760. doi:10.1158/1078-0432.CCR-17-0400
16. Schirripa M, Cremolini C, Loupakis F, et al. Role of NRAS mutations as prognostic and predictive markers in metastatic colorectal cancer. *Int J Cancer*. 2015;136(1):83-90. doi:10.1002/ijc.28955
17. Haigis KM, Kendall KR, Wang Y, et al. Differential effects of oncogenic K-Ras and N-Ras on proliferation, differentiation and tumor progression in the colon. *Nat Genet*. 2008;40(5):600-608. doi:10.1038/ng.115
18. Douillard J-Y, Oliner KS, Siena S, et al. Panitumumab–FOLFOX4 Treatment and RAS Mutations in Colorectal Cancer . *N Engl J Med*. 2013;369(11):1023-1034. doi:10.1056/nejmoa1305275
19. Karapetis CS, Khambata-Ford S, Jonker DJ, et al. *K-ras* Mutations and Benefit from Cetuximab in Advanced Colorectal Cancer. *N Engl J Med*. 2008. doi:10.1056/NEJMoa0804385
20. Mao C, Huang YF, Yang ZY, Zheng DY, Chen JZ, Tang JL. KRAS p.G13D mutation and codon 12 mutations are not created equal in predicting clinical outcomes of cetuximab in metastatic colorectal cancer: A systematic review and meta-analysis. *Cancer*. 2013;119(4):714-721. doi:10.1002/cncr.27804
21. De Roock W, Jonker DJ, Di Nicolantonio F, et al. Association of KRAS p.G13D mutation with outcome in patients with chemotherapy-refractory metastatic colorectal cancer treated with cetuximab. *JAMA - J Am Med Assoc*. 2010. doi:10.1001/jama.2010.1535
22. Tejpar S, Celik I, Schlichting M, Sartorius U, Bokemeyer C, Van Cutsem E. Association of KRAS G13D tumor mutations with outcome in patients with metastatic colorectal cancer treated with first-line chemotherapy with or without cetuximab. *J Clin Oncol*. 2012;30(29):3570-3577. doi:10.1200/JCO.2012.42.2592
23. Summers MG, Smith CG, Maughan TS, Kaplan R, Escott-Price V, Cheadle JP. BRAF and NRAS locus-specific variants have different outcomes on survival to colorectal cancer. *Clin Cancer Res*. 2017;23(11):2742-2749. doi:10.1158/1078-0432.CCR-16-1541
24. Rosenberg DW, Yang S, Pleau DC, et al. Mutations in BRAF and KRAS differentially distinguish serrated versus non-serrated hyperplastic aberrant crypt foci in humans. *Cancer Res*. 2007;67(8):3551-3554. doi:10.1158/0008-5472.CAN-07-0343
25. Van De Wetering M, Francies HE, Francis JM, et al. Prospective derivation of a living organoid biobank of

colorectal cancer patients. *Cell*. 2015. doi:10.1016/j.cell.2015.03.053
26. Roerink SF, Young MD, Alexandrov B, et al. Intra-tumour diversification in colorectal cancer at the single-cell level. *Nature*. 2018;556:457-462. doi:10.1038/s41586-018-0024-3
27. Vlachogiannis G, Hedayat S, Vatsiou A, et al. Patient-derived organoids model treatment response of metastatic gastrointestinal cancers. *Science (80-)*. 2018. doi:10.1126/science.aao2774
28. Verissimo CS, Overmeer RM, Ponsioen B, et al. Targeting mutant RAS in patient-derived colorectal cancer organoids by combinatorial drug screening. *Elife*. 2016. doi:10.7554/elife.18489
29. Post JB, Hami N, Mertens AEE, Elfrink S, Bos JL, Snippert HJG. CRISPR-induced RASGAP deficiencies in colorectal cancer organoids reveal that only loss of NF1 promotes resistance to EGFR inhibition. *Oncotarget*. 2019. doi:10.18632/oncotarget.26677
30. De Roock W, Claes B, Bernasconi D, et al. Effects of KRAS, BRAF, NRAS, and PIK3CA mutations on the efficacy of cetuximab plus chemotherapy in chemotherapy-refractory metastatic colorectal cancer: A retrospective consortium analysis. *Lancet Oncol*. 2010;11(8):753-762. doi:10.1016/S1470-2045(10)70130-3
31. Van Cutsem E, Köhne CH, Láng I, et al. Cetuximab plus irinotecan, fluorouracil, and leucovorin as first-line treatment for metastatic colorectal cancer: Updated analysis of overall survival according to tumor KRAS and BRAF mutation status. *J Clin Oncol*. 2011;29(15):2011-2019. doi:10.1200/JCO.2010.33.5091
32. Diaz LA, Sausen M, Fisher GA, Velculescu VE. Insights into therapeutic resistance from whole-genome analyses of circulating tumor DNA. *Oncotarget Oncotarget Oncotarget*. 2013;44(4):1856-1857. doi:10.18632/oncotarget.1486
33. Yonesaka K, Zejnullahu K, Okamoto I, et al. Activation of ERBB2 signaling causes resistance to the EGFR-directed therapeutic antibody cetuximab. *Sci Transl Med*. 2011. doi:10.1126/scitranslmed.3002442
34. de Bruin EC, Cowell C, Warne PH, et al. Reduced NF1 expression confers resistance to EGFR inhibition in lung cancer. *Cancer Discov*. 2014;4(5):606-619. doi:10.1158/2159-8290.CD-13-0741
35. Misale S, Di Nicolantonio F, Sartore-Bianchi A, Siena S, Bardelli A. Resistance to Anti-EGFR therapy in colorectal cancer: From heterogeneity to convergent evolution. *Cancer Discov*. 2014;4(11):1269-1280. doi:10.1158/2159-8290.CD-14-0462
36. Turke AB, Song Y, Costa C, et al. MEK inhibition leads to PI3K/AKT activation by relieving a negative feedback on ERBB receptors. *Cancer Res*. 2012;72(13):3228-3237. doi:10.1158/0008-5472.CAN-11-3747
37. Lamba S, Russo M, Sun C, et al. RAF Suppression Synergizes with MEK Inhibition in KRAS Mutant Cancer Cells. *Cell Rep*. 2014;8(5):1475-1483. doi:10.1016/j.celrep.2014.07.033
38. Infante JR, Fecher LA, Falchook GS, et al. Safety, pharmacokinetic, pharmacodynamic, and efficacy data for the oral MEK inhibitor trametinib: a phase 1 dose-escalation trial. *Lancet Oncol*. 2012;13(8):773-781. doi:10.1016/S1470-2045(12)70270-X
39. Prahallad A, Sun C, Huang S, et al. Unresponsiveness of colon cancer to BRAF(V600E) inhibition through feedback activation of EGFR. *Nature*. 2012;483(7387):100-104. doi:10.1038/nature10868
40. Corcoran RB, Dias-Santagata D, Bergethon K, Iafrate AJ, Settleman J, Engelman JA. BRAF gene amplification can promote acquired resistance to MEK inhibitors in cancer cells harboring the BRAF V600E mutation. *Sci Signal*. 2010;3(149). doi:10.1126/scisignal.2001148
41. Corcoran RB, Ebi H, Turke AB, et al. EGFR-mediated reactivation of MAPK signaling contributes to insensitivity of BRAF-mutant colorectal cancers to RAF inhibition with vemurafenib. *Cancer Discov*. 2012;2(3):227-235. doi:10.1158/2159-8290.CD-11-0341
42. Kopetz S, Desai J, Chan E, et al. Phase II pilot study of vemurafenib in patients with metastatic BRAF-mutated colorectal cancer. *J Clin Oncol*. 2015;33(34):4032-4038. doi:10.1200/JCO.2015.63.2497
43. Corcoran RB, Andre T, Atreya CE, et al. Research article combined BRAF, EGFR, and MEK inhibition in patients with BRAF V600E -mutant colorectal cancer. *Cancer Discov*. 2018;8(4):428-443. doi:10.1158/2159-8290.CD-17-1226
44. Verissimo CS, Overmeer RM, Ponsioen B, et al. Targeting mutant RAS in patient-derived colorectal cancer organoids by combinatorial drug screening. *Elife*. 2016. doi:10.7554/eLife.18489
45. Schumacher D, Andrieux G, Boehnke K, et al. Heterogeneous pathway activation and drug response modelled in colorectal-tumor-derived 3D cultures. *PLoS Genet*. 2019;15(3):e1008076. doi:10.1371/journal.pgen.1008076
46. Fujii M, Shimokawa M, Date S, et al. A Colorectal Tumor Organoid Library Demonstrates Progressive Loss of Niche Factor Requirements during Tumorigenesis. *Cell Stem Cell*. 2016;18(6):827-838. doi:10.1016/j.stem.2016.04.003
47. Matano M, Date S, Shimokawa M, et al. Modeling colorectal cancer using CRISPR-Cas9-mediated engineering of human intestinal organoids. *Nat Med*. 2015. doi:10.1038/nm.3802
48. Drost J, Van Jaarsveld RH, Ponsioen B, et al. Sequential cancer mutations in cultured human intestinal stem cells. *Nature*. 2015;521(7550):43-47. doi:10.1038/nature14415
49. Burgess MR, Hwang E, Mroue R, et al. KRAS Allelic Imbalance Enhances Fitness and Modulates MAP

Kinase Dependence in Cancer. *Cell*. 2017;168(5):817-829.e15. doi:10.1016/j.cell.2017.01.020
50. Lampson BL, Pershing NLK, Prinz JA, et al. Rare codons regulate KRas oncogenesis. *Curr Biol*. 2013;23(1):70-75. doi:10.1016/j.cub.2012.11.031
51. Weyandt JD, Carney JM, Pavlisko EN, Xu MM, Counter CM. Isoform-Specific effects of wild-type ras genes on carcinogen-Induced lung tumorigenesis in mice. *PLoS One*. 2016;11(12):1-11. doi:10.1371/journal.pone.0167205
52. To MD, Rosario RD, Westcott PMK, Banta KL, Balmain A. Interactions between wild-type and mutant Ras genes in lung and skin carcinogenesis. *Oncogene*. 2013;32(34):4028-4033. doi:10.1038/onc.2012.404
53. Li Q, Haigis KM, McDaniel A, et al. Hematopoiesis and leukemogenesis in mice expressing oncogenic Nras G12D from the endogenous locus. *Blood*. 2011;117(6):2022-2032. doi:10.1182/blood-2010-04-280750
54. Kruspig B, Monteverde T, Neidler S, et al. The ERBB network facilitates KRAS-driven lung tumorigenesis. *Sci Transl Med*. 2018. doi:10.1126/scitranslmed.aao2565
55. Moll HP, Pranz K, Musteanu M, et al. Afatinib restrains K-RAS-driven lung tumorigenesis. *Sci Transl Med*. 2018. doi:10.1126/scitranslmed.aao2301
56. Misale S, Arena S, Lamba S, et al. Blockade of EGFR and MEK Intercepts Heterogeneous Mechanisms of Acquired Resistance to Anti-EGFR Therapies in Colorectal Cancer. *Sci Transl Med*. 2014;6(224):224ra26-224ra26. doi:10.1126/scitranslmed.3007947
57. Ahronian LG, Corcoran RB. Effective MAPK Inhibition is critical for therapeutic responses in colorectal cancer with BRAF mutations. *Mol Cell Oncol*. 2016;3(1):1-3. doi:10.1080/23723556.2015.1048405
58. Sachs N, de Ligt J, Kopper O, et al. A Living Biobank of Breast Cancer Organoids Captures Disease Heterogeneity. *Cell*. 2018;172(1-2):373-386.e10. doi:10.1016/j.cell.2017.11.010
59. Tiriac H, Belleau P, Engle DD, et al. Organoid profiling identifies common responders to chemotherapy in pancreatic cancer. *Cancer Discov*. 2018;8(9):1112-1129. doi:10.1158/2159-8290.CD-18-0349
60. Metastatic C, Roock W De, Jonker DJ, Nicolantonio F Di, Sartore-bianchi A, Simes J. Association of KRAS p . G13D Mutation With Outcome in Patients With Chemotherapy-RefractoryMetastatic Colorectal Cancer Treated With Cetuximab. *JAMA*. 2013;304(16):1812-1820.
61. Poulin EJ, Bera AK, Lu J, et al. Tissue-specific oncogenic activity of K-RasA146T. *Cancer Discov*. April 2019:CD-18-1220. doi:10.1158/2159-8290.CD-18-1220
62. Morkel M, Riemer P, Bläker H, Sers C. Similar but different: distinct roles for KRAS and BRAF oncogenes in colorectal cancer development and therapy resistance. *Oncotarget*. 2015;6(25):20785-20800. doi:10.18632/oncotarget.4750
63. Van Emburgh BO, Arena S, Siravegna G, et al. Acquired RAS or EGFR mutations and duration of response to EGFR blockade in colorectal cancer. *Nat Commun*. 2016;7:1-9. doi:10.1038/ncomms13665
64. Gamba S, Camaj P, Heinemann V, et al. Effect of KRAS exon 2 mutations on antitumor activity of afatinib and gefitinib. *Anticancer Drugs*. 2015;26(4):371-378. doi:10.1097/CAD.0000000000000196
65. Sepulveda AR, Hamilton SR, Allegra CJ, et al. Molecular biomarkers for the evaluation of colorectal cancer: Guideline from the American society for clinical pathology, college of American pathologists, association for molecular pathology, and American society of clinical oncology. *Arch Pathol Lab Med*. 2017;141(5):625-657. doi:10.5858/arpa.2016-0554-CP
66. Gupta R, Sinha S, Paul RN. The impact of microsatellite stability status in colorectal cancer. *Curr Probl Cancer*. 2018;42(6):548-559. doi:10.1016/j.currproblcancer.2018.06.010
67. Smith MJ, Neel BG, Ikura M. NMR-based functional profiling of RASopathies and oncogenic RAS mutations. *Proc Natl Acad Sci*. 2013;110(12):4574-4579. doi:10.1073/pnas.1218173110
68. Hunter JC, Manandhar A, Carrasco MA, Gurbani D, Gondi S, Westover KD. Biochemical and Structural Analysis of Common Cancer-Associated KRAS Mutations. *Mol Cancer Res*. 2015;13(9):1325-1335. doi:10.1007/s40520-017-0795-7
69. Chen CC, Er TK, Liu YY, et al. Computational Analysis of KRAS Mutations: Implications for Different Effects on the KRAS p.G12D and p.G13D Mutations. *PLoS One*. 2013;8(2):6-13. doi:10.1371/journal.pone.0055793
70. Posch C, Sanlorenzo M, Vujic I, et al. Phosphoproteomic Analyses of NRAS(G12) and NRAS(Q61) Mutant Melanocytes Reveal Increased CK2α Kinase Levels in NRAS(Q61) Mutant Cells. *J Invest Dermatol*. 2016;136(10):2041-2048. doi:10.1016/j.jid.2016.05.098
71. Pershing NLK, Macalpine DM, Counter M, et al. Rare codons capacitate Kras -driven de novo tumorigenesis Find the latest version : Rare codons capacitate Kras -driven de novo tumorigenesis. 2015;125(1):222-233. doi:10.1172/JCI77627.Creation
72. Moll HP, Pranz K, Musteanu M, et al. Afatinib restrains K-RAS-driven lung tumorigenesis. *Sci Transl Med*. 2018;10(44):1-13. doi:10.1126/scitranslmed.aao2301
73. Fujii M, Shimokawa M, Date S, et al. A Colorectal Tumor Organoid Library Demonstrates Progressive Loss of Niche Factor Requirements during Tumorigenesis. *Cell Stem Cell*. 2016;18(6):827-838. doi:10.1016/j.

stem.2016.04.003
74. Love MI, Huber W, Anders S. Moderated estimation of fold change and dispersion for RNA-seq data with DESeq2. *Genome Biol*. 2014. doi:10.1186/s13059-014-0550-8
75. Garvin T, Aboukhalil R, Kendall J, et al. Interactive analysis and assessment of single-cell copy-number variations. *Nat Methods*. 2015. doi:10.1038/nmeth.3578
76. Postma M, Goedhart J. Plotsofdata—a web app for visualizing data together with their summaries. *PLoS Biol*. 2019. doi:10.1371/journal.pbio.3000202

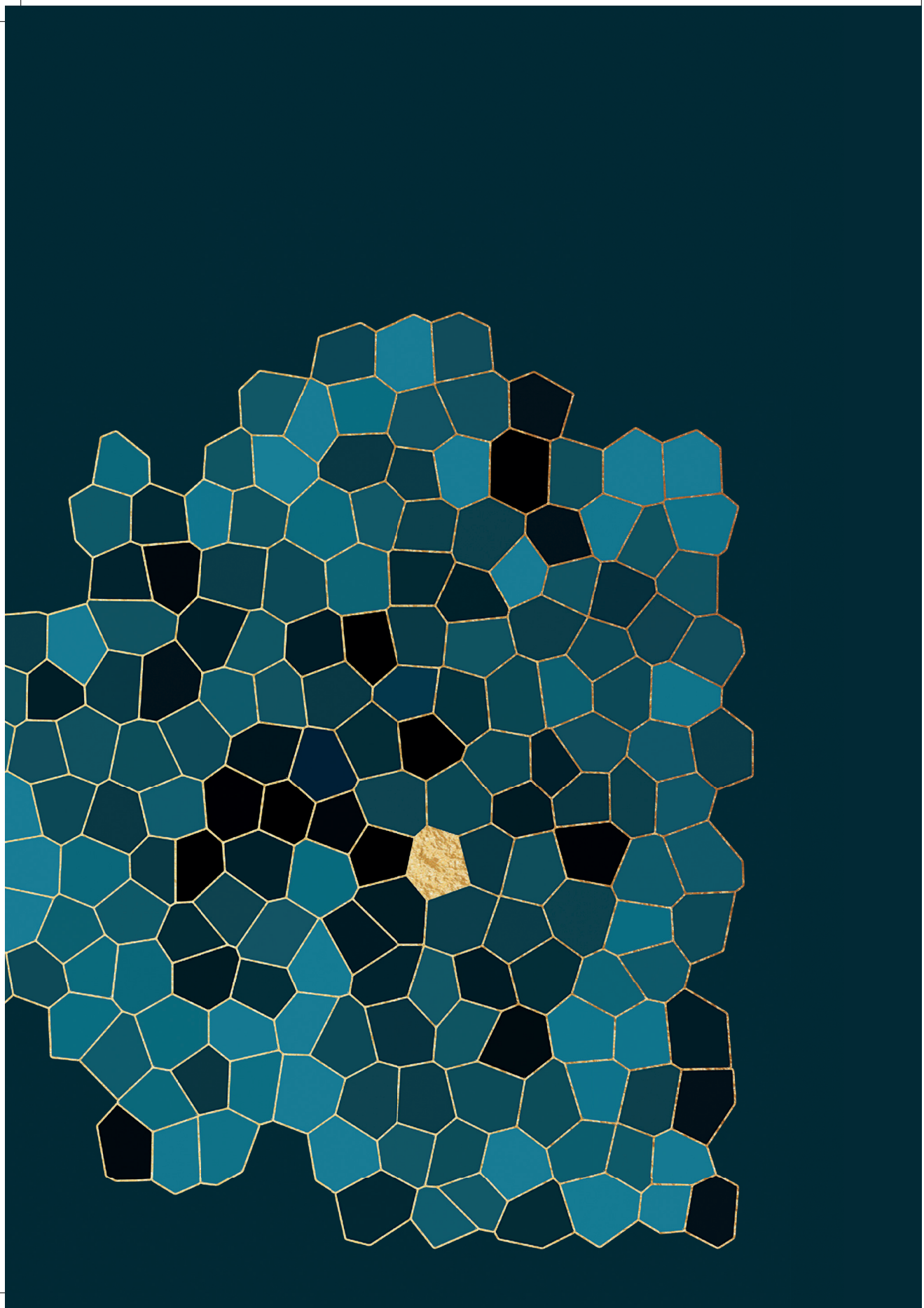

CHAPTER 6

SUMMARY & DISCUSSION

SUMMARY

The RAS family of small GTPases signal downstream of the epidermal growth factor receptor (EGFR) to induce the activation of a range of downstream signaling cascades, thereby regulating cell proliferation, migration, differentiation and survival[1,2]. Activating mutations in *RAS* are frequently detected in metastatic colorectal cancer (mCRC) patients (35-50%)[3] (COSMIC database) and are associated with resistance to EGFR inhibition[4,5]. As a consequence, this has led to the exclusion of RAS mutant mCRC patients from targeted therapy against the EGFR[6,7]. Besides oncogenic *RAS*, other genetic alterations that result in the aberrant activation of MAPK signaling, such as oncogenic mutations in *BRAF* (11%)[8–10] and *HER2* (2.7%)[11,12] and *MET* (7%)[11] amplifications, are also frequently found in mCRC and associated with anti-EGFR therapy resistance. Despite the overlapping effects of various MAPK pathway activating mutations, an increasing amount of evidence indicates that different oncogenic MAPK pathway mutations can have distinct effects on CRC development, progression and therapy response[13–22]. Better understanding of genotype-phenotype correlations will improve patient stratification for optimal treatment regimens. In this thesis, we used CRC patient-derived organoids (CRC PDOs) to investigate the similarities and discrepancies between various MAPK pathway mutations on cancer progression, niche independence, and therapy resistance.

Observations that are indicative that not all mutations in RAS isoforms and BRAF have equal outcome in mCRC was extensively described in **chapter 1**. This review outlines various sources of evidence that indicate that the current stratification of mCRC patients for treatment regimens, predominantly based on *RAS* and *BRAF* mutant status, might be too simplistic. Other factors besides the presence of oncogenic *RAS* status, such as isoform- and codon-specific mutations, should also be included. In addition, we describe the utility of CRC PDO biobanks and the CRISPR technology as physiological relevant cancer model systems to study and cross-compare oncogenic *RAS* and *BRAF* variants that change in isoform and codon specificity.

Subsequently, in **chapter 2** we provided a practical guide to optimize efficient engineering of isogenic cell as well as organoid lines expressing different oncogenes at endogenous expression levels. Several different strategies can be applied to introduce oncogenic mutations via CRISPR-induced homologous recombination (HR) and the preferred mode of integration, in particular towards oncogenes, strongly depends on the research question to be answered.

First, to investigate the effects of different oncogenic mutations during early tumorigenesis, we strongly advise to recreate heterozygous mutations by targeting the intronic region downstream of the exon of interest. Via this strategy, the allele that is not repaired by HR remains intact, which is reminiscent of the heterozygous oncogene expression in early stage cancer. This is important as allelic imbalance of the *KRAS* allele enhances its oncogenic potential and is observed during malignant transformation[3,23–26].

Second, the use of selection strategies that do not depend on niche growth factor depletion allows to study the intrinsic effects of different oncogenes on cancer progression and therapy resistance. For example, niche growth factor depletion and drug screening experiments on CRC PDOs showed that dependence on EGFR signaling was still observed in a fraction *KRAS*

mutant organoids[27–31] (**chapter 5**). In contrast, CRISPR-engineered *KRAS* mutant organoids can be selected by EGF-independent growth[29], but are then selected on a potential extreme phenotype.

Last, niche factor dependent selection strategies can be instrumental to screen the potential of multiple MAPK pathway mutations as strong oncogenic drivers of EGF independence and tumor progression. This approach revealed that partial EGF dependence as observed in *KRAS* mutant intestinal organoids was completely abolished in the co-presence of oncogenic PI3K mutations[28].

The last approach was used in **chapter 3** to screen whether RASGAP deficiencies can promote independence to EGFR signaling in CRC PDOs. Surprisingly, this strategy elucidated that the loss of only one out of nine expressed RASGAP isoforms, i.e. NF1, with a functional RASGAP domain was able to drive intrinsic resistance to EGFR inhibition. However, NF1-deficient CRC PDOs still showed responsiveness to EGFR inhibition, demonstrated by decreased organoid growth and ERK activation under limited EGF-induced signaling. Moreover, the effect of NF1 loss was less robust than activating mutations in *KRAS*. We hypothesized that this is the result of an increased ratio of total active RAS proteins in *KRAS* mutant over NF1-deficient organoids, with the latter only affecting the small subfraction of RAS proteins present near the activated EGFR. In contrast to autonomous signaling by oncogenic KRAS, the oncogenic effect of NF1 loss mainly manifested itself by amplifying the activity of RAS-MAPK signaling, as the effects on ERK activation and organoid growth were only observed in the presence of EGFR signaling. Together, these findings indicate that RASGAP functioning determines sensitivity towards EGF-dependent signaling in mCRC.

In **chapter 4**, we describe *BRAF* fusion genes. In particular, the specific effects on BRAF kinase activity that is imposed by gene fusion partners, other than simply replacing the autoinhibitory domain. Different *BRAF* fusion genes, as detected in mCRC patients, influenced BRAF localization and efficacy of downstream MAPK pathway activation. As a result, BRAF fusions residing at the plasma membrane (i.e. DLG1-BRAF), induced increased levels of downstream ERK activation compared to other BRAF oncogene variants. In addition, RNA sequencing of CRC organoids with various BRAF oncogenic fusion proteins revealed overlapping as well as distinct downstream signaling pathways. Importantly, all *BRAF* fusion genes conferred resistance to EGFR inhibition through sustained ERK activation. Detection of *BRAF* fusion genes should therefore be included in genetic screening of mCRC patients to avoid unnecessary anti-EGFR therapy.

Unfortunately, the high complexity of oncogenic fusion genes, together with minimal efficiency to delete large DNA fragments in organoids refrained us from applying genetic engineering to create endogenously expressed *BRAF* fusions. Although *in vitro* generation of fusion genes has been reported in cell lines[32], these approaches required niche factor depletion selection strategies, which can bias the generation towards EGF-independent *BRAF* fusion genes.

Intrinsic effects of a single oncogenic mutation in the RAS pathway (i.e. $KRAS^{G12D}$, $KRAS^{G13D}$, $NRAS^{G12D}$ and $BRAF^{V600E}$) are described in **chapter 5**. Whereas all CRISPR-engineered RAS pathway mutants induced increased tumor growth due to enhanced RAS-MEK-ERK activity compared to wild-type RAS/BRAF organoids, differential phenotypes were observed between oncogenic MAPK pathway variants. First of all, drug screening showed differential

sensitivities to MAPK pathway inhibition in CRC PDOs with oncogenic *RAS* and *BRAF* mutations. Second, under unperturbed conditions $KRAS^{G13D}$ mutant organoid xenografts exhibited enhanced tumor growth as compared to other MAPK pathway activating mutants, resembling observations from clinical studies in mCRC patients[18,19,33]. Last, both *in vitro* and *in vivo,* EGFR resistance was observed in $KRAS^{G12D}$ and $BRAF^{V600E}$ organoids as compared to $KRAS^{G13D}$, $NRAS^{G12D}$ and parental organoids. Resistance to EGFR inhibition in RAS mutant organoids correlated with sustained levels of residual activated ERK, underscoring that different *RAS* mutations induce different sensitivities to MAPK inhibition.

We will discuss our findings in the next section and describe how different mechanisms may be implicated in the regulation of MAPK pathway activation in CRC.

DISCUSSION

ONCOGENE-DEPENDENT MAPK PATHWAY ACTIVATION

The correlation between MAPK pathway activity and tumor outgrowth observed in **chapter 3** and **5** indicates that the level of MAPK pathway activity dictates the degree of cell proliferation and tumor growth. Our findings and results from other studies show that this can occur in an oncogene-dependent and -independent manner.

1. RAS oncogene-dependent MAPK pathway activity

The accelerated tumor growth observed in the presence of *KRAS*^{G13D} mutations, compared to other oncogenic *RAS* mutations, indicates that tumor growth is oncogene-specific (**chapter 5**). In support of this, genetic mouse models have shown that endogenous expression of *KRAS*^{G12D} in the intestine induced increased proliferation and decreased differentiation as compared to *KRAS*^{A146T} and *NRAS*^{G12D} oncogenes[13,14] by enhanced levels of ERK activation[13,14] (**Figure 1A**). Divergent phenotypes were also observed with different oncogenic *KRAS* and *NRAS* variants in genetic mouse studies on myeloid and lymphoid malignancies[15].

The different transforming potential of oncogenic variants of the same RAS isoform is likely caused by mutation-dependent alteration of sensitivity to RASGEF- and RASGAP-mediated activation and inactivation. For instance, GDP-GTP exchange rates are significantly increased in mutant KRAS^{G13D} proteins as compared to other KRAS mutants, making them less dependent on RASGEF proteins for activation[34,35]. Conversely, the activation of KRAS^{A146T} proteins are more sensitive to GEF- and GAP-mediated regulation compared to KRAS^{G12D} proteins, which can explain their limited transforming potential[14]. Moreover, genome analysis of mCRC patients showed that weak activating mutations in *KRAS*, such as A146T, more often co-occurred with loss-of-function mutations in *NF1*, whereas mutually exclusivity with frequently occurring KRAS (e.g. G12D) mutations was observed[36]. Similar differences might also be true for NRAS mutants, where mutations affecting codon 61 are less prone to GTP hydrolysis compared to codon 12 mutations[21,34,35]. Furthermore, binding affinities for downstream effectors might also be affected by different mutations, since codon 61 mutations show increased RAF binding affinity compared to G12D or G12V mutations[35]. Consistent with this, phosphoproteomic analysis of melanocytes revealed that different NRAS oncogenes activated different downstream signaling pathways. Expression of NRAS^{Q61L} proteins increased MAPK pathway activation, whereas NRAS^{G12V} proteins induced PI3K signaling. Moreover, NRAS codon 12 mutants were found to harbor additional low activating BRAF mutations to increase MAPK signaling[37]. Together, this suggests that the degree by which different RAS mutants can activate the MAPK pathway determines their oncogenic potential. Co-occurrence of weak mutant variants within the MAPK pathway are thus evolutionary advantageous to generate sufficient downstream MAPK activity, in contrast to semi-autonomous driver mutations like codon 61 in *NRAS* (**Figure 1A-B**). This is consistent with our observation in **chapter 5**, where we find that *KRAS* codon 12 and 13 mutations induce higher levels of activated RAS proteins compared to *NRAS* codon 12 mutants and can explain the preference of codon 12 and 13 mutations in *KRAS* over *NRAS*.

Although structural differences between oncogenic variants of the same RAS isoform are informative to understand downstream signaling and transformative capacity, the functional differences between oncogenic RAS isoforms is more complex. Whereas both KRAS and NRAS proteins are expressed in the gut[13,38], they seem to have different effects on downstream signaling cascades. It has been shown that the expression of $KRAS^{G12D}$ oncogenes in the crypt can drive hyperplasia by enhancing MAPK pathway activity, while the expression of $NRAS^{G12D}$ oncogenes provide a protective role by suppressing apoptosis via RAF-STAT3 signaling. Furthermore, the different effects of oncogenic RAS isoforms seem to be context-dependent, as $NRAS^{G12D}$ oncogenes were only able to drive colorectal tumorigenesis upon inflammation, but not upon the loss of APC expression[13,39]. Consistent with this, we observed that oncogenic G12D knock-in mutations in *KRAS* as well as *NRAS* in CRC PDOs promote tumor growth as compared to their parental RAS^{WT} CRC PDOs.

Differences in signaling between RAS isoforms can be explained by their distinct membrane localization, mode of activation and tissue-dependent expression levels. The different hypervariable regions (HVR) of RAS proteins causes RAS isoforms to localize to distinct regions in the membrane. Whereas KRAS molecules are localized to negatively charged non-ordered membrane domains, N- and HRAS proteins reside in highly ordered lipid raft microdomains[40,41]. This might result in their distinct interaction with upstream receptors and downstream effectors that are also recruited to dedicated locations in the membrane. For instance, it has been reported that EGFR migrates away from lipid rafts upon activation[42,43], possibly resulting in increased activation of nearby KRAS molecules at the expense of NRAS proteins. It is possible that other receptors residing in different compartments of the plasma membrane are better in activating NRAS. Consistent with this, differential sensitivities to different cytokines has been observed between $KRAS^{G12D}$ and $NRAS^{G12D}$ myeloid cells[15]. Furthermore, genetic mouse studies revealed that the anti-apoptotic effects of mutant NRAS proteins in CRC is specified by its localization as the replacement the HVR of HRAS with that of NRAS also suppressed apoptosis[44].

Besides their localization in the membrane, location- and tissue-dependent expression might also explain the different oncogenic potentials of RAS isoforms. For instance, a higher incidence of NRAS mutations is found in the left versus right colon[17,22,45,46], which correlates with enhanced expression of EGFR, HER2 and activating ligands[47–50] and suggests that NRAS mutant proteins are still partially dependent on upstream receptor activation. In addition, the relative expression of NRAS in the gut is much lower than in the lymphatic system[51,52], which might explain the increased proportion of NRAS mutations in RAS mutant chronic lymphocytic leukaemia[53]. A similar explanation might also hold true for the increased incidence of NRAS mutations compared to KRAS mutations in melanoma[52,53], where $NRAS^{G12V}$ overexpression exhibited increased tumorigenic potentials compared to $KRAS^{G12V}$ [54]. Contrarily, endogenous expression of $NRAS^{G12D}$ in melanocytes did not show increased tumor growth compared $KRAS^{G12D}$ mutant melanocytes[21], again indicating that the level of RAS isoform expression also determines their transformative capacity (**Figure 1C**).

2. RASGAP-dependent MAPK pathway activity

Similar to oncogenic RAS variants, the loss of different RASGAPs also impacts cell proliferation to different levels. The accelerated growth of *NF1* null CRC PDOs compared to

RASA1 null CRC PDOs correlated with their level of RAS-ERK signaling activity, suggesting that RASGAP-regulated MAPK activity levels determines the rate of proliferation. However, loss of NF1 turned out to be a weaker activator of downstream MAPK signaling activity as compared to autonomous $KRAS^{G12D}$ and still required some EGF-signaling input (**chapter 3**) (**Figure 1A**). Indeed, mCRC genome analysis showed that *NF1* truncating mutations often co-occurred with less frequent or weak activating mutations in *KRAS*, *HRAS*, *EGFR*, *HER2* and *MET*[36]. This is in line with other studies reporting that the loss of NF1, as well as other mutations in GEFs and GAPs, often co-occur with non-canonical mutations in *RAS* and *BRAF*, thereby increasing their combined MAPK signaling output[55–57]. Together, this underscores that multiple weak MAPK pathway activating mutations co-occur to obtain sufficient levels of MAPK signaling (**Figure 1A-B**).

Although deficiency of NF1 was sufficient to promote EGF independence in CRC PDOs (**chapter 3**), this does not rule out that other RASGAPs can partially restore the loss of GAP activity. This would suggest that the co-deletion of multiple RASGAPs might generate a sufficient degree of EGF independence, which is supported by few cases of co-occurring mutations in *NF1* and *RASA1* truncating mutations in mCRC[36] (**Figure 1A-B**). Similar observations have also been described for other cancers, showing that *NF1* mutations frequently co-occurr with other mutations in GEFs, EGFR, and negative feedback regulators, such as GAPs and dual-specificity phosphatases (DUSPs)[55,58,59]. Potentially, the co-deletion of *RASA1* and *NF1* could increase EGF independence in CRC PDOs, which would be consistent with the synergistic effects on developmental disease phenotypes as well as cancer progression upon loss of expression of both RASA1 and NF1 in mice[60,61].

Although above observations point towards partially redundant effects of RASGAPs, other studies favor nonoverlapping roles for RASGAPs[62]. In support of this notion, RAS binding affinity assays show that NF1 has increased binding affinity for RAS proteins as compared to RASA1[63,64]. Furthermore, RASGAPs also showed distinct GAP activity per RAS isoforms, where NF1 loss caused enhanced GTP loading of KRAS and HRAS, but not NRAS[65]. The loss of RASA1 resulted in increased activity of RRAS, but not K-, H-, or NRAS[66,67]. Cell line-based studies have shown that MAPK pathway activation is induced by H-, N-, and KRAS, whereas RALGDS and PI3K signaling is induced by RRAS proteins, suggesting that NF1 and RASA1 might as such regulate different signaling pathways[68,69]. Simultaneous loss of NF1 and RASA1 might thus promote MAPK as well as PI3K and RALGDS signaling pathways, which combined activation has been shown to effectuate EGF independence in intestinal organoids[28].

Overall, the level of MAPK signaling activity as well as PI3K and RALGDS pathway activation can be fine-tuned by various mutations, where combined activity levels affect the degree of EGF independence and as such stimulate cancer growth and progression.

3. Basal MAPK pathway activation does not influence therapy resistance

Drug screening experiments and analysis of MAPK pathway activaty in patient-derived CRC organoids in **chapter 3**, **4** and **5** showed that the basal level of ERK activity does not correlate with anti-EGFR therapy resistance. In **chapter 3**, we observed that NF1 loss promoted RAS-ERK activation as strong as oncogenic mutations in *KRAS* in the presence of EGF, but was less potent in conferring resistance to EGFR inhibition. In **chapter 4**, we showed that MAPK

activity is induced to different basal levels upon expression of different *BRAF* fusions, but all fusions displayed resistance to anti-EGFR therapy. In **chapter 5**, all oncogenic *RAS* and *BRAF* mutants increased basal MAPK activity, but still displayed differential responses to EGFR inhibition. Similar findings were also observed in a CRC PDO biobank reported by Schumacher et al. (2019)[30], showing that basal MAPK activity in CRC PDOs did not predict therapy response to EGFR inhibitors. For example, they observed that subclones of *KRAS* mutant CRC PDOs displayed varying degrees of basal MAPK pathway activation, which did not correlate with the level of resistance EGFR inhibition. Furthermore, different CRC PDOs exhibited very diverse MAPK pathway activation irrespective of their mutational *RAS* status and resistance phenotype[30].

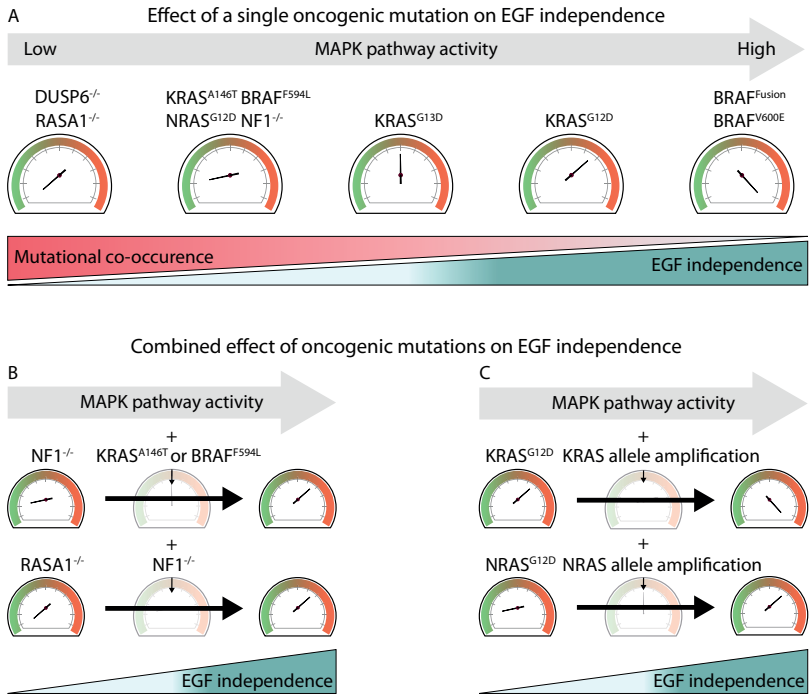

Figure 1. The level of MAPK pathway activation by oncogenic mutations determines oncogene co-occurrence and EGF independence.
(**A**) Schematic overview presenting effects of a single oncogenic mutation on MAPK pathway activity, co-occurrence with other MAPK pathway mutations and EGF independence. CRCs with weak MAPK pathway activating mutations (e.g. *NF1*$^{-/-}$, *NRAS*^{G12D}, *KRAS*^{A146T} and *BRAF*^{594L}) show less EGF-independent growth and higher mutational co-occurrence compared to CRCs with strong MAPK pathway activating mutations (e.g. *KRAS*^{G12D} and *BRAF*$^{V600E\ or\ Fusion}$). (**B**) Schematic overview presenting the combined effects of weak oncogene (as shown in A) co-occurrence on MAPK pathway activity and EGF-independent growth. (**C**) As in (B) showing the net effect of oncogene amplification of strong (*KRAS*) and weak (*NRAS*) MAPK pathway activating mutations on MAPK pathway activity and EGF-independent growth.

ONCOGENE-INDEPENDENT MAPK PATHWAY ACTIVATION

Oncogene-independent effects on EGF independence are supported by the observation that $BRAF^{V600E}$ CRC PDOs show similar responses to MAPK pathway inhibition, but with varying sensitivities (**chapter 5**). Similarly, drug screen experiments on CRC PDOs representative of multiple subclones derived from the same primary tumor showed that differential responses to EGFR inhibition were observed, although all clones contained the same, early on acquired, oncogenic *KRAS* mutation[30,31]. This indicates that other factors besides known oncogenic MAPK pathway mutations, such as copy number variations, epigenetic landscape, cellular tumor composition and the microenvironment, can influence the level of ERK activation.

1. Cell type- and cycle-dependent MAPK pathway activation

Observations from mouse intestinal organoids that express $KRAS^{G12V}$ oncogenes in an inducible manner indicate that the degree of MAPK activation by mutant *KRAS* occurs in a cell type-dependent manner. This difference in MAPK pathway activation was caused by differences in MEK-ERK signal transmission and feedback inhibition. $KRAS^{G12V}$-responsive cells showing high MAPK pathway activity exhibited fast MEK-ERK signal transmission and attenuated feedback inhibition. Conversely, $KRAS^{G12V}$-insensitive cells showed strong feedback inhibition, which was likely caused by increased expression of DUSPs[70] (**Figure 2A**). Similar findings were observed by single-cell signaling analysis of intestinal organoids, demonstrating cell type- as well as cell cycle-dependent MAPK signaling[71]. Similar mechanisms could also explain differential sensitivities to EGFR inhibition found in different CRISPR-engineered monoclonal NF1-deficient and *RAS/BRAF* mutant organoid lines (**chapter 3 and 5**).

2. Tumor environment-dependent MAPK pathway activation

Analysis of MAPK activity in CRC PDOs as well as in CRC tissues showed heterozygous levels of ERK activation irrespective the mutational status of *KRAS* or *BRAF*[30,72]. It was found that cells residing at the leading edge exhibited high ERK and WNT activity, thereby contributing to lineage persistence[72,73]. This heterozygous pattern of ERK activity suggests that MAPK pathway activation can be affected by factors emanating from stromal cells that surround the cells at the leading edge[74]. In support of this, co-culture systems showed that stromal cells could further upregulate signaling pathways that already contained oncogenic mutations like KRAS[71]. Potentially, such stroma might contribute to poor prognosis CRC patients[75]. It is possible that the secretion of growth factors, such as EGF, by stromal cells further increases MAPK pathway activation even in the presence of *KRAS* oncogenes (**Figure 2B**). This is supported by the observation that EGF stimulation of *KRAS* mutant CRC cells results in increased levels of ERK activity, possibly by activating wild-type RAS isoforms[72] (**chapter 3 and 5**).

KRAS oncogene-independent effects on tumor growth has also been observed in subclonal CRC organoid lines derived from the same tumor tissue, which is independent of surrounding factors. Xenograft experiments of these subclones showed slow outgrowth of $KRAS^{G12D/}PIK3CA^{H1047R}/TP53^{C24F}$ mutant organoids and rapid outgrowth of $KRAS^{G12D/}PIK3CA^{H1047R}/TP53^{C24F}/SMAD4^{R361H}$ lines[30]. Intriguingly, this study showed that the degree

of tumor outgrowth was not correlated with the level of ERK activity, with triple mutant organoids displaying high ERK activity and quadruple mutants showing low ERK activity[30]. Together, this indicates that MAPK pathway activity requires a certain threshold level, but that its absolute level does not dictate the strength of cell proliferation. In addition, niche factor depletion experiments in CRC PDOs and genetically engineered intestinal organoids demonstrated that frequent cancer mutations in CRC drive niche growth factor independence, i.e. WNT, EGF and BMP via APC, KRAS and SMAD4, respectively. Together, these mutations combined facilitate engraftment efficiencies at ectopic locations, which is most efficient in quadruple APC/KRAS/TP53/SMAD4 mutant organoid lines. However, differential effects of ERK activity were not assessed.

3. Location-dependent MAPK pathway activation

Single cell analysis of *BRAF* and *KRAS* mutant CRC PDOs (unpublished data) showed that not all cells within one organoid show synchronized and similar levels of ERK activity. This could be explained by the cell cycle phase and cell type[70,71], but might also be influenced by their relative location. A study by Takeda and Kiyokawa (2017)[76] showed that ERK activity was enhanced in intestinal cells residing next to damaged cells, thereby promoting resealing of the damaged area. This suggests that ERK activity can be modulated by spatial cues. Moreover, cell density can even affect the level of ERK activation in a *RAS* or *BRAF* mutated background via phosphatase-dependent regulation[77] (**Figure 2C**). However, it is questionable whether these differences can explain the differences in ERK activity observed in *BRAF* and *KRAS* mutant CRC PDOs, since their growth is less spatially restricted.

Besides the effect of the cellular location within one organoid or crypt, location along the intestinal tract is also likely to modify MAPK pathway activity. The expression of receptors of the HER family and upstream growth factors (like epiregulin and amphiregulin) is elevated in the left versus the right colon[47–50]. This suggests that certain MAPK pathway mutations that are partially dependent on upstream receptor activation, such as $NRAS^{G12D}$, are more abundant in the left compared to the right colon (**Figure 2D**). The outgrowth efficiency of transplanted $NRAS^{G12D}$ mutant CRC PDOs at different locations in the colon (right or left) might give indications about their dependence on tumor location.

Overall, these observations show that RAS-MAPK signaling and tumor growth can be affected irrespective of the mutational status of *RAS* or *BRAF*.

EXPERIMENTAL CANCER MODEL SYSTEMS FOR TESTING DRUG RESPONSE

The use of CRC-derived cell lines has been important for understanding the downstream signaling events by which MAPK pathway mutations drive tumorigenesis and have been widely used as preclinical cancer models for drug screening experiments. The rapid expansion and easy modification of cancer cell lines makes them suitable for high-throughput drug screening experiments and research on therapy resistance. However, in relation to their native tumors the genetic and histological features are significantly changed once cultured in two dimensional (2D) culture systems. As a consequence, many drugs that show promising effects in 2D cell cultures fail in clinical trials[78–83].

Conversely, patient-derived xenograft (PDX) models allows the growth of three dimensional

(3D) tumors that mimics features of the primary tumor and allows *in vivo* drug testing in a relatively physiological environment comprising stromal and immune cells. However, drug testing experiments in PDX models are slow, expensive and only low-throughput[78–80,84]. Consequently, an in-between cancer model such as CRC PDOs can be useful for initial investigation of drug responses *in vitro* before switching to *in vivo* PDX model systems.

The 3D organoid system has shown to faithfully recapitulate the histological and genetic features of their native tumors, and to resemble drug responses observed in patients they were derived from[31,80,85–89]. Moreover, we have shown that CRC PDOs can be genetically manipulated to investigate the direct effect of different MAPK pathway mutations. The organoid system purely consists of tumor cells and lacks the tumor microenvironment. As such, drugs affecting the tumor microenvironment (TME) cannot be scored when solely screening in CRC PDOs[89–91]. In addition, it has been shown that mutant *KRAS* CRCs can also have immunosuppressive effects[92–94], which might in turn affect the outcome of immune therapies. Advances in co-culture systems using CRC PDOs and matched immune cells showed that air-liquid interface PDOs could retain immune cells, which recapitulated PD1-dependent immune responses[90]. However, the derivation and maintenance of CRC PDOs using the air-liquid interface method show some limitations, since tissue architecture and stroma got lost after long-term passaging. Moreover, it still needs to be validated whether treatment outcomes to immunotherapy correlates with patient response. Other studies have also reported the development of additional co-culture systems, like PDOs with matched stromal and immune cells[95]. Further advances will facilitate research on the influence of MAPK pathway mutations on the interaction between tumor tissue and the microenvironment.

CONCLUDING REMARKS

Altogether, the data described in this thesis demonstrated that different oncogenic variants of *RAS*, *RASGAP* and *BRAF* induce different levels of tumor progression and resistance, likely by their mode of MAPK pathway activation. Furthermore, we have shown that CRC PDOs are a relevant model system to investigate therapy response and the effect of low frequency mutations in the MAPK pathway. Differences between endogenously expressed MAPK pathway oncogenes might not have been detected with overexpression strategies[96]. In this era, the fast pace of new technologies that are arising to enhance the efficiency of genetic engineering should aspire researchers to use endogenous oncogene expression methods over oncogene overexpression. In addition, we have encountered mutation-independent effects on MAPK pathway activity and organoid survival, which requires further investigation. Ultimately, therapy responses need to be validated using other PDOs and should be correlated with observations from the clinic in order to improve current stratification of mCRC patients for targeted therapy.

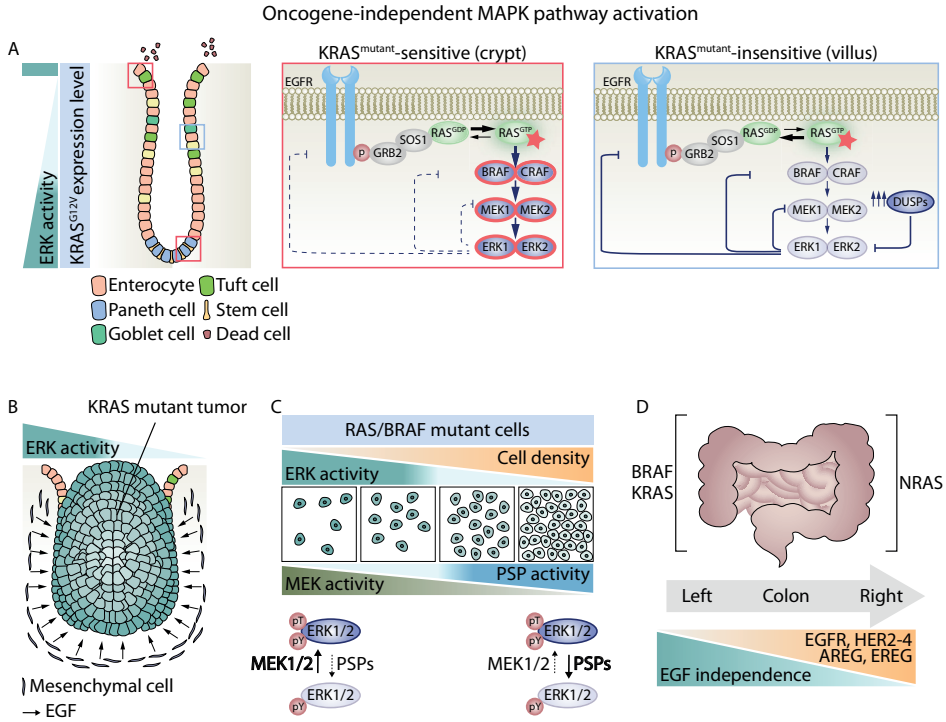

Figure 2. Summary of *RAS/BRAF* mutant-independent effects on MAPK pathway activation.
(**A**) MAPK pathway activity is regulated in a cell type-dependent manner irrespective of *RAS*' mutational state in intestinal organoids. (Left panel) In *KRAS* mutant (KRAS^{MT}) organoids high-to-low ERK activity is observed along the crypt-villus axis, respectively. Gradient at the left displays ERK activity. (Middle panel) KRAS^{MT}-sensitive cells in the crypt (Stem and Paneth cells) and at the top of the villus (cells undergoing apoptosis) show high ERK activity, which is correlated with fast RAS-RAF-MEK-ERK feedforward signaling and slow ERK-MEK-RAF feedback signaling. (Right panel) Towards the villus, low ERK activity is observed in KRAS^{MT}-insensitive cells (differentiated cells), which display slow RAS-RAF-MEK-ERK feedforward signaling and rapid ERK-MEK-RAF feedback signaling, likely caused by the upregulated expression of DUSPs. (**B**) In *RAS* mutant tumors, increased ERK activity is observed in cells residing at the leading edge compared to those in the center of the tumor. The secretion of ligands (e.g. EGF) by stromal cells can enhance EGFR-RAS-ERK pathway activity of *RAS* mutant tumor cells that reside at the rim of the tumor. Gradient at the top and in the tumor displays ERK activity. (**C**) *RAS* and *BRAF* mutant cells display cell density-dependent ERK activation. A decrease in active ERK (tyrosine (Y) and threonine (T) diphosphorylation) and increase in inactive ERK (tyrosine (Y) monophosphorylation) is observed at high cell density, independent of *RAS/BRAF* mutational state. At low cell density, high MEK1/2 activity induces ERK activation, which is reverted by high threonine/serine phosphatase activity (PSP) at high cell density. (**D**) Schematic overview depicting clinical features (EGF independence/anti-EGFR therapy resistance), genetic alterations (*RAS*/*BRAF* mutations) and gene expression patterns (HER family and growth factor expression levels) associated with right- and left-sided CRCs.

REFERENCES

1. Malumbres M, Barbacid M. RAS oncogenes: the first 30 years. *Nat Rev Cancer*. 2003;3:459. https://doi.org/10.1038/nrc1097.
2. Cox AD, Der CJ. Ras history: The saga continues. *Small GTPases*. 2010;1(1):2-27. doi:10.4161/sgtp.1.1.12178
3. Bos JL, Fearon ER, Hamilton SR, et al. Prevalence of ras gene mutations in human colorectal cancers. *Nature*. 1987;327(6120):293-297. doi:10.1038/327293a0
4. Karapetis CS, Khambata-Ford S, Jonker DJ, et al. *K-ras* Mutations and Benefit from Cetuximab in Advanced Colorectal Cancer. *N Engl J Med*. 2008. doi:10.1056/NEJMoa0804385
5. Douillard J-Y, Oliner KS, Siena S, et al. Panitumumab–FOLFOX4 Treatment and RAS Mutations in Colorectal Cancer . *N Engl J Med*. 2013;369(11):1023-1034. doi:10.1056/nejmoa1305275
6. Van Cutsem E, Cervantes A, Adam R, et al. ESMO consensus guidelines for the management of patients with metastatic colorectal cancer. *Ann Oncol*. 2016;27(8):1386-1422. doi:10.1093/annonc/mdw235
7. Sepulveda AR, Hamilton SR, Allegra CJ, et al. Molecular biomarkers for the evaluation of colorectal cancer: Guideline from the American society for clinical pathology, college of American pathologists, association for molecular pathology, and American society of clinical oncology. *Arch Pathol Lab Med*. 2017;141(5):625-657. doi:10.5858/arpa.2016-0554-CP
8. Peeters M, Oliner KS, Parker A, et al. Massively parallel tumor multigene sequencing to evaluate response to panitumumab in a randomized phase III study of metastatic colorectal cancer. *Clin Cancer Res*. 2013;19(7):1902-1912. doi:10.1158/1078-0432.CCR-12-1913
9. Loupakis F, Ruzzo A, Cremolini C, et al. KRAS codon 61, 146 and BRAF mutations predict resistance to cetuximab plus irinotecan in KRAS codon 12 and 13 wild-type metastatic colorectal cancer. *Br J Cancer*. 2009;101(4):715-721. doi:10.1038/sj.bjc.6605177
10. De Roock W, Claes B, Bernasconi D, et al. Effects of KRAS, BRAF, NRAS, and PIK3CA mutations on the efficacy of cetuximab plus chemotherapy in chemotherapy-refractory metastatic colorectal cancer: A retrospective consortium analysis. *Lancet Oncol*. 2010. doi:10.1016/S1470-2045(10)70130-3
11. Siravegna G, Mussolin B, Buscarino M, et al. Clonal evolution and resistance to EGFR blockade in the blood of colorectal cancer patients. *Nat Med*. 2015;21(7):795-801. doi:10.1038/nm.3870
12. Diaz LA, Sausen M, Fisher GA, Velculescu VE. Insights into therapeutic resistance from whole-genome analyses of circulating tumor DNA. *Oncotarget Oncotarget Oncotarget*. 2013;44(4):1856-1857. doi:10.18632/oncotarget.1486
13. Haigis KM, Kendall KR, Wang Y, et al. Differential effects of oncogenic K-Ras and N-Ras on proliferation, differentiation and tumor progression in the colon. *Nat Genet*. 2008;40(5):600-608. doi:10.1038/ng.115
14. Poulin EJ, Bera AK, Lu J, et al. Tissue-specific oncogenic activity of K-RasA146T. *Cancer Discov*. April 2019:CD-18-1220. doi:10.1158/2159-8290.CD-18-1220
15. Li Q, Haigis KM, McDaniel A, et al. Hematopoiesis and leukemogenesis in mice expressing oncogenic Nras G12D from the endogenous locus. *Blood*. 2011;117(6):2022-2032. doi:10.1182/blood-2010-04-280750
16. Van Emburgh BO, Arena S, Siravegna G, et al. Acquired RAS or EGFR mutations and duration of response to EGFR blockade in colorectal cancer. *Nat Commun*. 2016;7:1-9. doi:10.1038/ncomms13665
17. Summers MG, Smith CG, Maughan TS, Kaplan R, Escott-Price V, Cheadle JP. BRAF and NRAS locus-specific variants have different outcomes on survival to colorectal cancer. *Clin Cancer Res*. 2017;23(11):2742-2749. doi:10.1158/1078-0432.CCR-16-1541
18. Mao C, Huang YF, Yang ZY, Zheng DY, Chen JZ, Tang JL. KRAS p.G13D mutation and codon 12 mutations are not created equal in predicting clinical outcomes of cetuximab in metastatic colorectal cancer: A systematic review and meta-analysis. *Cancer*. 2013;119(4):714-721. doi:10.1002/cncr.27804
19. Tejpar S, Celik I, Schlichting M, Sartorius U, Bokemeyer C, Van Cutsem E. Association of KRAS G13D tumor mutations with outcome in patients with metastatic colorectal cancer treated with first-line chemotherapy with or without cetuximab. *J Clin Oncol*. 2012;30(29):3570-3577. doi:10.1200/JCO.2012.42.2592
20. De Roock W, Jonker DJ, Di Nicolantonio F, et al. Association of KRAS p.G13D mutation with outcome in patients with chemotherapy-refractory metastatic colorectal cancer treated with cetuximab. *JAMA - J Am Med Assoc*. 2010. doi:10.1001/jama.2010.1535
21. Burd CE, Liu W, Huynh M V, et al. Selection in Melanoma. 2015;4(12):1418-1429. doi:10.1158/2159-8290.CD-14-0729.Mutation-Specific
22. Ogura T, Kakuta M, Yatsuoka T, et al. Clinicopathological characteristics and prognostic impact of colorectal cancers with NRAS mutations. *Oncol Rep*. 2014;32(1):50-56. doi:10.3892/or.2014.3165
23. Burgess MR, Hwang E, Mroue R, et al. KRAS Allelic Imbalance Enhances Fitness and Modulates MAP Kinase Dependence in Cancer. *Cell*. 2017;168(5):817-829.e15. doi:10.1016/j.cell.2017.01.020
24. Soh J, Okumura N, Lockwood WW, et al. Oncogene mutations, copy number gains and mutant allele

specific imbalance (MASI) frequently occur together in tumor cells. *PLoS One*. 2009. doi:10.1371/journal.pone.0007464

25. Malapelle U, Sgariglia R, De Stefano A, et al. KRAS Mutant Allele-Specific Imbalance (MASI) assessment in routine samples of patients with metastatic colorectal cancer. *J Clin Pathol*. 2015. doi:10.1136/jclinpath-2014-202761
26. Hartman DJ, Davison JM, Foxwell TJ, Nikiforova MN, Chiosea SI. Mutant allele-specific imbalance modulates prognostic impact of KRAS mutations in colorectal adenocarcinoma and is associated with worse overall survival. *Int J Cancer*. 2012. doi:10.1002/ijc.27461
27. Fujii M, Shimokawa M, Date S, et al. A Colorectal Tumor Organoid Library Demonstrates Progressive Loss of Niche Factor Requirements during Tumorigenesis. *Cell Stem Cell*. 2016;18(6):827-838. doi:10.1016/j.stem.2016.04.003
28. Matano M, Date S, Shimokawa M, et al. Modeling colorectal cancer using CRISPR-Cas9-mediated engineering of human intestinal organoids. *Nat Med*. 2015. doi:10.1038/nm.3802
29. Verissimo CS, Overmeer RM, Ponsioen B, et al. Targeting mutant RAS in patient-derived colorectal cancer organoids by combinatorial drug screening. *Elife*. 2016. doi:10.7554/eLife.18489
30. Schumacher D, Andrieux G, Boehnke K, et al. Heterogeneous pathway activation and drug response modelled in colorectal-tumor-derived 3D cultures. *PLoS Genet*. 2019;15(3):e1008076. doi:10.1371/journal.pgen.1008076
31. Roerink SF, Young MD, Alexandrov B, et al. Intra-tumour diversification in colorectal cancer at the single-cell level. *Nature*. 2018;556:457-462. doi:10.1038/s41586-018-0024-3
32. Babin L, Piganeau M, Renouf B, et al. Chromosomal Translocation Formation Is Sufficient to Produce Fusion Circular RNAs Specific to Patient Tumor Cells. *iScience*. 2018. doi:10.1016/j.isci.2018.06.007
33. Metastatic C, Roock W De, Jonker DJ, Nicolantonio F Di, Sartore-bianchi A, Simes J. Association of KRAS p . G13D Mutation With Outcome in Patients With Chemotherapy-RefractoryMetastatic Colorectal Cancer Treated With Cetuximab. *JAMA*. 2013;304(16):1812-1820.
34. Smith MJ, Neel BG, Ikura M. NMR-based functional profiling of RASopathies and oncogenic RAS mutations. *Proc Natl Acad Sci*. 2013;110(12):4574-4579. doi:10.1073/pnas.1218173110
35. Hunter JC, Manandhar A, Carrasco MA, Gurbani D, Gondi S, Westover KD. Biochemical and Structural Analysis of Common Cancer-Associated KRAS Mutations. *Mol Cancer Res*. 2015;13(9):1325-1335. doi:10.1007/s40520-017-0795-7
36. Yaeger R, Chatila WK, Lipsyc MD, et al. Clinical Sequencing Defines the Genomic Landscape of Metastatic Colorectal Cancer. *Cancer Cell*. 2018. doi:10.1016/j.ccell.2017.12.004
37. Posch C, Sanlorenzo M, Vujic I, et al. Phosphoproteomic Analyses of NRAS(G12) and NRAS(Q61) Mutant Melanocytes Reveal Increased CK2α Kinase Levels in NRAS(Q61) Mutant Cells. *J Invest Dermatol*. 2016;136(10):2041-2048. doi:10.1016/j.jid.2016.05.098
38. Leon J, Guerrero I, Pellicer A. Differential expression of the ras gene family in mice. *Mol Cell Biol*. 2015;7(4):1535-1540. doi:10.1128/mcb.7.4.1535
39. Wang Y, Velho S, Vakiani E, et al. Mutant N-RAS protects colorectal cancer cells from stress-induced apoptosis and contributes to cancer development and progression. *Cancer Discov*. 2013. doi:10.1158/2159-8290.CD-12-0198
40. Parker JA, Mattos C. The Ras-Membrane Interface: Isoform-Specific Differences in the Catalytic Domain. *Mol Cancer Res*. 2015;13(4):595-603. doi:10.1158/1541-7786.MCR-14-0535
41. Nussinov R, Tsai CJ, Jang H. Oncogenic ras isoforms signaling specificity at the membrane. *Cancer Res*. 2018;78(3):593-602. doi:10.1158/0008-5472.CAN-17-2727
42. Mineo C, Gill GN, Anderson RGW. Regulated migration of epidermal growth factor receptor from caveolae. *J Biol Chem*. 1999. doi:10.1074/jbc.274.43.30636
43. Lambert S, Vind-Kezunovic D, Karvinen S, Gniadecki R. Ligand-independent activation of the EGFR by lipid raft disruption. *J Invest Dermatol*. 2006. doi:10.1038/sj.jid.5700168
44. Wang J, Liu Y, Li Z, et al. Endogenous oncogenic Nras mutation initiates hematopoietic malignancies in a dose- and cell type-dependent manner. *Blood*. 2011;118(2):368-379. doi:10.1182/blood-2010-12-326058
45. Irahara N, Baba Y, Nosho K, et al. NRAS mutations are rare in colorectal cancer. *Diagnostic Mol Pathol*. 2010;19(3):157-163. doi:10.1097/PDM.0b013e3181c93fd1
46. Cercek A, Braghiroli MI, Chou JF, et al. Clinical features and outcomes of patients with colorectal cancers harboring NRAS mutations. *Clin Cancer Res*. 2017;23(16):4753-4760. doi:10.1158/1078-0432.CCR-17-0400
47. Missiaglia E, Jacobs B, D'Ario G, et al. Distal and proximal colon cancers differ in terms of molecular, pathological, and clinical features. *Ann Oncol*. 2014;25(10):1995-2001. doi:10.1093/annonc/mdu275
48. Brulé SY, Jonker DJ, Karapetis CS, et al. Location of colon cancer (right-sided versus left-sided) as a prognostic factor and a predictor of benefit from cetuximab in NCIC CO.17. *Eur J Cancer*. 2015;51(11):1405-

1414. doi:10.1016/j.ejca.2015.03.015
49. Lee MS, McGuffey EJ, Morris JS, et al. Association of CpG island methylator phenotype and EREG/AREG methylation and expression in colorectal cancer. *Br J Cancer*. 2016;114(12):1352-1361. doi:10.1038/bjc.2016.87
50. Stintzing S, Tejpar S, Gibbs P, Thiebach L, Lenz HJ. Understanding the role of primary tumour localisation in colorectal cancer treatment and outcomes. *Eur J Cancer*. 2017;84:69-80. doi:10.1016/j.ejca.2017.07.016
51. Newlaczyl AU, Coulson JM, Prior IA. Quantification of spatiotemporal patterns of Ras isoform expression during development. *Sci Rep*. 2017;7:1-7. doi:10.1038/srep41297
52. Leon J, Guerrero I, Pellicer A. Differential expression of the ras gene family in mice. *Mol Cell Biol*. 2015. doi:10.1128/mcb.7.4.1535
53. Cox AD, Fesik SW, Kimmelman AC, Luo J, Der CJ. Drugging the undruggable RAS: Mission Possible? *Nat Rev Drug Discov*. 2014;13(11):828-851. doi:10.1038/nrd4389
54. Whitwam T, VanBrocklin MW, Russo ME, et al. Differential oncogenic potential of activated RAS isoforms in melanocytes. *Oncogene*. 2007. doi:10.1038/sj.onc.1210239
55. Stites EC, Trampont PC, Haney LB, Walk SF, Ravichandran KS. Cooperation between Noncanonical Ras Network Mutations. *Cell Rep*. 2015;10(3):307-316. doi:10.1016/j.celrep.2014.12.035
56. Lock R, Cichowski K. Loss of negative regulators amplifies RAS signaling. *Nat Genet*. 2015;47(5):426-427. doi:10.1038/ng.3299
57. Wan PT, Wan PT, Garnett MJ, et al. Mechanism of activation of the RAF-ERK signaling pathway by oncogenic mutations of B-RAF. *Cell*. 2004;116(6):855-867. papers2://publication/uuid/6A789316-AB6F-4316-B640-A6CE5046EAE0.
58. Zhao Z, Chen C-C, Rillahan CD, et al. Cooperative loss of RAS feedback regulation drives myeloid leukemogenesis. *Nat Genet*. 2015;47(5):539-543. doi:10.1038/ng.3251
59. Hayashi T, Desmeules P, Smith RS, Drilon A, Somwar R, Ladanyi M. RASA1 and NF1 are preferentially co-mutated and define a distinct genetic subset of smoking-associated non–small cell lung carcinomas sensitive to MEK inhibition. *Clin Cancer Res*. 2018;24(6):1436-1447. doi:10.1158/1078-0432.CCR-17-2343
60. Lubeck B a, Lapinski PE, Oliver J a, et al. Cutting Edge: Codeletion of the Ras GTPase-Activating Proteins (RasGAPs) Neurofibromin 1 and p120 RasGAP in T Cells Results in the Development of T Cell Acute Lymphoblastic Leukemia. *J Immunol*. 2015;195(1):31-35. doi:10.4049/jimmunol.1402639
61. Henkemeyer M, Rossi DJ, Holmyard DP, et al. Vascular system defects and neuronal apoptosis in mice lacking Ras GTPase-activating protein. *Nature*. 1995. doi:10.1038/377695a0
62. King PD, Lubeck BA, Lapinski PE. Nonredundant functions for Ras GTPase-activating proteins in tissue homeostasis. *Sci Signal*. 2013;6(264):re1. doi:10.1126/scisignal.2003669
63. Scheffzek K. The Ras-RasGAP Complex: Structural Basis for GTPase Activation and Its Loss in Oncogenic Ras Mutants. *Science (80-)*. 1997;277(5324):333-338. doi:10.1126/science.277.5324.333
64. Ahmadian MR, Kiel C, Stege P, Scheffzek K. Structural fingerprints of the Ras-GTPase activating proteins neurofibromin and p120GAP. *J Mol Biol*. 2003;329(4):699-710. doi:10.1016/S0022-2836(03)00514-X
65. Maertens O, Johnson B, Hollstein P, et al. Elucidating distinct roles for NF1 in melanomagenesis. *Cancer Discov*. 2013;3(3):338-349. doi:10.1158/2159-8290.CD-12-0313
66. Sung H, Kanchi KL, Wang X, et al. Inactivation of RASA1 promotes melanoma tumorigenesis via R-Ras activation. *Oncotarget*. 2016;7(17):23885-23896. doi:10.18632/oncotarget.8127
67. Li S, Nakamura S, Hattori S. Activation of R-Ras GTPase by GTPase-activating proteins for ras, gap1(m), and p120GAP [In Process Citation]. *JBiolChem*. 1997;272(31):19328-19332.
68. Nakhaeizadeh H, Amin E, Nakhaei-Rad S, Dvorsky R, Ahmadian MR. The RAS-effector interface: Isoform-specific differences in the effector binding regions. *PLoS One*. 2016;11(12):1-20. doi:10.1371/journal.pone.0167145
69. Drosten M, Dhawahir A, Sum EYM, et al. Genetic analysis of Ras signalling pathways in cell proliferation, migration and survival. *EMBO J*. 2010;29(6):1091-1104. doi:10.1038/emboj.2010.7
70. Brandt R, Uhlitz F, Riemer P, Giesecke C, Schulze S, El- IA. Cell type-dependent differential activation of ERK by oncogenic KRAS or BRAF in the mouse intestinal epithelium. *bioRxiv 340844*. 2018;(June):0-2. doi:https://doi.org/10.1101/340844
71. Qin X, Sufi J, Vlckova P, et al. Single-Cell Signalling Analysis of Heterocellular Organoids. *bioRxiv*. January 2019:659896. doi:10.1101/659896
72. Blaj C, Schmidt EM, Lamprecht S, et al. Oncogenic effects of high MAPK activity in colorectal cancer mark progenitor cells and persist irrespective of RAS mutations. *Cancer Res*. 2017. doi:10.1158/0008-5472.CAN-16-2821
73. Brandt R, Uhlitz F, Riemer P, et al. Cell type-dependent differential activation of ERK by oncogenic KRAS or BRAF in the mouse intestinal epithelium. *bioRxiv*. January 2018:340844. doi:10.1101/340844
74. Isella C, Terrasi A, Bellomo SE, et al. Stromal contribution to the colorectal cancer transcriptome. *Nat*

Genet. 2015;47(4):312-319. doi:10.1038/ng.3224
75. Calon A, Lonardo E, Berenguer-Llergo A, et al. Stromal gene expression defines poor-prognosis subtypes in colorectal cancer. *Nat Genet*. 2015;47(4):320-329. doi:10.1038/ng.3225
76. Takeda H, Kiyokawa E. Activation of Erk in ileal epithelial cells engaged in ischemic-injury repair. *Sci Rep*. 2017;7(1):1-11. doi:10.1038/s41598-017-16714-6
77. Kawabata N, Matsuda M. Cell density-dependent increase in tyrosine-monophosphorylated ERK2 in MDCK Cells expressing active ras or raf. *PLoS One*. 2016;11(12):1-15. doi:10.1371/journal.pone.0167940
78. Tuveson D, Clevers H. Cancer modeling meets human organoid technology. *Science (80-)*. 2019;364(6444):952-955. doi:10.1126/science.aaw6985
79. Drost J, Clevers H. Organoids in cancer research. *Nat Rev Cancer*. 2018. doi:10.1038/s41568-018-0007-6
80. Sachs N, de Ligt J, Kopper O, et al. A Living Biobank of Breast Cancer Organoids Captures Disease Heterogeneity. *Cell*. 2018;172(1-2):373-386.e10. doi:10.1016/j.cell.2017.11.010
81. Kamb A. At a crossroads in oncology. *Curr Opin Pharmacol*. 2010. doi:10.1016/j.coph.2010.05.006
82. Gazdar AF, Gao B, Minna JD. Lung cancer cell lines: Useless artifacts or invaluable tools for medical science? *Lung Cancer*. 2010. doi:10.1016/j.lungcan.2009.12.005
83. Gillet JP, Varma S, Gottesman MM. The clinical relevance of cancer cell lines. *J Natl Cancer Inst*. 2013. doi:10.1093/jnci/djt007
84. Ben-David U, Siranosian B, Ha G, et al. Genetic and transcriptional evolution alters cancer cell line drug response. *Nature*. 2018;560(7718):325-330. doi:10.1038/s41586-018-0409-3
85. Fujii M, Shimokawa M, Date S, et al. A Colorectal Tumor Organoid Library Demonstrates Progressive Loss of Niche Factor Requirements during Tumorigenesis. *Cell Stem Cell*. 2016;18(6):827-838. doi:10.1016/j.stem.2016.04.003
86. Tiriac H, Belleau P, Engle DD, et al. Organoid profiling identifies common responders to chemotherapy in pancreatic cancer. *Cancer Discov*. 2018;8(9):1112-1129. doi:10.1158/2159-8290.CD-18-0349
87. Van De Wetering M, Francies HE, Francis JM, et al. Prospective derivation of a living organoid biobank of colorectal cancer patients. *Cell*. 2015. doi:10.1016/j.cell.2015.03.053
88. Pauli C, Hopkins BD, Prandi D, et al. Personalized in vitro and in vivo cancer models to guide precision medicine. *Cancer Discov*. 2017;7(5):462-477. doi:10.1158/2159-8290.CD-16-1154
89. Vlachogiannis G, Hedayat S, Vatsiou A, et al. Patient-derived organoids model treatment response of metastatic gastrointestinal cancers. *Science (80-)*. 2018. doi:10.1126/science.aao2774
90. Neal JT, Li X, Zhu J, et al. Organoid Modeling of the Tumor Immune Microenvironment. *Cell*. 2018. doi:10.1016/j.cell.2018.11.021
91. Wang L, Wei Y, Fang W, et al. Cetuximab Enhanced the Cytotoxic Activity of Immune Cells during Treatment of Colorectal Cancer. *Cell Physiol Biochem*. 2017. doi:10.1159/000485404
92. Lal N, Beggs AD, Willcox BE, Middleton GW. An immunogenomic stratification of colorectal cancer: Implications for development of targeted immunotherapy. *Oncoimmunology*. 2015;4(3):1-9. doi:10.4161/2162402X.2014.976052
93. Lal N, White BS, Goussous G, et al. KRAS mutation and consensus molecular subtypes 2 and 3 are independently associated with reduced immune infiltration and reactivity in colorectal cancer. *Clin Cancer Res*. 2018;24(1):224-233. doi:10.1158/1078-0432.CCR-17-1090
94. Liao W, Overman MJ, Boutin AT, et al. KRAS-IRF2 Axis Drives Immune Suppression and Immune Therapy Resistance in Colorectal Cancer. *Cancer Cell*. 2019;35(4):559-572.e7. doi:10.1016/j.ccell.2019.02.008
95. Tsai S, McOlash L, Palen K, et al. Development of primary human pancreatic cancer organoids, matched stromal and immune cells and 3D tumor microenvironment models. *BMC Cancer*. 2018;18(1):1-13. doi:10.1186/s12885-018-4238-4
96. Di Nicolantonio F, Arena S, Gallicchio M, et al. Replacement of normal with mutant alleles in the genome of normal human cells unveils mutation-specific drug responses. *Proc Natl Acad Sci*. 2008;105(52):20864-20869. doi:10.1073/pnas.0808757105

6

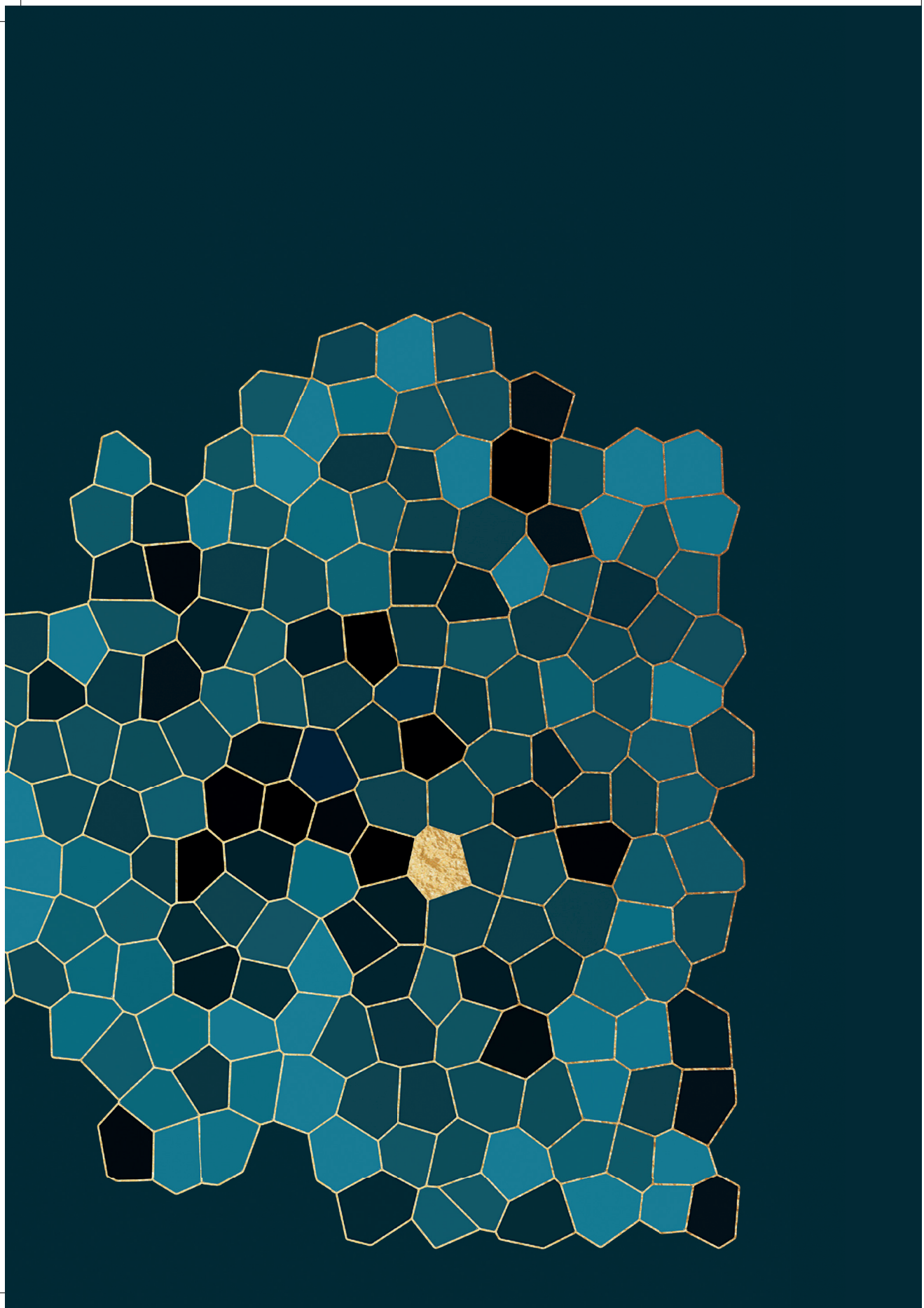

ADDENDUM

NEDERLANDSE SAMENVATTING

CURRICULUM VITAE

PUBLICATIELIJST

DANKWOORD

NEDERLANDSE SAMENVATTING

De dunne en dikke darm spelen een belangrijke rol in het menselijke verteringsstelsel. In de dunne darm wordt voedsel omgezet gezet in voedingsstoffen en in het bloed opgenomen via de darmwand. In de dikke darm worden voornamelijk water en zouten opgenomen, waarna het onverteerde voedsel het lichaam via de endeldarm verlaat. De dunne darm is gevormd als plooiing die bestaat uit invaginaties (crypten) en vingerachtige uitstulpingen (villi) die de oppervlakte van de darmwand vergroot en daarmee de opname van voedingsstoffen vergroot. Het aantal villi neemt af naar het einde van de dunne darm, waar minder voedingsstoffen worden opgenomen, en zijn geheel afwezig in de dikke darm. De darmwand bestaat uit een laag epitheelcellen die om de 3 á 4 dagen worden vernieuwd. Darmvilli bestaan uit post-mitotische, gespecialiseerde cellen die een rol spelen bij het opnemen van nutriënten (enterocyten), bij het metabolisme (entero-endocriene cellen), bij de verdediging tegen parasieten (tuftcellen), bij de productie van mucus (gobletcellen), en bij de "cross-talk" tussen het immuunsysteem en het darmlumen (M-cellen). In de crypten bevinden zich de delende stam- en "transit amplifying" (TA) cellen die nieuwe dochtercellen produceren. Naarmate er meer celdelingen zijn, bewegen deze dochtercellen zich naar het topje van de crypte of villus waar ze aan het lumen van de darm worden afgegeven, nadat ze celdood hebben ondergaan. Naast delende cellen bevinden zich tussen de stamcellen gespecialiseerde paneth- (dunne darm) of "deep crypt secretory" (dikke darm) cellen die antimicrobiële peptiden en groeifactoren voor stamcellen uitscheiden. De crypten waarin deze delende stamcellen zich bevinden, bieden bescherming tegen de agressieve omgeving van het darmlumen. Hoewel de villi zorgen voor een oppervlaktevergroting leidt het ook tot een verhoogde mate van stress. De cellen die zich namelijk in de villi en aan het einde van de crypte bevinden, worden blootgesteld aan bacteriële toxines en wrijving door de beweging van voedsel. Delende cellen daarentegen worden hiertegen beschermd door zowel de structuur van de crypte als door de antibacteriële mucuslaag die geproduceerd wordt door de gobletcellen en voor een fysieke barrière zorgen tegen microbiële producten.

De omgeving van de stamcellen onderin de crypte, de zogenaamde stamcelniche (stamcelzone), levert signalen (zoals liganden voor WNT-, EGF- en Notch-signaaltransductie) voor celdeling en het behoud van de stamcelidentiteit, terwijl signalen (zoals BMP) bovenaan de crypte specialisatie van cellen bevorderen (**Figuur 1**). WNT-liganden uit de stamcelniche, die geleverd worden door paneth- en mesenchymale cellen, kunnen binden aan het Frizzled-LRP5-LRP6 receptorcomplex aan de oppervlakte van de stamcel. Dit zorgt voor remming van de afbraak van het eiwit b-catenine door het adenomatous polyposis coli (APC) complex en resulteert in de translocatie van b-catenine naar de celkern om de expressie van genen te reguleren die het behoud van de stamcelidentiteit bevorderen. Naastliggende panethcellen leveren ook DLL1 en DLL4 liganden die Notch-receptoren in stamcellen binden en activeren, en daardoor de differentiatie van stamcellen naar gespecialiseerde cellen remt. De EGF-receptor (EGFR), een receptor-tyrosinekinase, wordt ook tot expressie gebracht in stamcellen. Activering van de EGFR door EGF of TGFa, uitgescheiden door panethcellen en het mesenchym, induceert onder andere celdeling en overleving. Competitie tussen delende stamcellen in de gelimiteerde ruimte van de crypte zorgt ervoor dat cellen aan de grens van de celde-

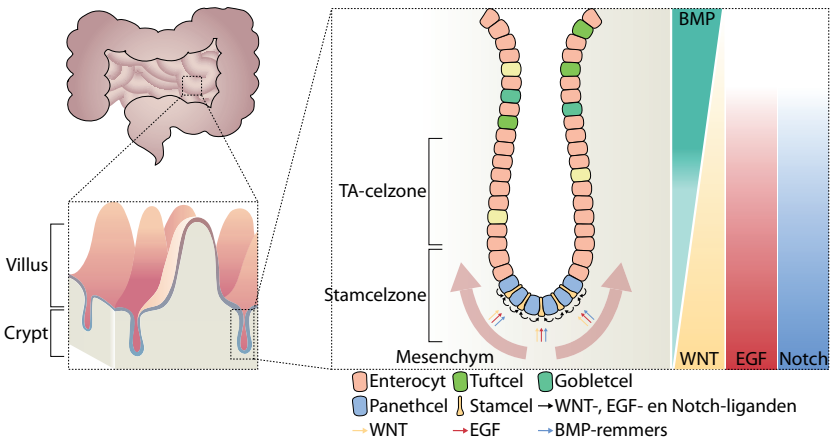

Figuur 1. Darmstructuur.
Het darmepitheel is opgebouwd in crypten en villi. Delende stam- en "transit amplifying" (TA) cellen in de crypte produceren nieuwe darmepitheelcellen die zich naar het topje van de crypte of villus bewegen. Buiten de stamcel- en TA-celzone bevinden zich gespecialiseerde cellen, zoals enterocyten, tuftcellen en gobletcellen. Panethcellen zijn de enige gespecialiseerde cellen die zich naar de bodem van de crypte bewegen. In de stamcelzone leveren paneth- en mesenchymale cellen signalen (BPM-remmers, WNT-, EGF- en Notch-liganden) voor celdeling en het behoud van de stamcelidentiteit, terwijl de omgeving bovenaan de crypte BMP-signalen leveren voor de specialisatie van cellen.

lingszone uit de stamcelniche worden geduwd en hun vermogen om te delen verliezen. Deze stamcelniche is nodig om de opbouw van de darm te waarborgen. Bijvoorbeeld: remming van WNT-signalering in de crypte kan het verlies van stamcellen veroorzaken, terwijl hyperactieve WNT-signalering kan leiden tot excessieve groei van het darmepitheel, wat kan resulteren in een adenoom. De stamcelniche functioneert dus ook als een beschermingsmechanisme tegen "productiefouten" (mutaties). Om te overleven en gemuteerde "nakomelingen" te produceren, moeten gemuteerde stamcellen competitie voeren met gezonde stamcellen die vaak een snellere delingscyclus hebben dan gemuteerde cellen. Gemuteerde stamcellen moeten dus de mogelijkheid krijgen om buiten de niche te delen voordat ze de stamcelzone worden uitgeduwd. Dus alleen mutaties die niche-onafhankelijk zijn en verhoogde delingssnelheid van een cel veroorzaken, kunnen leiden tot kankerontwikkeling. WNT-signalering speelt een essentiële rol in stamcelproductie en behoud. Vandaar dat vaak de eerste mutatie "hits" in darmkanker WNT-activerende signalen zijn, zoals het verlies van APC (prevalentie van 75%). Daaropvolgend leiden activerende mutaties in EGFR-signaaltransductie, zoals KRAS-mutaties (prevalentie van 35-50%), tot versnelde celdeling en zo cellen een selectief voordeel geeft om de crypte te domineren. Verhoogde activiteit van EGFR-signalering leidt tot ongecontroleerde celgroei en speelt een belangrijke rol in de progressie van darmkanker (**Figuur 2**).
De essentiële rol van EGFR-signalering in darmkanker wordt weerspiegeld in de effectieve behandeling van darmkankerpatiënten met antilichamen die gericht zijn op het remmen van de EGFR, mits er geen mutatie aanwezig is die de EGF-signaaltransductiecascade activeert onafhankelijk van de EGFR. Behandeling met EGFR-remmers in darmkankerpatiënten zonder mutaties in de EGF-signaaltransductiecascade leidt tot verminderde tumorgroei

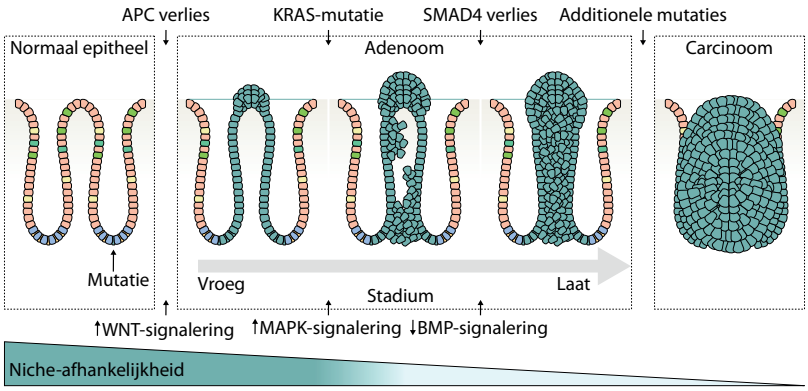

Figuur 2. De progressie van darmkanker.
De ontwikkeling van darmkanker bestaat uit een reeks van achtereenvolgende mutaties die de niche-afhankelijkheid van stamcellen voor celdeling verminderen. De eerste stap op weg naar darmkanker is vaak een mutatie dat verhoogde WNT-signalering (zoals het verlies van APC) tot gevolg heeft. Daaropvolgend vinden vaak activerende mutaties in de EGFR-signaaltransductie (zoals in het *KRAS* gen), inactiverende mutaties van BMP-signaaltransductie (zoals het verlies van SMAD4), en additionele mutaties (zoals het verlies van TP53) plaats die de ontwikkeling van een adenoom naar carcinoom bevorderen.

(**Figuur 3A-B**). Daarentegen vertonen darmkankerpatiënten met activerende mutaties in de EGF-signaaltransductiecascade resistentie tegen EGFR-remmende therapie (**Figuur 3C**). Een van de meest voorkomende activerende mutaties in de EGF-signaaltransductiecascade betreft het *KRAS*-gen, dat gemuteerd is in 35-50% van de darmkankergevallen en leidt tot resistentie tegen EGFR-remming. Mutaties in het *NRAS*-gen, het zusje (RAS isovorm) van KRAS, komen in 4% van darmkankergevallen voor en zijn ook geassocieerd met resistentie tegen EGFR-remmers. Dit heeft ertoe geleid dat patiënten met RAS-gemuteerde tumoren uitgesloten worden van EGFR-remmende therapie.
RAS-eiwitten zijn GTPases die schakelen tussen GDP-gebonden inactieve en GTP-gebonden actieve vormen, en worden gereguleerd door de EGFR. Actieve RAS-eiwitten kunnen een heel scala aan signaleringscascades aanzetten, die onder andere celdeling, -overleving, -migratie en -specialisatie tot gevolg hebben (**Figuur 4**). Eén van deze signaaltransductiecascades is de MAPK-signaaltransductiecascade die onder andere de celdeling reguleert. De activering van RAS-eiwitten moet nauwkeurig gereguleerd worden om excessieve celgroei te voorkomen. Terwijl guanine nucleotide exchange factoren (GEF) helpen RAS-eiwitten te activeren, zorgen RAS GTPase activerende eiwitten (GAP) voor de uitschakeling van RAS-eiwitten. Mutaties in *RAS*-genen (voornamelijk op codon 12, 13 en 61) leiden tot verhoogde RAS-activiteit door GEF-onafhankelijk activatie, GAP-ongevoeligheid, of beide. Ondanks dat mutaties op deze zogenaamde "hotspot" locaties in *RAS* voor verhoogde activiteit van de EGFR-signaaltransductiecascade zorgen, zijn er steeds meer aanwijzingen dat veel meer nuance nodig is in de verdeling van darmkankerpatiënten die ontvankelijk zijn voor therapie met EGFR-remmers. De ene *KRAS*-mutatie op locatie X heeft namelijk een ander effect dan dezelfde mutatie op locatie Y in de context van EGF-onafhankelijkheid. Bovendien lijken de effecten van dezelfde codonmutaties in verschillende RAS-isovormen (d.w.z in *KRAS* of *NRAS*) contextgevoelig.

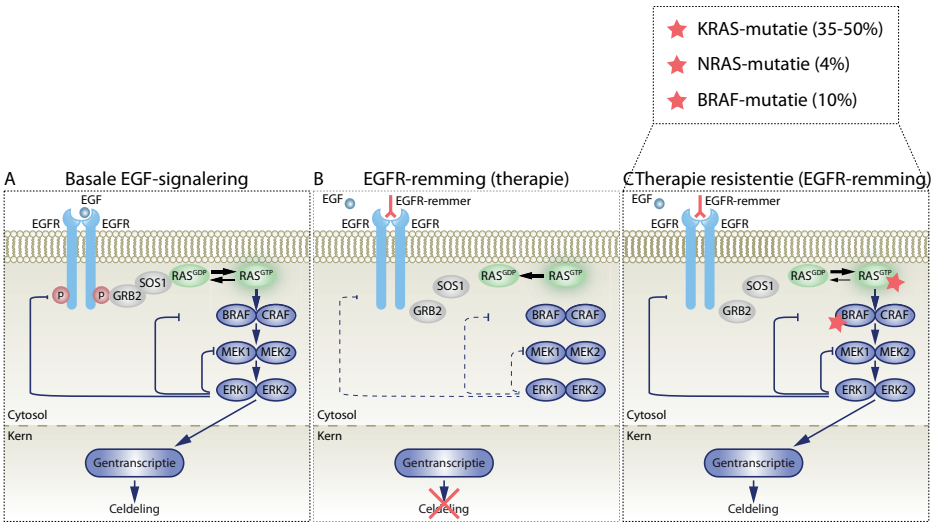

Figuur 3. Mutaties in de MAPK-signaaltransductiecascade en resistentie tegen EGFR-remmers.
(**A**) Activering van epidermale groeifactorreceptoren (EGFR) heeft onder andere de activering van de MAPK-signaaltransductie tot gevolg. De binding van groeifactoren (EGF) aan EGFR leidt tot de fosforylering en activering van de receptor. Het adaptereiwit GRB2 bindt vervolgens aan de receptor om daar weer een activator van RAS (SOS1) te binden en naar de celmembraan te brengen. Bij de celmembraan kan SOS1 RAS-eiwitten activeren. Actief RAS bindt en activeert RAF-eiwitten, resulterend in de activering van ERK via MEK. Actieve ERK-eiwitten hebben meer dan 200 substraten die zich zowel in het cytosol als in de kern bevinden. In de kern kan ERK transcriptiefactoren activeren om specifieke transcriptieprogramma's aan te zetten die nodig zijn voor celdeling. Actieve ERK-eiwitten zorgen ook voor een negatieve feedback regulatie van de MAPK-signalering om de activiteit van de signaaltransductie in toom te houden. (**B**) Therapie met EGFR-remmers wordt gebruikt in darmkankerpatiënten om de MAPK-signaaltransductie uit te zetten en op die manier de ongecontroleerde celdeling van kankercellen te remmen. (**C**) Activerende mutaties in de EGFR-MAPK-signaaltransductiecascade (zoals mutaties in het *KRAS*, *NRAS* en *BRAF* gen) komen vaak voor in darmkankerpatiënten en zorgen voor resistentie tegen therapie met EGFR-remmers. De frequentie van mutaties in de *KRAS*, *NRAS* en *BRAF* genen in darmkanker zijn als percentages weergegeven.

In de darm leiden namelijk NRAS-mutaties op codon 12 niet tot hetzelfde kankerinducerend vermogen als KRAS-mutaties op dezelfde locatie, terwijl dezelfde NRAS-mutaties wel de tumorgroei van bloedcellen kan induceren. Verder worden andere mutaties in de EGFR-signaaltransductiecascade ook geassocieerd met ongevoeligheid voor EGFR-remmers, zoals activerende mutaties in *BRAF*. Bovendien is in 25% van de gevallen het onderliggende mechanisme van resistentie tegen EGFR-remmende therapie niet bekend. In dit proefschrift wordt onderzoek beschreven naar welke mutaties in de EGFR-signaaltransductiecascade leiden tot EGF-onafhankelijkheid en resistentie tegen EGFR-remmers en naar het onderliggende mechanisme ervan.
Eerder onderzoek aan kankercellijnen heeft aangetoond dat oncogene mutaties in *RAS*- en *BRAF*-genen kunnen leiden tot resistentie tegen EGFR-remmers. In deze studies is echter voornamelijk gebruik gemaakt van oncogenoverexpressie in 2D cellijnen. De expressieniveaus van *RAS*- en *BRAF*-oncogenen zijn in deze studies vele malen hoger dan de fysiologische expressieniveaus in darmtumoren en kunnen daardoor verschillen in de mate van EGFR-ongevoeligheid tussen mutanten maskeren. Bovendien bevatten de darmkankercellij-

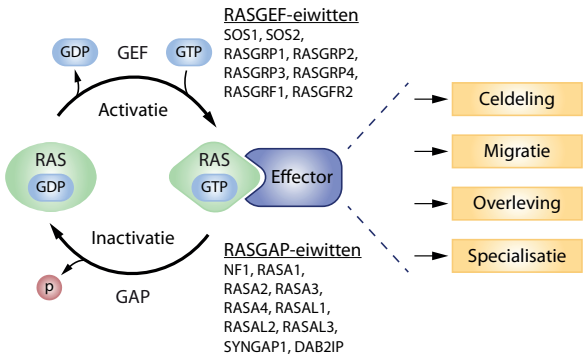

Figuur 4. Signalering van RAS-eiwitten.
RAS-eiwitten schakelen tussen GDP-gebonden inactieve en GTP-gebonden actieve vormen. Verschillende RAS-GEF-eiwitten stimuleren de activatie van RAS-eiwitten door de dissociatie van GDP te bevorderen, waarna RAS GTP kan binden. RASGAP-eiwitten versnellen de omzetting van GTP naar GDP en helpen op die manier om RAS-eiwitten uit te zetten. De binding van GTP zorgt voor een conformatieverandering van RAS-eiwitten, waardoor ze verschillende effectoren kunnen binden en activeren. De activering van deze effectoren heeft verschillende biologische processen tot gevolg, zoals celdeling, migratie, overleving en specialisatie.

nen die gebruikt worden vaak al activerende mutaties van de EGFR-signaaltransductiecascade en lijken ze qua morfologie en behandelingsrespons vaak niet op de originele tumor. Met behulp van 3D darmorganoïden afkomstig van darmkankerpatiënten hebben we verschillende oncogene mutaties en deleties in verschillende spelers van de EGFR-signaaltransductiecascade endogeen aangebracht. De morfologie en respons van darmorganoïden zijn meer overeenkomstig met die van de originele darmtumoren in patiënten en fungeren dankzij hun schaalbaarheid als een fysiologisch belangrijk *in vitro* darmkankermodel. Met behulp van de CRISPR-Cas9-techniek hebben we verschillende endogene mutaties of deleties in *RASGAP*, *KRAS*, *NRAS* en *BRAF* genen aangebracht om de fysiologische expressie van deze oncogenen te bewerkstelligen.

In **hoofdstuk 1** van dit proefschrift wordt omschreven wat de overeenkomstigheden en verschillen tussen KRAS-, NRAS- en BRAF-oncogenen zijn in darmkankerontwikkeling, histologie, en resistentie tegen EGFR-remmende therapie. Tot slot beschrijven we aan de hand van verschillende studies de waarde van darmkankerorganoïdbiobanken en genoombewerking als een darmkankermodel om de verschillen tussen *RAS*- en *BRAF*-mutaties op tumorgroei en respons op therapie te onderzoeken.
In **hoofdstuk 2** gaan we dieper in op de methoden van genoombewerking met behulp van de CRISPR-Cas9-techniek en leveren we een gebruiksaanwijzing voor context-afhankelijke benaderingen van genoombewerking. We omschrijven de specificiteit en efficiëntie van verschillende CRISPR-nucleases, het optimale design om bewerkingen in het genoom te integreren, selectietechnieken van cellen met juiste genoombewerkingen, en additionele strategieën om de efficiëntie van dit proces te verhogen.
In **hoofdstuk 3** tonen we aan de hand van deleties en nichefactordepletie in darmkankerorganoïden aan dat RASGAP-eiwitten een rol spelen in EGF-onafhankelijkheid (**Figuur 5**). The-

rapie met EGFR-remmers leidt over het algemeen tot een gunstig effect in darmkankerpatiënten met wildtype *RAS* en *BRAF*-tumoren. Echter, in 25% van de gevallen treedt er resistentie op waarvan de onderliggende mechanismen niet bekend zijn. Onderzoek naar RASGAP-eiwitten in huid- en longkanker leerde dat het verlies van deze eiwitten kan leiden tot verhoogde RAS-activiteit en het verlies een rol kan in EGF-onafhankelijkheid. De RASGAP-familie bestaat uit 10 verschillende eiwitten die allemaal de capaciteit beschikken om RAS-eiwitten uit te schakelen. Desalniettemin lijken niet alle functies van een bepaald RASGAP-eiwit overgenomen te kunnen worden door een andere RASGAP-isovorm. We hebben in hoofdstuk 3 onderzocht of het verlies van alle of slechts één enkel RASGAP-eiwit kan leiden tot EGF-onafhankelijke groei van darmkankerorganoïden en het onderliggende mechanisme hiervan. Dit hebben we gedaan door van alle tien de RASGAP-eiwitten er stuk voor stuk steeds één uit te schakelen met behulp van CRISPR-Cas9 in organoïden afkomstig van darmtumoren (wildtype voor de EGFR-signalering) of in organoïden die een darmtumor nabootsen. Met behulp van EGFR-remmers laten we zien dat het verlies van alleen één RASGAP-eiwit (NF1) leidt tot EGF-onafhankelijkheid wegens verhoogde RAS-activiteit en MAPK-signaaltransductie. Echter, het verlies van NF1 zorgt niet voor dezelfde mate van EGF-onafhankelijkheid als KRAS-mutanten en lijkt te leiden tot een grotere gevoeligheid voor complete remming van de MAPK-signaaltransductiecascade. Dit suggereert dat darmkankerpatiënten met tumoren die NF1 niet tot expressie brengen ook resistent zijn tegen EGFR-remmende therapie en van deze behandeling zouden moeten worden uitgesloten. Daarentegen kunnen deze tumoren potentieel wel worden behandeld met meerdere remmers die de MAPK-signalering volledig uitzetten.

Darmkankerpatiënten met activerende *BRAF*-mutaties (10%) vertonen ook resistentie tegen EGFR-remmers. Behalve mutaties in het *BRAF*-gen zijn er ook *BRAF*-genfusies gevonden in patiënten met darmkanker. Hierbij fuseert een deel van het *BRAF*-gen met een deel van een ander gen. Op die manier ontstaat er een eiwitproduct dat bestaat uit het functionele kinase domein van BRAF, dat andere eiwitten (MEK1/2) in de MAPK-signaaltransductiecascade kan activeren, en een deel van een ander eiwit. Het nieuwe eiwit is dus als het ware een chimera uit de Griekse mythologie, een monster samengesteld uit meerdere dieren. In deze BRAF-fusie-eiwitten is het remmende deel van BRAF verloren gegaan, waardoor het BRAF-eiwit continue geactiveerd is. Dit suggereert dat BRAF-genfusies mogelijk ook resistentie tegen EGFR-remming kunnen veroorzaken. Om dit te onderzoeken, hebben we in **hoofdstuk 4** verschillende BRAF-fusie-eiwitten en een activerende BRAF-mutant ($BRAF^{V600E}$) tot expressie gebracht in darmkankerorganoïden (**Figuur 5**). We laten zien dat onafhankelijk van de fusiepartner BRAF-fusie-eiwitten, net als $BRAF^{V600E}$, resistentie tegen EGFR, BRAF en MEK-remmers veroorzaken. Daarentegen varieert de mate van resistentie tussen de verschillende BRAF-fusie-eiwitten. Bovendien beïnvloedt de fusiepartner ook de locatie van het eiwit in de cel, de activiteit van de MAPK-signaaltransductiecascade en het transcriptieprogramma dat geactiveerd wordt. Dus ondanks de verschillen tussen BRAF-genfusies vertonen ze allemaal resistentie tegen remming van de EGFR-signaaltransductiecascade.

Net als RASGAP en BRAF-fusie-eiwitten zijn niet alle RAS isovormen hetzelfde. Sterker nog, er lijkt zelfs een nuance te zijn tussen verschillende activerende mutaties in dezelfde RAS isovorm. Desondanks worden alle RAS-mutaties over één kam geschoren en worden darmkankerpatiënten met RAS-mutaties uitgesloten van therapie met EGFR-remmers.

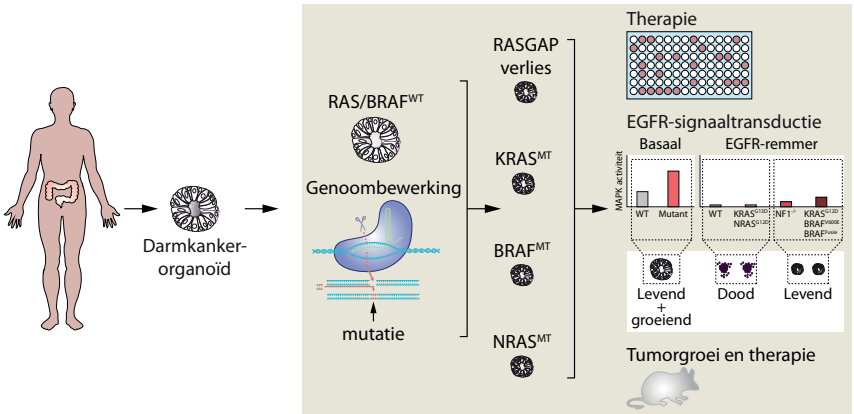

Figuur 5. Verschillende mutaties in de MAPK-signaaltransductiecascade laten verschillen in tumorgroei en resistentie tegen EGFR-remmers zien.
Met behulp van genoombewerking in darmkankerorganoïden die wildtype zijn voor EGFR-RAS-signalering hebben we onderzocht wat de effecten van verschillende mutaties (het verlies van RASGAP-eiwitten en mutaties in *KRAS*, *NRAS*, en *BRAF*) in de MAPK-signaaltransductiecascade zijn op EGF-onafhankelijkheid. Alle mutaties laten verhoogde ERK-activatie zien ten opzichte van wildtype RAS/BRAF. In de aanwezigheid van EGFR-remmers in darmkankerorganoïden worden echter de verschillen tussen mutanten zichtbaar. Behandeling met EGFR-remmers laat zien dat wildtype RAS/BRAF en $KRAS^{G13D}$ en $NRAS^{G12D}$ organoïden afhankelijk zijn van EGF-signalering voor overleving. Organoïden met $KRAS^{G12D}$, $BRAF^{V600E}$ en $BRAF^{fusie}$ mutaties of NF1-deficiëntie laten daarentegen EGF-onafhankelijkheid zien voor overleving, maar niet voor celgroei. EGF-onafhankelijkheid voor overleving is echter minder groot in organoïden die geen NF1 tot expressie brengen ten opzichte van $KRAS^{G12D}$, $BRAF^{V600E}$ en $BRAF^{fusie}$ mutanten. Transplantatie van wildtype RAS/BRAF, $KRAS^{G12D}$, $KRAS^{G13D}$, $NRAS^{G12D}$ en $BRAF^{V600E}$ organoïden in muizen laat zien dat onder fysiologische EGF-concentraties alle mutanten versnelde tumorgroei laten zien ten opzichte van wildtype RAS/BRAF-tumoren. Onder de mutanten is de groei van $KRAS^{G13D}$ gemuteerde tumoren het snelst. De effecten van EGFR-remmers op de verschillende mutanten blijven echter *in vivo* hetzelfde.

Behalve mutaties in *RAS* worden *BRAF*-mutaties ook geassocieerd met resistentie tegen EGFR-remmers. Er zijn echter vaak verschillen in andere factoren te vinden tussen *KRAS*- en *BRAF*-gemuteerde darmtumoren, zoals de histologie van de tumor, de locatie in de darm en de hoeveelheid mutaties. In **hoofdstuk 5** onderzoeken we de verschillen tussen *RAS*- en *BRAF*-mutaties door ze via de CRISPR-Cas9-methode te introduceren in darmkankerorganoïden (**Figuur 5**). Deze organoïden verschillen dus enkel in het aangebrachte oncogen dat ze tot expressie brengen. Door deze benadering laten we zien dat alle RAS ($KRAS^{G12D}$, $KRAS^{G13D}$ en $NRAS^{G12D}$) en BRAF ($BRAF^{V600E}$) mutanten leiden tot verhoogde activatie van de EGFR-signaaltransductiecascade en versnelde tumorgroei. Daarentegen, alleen $KRAS^{G12D}$ en $BRAF^{V600E}$ mutaties zijn voldoende om volledige resistentie te bieden tegen remming van de MAPK-signaaltransductiecascade. $KRAS^{G12D}$ en $BRAF^{V600E}$ mutanten zijn echter nog steeds gedeeltelijk afhankelijk van EGF-signalering, aangezien de activiteit van de MAPK-signaaltransductiecascade en tumorgroei verminderd zijn tijdens EGFR-remming. Samenvattend impliceert deze studie dus dat er meer nuance nodig is in de verdeling van darmkankerpatiënten met *RAS*-mutaties om in aanmerking te komen voor EGFR-gerichte therapie.
Tot slot worden in **hoofdstuk 6** de bevindingen in dit proefschrift samengevat en uitvoerig bediscussieerd.

CURRICULUM VITAE

Jasmin Post is geboren op 1 april 1989 te Mississauga, ON, Canada. In 2007 behaalde zij haar atheneumdiploma aan het Sint Bonifatius Lyceum te Utrecht. Hetzelfde jaar begon zij met de opleiding Biologie aan de Universiteit van Utrecht. Na afronding van haar Bachelor, begon zij in 2012 aan de Master Biology of Disease, die ze in 2014 afrondde. Tijdens deze Master-opleiding heeft Jasmin een onderzoeksstage van 9 maanden gedaan bij de afdeling Molecular Cancer Research in het UMC Utrecht, onder begeleiding van dr. Tale Sliedrecht in het lab van prof. dr. Geert Kops. Jasmin heeft een tweede onderzoeksstage van 8 maanden gedaan bij de afdeling Anatomy aan de University of Califoria San Francisco, onder begeleiding van dr. Yvonne Vercoulen in het lab van dr. Jeroen Roose. In juni 2014 is Jasmin begonnen als onderzoeker in opleiding bij de afdeling Molecular Cancer Research, UMC Utrecht, in het laboratorium van dr. Hugo Snippert, waar ze gewerkt heeft aan het onderzoek beschreven in dit proefschrift.

PUBLICATIONS

1. Disease modeling in tumor organoids: discriminating between oncogenic RAS and BRAF variants. **Jasmin B. Post**, Jeanine M.L. Roodhart and Hugo J.G. Snippert. Trends in Cancer. 2019 Sep (*under review*).

2. BRAF fusion gene partners influence oncogenic BRAF activity. Christina S. Stangl, **Jasmin B. Post**, Markus J. van Roosmalen, Nizar Hami, Ingrid Verlaan-Klink, Harmjan R. Vos, Robert M. van Es, Marco J. Koudijs, Emile E. Voest, Hugo J.G. Snippert and W.P. Kloosterman. Molecular Cancer Research. 2019 Aug (*under review*).

3. CRISPR-mediated RASGAP deficiencies in colorectal cancer organoids reveal that only loss of NF1 promotes resistance to EGFR inhibition. **Jasmin B. Post**, Nizar Hami, Alexander E.E. Mertens, Suraya Elfrink, Johannes L. Bos and Hugo J.G. Snippert. Oncotarget. 2019. 10(14): 1440-1457.

4. How to create state-of-the-art genetic model systems: strategies for optimal CRISPR-mediated genome editing. Yannik Bollen, **Jasmin B. Post**, Bon-Kyong Koo and Hugo J.G. Snippert. Nucleic Acids Research. 2018. 46(13): 6435–6454.

5. Baculoviral delivery of CRISPR/Cas9 facilitates efficient genome editing in human cells. Sanne Hindriksen, Arne J. Bramer, My A. Truong, Martijn J.M. Vromans, **Jasmin B. Post**, Ingrid Verlaan-Klink, Hugo J.G. Snippert, Susanne M.A. Lens, Michael A. Hadders. PLoS One. 2017. 12(6): e0179514.

DANKWOORD

Ik zou het bijna het einde van een tijdsperk kunnen noemen, want zo voelt het ongeveer wel. Na twee stages en een promotieonderzoek van 5,5 jaar ga ik het gezellige Stratenum verlaten. De afgelopen jaren heb ik hier met veel plezier rondgelopen wat uiteindelijk heeft geleid tot dit proefschrift wat ik nu eindelijk als boek in mijn handen kan vasthouden. Dit heb ik natuurlijk niet helemaal alleen gedaan en ik wil daarvoor graag enkele mensen bedanken. Na een met koffievlekken doordrongen begin van mijn promotietijd hoop ik toch echt dit laatste deel van het proefschrift vlekkeloos af te ronden door niemand vergeten te bedanken. Dus daar gaan we dan: "Iedereen bedankt!"

Grapje!

Hier gaan we dan echt:

Hugo (of moet ik zeggen Neo), ik kan me de eerste keer dat ik je ontmoette nog goed herinneren. Een jonge vent zat voor me die bijna overliep van enthousiasme en nieuwe ideeën. Dit enthousiasme van jou was zo aanstekelijk dat ik niet kon wachten om te beginnen. Jouw creativiteit leidde ertoe dat we talloze projecten hebben geprobeerd (en zoals dat in het onderzoek gaat helaas ook behoorlijk wat hebben moeten schrappen). Soms voelde het in het begin dan ook alsof ik maar wat pasta tegen de muur probeerde te gooien tot er eindelijk een sliertje bleef plakken. En gelukkig, dat lukte! Ik heb het altijd ontzettend fijn gevonden dat je zo betrokken was bij het opstarten van alle projecten en dat je deur altijd open stond voor overleg, een brainstormsessie of gewoon een praatje. Het is leuk om te zien hoe de groep gegroeid is, zowel in expertise als in grootte, en waar jij je vele ideeën over uit kan storten. Ik wil je ontzettend bedanken voor je begeleiding afgelopen jaren en de stimulatie om me te blijven ontwikkelen. Ik ben ontzettend benieuwd hoe het lab eruit zal zien na de volgende 5 jaar.

Hans, samen met Hugo bedacht je het "flippable KRAS"-project waar ik aan mocht beginnen. Helaas is dit nooit helemaal van de grond gekomen, maar hieruit zijn gelukkig wel veel mooie andere (RAS-)projecten gevloeid. Als een soort Godfather van mijn onderzoeksonderwerp zorgde jij ervoor dat ik soms weer op scherp werd gesteld wanneer nodig, hield je een oogje in het zeil en zorgde je voor focus. Ik zal dan ook nooit meer de welbekende zin van jou tijdens werkbesprekingen "Maar wat is het doel van dit experiment?" vergeten. Ik heb ontzettend veel gehad aan je begeleiding in het begin van mijn promotietraject en het was fijn om af en toe terug te kunnen vallen op zo'n ervaren onderzoeker.

Jacco, jij was de andere jongeman (naast Hugo) aan tafel die ook overstroomde van energie. Hoewel ik in eerste instantie solliciteerde voor een project dat gedeeld zou zijn tussen jouw en Hugo's lab, kwam ik uiteindelijk op een ander project terecht in het Snippert lab. Desondanks heb ik altijd met erg veel plezier de Van Rheenen retraites meegemaakt waar het duidelijk werd dat jij altijd de tijd neemt voor het grondig doorspitten van projecten. Een samenwerking tussen onze labs die uit één van deze retraites vloeide, heeft dan ook uiteindelijk tot een mooi hoofdstuk in dit boekje geleid.

Mijn lieve paranimfen, **Koen** en **Loes**, wat ontzettend fijn dat jullie de afgelopen jaren ook op de derde van het Stratenum rondliepen. **Koen**, met jou was het altijd een feestje op de kamer of op het lab. Ik heb met jou echt over alles kunnen lullen: van wetenschap tot scheermesjes, en dat vanaf Hippo Monday tot en met Suit-it-Up Friday. Ik zou het beeld van jou dat je tijdens Dubrovnik op het golfkarretje van het hotel sprong om zo rondjes rond de rotonde te rijden nooit vergeten. Heel veel succes in Bazel en ik kom je opzoeken! **Loes**, in San Francisco kwam ik erachter wat een fantastisch persoon jij bent. Je bent altijd in voor een uitje, van festivals of kamperen tot een borrel of gewoon een goede grap. Ik was dus ook ontzettend blij toen jij vertelde dat je ervoor had gekozen om op het Stratenum te komen werken. Je bent echt een sfeermaker en onze trip naar Noorwegen was ook een feestje om nooit te vergeten ("Hi, I'm single"). Nog eventjes, en je mag een stuk zoals dit ook gaan schrijven. Zet hem op nog even, ik verheug me nu al op het feestje!

De **Snippies**, wat was het fijn om de afgelopen jaren in zo'n gezellig lab te zitten waar iedereen zo behulpzaam is. Vergeleken met het begin is de groep behoorlijk gegroeid en bestaat het uit nogal uiteenlopende persoonlijkheden. Op een ding lijken we wel op elkaar, want iedereen heeft hard werken met een goede portie lol hoog in het vaandel staan. **Carla** en **René**, hoewel jullie al enkele jaren weg zijn, wil ik jullie bedanken voor jullie input in de drug screen-experimenten en persoonlijke interesse. De twee newbies, **Joris** en **Julian**, wat fijn dat jullie terug zijn. Heel veel succes (en neem nooit meer het woord "prullenbakkencollege" in de mond)!

Bas, wat is het fijn om jou om je heen te hebben, zowel op wetenschappelijk als op muzikaal en sociaal gebied. Het is elke keer weer een verrassing wat jij uit je laatje trekt: 60 dozen Cup-a-Soup of een yoghurtbak met schimmel. Dankzij jouw FRET-probe hebben we een stukje van de biologie beschreven in hoofdstuk 5 beter kunnen begrijpen en het werkte erg stimulerend om daar soms samen over te kunnen sparren. Bedankt voor alle wijze lessen en je grappen en grollen! P.S. Ik moet nog steeds dat nummer van jouw timer hebben, want man, man, wat een lekker deuntje is dat! **Ingrid**, de labmoeder van de Snippies. Wat heb jij veel voor mij gedaan: het kweken van organoidcultures plus het pikken en de sequencing van honderden clones. Ontzettend veel dank hiervoor. **Lotte**, bijna tegelijkertijd begonnen en eindigen wij onze promotietijd. Hoewel je uiteindelijk meer in het Van Rheenen lab was te vinden, was het altijd erg gezellig als je eventjes bij ons kwam buurten. Bovendien was je een hele fijne buddy om samen mee de kamer te delen als we naar een meeting of retraite gingen. Zo heb jij dat vast ook gevoeld toen ik de badkamer liet overstromen en je kleren zeiknat waren geworden… Veel succes met de laatste loodjes! **Maria H**, it was great to have you as a team player and coffee-drinking-buddy in the Snippert group (it didn't matter if it was just a normal Americano, Iced Coffee, or Espresso Martini). I'm always amazed by your scientific input during work discussions, which was something I valued very much. Good luck with all the projects! **Yannik**, jij bent denk ik één van de mensen in het lab met de meest grappige en uitzonderlijke eigenaardigheden: de drive om langer te leven door middel van "intermittent fasting" (ik ruik de broccoli nog steeds), het drinken van shakes en het insmeren met factor 50. Jouw passie voor het ontwerpen van CRISPR-gebaseerde editing tools heeft geleid tot een mooi hoofdstuk in dit proefschrift. Het was erg leuk om daaraan bij te mogen dragen! **Nizar**, de hulk van het Snippert Lab. Ik heb genoten van al je verhalen tijdens de lunch en jouw liefde voor woordgrappen die vaak niet voor herhaling vatbaar zijn. Ik heb zo ontzettend veel gehad aan jouw tomeloze inzet en medewerking aan drie hoofdstukken in dit proefschrift! Als ik op het laatste moment vroeg of het toch anders geanalyseerd kon worden, dan deed je dat meteen. Veel dank daarvoor en je hoge tollelollerantie! **Sander**, wat was het fijn om jouw buurvrouw te mogen zijn op het kantoor. Jouw luisterend oor, hoge "chillheidsgehalte" en gevoel voor humor is iets wat ik erg kon waarderen. En verbazingwekkend is het toch: Zo snel en competitief je bent op de fiets, zo langzaam dat je bent tijdens de lunch. **Petra**, als side-kick van Yannik begon je bij ons op het lab, maar je bent inmiddels uitgegroeid tot een echte allrounder die alles wil leren. Mooi om te zien dat zo'n jonge meid zulke drive heeft om te groeien! **Michiel** en **Suzanne**, ik heb wel eens vaker gezegd dat jullie wat mij betreft te laat zijn gekomen. Het is namelijk zo leuk om jullie in het lab te hebben. **Michiel**, jouw vrolijkheid is zo aanstekelijk dat het bijna elk mislukt experiment weer goed maakt. Ook heb ik erg graag gebruik gemaakt

van jouw "Verzamelaaracties" voor de luie "Jagers" in de groep. Bovendien, heb ik nog nooit iemand zo zien springen toen we naar de Matrix gingen en jij het rode drankje naar je zag lonken. **Suzanne**, jouw zelfspot en lachsalvo's zijn echt heerlijk om naar te luisteren. Ik vind het knap hoe je twee banen combineerde, maar nog steeds de vrolijkheid zelve bleef. Jij hebt altijd feilloos in de gaten als iemand wat minder goed in zijn vel zit en handelt daar dan ook naar (net zoals je altijd door hebt als er een goede cocktail op de kaart staat). **Suraya**, wat was jij een topstudent! Je pakte zo veel zo snel op en dat heeft tot mijn eerste onderzoeksartikel geleid! En het is echt waar wat ze zeggen: een mens weet niet wat hij mist, maar als ze er niet is, weet een mens pas wat hij mist. Veel succes met je promotieonderzoek!

Christina, **Wigard** en **Ellen**, ontzettend bedankt voor de fijne samenwerkingen die hebben bijgedragen aan de totstandkoming van hoofdstukken 4 en 5! **Christina**, I really enjoyed our collaboration and I am happy that you asked me to join forces with you. Besides scientific interest, which resulted in chapter 4, we also shared our love for laughter and food! I wish you all the best with finishing up the final part of your PhD. Go, go, go!

De Rooij groep en **Gloerich** groep, 5,5 jaar lang heb ik ook van jullie aanwezigheid mogen genieten. Ik heb veel gehad aan de discussies en jullie expertise op onze wekelijkse woensdagochtendmeetings. **Johan** en **Martijn**, jullie oog voor detail en brede kennis heeft me geholpen bij het bijsturen van projecten, bedankt! **Antoine**, the guy with the hoodie! Thanks for all the feedback during work discussions and good luck with your projects! **Daan**, de sidekick van Antoine, ook veel succes toegewenst! **Lisa**, almost there! Succes met de laatste loodjes! **Mirjam** en **Jooske**, jullie ook veel succes met jullie projecten. **Marjolein**, bedankt voor het verzorgen van alle labprotocollen en je hulp bij pull-down experimenten. **WJ**, dacht je van de Postjes af te zijn, kwam er toch nog één op de werkvloer… Dankjewel voor de gesprekken bij de koffie, de grappen op Spetses, of je hulp tijdens de weekenden! Nu ben je dan eindelijk echt van ze af… De Postjes.

Lucas, ik mis je cowboyboots en je houthakkersblouse op het kantoor. Ook jouw kritische blik tijdens werkdiscussies heeft me erg geholpen.

Fried, bedankt dat je een oogje in het zeil hield en voor je adviezen. Vooral tijdens het begin van mijn promotieonderzoek heb ik hier veel aan gehad. Succes! Fried's Angels, **Susan** en **Denise**, wat was het gezellig om jullie op het lab te hebben. Ik heb zo met jullie kunnen lachen, vooral als er voor de koelkast gedanst werd. Heel stiekem hebben jullie toch wat bijgedragen aan dit boekje, want ik heb behoorlijk wat Wattmanpapiertjes en buffers van jullie gejat. Dankjewel!

Holger, een onderzoeker pur sang. Met behulp van 3D brillen en jouw uitleg heb ik de structuur van RAS-eiwitten beter kunnen begrijpen. Bedankt voor de discussies tijdens de werkbesprekingen.

De leden van de leescommissie: **Boudewijn Burgering**, **René Bernards**, **Jan-Paul Medema**, **Jarno Drost** en **Madelon Maurice**, bedankt voor het lezen en beoordelen van mijn proef-

schrift.

Burgering, **Dansen**, **Vercoulen** en **Rodriguez-Colman** groep, dank voor jullie interesse en input in mijn projecten tijdens werkbesprekingen. Ik wil jullie ook voornamelijk bedanken voor de goede sfeer die op de derde van het Stratenum hangt. **Boudewijn**, bedankt voor je input tijdens de evaluatie van mijn projecten voor de hoofdstukken van dit proefschrift. Jouw visie heeft tot een andere benadering van het project beschreven in hoofdstuk 4 geleid. **Tobias**, jouw kennis en kritische blik zet iedereen op de dinsdagmeetings weer op scherp. **Harm-Jan** en **Robert**, de mannen van de Mass Spec, bedankt voor jullie bijdrage aan hoofdstuk 4! **Yvonne**, door jou ben ik uiteindelijk op de plek geëindigd waar ik nu zit. Jij tipte me op een PhD-positie in het lab van Hugo na een stage bij jou in SF. Ik heb mede dankzij jou een ontzettend leuke tijd gehad in SF en wat leuk dat je uiteindelijk ook weer in NL op dezelfde verdieping werkt. Tijdens mijn stage bij jou heb ik veel technieken opgedaan waaraan ik ontzettend veel heb gehad tijdens mijn promotieonderzoek. Ik kan geen Western Blot meer zien!

Jeanine, het was erg verfrissend om een arts bij de discussies te hebben tijdens onze retraite. Dit heeft tot een mooie samenwerking en hoofdstuk 1 geleid! Bedankt!

Van Rheenen groep, bedankt voor jullie feedback op de presentaties tijdens de jaarlijkse retraites. Hoewel mijn onderwerp nogal ver van jullie straatje vandaan lag, heb ik gelukkig dat op sociaal vlak nooit zo ervaren. Bedankt! **Jeroen**, bedankt voor de fijne samenwerking waarbij tig muizen van pas kwamen. Dit heeft geresulteerd in een mooie afsluiter van hoofdstuk 5. Veel succes nog bij Jacco!

Marianne en **Cristina**, de ladies waar je voor alle vragen terecht kon. Veel dank hiervoor! **Marianne**, bedankt voor het in de gaten houden wanneer er een voortgangsgesprek moest worden ingepland of voor je hulp bij het invoeren van online-documenten. Ik heb genoten van de schaterlachen wanneer je aan de koffietafel zat met Cheuk en Marjoleine.

Marcel, **Cheuk** en **Marjoleine**, bedankt voor het op orde houden van het lab en alle bestellingen die gedaan moesten worden.

De **ICT-boys**, bedankt voor het fiksen van mijn laptop als hij weer eens gecrasht was of bij het helpen van alle ICT-gerelateerde problemen waar ik de ballen van begrijp!

Ik wil ook nog wat mensen buiten de academische wereld bedanken die indirect hebben bijgedragen aan mijn promotietijd. Helaas is er niet genoeg ruimte om iedereen te bedanken, maar jullie enthousiasme en interesse in mijn werk (wanneer ik een poging tot uitleggen waagde) zetten alles altijd weer in perspectief en kon ik trots zijn op wat ik deed.

Mijn lieve vriendinnetjes van **JC Hoepel**, de **ZHS** en **VVV'tjes** wil ik toch even expliciet bedanken. Jullie waren altijd op de hoogte van mijn promotieperikelen en jullie stonden te juichen toen ik vertelde dat de datum van mijn verdediging vast stond. Ook al had ik een baaldag en begrepen jullie er soms de ballen van, jullie stonden altijd voor me klaar. De etentjes,

borrels, weekendjes weg en vakanties hebben voor de nodige ontspanning gezorgd en jullie support en vriendschap is me ontzettend waardevol.

De **Vinkjes** en **Hartjes**: Lieve **Bram**, **Lies**, **Eva** en **Tim**, jullie toejuiching vanaf de zijlijn (zoals jullie appjes tijdens het afronden van mijn proefschrift) is van onschatbare waarde. Niet alleen jullie wetenschappelijke interesse in mijn werk (bijvoorbeeld wanneer Bram weer met CRISPR-artikel aan kwam zetten of Eva die haar promotieperikelen met mij kon delen), maar vooral de andere fijne momenten wanneer het niet over werk ging, hebben mij erg geholpen tijdens mijn promotietijd. Bedankt voor alle gezelligheid en de avonden dat Huug en ik 's avonds nog even aan konden schuiven.

Papa en **Lodewijk**. Nature versus Nurture. Ik denk dat ons gezin daar een perfect voorbeeld van is. De nerdgenen zijn duidelijk doorgegeven en de proeven met slakken hadden kennelijk als klein kind een grote indruk op me achtergelaten. Wat was het fijn om de kleine overwinningen met jullie te delen, maar ook om mijn hart soms te kunnen luchten als ik even helemaal klaar was met het onderzoek doen. Lieve **Lodewijk**, bedankt voor je luisterend oor maar ook je doelgerichte aanpak. Je was altijd geïnteresseerd (al ging het over onderzoek of de volgende stap in mijn carrière) en bereid om mijn proefschrift door te lezen of mijn Nederlandse samenvatting na te kijken. Dankzij jouw plan de campagne heb ik maar mooi dit laatste jaar volbracht. Lieve **Pap**, ook al zit je ver weg, de successen kon ik gelukkig via een berichtje of telefoontje altijd met je delen. Het betekent heel veel voor me dat je vandaag dichtbij bent om dit succes met me te vieren! Ik denk alleen dat de droom om een Post lab met je kinderen op te richten misschien niet van de grond zal komen… Lieve **mam**, ik vind jou echt een powervrouw die barst van de energie en creativiteit. Bovendien moet je je maar kunnen redden in zo'n gezin vol nerds. Je hebt me geleerd mijn eigen boontjes te doppen en mijn hart te volgen. Ondanks je overvolle agenda's maak je altijd ruimte vrij voor je kinderen en kleinkinderen. Meerdere malen tijdens mijn promotietijd heb ik bij je aan kunnen kloppen voor advies of voor een plaspauze tijdens mijn rit naar het Stratenum. En de radiostilte tijdens de laatste fase van mijn promotietraject, die nam je gelukkig voor lief. Dear **Isa**, a woman who knows all the ins-and-outs of a successful career in science. Although we both like science, we mainly share our love for traveling, cooking and fashion. Besides the fact that you're passionate about your work, your top priority is your family. I'm happy that you are here to share this moment with me! Lieve **Maarten** en **Sanne**, wat is het fijn dat je bij jullie altijd aan kan komen kloppen. Als ik vrijdag op de fiets bel voor een borreltje, kan ik altijd langs komen waaien om vervolgens pas rond middernacht te vertrekken. Gelukkig kan dat sinds vorig jaar een stuk gemakkelijker als (bijna) buren. Dankjulliewel voor jullie interesse, maar vooral voor alle gezelligheid! Lieve **Anneke** en **Stefan**, heerlijk dat ik zoveel van deze tijd met jullie heb kunnen delen en dat jullie me altijd heel goed begrepen. Steef, je had natuurlijk alles al via An meegekregen en wist dat een glas rode wijn en lekkere stinkkaas soms de beste remedie was. **An**, je bent als een echte grote zus voor mij en we hebben zoveel gemeen. Aan de meeste dingen (de basis- en middelbare school, studie en een stage in SF) begon ik pas nadat jij het had afgerond. Daarom was het des te leuker dat ik het begin van mijn promotietijd met jou heb mogen delen. Vaak was ik in het begin nog "het zusje van", maar gelukkig word ik inmiddels gewoon Jasmin genoemd. Ik heb veel met je kunnen delen, niet alleen de praktische dingen van het labwerk,

maar vooral ook de sociale dingen op de werkvloer. Samen kunnen we ook uren hebben over de dingen die we willen gaan doen. Bedankt voor alle adviezen! En wie weet, misschien is het de volgende keer omgedraaid en begin ik iets eerst voordat jij het doet… ;-) **Alex**, the last geek in the running for a position in the Post Lab… It is fun to see how much you have changed the last few years: from a dedicated nerd to a partying college dude back again to a dedicated scientist! My best career advice is: follow your heart in what you like to do the most (may it be a PhD or veterinary school). But for now: enjoy every bit of freedom and partying before you will start your career!

En dan, tot slot, mijn lief! **Huug**. Volgens jou had ik twee bazen die Hugo heetten, eentje op werk en eentje thuis. Jouw nummer staat dan ook onder de naam van Hugo Boss in mijn telefoon. Alleen voelde dit misschien het afgelopen jaar niet zo voor je, gezien de vele avonden dat je voor me hebt gekookt en gezorgd! Jij staat altijd voor me klaar en hebt me ook veel geleerd over hoe ik dingen aan kan pakken op werk. Zonder jou was deze promotietijd toch echt een stuk saaier geweest, want thuis of op reis is het met jou echt een feestje. Alleen dit jaar zaten we in hetzelfde schuitje en waren we allebei ontzettend druk: ik met het afronden van mijn proefschrift, jij met het afronden van je studie (en dat naast je drukke baan). Dat hebben we nu allebei maar mooi afgerond. Gelukkig maar, want het begon verdomde stil te worden in huis. Ik ben ontzettend gelukkig met jou en op naar het volgende feestje! I love you.

Jasmin